

# Organising Molecules at the Solid - Liquid Interface

Inauguraldissertation

zur

Erlangung der Würde eines Doktors der Philosophie

vorgelegt der

Philosophisch-Naturwissenschaftlichen Fakultät

der Universität Basel



von

**M. A. Umut Soydaner**

aus Istanbul, Türkei

Basel, 2012

Original document stored on the publication server of the University of Basel  
**edoc.unibas.ch**



This work is licenced under the agreement „Attribution Non-Commercial No Derivatives –  
2.5 Switzerland“. The complete text may be viewed here:

**[creativecommons.org/licenses/by-nc-nd/2.5/ch/deed.en](http://creativecommons.org/licenses/by-nc-nd/2.5/ch/deed.en)**





## Attribution-Noncommercial-No Derivative Works 2.5 Switzerland

---

You are free:



to Share — to copy, distribute and transmit the work

Under the following conditions:



**Attribution.** You must attribute the work in the manner specified by the author or licensor (but not in any way that suggests that they endorse you or your use of the work).



**Noncommercial.** You may not use this work for commercial purposes.



**No Derivative Works.** You may not alter, transform, or build upon this work.

- For any reuse or distribution, you must make clear to others the license terms of this work. The best way to do this is with a link to this web page.
- Any of the above conditions can be waived if you get permission from the copyright holder.
- Nothing in this license impairs or restricts the author's moral rights.

**Your fair dealing and other rights are in no way affected by the above.**

This is a human-readable summary of the Legal Code (the full license) available in German:

<http://creativecommons.org/licenses/by-nc-nd/2.5/ch/legalcode.de>

**Disclaimer:**

The Commons Deed is not a license. It is simply a handy reference for understanding the Legal Code (the full license) — it is a human -readable expression of some of its key terms. Think of it as the user-friendly interface to the Legal Code beneath. This Deed itself has no legal value, and its contents do not appear in the actual license. Creative Commons is not a law firm and does not provide legal services. Distributing of, displaying of, or linking to this Commons Deed does not create an attorney-client relationship.



Genehmigt von der Philosophisch-Naturwissenschaftlichen Fakultät der Universität  
Basel auf Antrag der Herren:

Prof. Dr. Marcel Mayor

Prof. Dr. Wolf-Dietrich Woggon

Basel, den 22. Juni.2010

Prof. Dr. E. Parlow  
(Dekan)



The work presented here was initiated and supervised by Prof. Dr. Marcel Mayor at the Chemistry Department of the University of Basel, between 2005 and 2010.

Excerpts from this work are published in:

Soydaner, U., Peterle, T., Ringler, P., Mayor, M., "A novel thiol-thioether hybrid ligand for the direct synthesis of gold nanoparticles" *in preparation*.

Raimondo, C., Reinders, F., Soydaner, U., Mayor, M., Samorì P., "Light-responsive reversible solvation and precipitation of gold nanoparticles" *Chem. Commun.*, 2010, 46 (7):1147-9

Boz, S., Stöhr, M., Soydaner, U., Mayor, M., "Protecting-group-controlled surface chemistry - organization and heat-induced coupling of 4,4'-di(tert-butoxycarbonylamino)biphenyl on metal surfaces", *Angew. Chem. Int. Ed.*, 2009, 48(17):3179 – 83. "Schutzgruppengesteuerte Oberflächenchemie - Organisation und temperaturinduzierte Kupplung von 4,4'-Di(tert-Butoxycarbonylamino)biphenyl auf Metalloberflächen" *Angewandte Chemie*, 2009, 121(17):3225-9





## Acknowledgments

I want to express my gratitude to Prof. Dr. Marcel Mayor for giving me the opportunity to work on such an interesting and challenging project. Furthermore, I sincerely thank to Prof. Dr. Wolf D. Woggon for accepting co-examination of my thesis as well as being a mentor in the beginning of my research life and Prof. Dr. Edwin C. Constable for accepting to be the chairman.

I would like to thank to Dr. Meike Stöhr for the fruitful collaboration and especially to Serpil Boz for her experimental work and all the stimulating and scientific discussions. Moreover, I would also like to thank Dr. Philippe Ringler for the measurement of the TEM micrographs.

I would like to thank Dr. Daniel Häussinger for NMR measurements, Dr. Heinz Nadig for EI- and FAB-MS and M. Werner Kirsch for elemental analysis. I am also thankful to Brigitte Howald, Marina Mambelli Johnson and Beatrice Erismann for their administrative support as well as the complete 'Werkstatt' and 'Materialausgabe' team. These are the people who keep the Department of Chemistry running.

I would like to thank to the colleagues from the Department of the Chemistry and the entire Mayor group all for the warm environment and the unforgettable memories. My thanks go to Sergio Grunder for being my first lab mate, Dr. Nicolas Weibel and Torsten Peterle for their help and useful suggestions, Sandro Gabutti and David Muñoz for their friendship, Thomas Eaton for proofreading, Viviana Horhoiu and Agnieszka Glowinska for making lab work fun and their contribution to a nice and multicultural environment.

I would like to acknowledge the NCCR "Nanoscale Science", University of Basel and SNF for financial support.

I am indebted to my parents and my sister for all their help and guidance as I started to make my way in the world.

Last but not least, I am deeply grateful to my wife Banu Sürücü for her presence in my life, never-ending love and supporting me all the time and to our son Arda for bringing "joie de vivre" to our life. Without them, this research would never have come so far.

Golf kadar...

Si la jeunesse savait,  
si la vieillesse pouvait....



---

<b>TABLE OF CONTENTS</b>		<b>Page</b>
i.	LIST OF FIGURES	i
ii.	LIST OF SCHEMES	lv
iii.	ABBREVIATIONS	Vi
1.	INTRODUCTION	1
1.1.	Towards the Gold Nanoparticles	1
1.2.	Properties of Gold Nanoparticles	4
1.2.1.	Surface Plasmon Resonance	5
1.2.2.	Quantum Size Effects	5
1.3.	Synthesis of Gold Nanoparticles	9
1.3.1.	Turkevich Method	10
1.3.2.	Phosphine Ligands	10
1.3.3.	Brust-Schiffrin Method	12
1.4.	Functionalization of Nanoparticles	13
1.4.1.	Post-Synthetic Modification	14
1.4.2.	Ligand Exchange	14
1.5.	Purification of Nanoparticles	17
1.6.	Characterization of Nanoparticles	17
1.7.	Preparation of Ordered Nanoparticles	18
1.8.	From Molecules to Structures	20
1.8.1.	Molecules on the Surface	22
2.	AIM OF THE THESIS	35
3.	RESULTS AND DISCUSSION	37
3.1.	Synthesis of New Ligands for Enwrapping Au <sub>55</sub> Nanoparticles	37
3.2.	Synthesis New Gold Nanoparticles Stabilized by Thioether Based Ligands	64
3.3.	2D Assemblies of Preorganised Molecules	87
3.3.1.	Protection Group Controlled Surface Chemistry	87
3.3.2.	Selective Cleavage of Protection Group	100
3.3.3.	Self-Assembly Pattern of Asymmetric Thermally Interlinkable Structure	107
4.	SUMMARY AND CONCLUSION	117
5.	EXPERIMENTAL PART	119
5.1.	General Remarks	119
5.1.1.	Chromatographic Methods	119
5.1.2.	Spectroscopic Methods	120

## Table of Contents

---

5.2.	Synthetic Procedures for Gold Nanoparticles	121
5.3.	Synthetic Procedures for 2D Assemblies of Preorganized Structures	165
6.	REFERENCES	177
7.	CURRICULUM VITAE	186

<b>i. LIST OF FIGURES</b>		<b>Page</b>
Figure 1.1.	Sarcophage of Touthankamon and Lycurgus cup	1
Figure 1.2.	Faraday's colloidal ruby gold	2
Figure 1.3.	Number of articles published containing the concept on gold nanoparticles since 1991	3
Figure 1.4.	Some potential application areas of nanoparticles	4
Figure 1.5.	Origin of surface plasmon resonance	5
Figure 1.6.	Formation of a metallic band structure	6
Figure 1.7.	Kubo criterion	7
Figure 1.8.	Experimental arrangement and conditions to measure current-voltage (I-U) characteristics of gold nanoparticles	7
Figure 1.9.	I-U curve of $Au_{55}(PPh_3)_{12}Cl_6$ at room temperature	8
Figure 1.10.	Diagram of a gold MPC	9
Figure 1.11.	Preparation of citrate-stabilized nanoparticle	10
Figure 1.12.	Synthesis of $Au_{55}(PPh_3)_{12}Cl_6$	11
Figure 1.13.	Organization of full shell metal clusters	12
Figure 1.14.	Idealized computational model structure of a thioether ligand gold cluster complex and the employed ligand structure	15
Figure 1.15.	Examples of images obtained by lithographic method	19
Figure 1.16.	Schematic representation of the self-assembly of a supramolecular aggregate	21
Figure 1.17.	Hydrogen bond arrays based G-C base pair	21
Figure 1.18.	STM images of isophthalic acid derivatives	22
Figure 1.19.	STM image of terephthalic acid derivatives	23
Figure 1.20.	STM images of PVBA on Ag(111)	24
Figure 1.21.	STM images of 1-NN on Au(111)	24
Figure 1.22.	STM images of the 2D structure formed by TCPP and stearic acid	25
Figure 1.23.	Arrangement of trimesic acid molecules on graphite surface	26
Figure 1.24.	Schematic diagrams showing the structure of NTCDA and NTCDI	27
Figure 1.25.	STM image of NTCDI on Ag-Si(111)	27
Figure 1.26.	Quartets of guanine formed by self-assembly on Au(111)	27
Figure 1.27.	Structures of melamine and cyanuric acid complexes	28
Figure 1.28.	STM images of $C_{60}$ heptamers in PTCDI-melamine supramolecular network.	29

Figure 1.29.	STM images of Cu-Pc and PTCDA on Cu(111)	29
Figure 1.30.	STM image of SubPc and C <sub>60</sub> on Ag(111)	30
Figure 1.31.	Steering the size and aspect ratio of rectangular molecular-scale compartments	30
Figure 1.32.	STM images and diagrams showing the process of controlling the initiation and termination of linear chain polymerization	32
Figure 1.33.	Proposed structure of the molecules arising from the UV induced formation of “clothlike” macromolecules	32
Figure 1.34.	STM image of the TTA-DIA monolayer structure on graphite	33
Figure 1.35.	Nano-architectures of covalently bound Br <sub>4</sub> TPP molecular networks	34
Figure 2.1.	Ligand enwrapping gold nanoparticles	35
Figure 2.2.	Schematic view of H-bonding of 4,4'-diaminobiphenyl molecules	36
Figure 3.1.1.	Schematic representation of the expected ligand exchange and enwrapping of Au <sub>55</sub> nanoparticles with dimeric macrocycle ligands	37
Figure 3.1.2.	<sup>1</sup> H-NMR spectrum of ligand <b>B</b>	58
Figure 3.1.3.	<sup>31</sup> P-NMR spectrum of ligand <b>B</b>	59
Figure 3.2.1.	Model depicting the minimized energy calculations of preligand <b>E</b>	79
Figure 3.2.2.	UV-Vis spectrum of gold nanoparticles stabilized with ligand <b>E</b>	82
Figure 3.2.3.	<sup>1</sup> H-NMR spectrum of ligand <b>E</b> with gold nanoparticles	83
Figure 3.2.4.	TEM picture of gold nanoparticles stabilized with ligand <b>E</b>	85
Figure 3.2.5.	Histogram of gold nanoparticles stabilized with ligand <b>E</b>	86
Figure 3.2.6.	Models depicting the minimized energy calculations of ligand <b>E</b>	87
Figure 3.3.1.	Candidates for the formation of well-ordered molecular patterns	88
Figure 3.3.2.	STM image of <b>50</b> on Ag(111)	89
Figure 3.3.3.	STM images of <b>50</b> on Cu(111)	90
Figure 3.3.4.	STM images and suggested models of <b>50</b> on Cu(111)	91
Figure 3.3.5.	STM image of <b>50</b> on Ag(111) annealed ~200 °C	92
Figure 3.3.6.	STM image of <b>50</b> on Cu(111) annealed at 196 °C	93
Figure 3.3.7.	HPLC spectrum of the azo derivative <b>62</b> (top), the DMF extract of the Ag nanoparticles (middle in red) and of the urea derivative <b>60</b>	99
Figure 3.3.8.	STM image of <b>50</b> on Cu(111) annealed at > 198 °C.	100
Figure 3.3.9.	Close up STM image of <b>65</b> on Ag (111)	102
Figure 3.3.10.	STM image of <b>65</b> on Ag (111)	102
Figure 3.3.11.	STM image of <b>65</b> on Cu (111)	103



---

Figure 3.3.12.	STM images of <b>65</b> on Ag (111) annealed at 160 °C	104
Figure 3.3.13.	STM images of <b>65</b> on Ag (111) annealed at 168 °C	105
Figure 3.3.14.	XPS measurements of <b>65</b> on Ag(111)	105
Figure 3.3.15.	STM images of <b>65</b> on Cu(111)	106
Figure 3.3.16.	STM images of <b>66</b> on Ag(111)	108
Figure 3.3.17.	Close up STM image of <b>66</b> on Ag (111)	109
Figure 3.3.18.	STM image of <b>66</b> on Ag(111) at low coverage	109
Figure 3.3.19.	STM image of <b>66</b> on Ag(111) at high coverage	110
Figure 3.3.20.	STM image of <b>66</b> on Ag(111) annealed at 155 °C	111
Figure 3.3.21.	Close up STM image of <b>66</b> on Ag (111) annealed at 155 °C	111
Figure 3.3.22.	STM image of <b>66</b> on Ag (111) annealed at 168 °C	112
Figure 3.3.23.	STM image of <b>66</b> on Cu(111) at low coverage	113
Figure 3.3.24.	STM images of left and right hexamers of <b>66</b> on Cu(111)	113
Figure 3.3.25.	Coverage dependent growth of self-assembled structures of <b>66</b> on Cu(111)	114
Figure 3.3.26.	Parallel arrangement of <b>66</b> on Cu(111)	114
Figure 3.3.27.	STM image of <b>66</b> on Cu(111) annealed at 160 °C.	115
Figure 4.1.	Suggested assembly of gold nanoparticles stabilized with two of ligands <b>E</b>	117
Figure 4.2.	Preorganized molecular building blocks interlinked on the surface.	118

<b>ii. LIST OF SCHEMES</b>		<b>Page</b>
Scheme 3.1.1.	Retrosynthetic analysis of symmetric ligand <b>A</b>	37
Scheme 3.1.2.	Synthesis of 1,3,5-tris(bromomethyl)benzene	40
Scheme 3.1.3.	Strategy to synthesize (3,5-bis(bromomethyl)benzyl)(hexyl)sulfane	41
Scheme 3.1.4.	Suggested mechanism for polymerization of bis(bromomethyl)benzyl)sulfane	41
Scheme 3.1.5.	Strategy to synthesize (3,5-bis(chloromethyl)benzyl)(hexyl)sulfane	42
Scheme 3.1.6.	Retrosynthetic analysis of asymmetric ligand <b>B</b>	43
Scheme 3.1.7.	Retrosynthetic analysis of polar group containing building block	43
Scheme 3.1.8.	Synthesis of the polar chain	44
Scheme 3.1.9.	Synthesis of first building block of ligand <b>B</b>	45
Scheme 3.1.10.	Alternative synthesis of first building block of ligand <b>B</b>	46
Scheme 3.1.11.	Retrosynthetic analysis of second building block of ligand <b>B</b>	47
Scheme 3.1.12.	Strategy towards synthesis of second building block of ligand <b>B</b>	49
Scheme 3.1.13.	Retrosynthetic analysis of 1,3,5-tris(mercaptomethyl)benzene building block	50
Scheme 3.1.14.	Synthesis of polar thio building block	51
Scheme 3.1.15.	Synthesis of 1,3,5-tris(mercaptomethyl)benzene building block	52
Scheme 3.1.16.	One pot synthesis and deprotection of THP of 1,3,5-tris(mercaptomethyl)benzene building block	53
Scheme 3.1.17.	Alternative synthesis of 1,3,5-tris(mercaptomethyl)benzene building block	54
Scheme 3.1.18.	Synthesis of of dithiol building block	55
Scheme 3.1.19.	Synthesis of dimer <b>B</b>	56
Scheme 3.1.20.	Retrosynthetic analysis of benzo 1,3,5-tris(mercaptomethyl)benzene dithiol building block	61
Scheme 3.1.21.	A new approach to the synthesis of a 1,3,5-tris(mercaptomethyl)benzene dithiol building block	62
Scheme 3.1.22.	Synthesis of ligand <b>C</b>	63
Scheme 3.2.1.	Linear oligomeric multidentate thioether ligands	64
Scheme 3.2.2.	Retrosynthetic analysis of cyclic thiol-thioether hybrid multidentate ligand <b>D</b>	66
Scheme 3.2.3.	Retrosynthetic analysis building blocks	66
Scheme 3.2.4.	Synthesis of of bis(halomethyl)benzylsulfane	69

---

Scheme 3.2.5.	Retrosynthetic analysis of 1,3,5-tris(mercaptomethyl)benzene building block	70
Scheme 3.2.6.	Alternative synthesis of 1,3,5-tris(mercaptomethyl)benzene dithiol building block	71
Scheme 3.2.7.	Synthesis of ligand <b>D</b>	72
Scheme 3.2.8.	Retrosynthetic analysis of ligand <b>E</b>	75
Scheme 3.2.9.	Synthesis of one masked, one free thiol containing <i>tert</i> -butylbenzylic compound	77
Scheme 3.2.10.	A new approach to the synthesis of ligand with bulkier linker	78
Scheme 3.2.11.	The synthesis of ligand <b>E</b>	80
Scheme 3.3.1.	Hypothesized chemical reaction sequence	95
Scheme 3.3.2.	Synthesis of biphenyl <b>53</b>	96
Scheme 3.3.3.	Synthesis of biphenyl <b>59</b>	96
Scheme 3.3.4.	Synthesis of <b>60</b>	97
Scheme 3.3.5.	Simulation of surface reactions	97
Scheme 3.3.6.	Synthesis of biphenyl <b>62</b>	98
Scheme 3.3.7.	Synthesis of fluorinated derivative of <b>50</b>	101
Scheme 3.3.8.	Synthesis of asymmetric derivative of <b>50</b>	108

**iii. ABBREVIATIONS**

Ac	Acetyl
Å	Angstrom
AIBN	2,2'-azobis(2-methylpropionitrile)
Anhyd.	Anhydrous
aq.	Aqueous
BOC	<i>N-tert</i> -butoxycarbonyl
<i>br</i>	Broad
BTC	Bis(trichloromethyl)carbonate
Bu	Butyl
<i>d</i>	Duplet
DMAP	Dimethylaminopyridine
DCM	Dichloromethane
DHP	3,4-Dihydro-2H-pyran
DMF	<i>N,N</i> -dimethylformamide
DMSO	Dimethylsulfoxide
EA	Elemental Analysis
EI	Electron Impact
eq.	Equivalent
ESI	Electron Spray Ionization
Et	Ethyl
EtAc	Ethylacetate
EtOH	Ethanol
FAB	Fast Atom Bombardment
FG	Functional Group
GPC	Gel Permeation Chromatography
h	Hour
HPLC	High Performance Liquid Chromatography
HRXPS	High Resolution X-ray Photoelectron Spectroscopy
<i>hν</i>	Light
KSAc	Potassium thioacetate
NaH	Sodium hydride
<i>m</i>	Multiplet
M	Molar

---

<i>m/z</i>	Mass per charge
MALDI	Matrix-Assisted Laser Desorption-Ionization
Me	Methyl
mg	Milligram
min	Minute
mL	Milliliter
ML	Monolayer
mmol	Millimole
MeOH	Methanol
MP	Melting Point
MS	Mass Spectrometry
Ms	Mesyl
NBS	<i>N</i> -Bromosuccinimide
nm	Nanometer
NMR	Nuclear Magnetic Resonance
PG	Protecting Group
Ph	Phenyl
PMB	<i>p</i> -methoxybenzyl
ppm	Parts per million
PPTS	Pyridinium <i>p</i> -toluenesulfonate
<i>q</i>	Quartet
quant.	Quantitative
<i>R<sub>f</sub></i>	Retention factor
RT	Room temperature
<i>s</i>	Singlet
STM	Scanning Tunneling Microscopy
<i>t</i>	Triplet
<i>Tert</i>	Tertiary
TBAF	Tetra- <i>n</i> -butylammonium fluoride
TBME	<i>t</i> -butyl methyl ether
TEA	Triethylamine
TEM	Transmission Electron Microscopy
TFA	Trifluoroacetic acid
THF	Tetrahydrofuran

## Abbreviations

---

THP	Tetrahydropyran
TLC	Thin Layer Chromatography
TOAB	tetra- <i>n</i> -octylammonium bromide
TOF	Time of Flight
TPP	Triphenylphosphine
Trt	Trityl
UV-Vis	Ultraviolet and visible
v/v	Volume per volume
XPS	X-ray photoelectron spectroscopy

## INTRODUCTION

### *1.1. Towards the Gold Nanoparticles*

The extraction of gold started in the 5<sup>th</sup> millennium B.C. near Varna (Bulgaria). It became rapidly prevalent not only for its scarcity but also for its resistivity against the corrosion and its softness, which enabled it to be hammered into pieces of jewellery. The production of gold reached 10 tons per year in Egypt around 1200-1300 B.C. when the statue of Touthankamon was constructed.



**Figure 1.1.** Sarcophagus of Touthankamon (left), Lycurgus Cup (right)

“Soluble” gold (gold colloids) have been probably appeared around the 5th or 4th century B.C. in Egypt. Following their discovery, gold colloids have been used for well over a thousand years for both aesthetic and curative purposes some of which still continues today such as production of ruby glass and coloring of ceramics. Perhaps the most famous example is the Lycurgus Cup, which was made in the 5th to 4th century B.C. Its color is ruby red in transmitted light and green in reflected light, which is due to the presence of gold colloids <sup>[1]</sup>. In addition to the Lycurgus cup, use of gold nanoparticles could also be seen at the windows of many medieval churches.

The color of gold nanoparticles arises from unique resonance frequency, so called surface plasmon resonance (SPR), which results from the restoring force that tries to compensate collective oscillation of conduction electrons caused by the electric field of the incoming radiation, for example light <sup>[2]</sup>. Although many metals show plasmon resonance, their plasma frequency lies in the UV part of the spectrum <sup>[3]</sup>. However, gold and other coinage metals are exceptional. They are not only more noble and form air-stable colloids but also

their plasma frequency is pushed into the visible part of spectrum (between 500 and 600 nm) due to the to d–d band transitions <sup>[4]</sup>.

The reputation of soluble gold until the Middle Ages was to display fabulous curative powers for various diseases, such as heart and venereal problems, dysentery, epilepsy, and tumors, as well as for diagnosis of syphilis. The curative use of gold colloids was well detailed in what is considered as the first book on colloidal gold, published by the philosopher and medical doctor Francisci Antonii in 1618 <sup>[5]</sup>. Afterwards, the German chemist Johann Kunckels published another book, <sup>[6]</sup> in 1676, in which he concluded, well before Michael Faraday, that “gold must be present in such a degree of communitation that it is not visible to the human eye”. During 16<sup>th</sup> and 17<sup>th</sup> centuries there have been numerous studies on stability<sup>[7]</sup> and the coloration<sup>[8]</sup> of the gold colloids. However the real breakthrough in the scientific study of these particles was achieved by Faraday <sup>[9]</sup>, whose gold colloid films have survived to this day. In 1857, Faraday reported the formation of deep red solutions of colloidal gold by reduction of an aqueous solution of chloroaurate ( $\text{AuCl}_4^-$ ) using phosphorus in carbon disulfide (a two-phase system) <sup>[9]</sup>. The methods for producing gold colloids have since extended to many other elements, notably Ag, Pt and some transition metals <sup>[10]</sup>.



**Figure 1.2.** Faraday’s colloidal ruby gold. Reproduced by courtesy of the Royal Institution of Great Britain.

In contrast to the long history of gold, the development of its chemistry delayed because of its noble character since it could be only dissolved in oxidizing media like aqua regia limiting the scope of the potential experiments. In the mid-19th century Faraday <sup>[9]</sup> reported the initial formal studies of the interactions between gold colloids and light, subsequently in the 20th century, the physical descriptions such as Mie theory <sup>[11]</sup> were able to explain and predict the



optical properties of gold nanoparticles. In addition, descriptions of gold nanoparticles as zero-dimensional quantum wells and the theory of Coulomb blockade have initiated the analysis of their electronic properties. It is expected that the electronic properties of nanoparticles may offer solutions to the limits of Moore's law rendering them particularly interesting for future applications <sup>[12-18]</sup>. In the past decade, gold colloids have been the subject of a considerably increased number of books and reviews. Current effort is focused on colloids with particles smaller than 100 nm, known-as “nanoparticles”. Particularly interesting are the particles in the size range between 1 and 10 nm, where they can neither be treated as single molecule nor as bulk materials <sup>[19]</sup>. The subject is currently intensively investigated, due to fundamental and applied aspects relevant to the quantum size effect. The recent growth in the number of publications observed in Figure 1.3 reveals the recognition of the new and changing properties on the nanoscale.

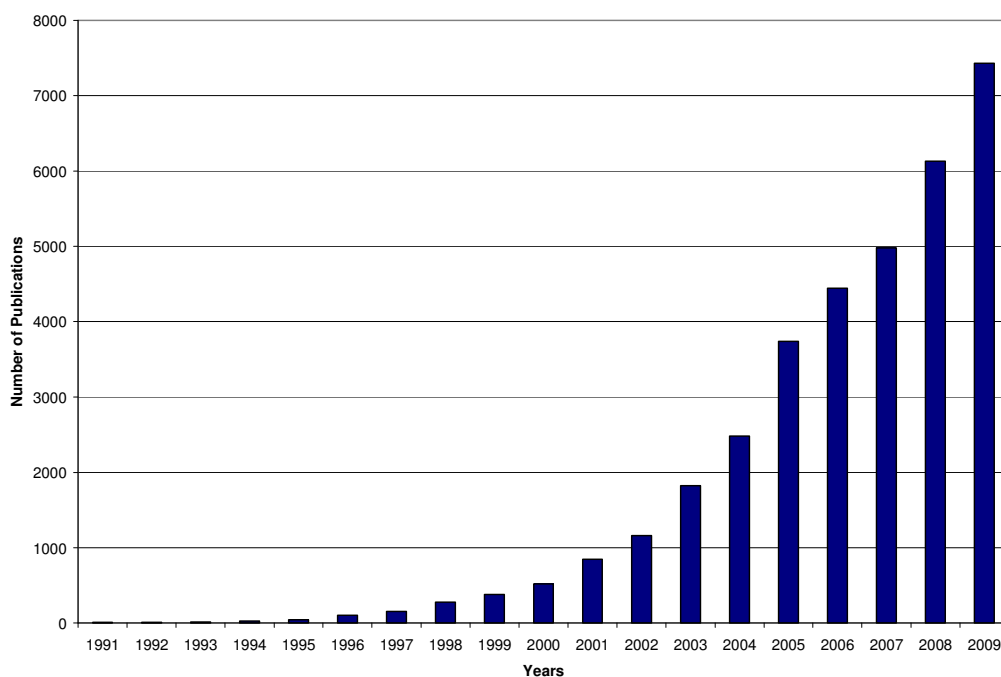


**Figure 1.3.** Number of articles published containing the concept on gold nanoparticles since 1991. Data collected from Scifinder 2010.

The nanometer scale is also important for several applications, which also includes those in biological systems <sup>[20-22]</sup> (Figure 1.4). Many proteins are around tens of nm in size. Since structures can be accurately designed in nanometer scale, they could be incorporated into

biological systems owing to their similar size scales. Aside from the similar size and correspondingly large surface-to-volume ratio, certain nanomaterials are attractive probe candidates because of their chemically tailorable physical properties. Moreover, their remarkable target binding properties and overall structural robustness yield novel hybrid nanobiomaterials. Nanotechnology for life sciences comprise an effort to address problems ranging from painful and inefficient drug delivery to the need for faster medical diagnosis and analysis.

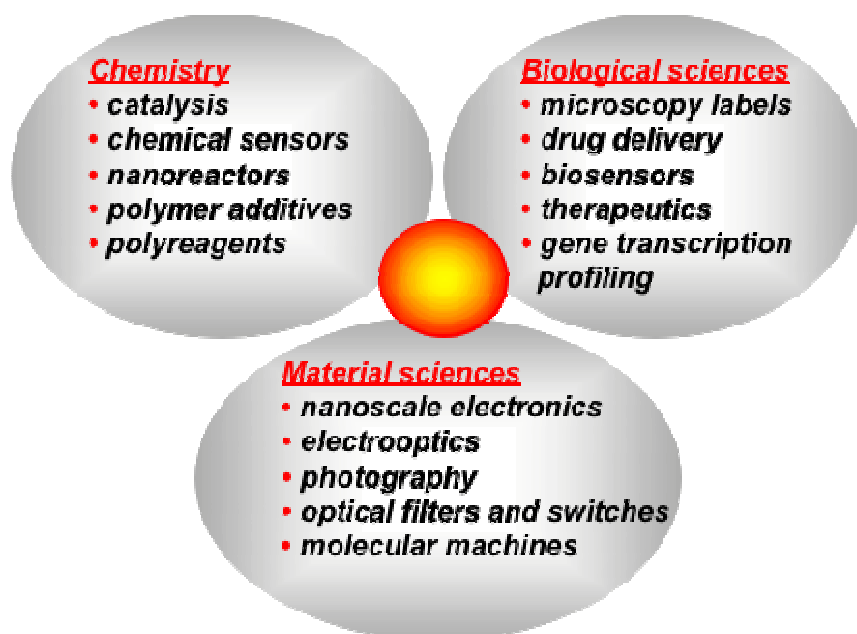


**Figure 1.4.** Some potential application areas of nanoparticles.

## ***1.2. Properties of Gold Nanoparticles***

Nanoparticles can have fundamentally different properties compared to their bulk counterparts <sup>[19]</sup>. For instance, they can exhibit SPR, their melting point is lower than that of bulk metals <sup>[23, 24]</sup> and their charging can be a quantized single-electron event <sup>[25, 26]</sup>. Virtually any chemical functionality can be bound to them by simple surface reactions <sup>[27, 28]</sup> and different metal compositions can be used to tailor the electronic properties of the core <sup>[10, 26]</sup>. Remarkably, most of these properties are size-dependent and can be adjusted by changing the nanoparticle size.

### 1.2.1. Surface Plasmon Resonance (SPR)

Nanoparticles exhibit distinct optical properties. For instance, photoluminescence spectra of semiconductor particles are governed by the opening of gaps in the band structure and the spatial confinement of excitons inside the nanoparticle [23, 29]. In metallic particles, the most prominent feature is the surface plasmon excitation [30]. An important characteristic of gold, silver and other noble metal nanoparticles is the SPR in the visible spectrum, which gives rise to intense colors. SPR is due to the collective oscillation of the conduction band electrons on the particle surface induced by the interacting electromagnetic field. SPR is very sensitive to the size of the particles. It is not observed for bulk materials but also vanishes for radii less than 2 nm since the incident light was absorbed by the electrons which behave like a wave due to quantum effects. For 2 - 20 nm particles, the position and the intensity of SPR is well defined by the Mie theory [2, 31] and can be used to obtain information about the concentration and polydispersity of the nanoparticle sample. Aggregation also affects surface plasmon resonance as the SPR of a single particle changes if it is brought in close proximity to another particle. The sensitivity of the plasmon frequency to the environment of the nanoparticle opens the way for application of such particles as sensors [32, 33].

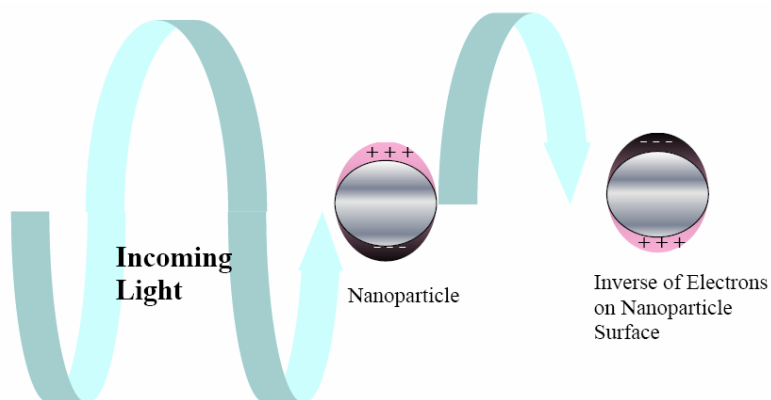


**Figure 1.5.** Origin of surface plasmon resonance due to coherent interaction of the electrons in the conduction band with electromagnetic field.

### 1.2.2. Quantum Size Effects

When the size of a metal is reduced to a particle of a few nanometres in diameter, bulk descriptions of the electronic structure are no longer valid [34]. In bulk, metallic gold, the electronic properties are characterized by the valence and conductance bands containing an

infinite number of bonding and antibonding orbitals respectively. The Fermi level lies within the conductance band, allowing the metal to conduct using only thermal energy (Figure 1.6.c). When the dimensions of the metal are reduced to a few tens of nanometers, discrete energy levels start to appear at the band edges due to confinement of space and decrease in the number of electrons (Figure 1.6.b). Although the properties of the gold nanoparticle remain largely metallic, some molecular transitions may be observed under certain conditions such as low temperature. As the size is further decreased to below 2 nm, the (pseudo) continuous bands will split into discrete levels, molecular orbitals, within the band structure can be observed (Figure 1.6.a) [35]. For instance, Au<sub>55</sub> clusters have a gap of ~ 0.25 eV [36]. As a consequence, the nanoparticle loses the majority of its metallic character and exhibits size-induced metal-to-insulator transition [23, 37, 38]. These changes in the electronic structure with size point out the need for access to gold nanoparticles with well-defined core diameter [12].

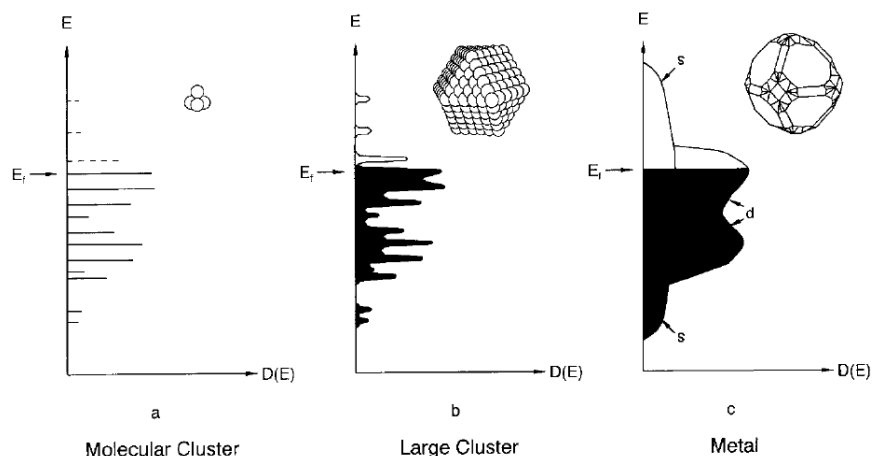


**Figure 1.6.** Formation of a metallic band structure. Adapted from [39]. On the way from a molecule a) via nanosized clusters b) the quasi delocalisation of valence electrons increases until the bulk state c) is reached.  $E_f$ =Fermi energy, DOS = Density of states.

The above mentioned discrete nature gives rise to Quantum Size Effects (QSE) [23, 24, 35, 37, 40]. The energy required to add an electron to a system, energy known as the Coulomb charging energy ( $E_c = e^2/2C$ ), is almost zero for bulk gold. However, in small gold nanoparticles, electrons are subject to substantial confinement leading to strong Coulombic repulsion and a subsequent increase in Fermi energy ( $E_f$ ). Indicated by Kubo criterion, the

QSE begin to take place when the level spacing at the Fermi level  $\delta(E_F)$  exceeds the thermal energy of the electrons ( $k_B T$ ), leading to single electron transition (SET) events [12, 34, 41-43].

$$\delta(E_F) \approx \frac{3}{2} \frac{E_F}{N_A z} > k_B T$$

**Figure 1.7.** Kubo criterion.  $N_A$ : Avogadro constant,  $k_B$ : Boltzmann constant;  $z$ : the number of valence electrons per atom.

When a nanoparticle is placed between two electrodes (Figure 1.8), a double tunneling junction will be formed due to the small size of the cluster and the band splitting. In order for electrons to tunnel between the source and the drain through the nanoparticle, a minimum energy known as the Coulomb charging energy must be applied [23, 44-46]. The nanoparticle is charged with one elementary charge by the tunnelling electron, causing a voltage build up  $U = e/C$ . If the capacitance is very small, the voltage build up can be large enough to prevent another electron from tunnelling.

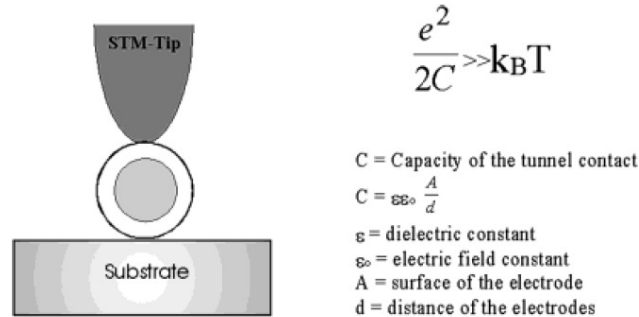


**Figure 1.8.** Experimental arrangement and conditions to measure current-voltage (I-U) characteristics. Adapted from [39].

The conductivity of such a device is therefore limited by a Coulomb blockade [47, 48]. Between -500 mV and +500 mV, conductivity is not observed meaning that a single electron is trapped in the cluster until a voltage less than 500 mV is reached (Figure 1.9). If the bias voltage is increased, a stepwise increase of the conductivity is expected [23, 45, 46, 49]. Within the Coulomb blockade region, the SET is in the “off” or “0” state, and at high enough gate voltages, the SET will be in the “on” or “1” state [12, 50].

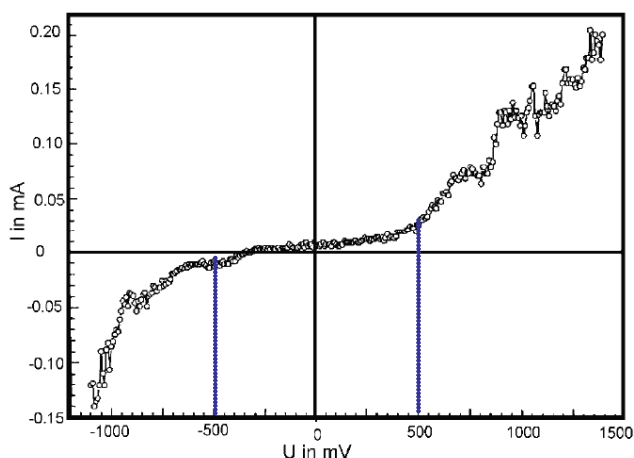


**Figure 1.9.** I-U curve of  $\text{Au}_{55}(\text{PPh}_3)_{12}\text{Cl}_6$  at room temperature. There is a well-pronounced Coulomb blockade between -500 mV and +500 mV. Adapted from [39].

Moreover, if the nanoparticle under investigation is sufficiently small, these effects can be observed at room temperature [51, 52]. In an ideal case it is possible to observe SET, however, only if the thermal energy of the electrons ( $k_B T$ ) is very small compared with the Coulomb charging energy. As the capacity  $C$  directly depends on the surface of the particle this means that the smaller the particle, the larger the electrostatic energy becomes. If  $C$  is small enough,  $T$  could be increased up to room temperature. All former measurements in literature had to be done at very low temperature to observe SET. However,  $\text{Au}_{55}(\text{PPh}_3)_{12}\text{Cl}_6$  for the first time allowed the observation of SET processes at room temperature. To sum up, careful control over the size and composition as well as the purity of gold nanoparticles is crucial for observing and utilizing the unique electronic properties of these materials.

Another important general property of nanoparticles is their surface-to-volume ratio. Small particles have a large proportion of their atoms at the surface. This will lead to different binding energies, since the surface atoms will have a lower coordination number than bulk atoms. For instance, the Au–Au binding is stronger in gold clusters than in bulk gold, leading to a smaller bond length [53]. The reactivity of small particles differs from that of the bulk material, due to this difference in the interatomic bonding. In combination with the large surface exposure and defect free close shell structures makes gold nanoparticles potent oxidation catalysts [23, 54]. Another important example is the low temperature oxidation of CO (carbon monoxide) by gold particles [55-57].

### 1.3. Synthesis of Gold Nanoparticles

The goal in preparing gold nanoparticles is to produce a population of narrowly dispersed gold cores. Most commonly, a Au(III) salt is reduced to Au(0) to form an activated species, either in a single step or via an Au(I) intermediate followed by reduction to Au(0). These activated Au(0) species are thermodynamically unstable and rapidly aggregate to form nuclei because in any colloidal material reduction of the surface-to-volume ratio is favourable for reducing the surface free energy<sup>[58]</sup>. To prevent aggregation of gold nanoparticles these activated Au(0) species are commonly passivated and stabilized by an organic ligand shell (Figure 1.10).

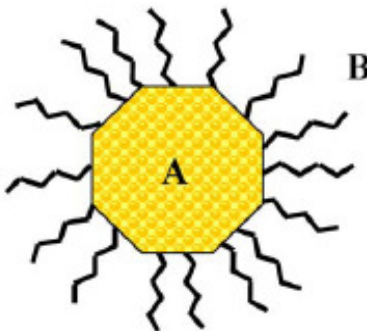


**Figure 1.10.** Diagram of a monolayer protected cluster (MPC). A) Inner gold core. B) Outer passivating organic monolayer, which electrically insulates the inner core.

In order to produce a uniform, narrowly distributed population of gold nanoparticles, the activated species must be homogeneously dissolved throughout the reaction medium, and the nucleation should occur simultaneously. To meet these criteria, reactions are typically carried out in small volumes with millimolar concentrations of reactants using constant, vigorous stirring. The rate of activated species formation, and thus the rate of nucleation, is controlled by choice of the reducing agent, the concentration or the temperature.

Although hundreds of methods have now been reported for the preparation of gold nanoparticles, they can generally be categorized by the type of organic ligand they are prepared with. These categories include (i) non-specific ligands, such as citrates, (ii) phosphines, such as triphenyl phosphine and (iii) thiols, such as dodecanethiol. Methods

resulting in formation of nanoparticles containing these classes of ligands are discussed below.

### 1.3.1. Turkevich Method

The most common method of synthesizing gold nanoparticles is through the use of citrate (Figure 1.11). Turkevich *et al.* reported that adding sodium citrate to a boiling solution of chlorauric acid led to the formation of nanoparticles<sup>[59]</sup>.

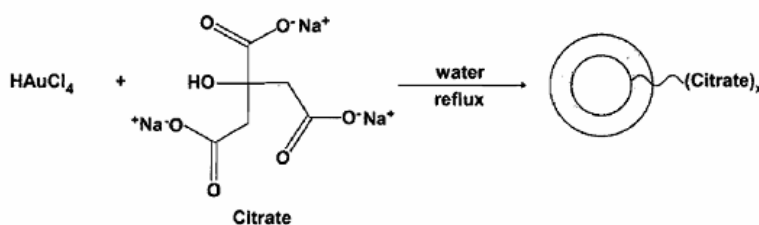


**Figure 1.11.** Preparation of citrate-stabilized nanoparticles.

Later work revealed that variations in temperature and the ratio of reactants allowed for control over the average core size from 10 to 100 nm<sup>[60]</sup>. More recent work showed that Au-citrate solutions allowed for the synthesis of nanoparticles less than 10 nm in average core size<sup>[171]</sup>. Despite being the most common method of producing nanoparticles, citrate-stabilized nanoparticles are disadvantageous for several reasons. First, they cannot be isolated from solution, making it difficult to store or study them in the solid state. Second, with minimal changes in pH or ionic strength their stability is diminished. Finally, and most significantly, their functionalisation, either through ligand exchange or via derivatisation of carboxylic acids in the ligand shell, is rather limited.

As noted, the synthesis of gold nanoparticles using non-specific ligand shells typically yields nanoparticles with large (> 5 nm) cores. The strongly enhanced plasmon resonance renders the large nanoparticles effective for optical and biological applications as tagging agents. In addition, larger nanoparticles produced by these methods have also been utilized as precursors in seeded growth reactions. On the other hand, despite their intriguing electronic properties at very low temperatures, large nanoparticles are not particularly suited for single electronics applications. For this reason, there has been significant effort put into the synthesis of smaller nanoparticles.



### 1.3.2. Phosphine Ligands

Though not as common as citrate preparations, another important class of gold nanoparticles is stabilized using phosphine ligands. The small size of gold nanoparticles stabilized with phosphine ligands, (typically less than 2 nm) along with their predicted room-temperature Coulomb blockade properties makes them particularly attractive for room temperature SET applications.

The earliest syntheses were derived from cluster chemistry, and some of the first molecular gold clusters contained just a few gold atoms. Initially,  $\text{Au}_5$  and  $\text{Au}_{11}$  were reported, and this was followed by a number of other molecular species up to  $\text{Au}_{39}$ .<sup>[61-64]</sup> The shift from sub-nanometer cluster chemistry to nanoparticle synthesis began with Schmid's synthesis of  $\text{Au}_{55}$  with 1.4-nm average core diameter<sup>[65]</sup>. These particles were synthesized in two steps. First,  $\text{HAu}^{(\text{III})}\text{Cl}_4 \cdot 3\text{H}_2\text{O}$  is reduced to  $\text{PPh}_3\text{Au}^{(\text{I})}\text{Cl}$ , by addition of triphenylphosphine<sup>[66]</sup>. Then, the next step requires the stronger reducing agent diborane,  $\text{B}_2\text{H}_6$ . A reaction equation completely describing the stoichiometry has never been elucidated for this reaction.

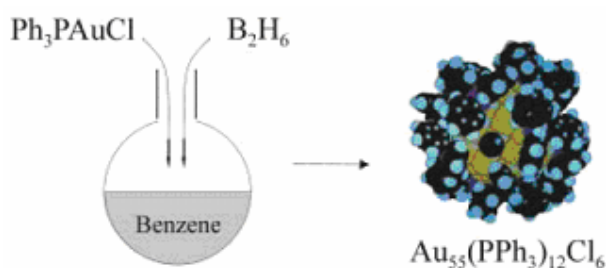
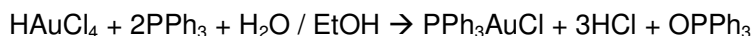


**Figure 1.12.** Synthesis of  $\text{Au}_{55}[\text{PPh}_3]_{12}\text{Cl}_6$ .

It is known that face centered clusters or hexagonal closed packed structures of transition metals contain  $10n^2+2$  atoms, so-called magic numbers, with  $n$  being the number of shell around the central atom<sup>[26]</sup>. Interestingly, it has been shown that the growth of gold nanoparticles generally proceeds through the formation of magic number clusters, which exhibit high electronic stability.

The properties of  $\text{Au}_{55}$  cluster have been extensively studied<sup>[18, 51, 53]</sup>. Both the stoichiometry and geometry of  $\text{Au}_{55}[\text{PPh}_3]_{12}\text{Cl}_6$  have been subject of a debate<sup>[67, 68]</sup>. It is suggested that  $\text{Au}_{55}$  cluster should be surrounded by two closed shells of gold atoms. The inner shell of  $\text{Au}_{55}$

cluster should be formed by a central gold atom surrounded by 12 neighboring atoms. In the outer shell of  $\text{Au}_{55}$  cluster, twelve atoms should be situated at the vertices, twenty four at the edges and six at the centres of the (100) facets. The proposed  $\text{Au}_{55}$  cluster has six (100) and eight (111) facets. Moreover, high electronic stability of  $\text{Au}_{55}$  clusters also implies face-centered cubic arrangement, giving it the cuboctahedral shape, as seen in figure 1.13. It is also proposed that the well defined geometry of the  $\text{Au}_{55}$  cluster leads to monodisperse and more stable compounds than the bulk gold <sup>[70]</sup>, since geometrically full shell clusters are much more stable than clusters with incomplete outer shells <sup>[35]</sup>. Nevertheless, the proposed structure has become widely accepted, owing to the increasing amount of evidence <sup>[51, 53, 69]</sup>.

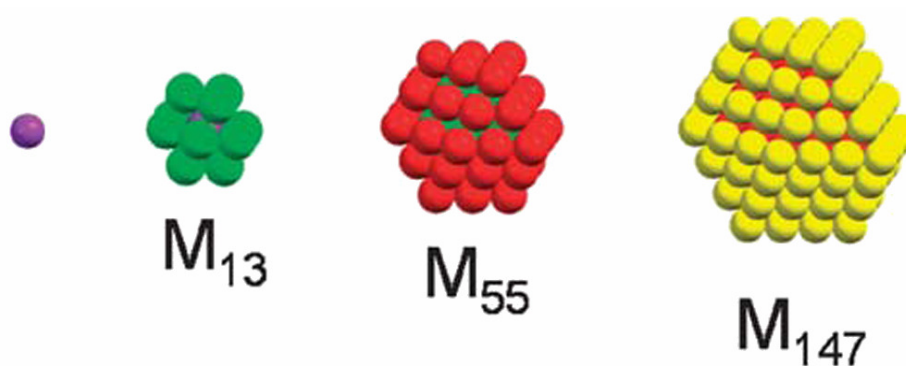


**Figure 1.13.** Organization of full shell metal clusters. A central metal atom (purple) is surrounded by 12 others (green) to form a full shell cluster  $\text{M}_{13}$ . 42 atoms (red) can be densely packed on the first shell to form a  $\text{M}_{55}$  2<sup>nd</sup> shell cluster, followed by 92 atoms on the 3<sup>rd</sup> shell (yellow) to give  $\text{M}_{147}$  <sup>[43]</sup>.

One drawback for phosphine-stabilized nanoparticles is the limited functionality available with compatible phosphine ligands and the fact that many phosphine-stabilized nanoparticles, for example,  $\text{Au}_{55}[\text{PPh}_3]_{12}\text{Cl}_6$ , are not stable in solution <sup>[71, 72]</sup>. In solution, part of the phosphine ligands detaches from the gold surface and leads to formation of irreversible coagulation of gold nanoparticles to bulk gold <sup>[73, 74]</sup>. Recent studies have demonstrated that phosphine-stabilized nanoparticles can undergo ligand exchange reactions with a wide variety of thiols, leading to nanoparticles that are stable in solution for extended periods <sup>[75, 76]</sup>.

### 1.3.3. Brust-Schiffrin Method

In 1994, Brust *et al.* reported the direct synthesis of gold nanoparticles containing dodecanethiol ligands by use of tetraoctyl ammonium bromide (TOAB) <sup>[77]</sup>. In this method, aqueous sodium borohydride is used to reduce  $\text{HAuCl}_4$  in toluene in the presence of

stabilising thiols and TOAB, to form toluene soluble 5 to 6-nm gold nanoparticles. Although the ability to synthesize a diverse range of core sizes is limited, this method provides advantages with respect to Turkevitch method and the resulting nanoparticles can be isolated from solution. Moreover, the ligand can be exchanged to yield both thiol and amine stabilized nanoparticles<sup>[78, 79]</sup>. Furthermore, thiol coating makes the particles extremely stable and they can be repeatedly dried and redispersed in various solvents without degradation.

Following these initial reports, syntheses have been developed for a wide variety of organic- and water-soluble nanoparticles containing a number of functional groups. Subsequent studies showed that a monophasic procedure could be used to prepare alcohol-soluble gold nanoparticles and eventually water-soluble gold nanoparticles<sup>[80]</sup>. Murray's group showed that the core size of nanoparticles prepared in this fashion might be tailored by varying the ligand to gold ratio during the reaction<sup>[81]</sup>. In general, the direct synthesis of thiol-capped gold nanoparticles leads to nanoparticles in the 2 to 8-nm size regime and tends to result in a greater degree of size dispersity than, for example, phosphine-stabilized nanoparticles. The synthesis has since been further modified to get more monodisperse gold nanoparticles [28, 82, 83].

## **1.4. Functionalization of Nanoparticles**

Upon synthesis, gold nanoparticles often contain an improperly functionalized ligand shell. However, this is not useful for the applications such as assembly or targeting, which require nanoparticles with specific peripheral functional groups. The presence of peripheral functionality allows for tuning the interactions between the gold nanoparticle and its environment, such as solubility, reactivity and self-assembly. Two general approaches have been devised for the introduction of functional groups into the periphery of the ligand shell: (i) post-synthetic modification of the existing ligands or (ii) ligand exchange to replace the existing ligands with ligands containing a desired functionality.

### **1.4.1. Post-Synthetic Modification**

Post synthetic modifications are used to attach molecules containing a desired functionality to the periphery of the nanoparticle using an existing functional group on the nanoparticle. For instance, Templeton *et al.* investigated the  $\text{SN}_2$  reactivity of bromo groups on the periphery of gold nanoparticles<sup>[84]</sup>. In particular, the effect of the chain length of the ligand shell (4, 8 and 10 carbons) and the bulkiness of the nucleophile on packing density of

ligands were investigated. Subsequently, it was shown that terminal —COOH groups could be modified by alcohols and amines to form the resulting amides and esters <sup>[85]</sup>. Other post-synthetic modifications included coupling reactions <sup>[84, 85]</sup>, polymerization <sup>[86]</sup> and peripheral group transformations <sup>[87]</sup>.

Post-synthetic modification offers the opportunity to start with a common precursor nanoparticle and, through well-known chemical transformations, obtain functionalized nanoparticles. However, the success of this approach is limited not only by the stability of the gold nanoparticle under the reaction conditions, but also by the reactivity and bulkiness of the peripheral functionality to be modified. Furthermore, complete functionalisation of nanoparticles might not be achieved in most of the cases leading a mixture of functionalised and non-functionalised nanoparticles <sup>[75]</sup>. Therefore, the functionalisation of particles is usually characterized qualitatively by infrared spectroscopy, X-ray diffraction, transmission electron microscopy etc. The quantitative analysis of the functionalised particles is performed indirectly which requires further reactions of nanoparticles and measuring the quantity of formed products. Consequently, the determination of the extent of functionalization is rather difficult. Because of these obstacles, ligand exchange is often employed.

### 1.4.2. Ligand Exchange

One of the most intriguing properties of noble metal clusters is the ligand exchange reaction where the existing ligand shell on a gold nanoparticle is either partially or fully displaced by another ligand that contains the desired functionality through simple chemisorption and desorption <sup>[26-28, 75, 84]</sup>. Most commonly, the gold nanoparticle is synthesized with a small, labile ligand shell that can be easily displaced in subsequent steps. Generally, the gold nanoparticles are dispersed in a suitable solvent, followed by addition of an excess of the ligand, typically a thiol, either under monophasic or biphasic conditions. This is allowed to stir for several hours or days either under ambient conditions or at elevated temperatures. Following the exchange, excess and exchanged ligands are removed by suitable purification methods, yielding the ligand-exchanged product. In all cases, removal of the excess ligand is important following ligand exchange because it has been shown that excess ligands lead to destabilization of the nanoparticles. In order to introduce the desired functionality, a variety of ligand exchange methods have been developed for different classes nanoparticles.

### Phosphine Ligand Exchange

Ligands like phosphines which are binding less strongly to gold than thiols may be replaced. Phosphine stabilized nanoparticles ligand exchange chemistry for triphenyl phosphine (TPP) stabilized nanoparticles was well-described by Woehrle *et al.* [76, 88]. The ligand exchange of 1.4 nm TPP stabilized nanoparticles, under both single and biphasic conditions, showed that the TPP was displaced as a  $\text{Au}(\text{PPh}_3)\text{Cl}$  compound followed by association of the incoming thiol during the ligand exchange process. Even though some loss of gold from the surface was observed, reductions in core diameter were negligible and the  $\text{Au}_{55}$  clusters were reported to be more stable when the phosphine ligands are exchanged for thiols or thioethers [66, 89-91]. Similarly, 0.8-nm TPP stabilized nanoparticles ( $\text{Au}_{11}$ ), have been exchanged with both functionalized phosphines and thiols to yield ligand-exchanged products.

In 2001, von Kiedrowski *et al.* reported the phase-transfer synthesis of gold clusters stabilized by tridentate benzylic thioether ligands based on 1,3,5-tris(mercaptomethyl)benzene scaffolds using water-soluble ligands [92].

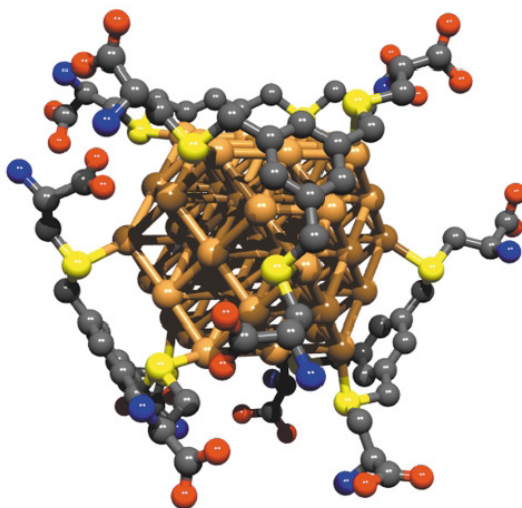


**Figure 1.14.** Idealized computational model structure of a thioether ligand gold cluster complex and the employed ligand structure. Adapted from [92].

The stoichiometry that is expected for the thiol-coated  $\text{Au}_{55}$  clusters thus formed depends on steric factors. With alkylthiols, a stoichiometry of  $\text{Au}_{55}[\text{SR}]_{26}$  is expected: twelve apical thiols, one thiol on each of the eight 111-faces and one on each of the six 100-faces. Indeed,

Brown claims to have obtained  $\text{Au}_{55}\text{L}_{26}$ , where  $\text{L}=\text{SC}_{12}\text{H}_{25}$  [91]. Schmid finds  $\text{Au}_{55}\text{L}_{12}$  with very bulky substituents that apparently occupy only the apical positions [89, 90].

### Thiol Ligand Exchange

Nanoparticles synthesized directly with thiol ligands are appealing because they offer the ability to obtain stable nanoparticles coated with a functionalized ligand shell in a single step. Unfortunately, the scope of direct thiol stabilized nanoparticle synthesis is limited by the stability of thiols with respect to disulfide formation. Although, it was reported that the disulfide ligands can be used for direct synthesis of gold nanoparticles, the stability of the particles is much lower than thiol counterparts [93, 94]. For this reason, thiol-thiol ligand exchange is often required to obtain nanoparticles with the desired functionality. However thiol-thiol ligand exchanges are often more difficult than exchanges on TPP or 4-dimethylaminopyridine (DMAP) stabilized nanoparticles.

Murray *et al.* suggested that ligand dissociation and exchange occurs via a concerted mechanism whereby an incoming ligand transfers a proton to the sulfur of an outgoing ligand [28]. It has been further hypothesized that certain locations on a nanoparticle are more reactive during ligand exchange. For both steric and electronic reasons, edge and vertex sites, areas where gold atoms have few nearest neighbors, are considered to have the highest reactivity, followed by edge sites, near-edge face sites and interior face sites [95]. It is likely that the vertex sites are the most reactive because; (i) the gold atoms at the vertex have the highest potential, and therefore show the highest reactivity (i.e. for redox chemistry) and, (ii) ligands at these sites are not stabilized by Van der Waals interactions. By similar arguments, interior surface sites show the greatest stability because the gold surface is more uniform and there is much higher ligand packing density, which increases the stability of the monolayer [28, 96, 97].

Several other factors have been shown to be important during the ligand exchange process. First, it has been shown that ligand exchange occurs most readily when the precursor particle has a ligand shell that is composed of short chain length and that is labile. Longer chain lengths lead to greater monolayer stability and lower exchange rates. It has also been shown that for the same reasons, incoming ligands that have favorable Van der Waals or hydrogen bonding interactions will show higher exchange rates. The concentration of incoming ligand also plays a large role. Although there is a one-to-one ligand exchange ratio, a high concentration of incoming ligand is required to force the ligand exchange

reaction to completion. The reason for this is that there is significant equilibrium of thiols on the surface and in solution. As with any equilibrium situation, pushing the reaction towards completion requires a significant excess of the incoming thiol. Additionally, time and temperature also play a role in forcing the reaction <sup>[98]</sup>.

### **1.5. Purification of Nanoparticles**

Purification of the desired product is one of the most critical aspects of nanoparticle preparation. Following synthesis, the product is often contaminated with excess free ligand, precursor molecules, salts and nanoparticles with undesired sizes. These impurities will often interfere on the properties of the gold nanoparticles along with their interactions with the environment, either for self-assembly or for assessing the toxicology.

The method used for purification of nanoparticles largely relies on the nanoparticle characteristics and the composition of the impurity to be removed. For instance, purification of water-soluble, thiol-stabilized nanoparticles could be challenging, as the desired material and the impurities, both salts and free ligand, often have similar solubility.

Extractions and solvent washes are beneficial for removal of the free ligand and other organic impurities, but tend to leave residual salts behind. Size exclusion chromatography is useful for removing both salts and free ligand, however the nanoparticles tend to irreversibly precipitate on the chromatography supports, leading to decreased yields. Centrifugation is another method for removing both types of impurity, but requires considerable amount of time for sufficient purification.

### **1.6. Characterization of Nanoparticles**

One of the significant challenges in gold nanoparticle synthesis is sufficient characterization in order to determine average core diameter and shape, ligand shell composition and impurity profile of the synthesized material. Defining a precise picture of the gold nanoparticles allows for a better understanding of the optical and electronic properties and contributes in the development of structure-function relationships. In order to establish the size and shape of the gold nanoparticle core, Transmission Electron Microscopy (TEM) and UV-Visible spectroscopy (UV-Vis) are often used. UV-Vis is a rapid and routine characterization method used for assessing gold nanoparticle samples. It allows access to

the optical properties of gold nanoparticles, primarily through the plasmon resonance exhibited at ~520 nm. While UV-Vis allows determining of collective properties for a qualitative assessment of particle size and shape, TEM provides a more quantitative determination of individual properties like size distribution. Additionally, electron diffraction experiments can also be carried out, allowing for an assessment of atomic packing and orientation, which is useful for shaped gold nanoparticles. In the area of nanoparticle study, NMR is used primarily to verify the composition of the ligand shell and to identify any impurities in the sample.  $^1\text{H}$ -NMR can be used to determine the identity of ligands bound to the surface versus those in solution or weakly bound. Due to the effects of the nanoparticle core and the proximity of bound ligands to one another, integration and thus quantification of the relative concentrations of different species associated with the nanoparticle is usually not applicable, thus other methods such as elemental analysis (EA), thermogravimetric analysis (TGA) and x-ray photoelectron spectroscopy (XPS) are used for quantification. EA or TGA offers the ability to determine the percentage of organic material in a nanoparticle sample. It is also possible to calculate the theoretical amount of ligand associated with the surface of a gold nanoparticle <sup>[99]</sup>. XPS is a useful technique for analyzing solid-state samples and is used to identify elements present within a sample and to determine their relative abundances in relation to each other. It allows for similar assessments, and also allows for the determination of how much inorganic impurities (e.g. excess salts) exist in the sample. Using these characterization methods, it is possible to obtain a fairly accurate picture of the gold nanoparticle sample.

### **1.7. Preparation of Ordered Nanoparticles**

An object of a certain volume can be made in two ways: either sculpturing from bulk source material which has a larger volume in comparison to the intended object, or making a mosaic starting from tiny source material whose volume is far less than that of the object. In making small structures, the former is typically referred as *top-down*, and the latter is called *bottom-up* approach. Both approaches comprise a rich variety of tools with their specific advantages and drawbacks.

The general top-down approach often uses the traditional workshop or micro fabrication methods where externally-controlled tools are used to cut, mill, and shape materials for generating a pattern or structure and to reduce it to the desired size <sup>[100]</sup>. The mass production of miniaturized devices has been developed through top-down technologies as



optical projection lithography and etching <sup>[101]</sup>. The limit of this method is the diffraction limit given by the wavelength of the incident beam. X-rays <sup>[102]</sup> or electron-beams <sup>[103]</sup> have been used as beam sources with smaller wavelength. However, such technologies become very expensive: X-ray lithography requires synchrotron radiation and electron-beam lithography requires ultra-high vacuum. Several methods in the projection scheme are still pursued with novel ideas such as optical interference lithography <sup>[104, 105]</sup>. Although, much smaller nanostructures can be build using new lithographic methods the fabrication of each structure is a costly process <sup>[106]</sup>. Recently, an imprinting technique, in which a compression molding is used to create a thickness contrast pattern <sup>[107]</sup>, is reported. Because the technique does not require lithography and an etching process, the time required to fabricate nanostructure with a resolution of 10 nm requires only a few seconds <sup>[108]</sup>. While there is an ongoing technological progress over a few decades in the development of lithography and other top-down methods, the manipulation of matter at the atomic scale is still in its infancy.

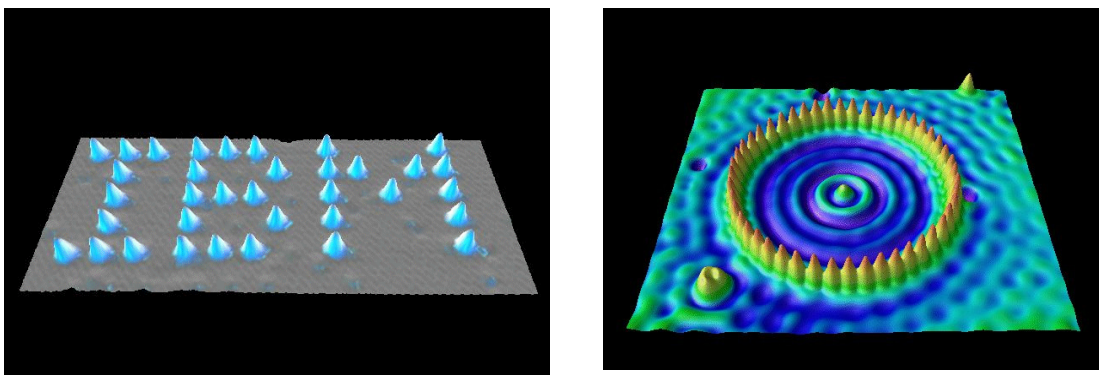


**Figure 1.15.** Examples of images obtained by lithographic methods.

*Bottom-up* approaches use the inherent properties of the materials: self-replication or self-assembling. In his famous visionary talk “There’s Plenty of Room at the Bottom” in 1959, Richard Feynman outlined how to merge chemistry, biology and physics to produce materials, whose functional units would be of a nanoscopic dimensions and whose capability in information storage would be comparable with the molecular structures known in biology <sup>[109]</sup>. Naturally, bio-molecules are good examples of self assembled nanostructures. Therefore, one can expect that the molecular self-assembly concepts are envisioned to play a major role.

## 1.8. *From Molecules to Structures*

Supramolecular chemistry is often defined as “the chemistry beyond the molecule” or “the chemistry of the noncovalent bond” [110-112]. The terminology of supramolecular chemistry was defined starting in the 1970s and new concepts were introduced by several different working groups. In 1987 the Nobel Prize in chemistry was awarded to C. J. Pedersen, D. J. Cram, and J.-M. Lehn for “pioneering an important contribution in the field of molecular recognition by non natural receptors.”

Noncovalent interactions, molecular recognition, and self-assembly are keywords that have to be considered for understanding the principles of supramolecular chemistry. The spatial arrangement of the building blocks and the supramolecular assemblies is determined by the directional intermolecular interactions. These bonds, non-covalent in nature, are of weak or intermediate strength. The various bonding types comprise metal-ligand interactions [113, 114], hydrogen bonding [115-117],  $\pi$ - $\pi$  stacking [118], van der Waals [119] or dipolar coupling [120, 121]. Each bonding type represents a different class of interactions differing in their directionality, degrees of strength, and dependence on distance and angles.

The formulation of fundamental principles of molecular recognition goes back to the early 20th century, when Emil Fischer and Paul Ehrlich introduced the terms “lock and key principle” [122] and “receptor-substrate” [123]. Molecular recognition is the specific interaction between two molecules, which are complementary in their geometric and electronic features (like two fitting pieces of a jigsaw puzzle). The lock and key principle laid the foundation for host-guest chemistry.

Molecular self-assembly relies on the specific interactions between complex molecules including a wide variety of functional groups. Self-organization describes the modular assembly of simple building blocks into complex architectures, whose topology is determined by the kinetics and thermodynamics of the assembly process. The rapid reversibility of the process ensures that any errors that may have occurred during assembly can be corrected. The abundance of self-assembly processes in nature clearly demonstrates its power in the construction of functional biological structures.

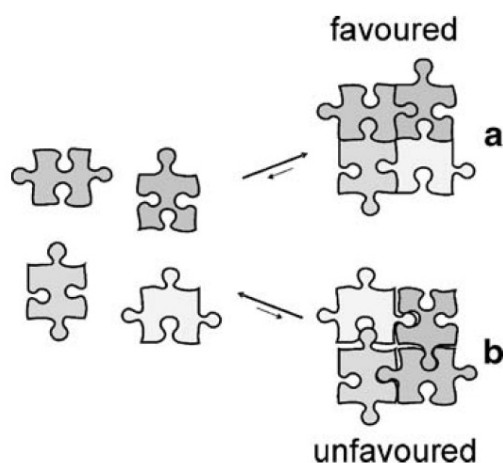


**Figure 1.16.** Schematic representation of the self-assembly of a supramolecular aggregate a by molecular recognition and noncovalent interactions between molecular building blocks. Poor complementarity of the building blocks will destabilize the obtained aggregate b, while the binding between complementary units leads to strong aggregation in the case of a. Adapted from [124].

Among the mentioned non-covalent forces above, hydrogen bonding is one of the most important intermolecular interactions. The strength of hydrogen bonds is typically around 20  $\text{kJMol}^{-1}$ , but can even be as strong as 163  $\text{kJ Mol}^{-1}$ , as has been reported for the  $\text{F}\cdots\text{HF}$  interaction [125]. However, a single hydrogen bond is still very weak compared to covalent bond and a combination of hydrogen bonds is usually needed to form a more stable interaction. Not only the number of hydrogen bonds determines the stability of the assembly, but also the arrangement of the donor (D) and acceptor (A) sites plays a significant role [126]. The differences in stability of hydrogen bonded supramolecular species can be largely attributed to attractive and repulsive secondary interactions. Stabilization arises from electrostatic attraction between positively and negatively polarized atoms in adjacent hydrogen bonds, whereas destabilization is caused by electrostatic repulsions between two positively or negatively polarized atoms (Figure 1.17).

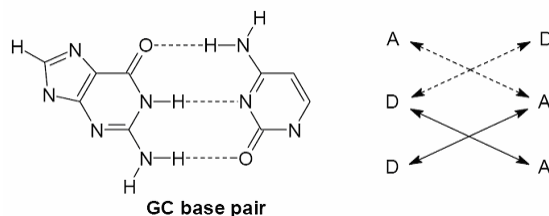


**Figure 1.17.** Hydrogen bond arrays based G-C base pair; attractive (solid arrows) and repulsive (dotted arrows) secondary interactions.

### 1.8.1. Molecules on the surface

Molecular recognition between the molecular building blocks is essential to enable an effective aggregation by noncovalent interactions, which in reversible self-assembly processes leads to stable and well-defined supramolecular species. By use of this principle to construct large ensembles of molecules, supramolecular chemistry bridges the gap between the picometer dimensions of molecules and the nanoworld. Therefore, the understanding of its fundamental basics is crucial for a successful chemical “bottom-up” approach toward nanotechnology <sup>[127]</sup>. The invention of scanning probe microscopy techniques has opened new doorways to study these concepts on surfaces <sup>[128]</sup>.

At solid substrates, hydrogen bonds can be present in molecular structures and these may consequently be highly ordered with specific directionality. For instance, alkylated isophthalic acid (1,3-benzenedicarboxylic acid) and terephthalic acid (1,4-benzenedicarboxylic acid) derivatives are versatile compounds displaying hydrogen bonding. 5-Alkoxyisophthalic acid derivatives form close-packed arrays of interdigitating hydrogen-bonded ribbons (Figure 1.18.a) <sup>[129, 130]</sup>. In contrast to the 3D crystals, the alkyl chains and the isophthalic acid groups are confined in the same plane. As a result, the hydrogen bonding motif does not reflect the traditional dimer formation of the carboxylic acid functions but a more complex 2D hydrogen bonding pattern is formed. By changing the location and the nature of the alkyl chains on the isophthalic acid groups, various other 2D motifs can be formed (Figure 1.18.b-d).

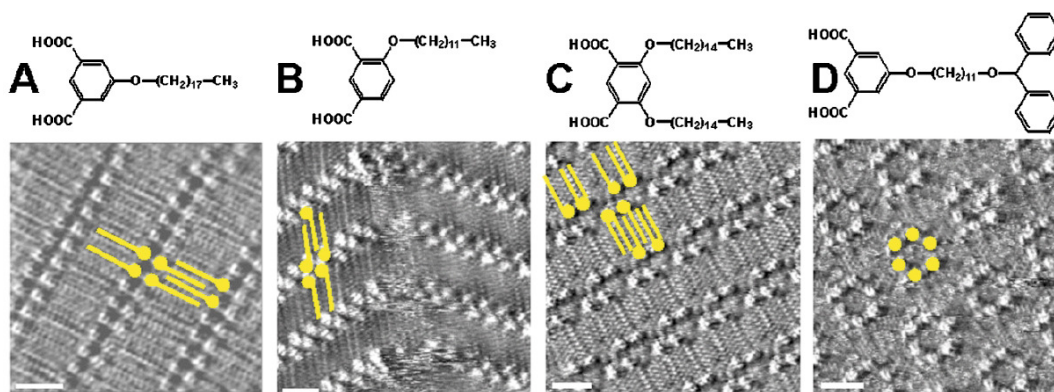


**Figure 1.18.** STM images of isophthalic acid derivatives, illustrating the effect of number, position and nature of the alkyl chains on the 2D ordering. The “discs” represent isophthalic acid groups. The lines are alkyl chains. In c, not all alkyl chains are adsorbed on the surface. In d, the isophthalic acid groups form a hexamer. The scale bar indicates 2 nm <sup>[129, 130]</sup>.

Some functionalised hydrocarbons may display stabilizing hydrogen bonding along the lamella axis. For example, in monolayers of dialkylated terephthalic acid derivatives the terephthalic acid groups (bright) are linked by hydrogen bonds (the distance between the terephthalic acid groups is the same as the distance found in 3D crystals), and the alkyl chains, which are oriented perpendicular to the lamella axis, are interdigitated (Figure 1.19.a). In this way, infinite 1D arrays of hydrogen-bonded terephthalic acid groups are formed. Other examples of infinite 1D arrays include those formed by urea or amide derivatives <sup>[131]</sup>. The urea function provides an especially strong intermolecular interaction. As a result, it was demonstrated that 1D rows or incomplete rows could be formed and imaged at the solid–liquid interface. Those hydrogen bonded arrays and the adsorbate–substrate interactions are strong enough to immobilise the molecules on the substrate, without forming a two-dimensional network (Figure 1.19.b) <sup>[131]</sup>.

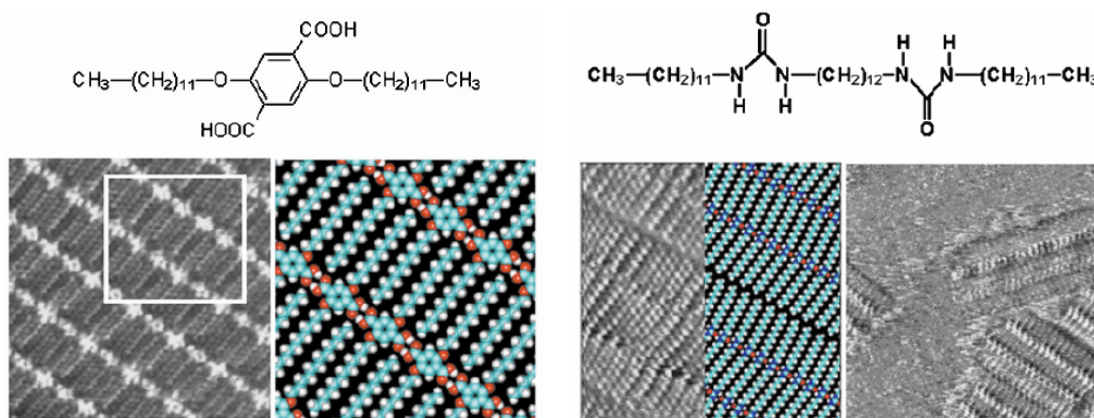


**Figure 1.19.** STM image at the solid (HOPG)–liquid (phenyloctane) interface of (left) a terephthalic acid derivative. The bright structures are the terephthalic acid groups. The model refers to the area indicated. (right) A bis-urea derivative. Left: STM image and molecular model Right: STM image with incomplete surface coverage (17.7 nm x 17.7 nm) <sup>[130, 131]</sup>.

Another interesting example is the supramolecular ordering of 4-[*trans*-2-(pyrid-4-vinyl)]benzoic acid (PVBA), surfaces <sup>[132, 133]</sup>. This molecule carries a benzoic acid function and a pyridine function. The former one can act as hydrogen bond donor and acceptor while the latter functionality is a hydrogen bond acceptor. Arrangements of PVBA molecules, which becomes chiral upon adsorption on a Ag(111) surface as it is confined to a 2D plane, was studied extensively and the resulting two enantiomers were labelled as  $\lambda$  and  $\delta$ . Twin chains form “nanogratings” extending over micrometer-size domains. This is surprising given that adjacent twin rows are nanometers apart from each other and no interaction is possible between adjacent chains. The achiral equivalent 4-[(pyrid-4-yl-ethynyl)]benzoic acid (PEBA)

was also studied. In contrast to PVBA, PEBA organises in islands, which consist of parallel chains. This difference may arise different lateral interactions between molecules are responsible for the differences in the 2D patterning, although, the main intermolecular interaction is head-to-tail hydrogen bonding for both molecules.

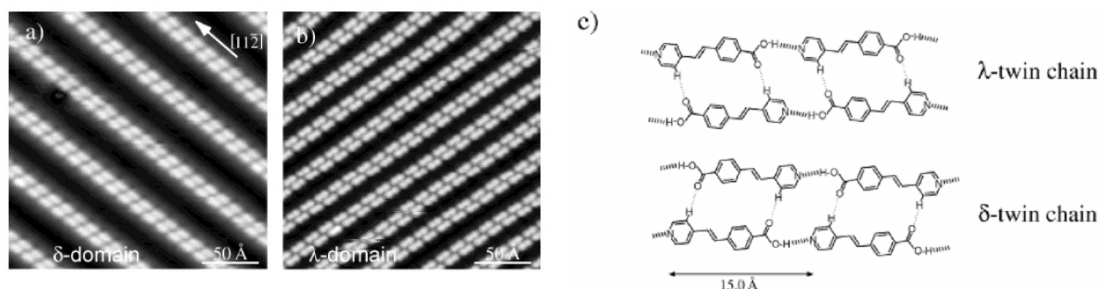


**Figure 1.20.** a)  $\delta$  PVBA on Ag(111) at 300K. b) PVBA “nanograting” on Ag(111) formed at 300K. c) schematic showing the two enantiomers of PVBA,  $\delta$  and  $\lambda$ , and the two resulting chiral double chains, with OH $\cdots$ N and weak lateral CH $\cdots$ OC hydrogen bonds<sup>[133]</sup>.

Hydrogen bonded clusters of molecules have been observed which appear self terminating in size, and do not extend to give larger arrays. These structures were investigated via the phases formed by 1-nitronaphthalene (NN) on Au(111). 1D chains and both chiralities of 10-molecule clusters were observed using STM. The arrangement of molecules became pseudo-chiral on adsorption, though the molecules are not geometrically enantiomeric when not restricted to a plane as with PVBA. The 1D rows form at 0.1 monolayer (ML) coverage with clusters forming at 0.2 ML coverage. High-resolution STM images and local density calculations reveal the orientations of individual molecules<sup>[134-136]</sup>.

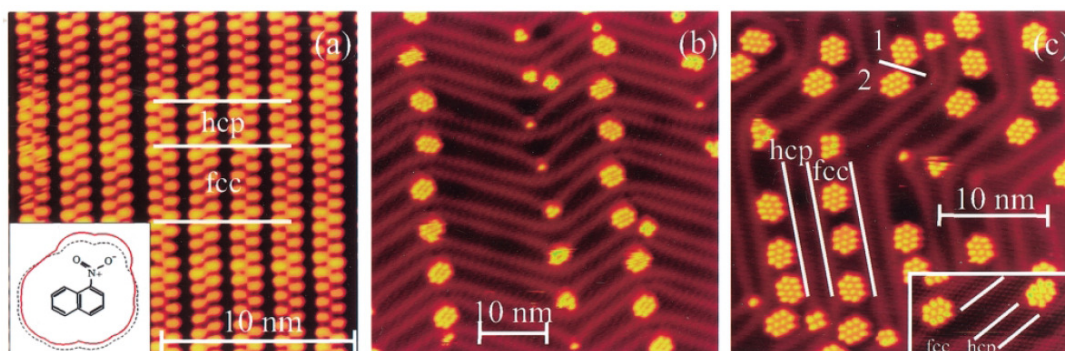


**Figure 1.21.** STM images at 50 K of a reconstructed Au(111) surface with adsorbed NN; a) 0.7 ML NN. Inset: Structural formula of NN. The dashed line encloses the “exclusion” area resulting from steric repulsion. The distance of the red line from the dashed line indicates the strength of a negative electrostatic potential. b) 0.1 ML NN at 65 K. c) 0.2 ML NN at 50 K. Inset: 0.2 ML NN at 10 K<sup>[135]</sup>.

Lei *et al.* reported on the surface stabilised porphyrin and phthalocyanine 2D network formation connected by hydrogen bonds (Figure 1.22) <sup>[137]</sup>. They have co-deposited a porphyrin derivative and stearic acid on highly oriented pyrolytic graphite (HOPG). It was observed that adsorption of the porphyrin derivative alone on the surface of HOPG did not yield observable molecular images while in presence of stearic acid, 2D islands of the porphyrin derivative were absorbed, surrounded by lamellae of stearic acid (Figure 1.22.a). In the porphyrin domains, the molecules are arranged with 4-fold symmetry (Figure 1.22.b). The 2D ordering is a compromise between the intermolecular interactions (hydrogen-bonding) and the minimization of the surface free energy: in the hypothetical closest packing, no hydrogen bonding is possible; those configurations with optimal hydrogen bonding would lead to large voids; the observed packing is a compromise between both (Figure 1.22.c).

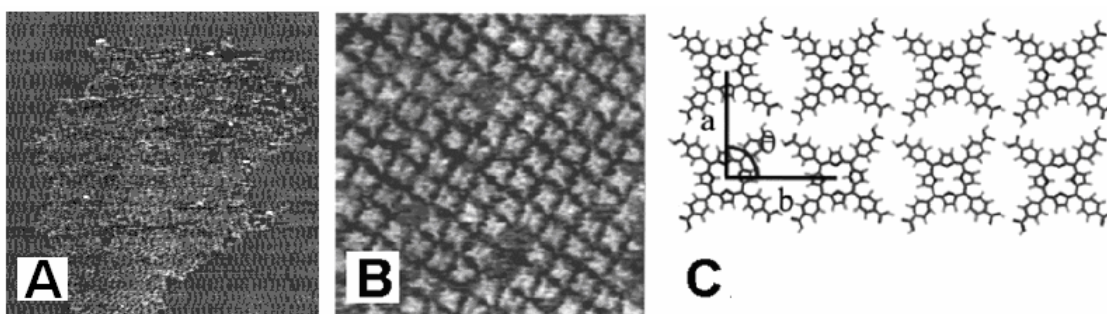


**Figure 1.22.** a) STM image of the 2D structure formed by TCPP and stearic acid, ( $200 \times 200 \text{ nm}^2$ ) b) STM image of the TCPP hydrogen-bonded network ( $22 \times 22 \text{ nm}^2$ ), and c) molecular packing of a porphyrin derivative. Note that the hydrogen bonding between the carboxylic acid groups is not optimal, but allows a dense packing <sup>[137]</sup>.

Hydrogen bonding between molecules need not necessarily lead to the formation of a single phase under a set of growth conditions, and different ordered phases can form together. The substrate on which the molecules are deposited also plays a crucial role in the possible ordering of the molecules, as does the temperature of the surface. Due to the trigonal exodentate functionality, trimesic acid deposited in vacuum onto Cu(100) was found at low temperatures (around 200K) to form two dimensional hexagonal (honeycomb) networks structure stabilised by carboxylic acid hydrogen bonding interactions between neighbouring molecules <sup>[138]</sup>.

Increasing the temperature to room temperature allows the molecules to rearrange themselves, forming a stripe motif with molecules oriented such that they no longer lie flat,

but the plane of the molecules is oriented perpendicular to the surface. Heckl *et al.* found that in addition to the honeycomb lattice, trimesic acid forms also a flowerlike motif on natural grown graphite <sup>[139]</sup>. These two phases are labelled as a hexagonal phase and a flower phase, and they can coexist due to different possible bonding geometries in which the molecules arrange to form hydrogen bond stabilised networks (Figure 1.23).

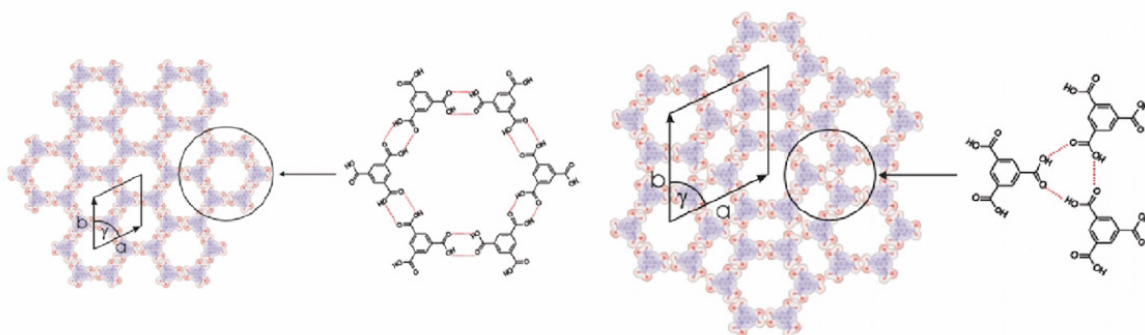


**Figure 1.23.** Trimesic acid molecules can arrange in different hydrogen bonding configurations hexagonal (left) and flower (right) to give these two structures on graphite <sup>[139]</sup>.

Hydrogen bonded molecular structures can be engineered through careful choice of functional groups, and can be considered as single entities. It is found that diimide interactions in naphthalene tetracarboxylic diimide (NTCDI) on Ag:Si(111) mediate the formation of 1D rows and close packed islands. The similar molecule NTCDAs (dianhydride) was also deposited on Ag:Si(111) and image of loosely bound molecules were observed. Thus the functional groups of adsorbate molecules can control, to some extent, the possibility of hydrogen bonded array formation. The researchers demonstrate the manipulation of a row of hydrogen bonded NTCDI molecules across the surface as a single object using the STM tip (Figure 1.25) <sup>[140]</sup>.



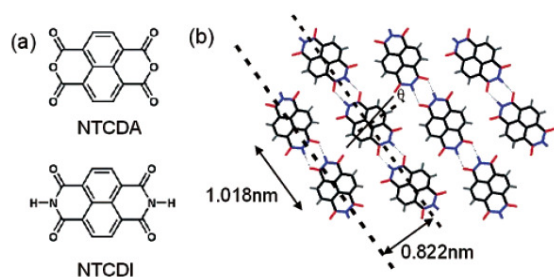


**Figure 1.24.** a) Schematic diagrams showing the structure of NTCDA and NTCDI. b) Bulk crystal structure of NTCDI. Molecules are canted to the direction of the parallel rows within the crystal by an angle  $\theta = \pm 13.9^\circ$  [140].

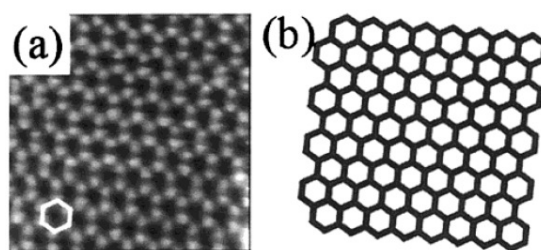


**Figure 1.25.** a) STM image ( $6 \times 6 \text{ nm}^2$ , sample voltage +1 V, tunnel current 0.5 nA) of the Ag/Si(111) surface. b) simplified schematic of the surface with vertices corresponding to positions of Ag trimers [140].

Cooperative hydrogen bonding can be present in ordered molecular surface structures. An example is demonstrated by Otero *et al.* [141], who presented STM images of guanine deposited at room temperature on Au(111) in UHV conditions. Guanine molecules are found to group into quartets of four molecules in a square arrangement, which the authors model computationally using density functional theory (DFT). These findings confirm that the quartet arrangement is more stable than a molecular dimer through stabilisation by cooperative hydrogen bonding. One may expect at first that a dimer structure would form as nucleic acids do in DNA. The guanine quartets pattern the surface to give a network structure. Figure 1.26 shows the quartet arrangement observed. After annealing the sample, the guanine molecules rearranged to form a self-assembled monolayer with a 30% increase in packing density, though hydrogen bonding was still present [141].

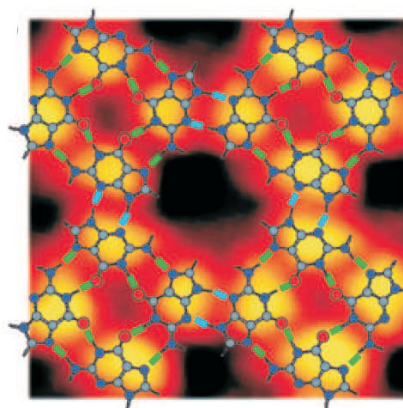


**Figure 1.26.** Cooperative hydrogen bonds (shown in green) stabilise quartets of guanine on Au(111); these quartets hydrogen bond (shown in blue) to form a network over the surface. Adapted from [141].

In many self-assembling structures, the components are held together by arrays of several hydrogen bonds. One early example is the formation of a 'rosette-like' insoluble complex between melamine and cyanuric acid discovered by Whitesides and co-workers<sup>[142]</sup>. Lehn *et al.* adapted this hydrogen-bonding motif by blocking one face of each of the subunits with alkyl chains<sup>[143]</sup>. Steric interactions cause these compounds to form a linear molecular ribbon, which is a non-covalently linked polymer. This work has recently been extended by Perdigao *et al.*, who studied two dimensional melamine-cyanuric networks on the silver terminated silicon surface Ag:Si(111)<sup>[144]</sup>.

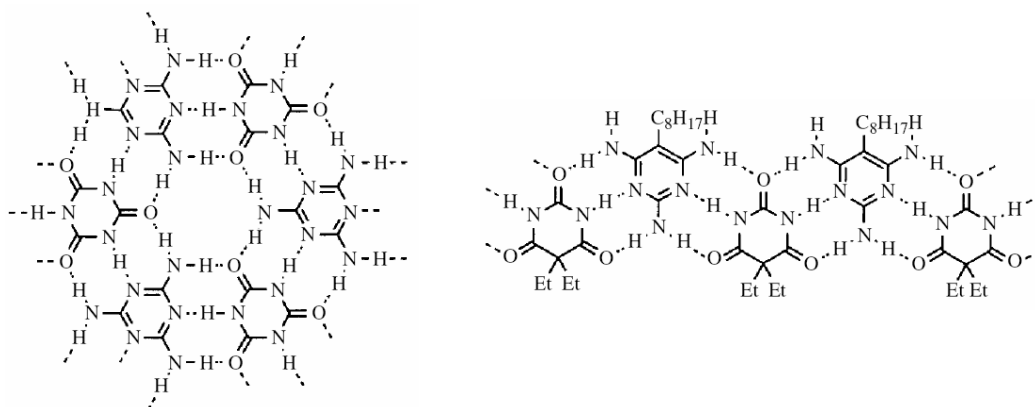


**Figure 1.27.** Melamine and cyanuric acid form an insoluble 'rosette-like' complex (left)<sup>[142]</sup>, whereas sterically hindered analogues form a molecular ribbon (right)<sup>[143]</sup>.

Theobald *et al.* studied the perylene derivative perylene-3,4,9,10-tetracarboxylic-3,4,9,10-diimide (PTCDI) and melamine on Ag:Si(111) and found them to form a supramolecular hexagonal hydrogen bonded network (Figure 1.28)<sup>[115]</sup>. At the vertex of each hexagonal pore a triangular melamine molecule is bonded to three PTCDI molecules by means of a triple hydrogen bond consisting of two O...H-N bonds and a central N...H-N bond. This triple hydrogen bonding configuration provides the network stability. The network was then used as a template in which clusters of guest molecules were housed. Heptameric clusters of C<sub>60</sub> molecules (Figure 1.28) and different sized clusters of C<sub>84</sub> were observed to rest inside the network pores, and these clusters could then be manipulated using the STM tip and were placed in different pores in the network<sup>[115, 145]</sup>.

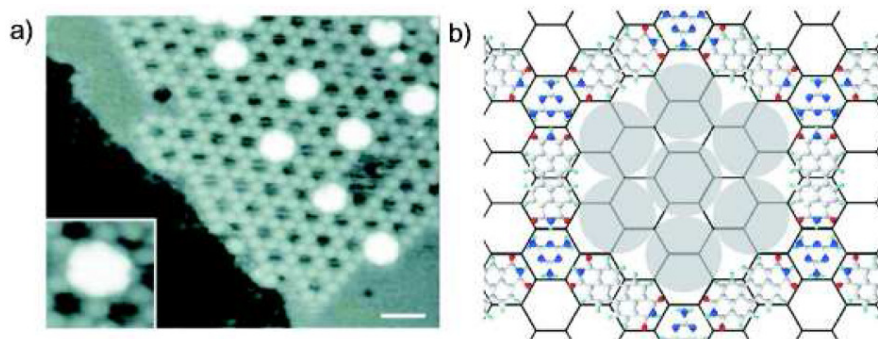


**Figure 1.28.** a) C<sub>60</sub> heptamers captured in a PTCDI-melamine supramolecular network. Scale bar indicates 5nm; b) schematic of the supramolecular bonding and placement of the C<sub>60</sub> heptamers in the network pores. Adapted from [115].

Aside from hydrogen bonding, other supramolecular forces like adsorbate-substrate interactions, surface defect densities, steric factors, temperature, adsorbate abundance, and many other factors may lead to formation of well ordered structures.

For example, two planar molecular species can form close packed ordered structures on a surface due to the steric repulsion. Perylene-3,4,9,10-tetracarboxylic-3,4,9,10-dianhydride (PTCDA) and copper phthalocyanine (Cu-Pc) on Cu(111) were investigated [146]. These two molecules interacted on the surface to form domains of molecules comprised of 3-molecule chevrons; one Cu-Pc was bound to two PTCDA molecules and this unit was repeated to build up an ordered close packed phase. Another phase was observed consisting of rows of Cu-Pc molecules alternating with zig-zag rows of PTCDA, forming a second close packed structure (Figure 1.29).

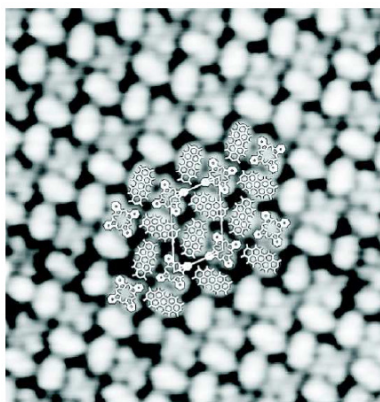


**Figure 1.29.** Cu-Pc and PTCDA molecules on Cu(111) forming an intermixed phase (15 x 15 nm<sup>2</sup>). Adapted from [146].

The phases observed involving two molecular species could rely on the relative concentrations of each species. de Wild *et al* investigated the phases formed by depositing chloro[subphthalocyaninato]boron(III) (SubPc) and  $C_{60}$  on Ag(111) <sup>[120]</sup>. The intermixed phases formed were found to be coverage dependent, and by changing the ratio of SubPc: $C_{60}$  on the surface several different motifs were observed (Figure 1.30) including 1D  $C_{60}$  chains and star motifs.

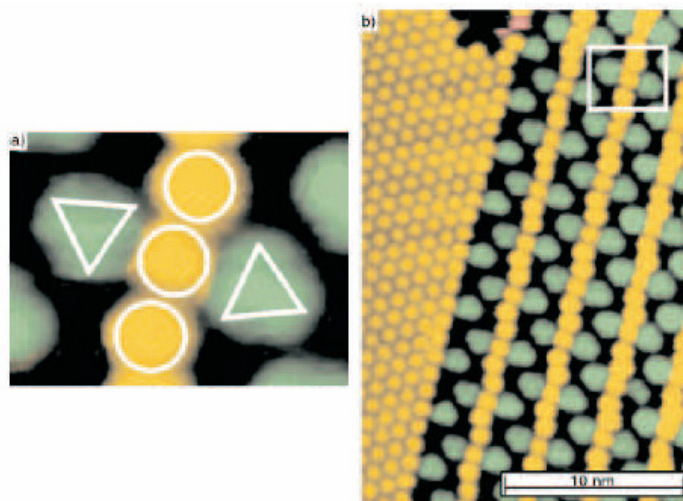


**Figure 1.30.** SubPc and  $C_{60}$  form coverage dependent intermixed phases on Ag(111). This image shows how two triangular SubPc molecules bond to a  $C_{60}$  molecule to form staggered chains, next to a region of close packed  $C_{60}$ . Adapted from [120].

Further, in a study by Langner *et al.*, two bipyridines (ligand **1a**, 1,4-bipyridyl-benzene; ligand **1b**, 4,4'-bipyridyl-biphenyl) and three *bis*-carboxylic acids (ligand **2a**, 1,4-benzoic-dicarboxylic acid; ligand **2b**, 1,4'-biphenyl-dicarboxylic acid; ligand **2c**, 4,1',4',1'-terphenyl-1,4'-dicarboxylic acid) were used during the coordination of iron atoms and highly ordered supramolecular arrays produced from redundant ligand mixtures by molecular self-recognition and -selection, enabled by efficient error correction and cooperativity (Figure 1.31) <sup>[147]</sup>.

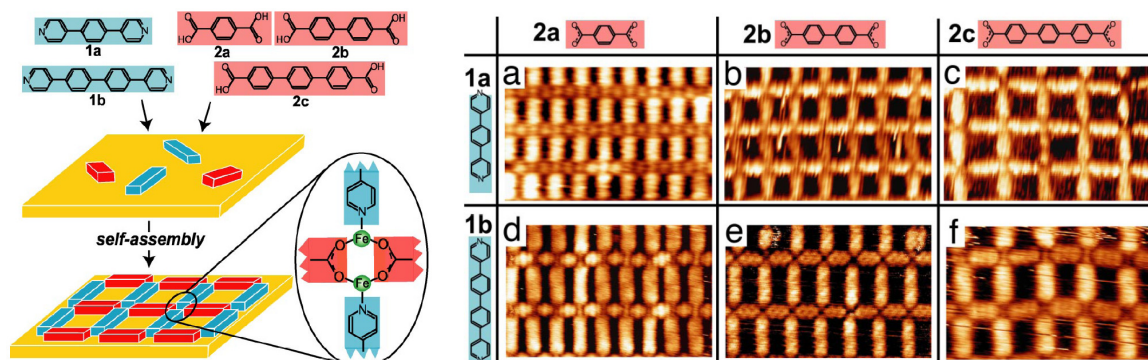


**Figure 1.31.** Complementary molecular ligands deposited with Fe atoms on Cu(100) self-assemble into regular rectangular arrays (left). Steering the size and aspect ratio of rectangular molecular-scale compartments via the backbone length of the ligands in self-assembled iron coordination networks (right). STM images show six possible binary combinations  $[(\text{Fe}_2)(1)_{2/2}(2)_{2/2}]_n$  of bipyridine (ligands 1a and 1b) and bis-carboxylic acid (ligands 2a, 2b, and 2c) ligands. All images are  $9.4 \times 6.0 \text{ nm}$  <sup>[147]</sup>.

No extended molecular networks on surfaces stabilized by interactions that are covalent have been realized yet. In contrast to supramolecular structures, these chemical bonds could facilitate efficient charge transport <sup>[148]</sup> and high stability <sup>[149]</sup>. Such large networks are difficult to make by traditional repetitive chemical synthesis. It has been shown that the STM can be used to create covalent bonds between single molecules on a surface <sup>[150, 151]</sup>. The covalent connection is typically achieved by either activating the precursor components by applying an electrical bias pulse such that transient intermediates are formed which react with one another, or by photochemical treatment after the components have been brought, either manually or by self-assembly, into tight enough contact. However, this method is not suitable for applications where a large number of molecules need to be connected in a desired architecture.

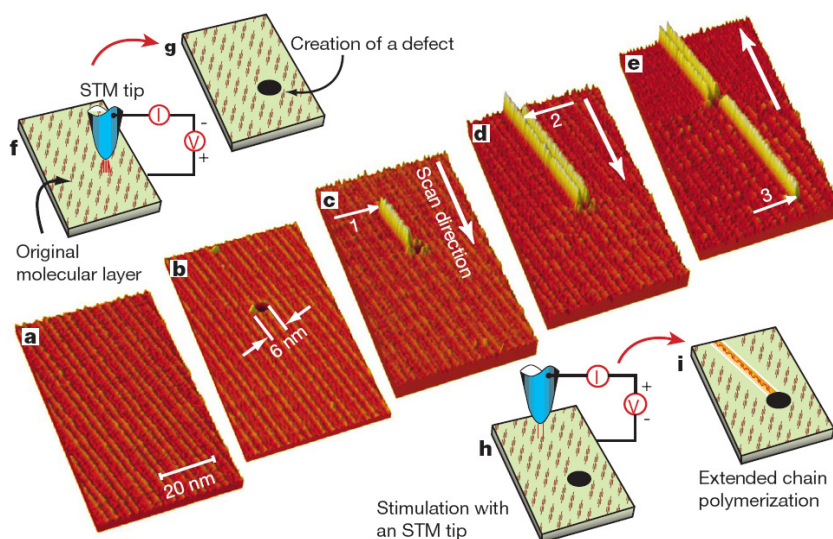


**Figure 1.32.** STM images and diagrams showing the process of controlling the initiation and termination of linear chain polymerization with an STM tip <sup>[152]</sup>.

The first such approach in this area was reported by Takami et al., who irradiated monolayers of 1,15,17,31-dotriacontatetrayne under UHV conditions with UV light and investigated the product by STM (Figure 1.33) <sup>[153]</sup>. Although the image showed periodic features with reasonable dimensions, it is still questionable how many of the diacetylene units and—perhaps even more so—how many of the terminal acetylene units have actually reacted to give the proposed periodic fisherman’s net with a defined mesh size.

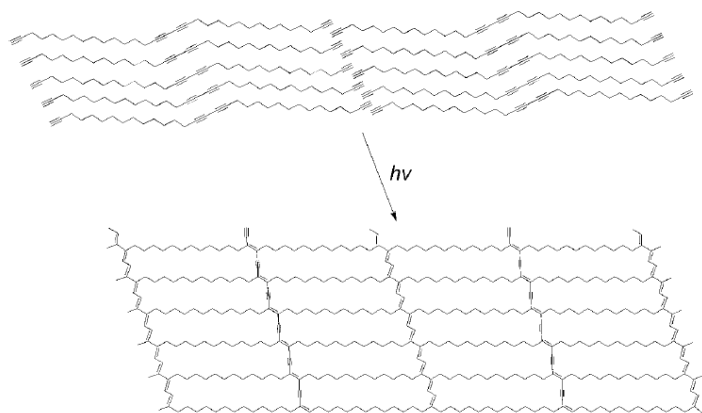


**Figure 1.33.** Proposed structure of the product arising from the UV induced formation of “clothlike” macromolecules. Adapted from [153].

A related topochemical polymerization was also reported by De Schryver and co-workers in which a terephthalic acid (TTA) transferred onto HOPG by the horizontal lifting method<sup>[154]</sup>. The terephthalic acid and diacetylene (DIA) units formed alternating parallel linear arrays in 2D lamellae, in which the latter units were aligned at a distance and an angle allowing for topochemical polymerization which can be induced by UV irradiation.

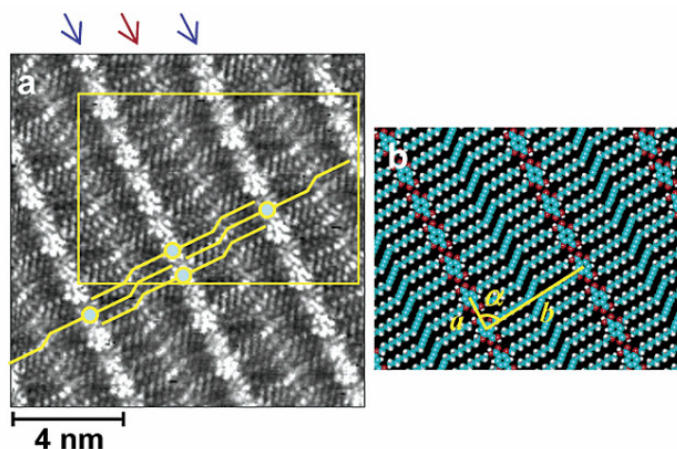


**Figure 1.34.** a) STM image of the TTA-DIA monolayer structure on graphite deposited by the horizontal lifting method. Blue arrows point to the TTA groups and the red arrow indicates the diacetylene moieties in the side chain. b) Molecular model of the area outlined in a) and the unit cell parameters. Adapted from [154].

The most recent case stems from the research group of Grill and Hecht. Porphyrin derivative was activated thermally before or while being deposited under UHV on a Au(111) surface so that the carbon–bromine bond was homolytically cleaved<sup>[155]</sup>. In the absence of any reagent with which the highly active centers of these intermediates could react, and by exploiting their high diffusivity on the surface, some single molecule products could be characterized and proven unequivocally by STM.

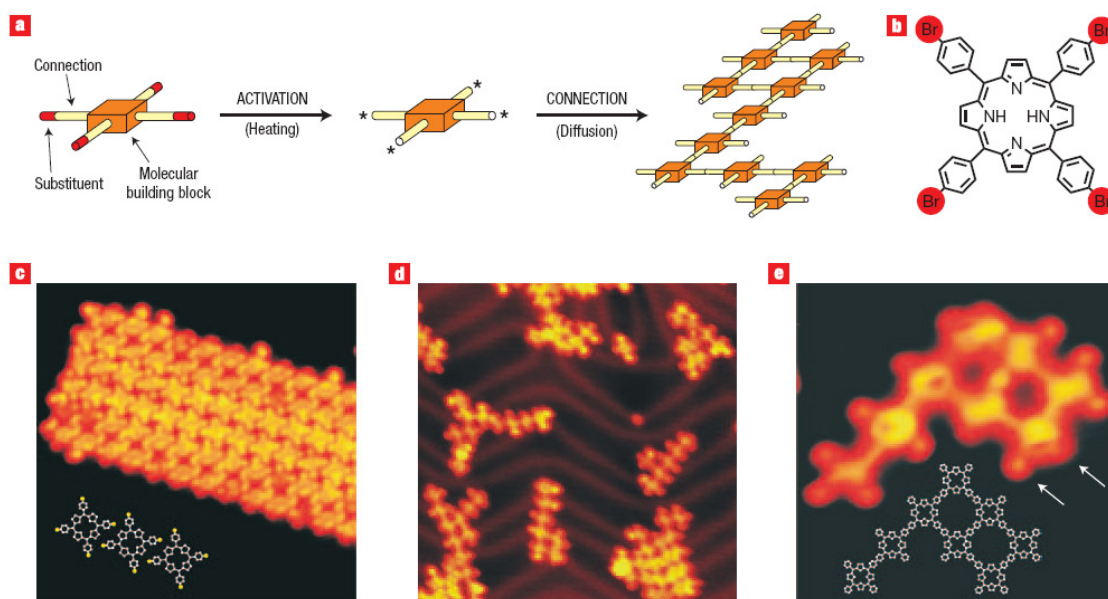


**Figure 1.35.** Nano-architectures of covalently bound Br<sub>4</sub>TPP molecular networks <sup>[155]</sup>.

The covalent nature of the products was proven by dragging experiments. Related approaches were recently published by Amabilino, Raval, and co-workers <sup>[156]</sup> as well as Zwaneveld and coworkers <sup>[157]</sup>.



## 2. AIM OF THE THESIS

Metal nanoparticles, and in particular monodispersed gold clusters, have attracted substantial attention in recent years owing to their small size and quantum properties leading to a wide range of potential applications as molecular devices and catalysts compared to their macromolecular counterparts. To make use of gold nanoparticles for fundamental or applied research, access to well-defined nanoparticles samples whose properties can be tuned through chemical modification is desirable.

The aim of this thesis with respect to gold nanoparticles is two fold. First, multidentate thioether based ligands were designed based on structural considerations, and synthesized. Then, the interactions of these novel well-defined ligands with  $\text{Au}_{55}$  nanoparticles were investigated. Once the successful ligand exchange between the triphenylphosphanes and our concept ligands was achieved, a composite dimer and a composite dimer with tunable linker may become accessible leading to a one-dimensional arrangement of the gold nanoparticles.

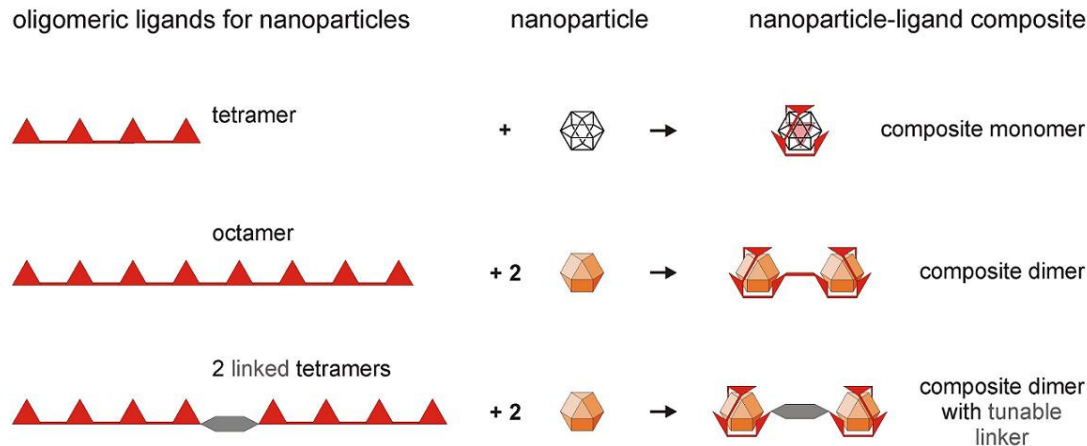


**Figure 2.1.** Ligand enwrapping gold nanoparticles

Alternatively, the potential of multidentate macrocyclic ligands as stabilizing and size steering additives during the direct synthesis of new gold clusters with the Brust-Schiffrin method shall be investigated. Through careful selection of the passivating ligands and/or reaction conditions, the power of the concept to produce new gold nanoparticles tailored to possess desired properties shall be investigated. Since the physical and chemical properties

of gold nanoparticles are known to be dramatically affected by their size, shape and spatial arrangement, these were the parameters we hoped to be able to steer by the ligands.

The study and the construction of nanomaterials became available with the development of the STM. In a bottom-up approach, nanostructures are constructed from molecular components which assemble themselves chemically by the principles of molecular recognition. Supramolecular chemistry based self-assembling techniques appear to be most promising in the design and development of a variety of nanomaterial structures. However, the formation of such thermodynamically controlled aggregated structures is reversible in most cases and the interaction between the molecular components is usually weak. A very appealing concept to obtain structures with higher stability is to benefit from the supramolecular order of pre-organized structures and to interlink the individual molecular building blocks to macromolecules.

In the second part of this study, we investigate the potential of *tert*-butoxycarbonyl (BOC) protected arylamine structures as supramolecularly organized building blocks which might be subsequently interlinked via reactive intermediates accessed by deprotection chemistry. This concept may pave the way towards molecule-based covalently linked 2D functional structures that are so far only achievable at larger scale by lithography techniques.

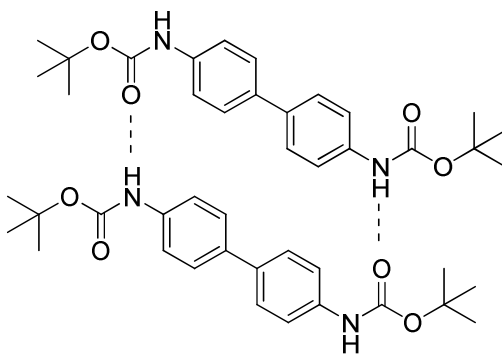


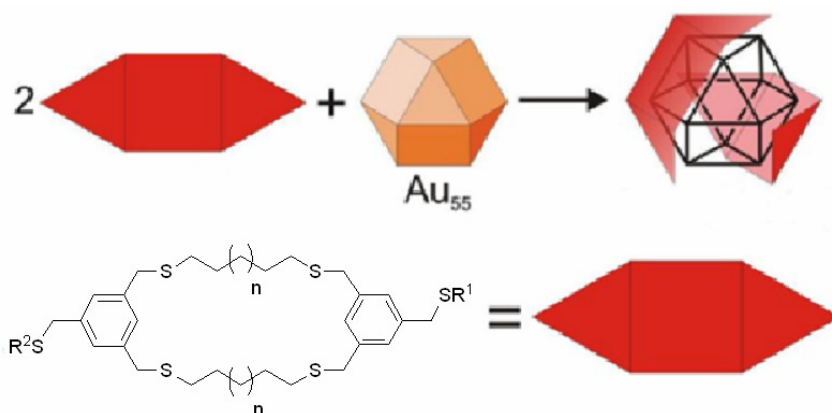
**Figure 2.2.** Expected H-bonding of 4,4'-diaminobiphenyl molecules as example of the supramolecular self assembly of BOC protected arylamines.

### 3. RESULTS AND DISCUSSION

#### 3.1. Synthesis of New Ligands for Enwrapping Au<sub>55</sub> Nanoparticles

The successful exchange of phosphine ligands of Au<sub>55</sub> clusters, also known as Schmid's clusters, using different water soluble trithioether based ligands derived from 1,3,5-tris(mercaptomethyl)benzene scaffolds while nanoparticles size and monodispersity remain intact were reported by von Kiedrowski [92]. The elemental analysis data suggested that the Au<sub>55</sub> cluster were covered with four ligands derived from 1,3,5-tris(mercaptomethyl)benzene scaffolds. More importantly, ligands derived from 1,3,5-tris(mercaptomethyl)benzene scaffolds improved the stability of Schmid's clusters in solution.

Our goal was to design interconnected hexadentate benzotrithioether ligand derived from 1,3,5-trimethylbenzene scaffolds to investigate their potential as multidentate ligands for stabilizing Au<sub>55</sub> clusters. As displayed in figure 3.1.1, the hexadentate ligand was expected to cover half of the surface of Au<sub>55</sub> clusters. Thus our first target structures were the macrocycles **A-C** (Figure 3.1.1).



$n=0$ ,  $R^1 = R^2 = C_6H_{13} \rightarrow$  ligand **A**

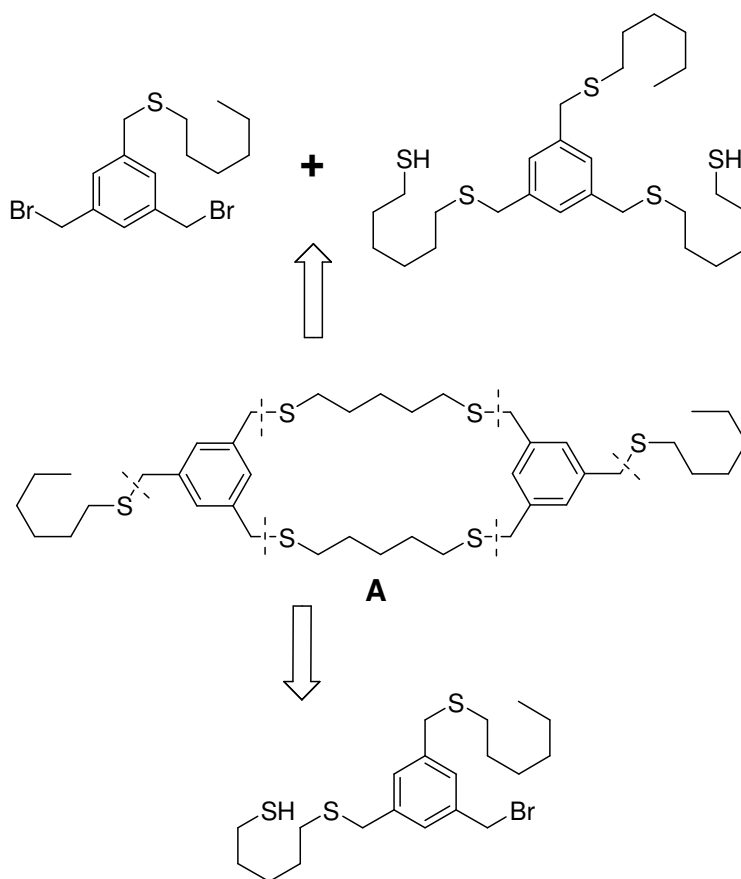
$n=0$ ,  $R^1 = C_6H_{13}$ ,  $R^2 = (CH_2)_5O(CH_2)_2OMe \rightarrow$  ligand **B**

$n=1$ ,  $R^1 = C_6H_{13}$ ,  $R^2 = (CH_2)_5O(CH_2)_2OMe \rightarrow$  ligand **C**

**Figure 3.1.1.** Schematic representation of the expected ligand exchange and enwrapping of Au<sub>55</sub> nanoparticles with dimeric macrocycle ligands.

A symmetrical ligand was preferred in order to achieve the final product in fewer steps. The presence of a methylene spacer between the benzene rings and the sulfur atoms induced a bent geometry allowing all three sulfur atoms to point towards the corners of the 111 triangle of Au<sub>55</sub> clusters. In contrast to this, direct connection of sulfur atoms to the benzene ring would result in a flat core that would be less ideal for covering (111) triangles of Au<sub>55</sub> clusters surfaces. Furthermore, these mercaptomethylbenzene groups could be obtained by nucleophilic substitution of benzylhalides allowing a straight forward synthetic approach to the desired structure. This strategy was further encouraged by the excellent properties of sulfur as nucleophile. The length of the spacers which interlink both 1,3,5-tris(mercaptomethyl)benzene cores were estimated around 5-to-6 carbon atoms, assuming an arrangement as described by previous molecular modeling data<sup>[158]</sup>. Furthermore, alkyl chains were added to the ligand to improve its solubility and processability in organic solvents (Figure 3.1.1).

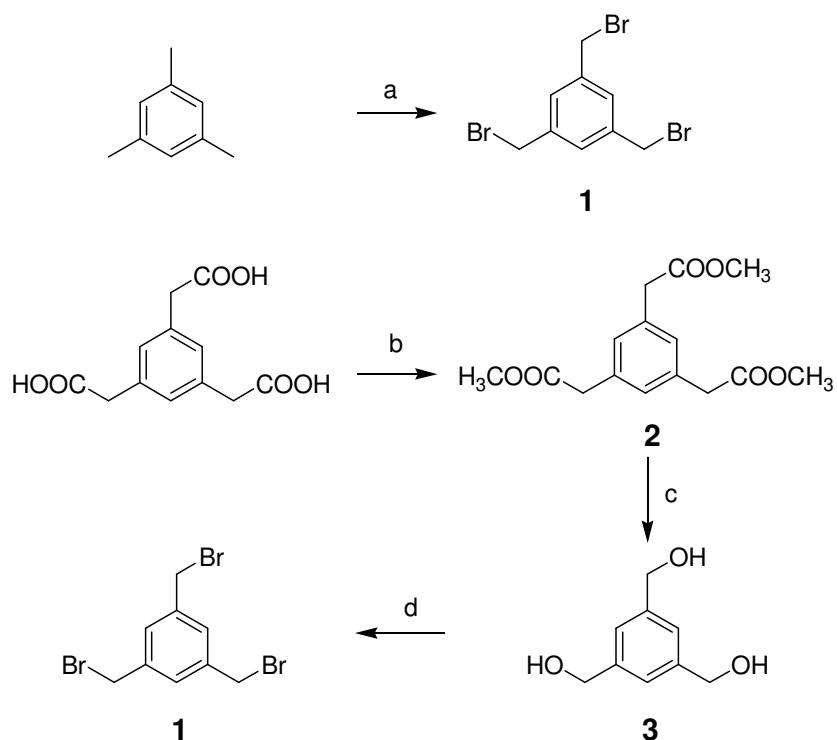
The macrocyclic ligand must be synthesized by a ring closing reaction. As displayed in scheme 3.1.1, either the dimerisation of a suitably functionalized precursor or twofold reaction of two different bifunctional starting materials could be considered. However, the presence of leaving group and nucleophile interlinked by a flexible chain in the case of dimerisation of a suitably functionalized precursor would provide a competing intramolecular reaction strongly disfavoring the viability of this approach. In our first strategy, we thus suggested the reaction between the dibromine and the dithiol precursors which were expected to yield in the desired hexadentate ligand **A**. To favor the ligand formation over polymerization, high dilution conditions were considered.



**Scheme 3.1.1.** Retrosynthetic analysis of symmetric ligand **A**.

The synthesis of the both required building blocks was achieved in a straightforward manner starting from 1,3,5-tris(bromomethyl)benzene, **1**. **1** was synthesized either from mesitylene via bromination or from 1,3,5-benzenetricarboxylic acid via esterification, reduction to corresponding triol and subsequent substitution of benzylic alcohols with bromines. Synthesis of **1** via bromination of mesitylene required low cost commercially available starting materials. However, the achieved yields were low due to partial over bromination of benzylic positions. Moreover, the low polarity of both **1** and the side products made its purification by column chromatography ineffective. The successive recrystallizations were time consuming, challenging and reduced the total yield to 22%. Another drawback of this synthetic approach to **1** was the toxicity of carbon tetrachloride, as solvent during the bromination. An alternative strategy based on esterification, reduction to corresponding triol and subsequent substitution with bromine required more costly starting materials and more synthetic steps, but led to improved over all yields and superior quality (purity) of the target compound **1**. 1,3,5-benzenetricarboxylic acid was refluxed overnight in methanol (MeOH)

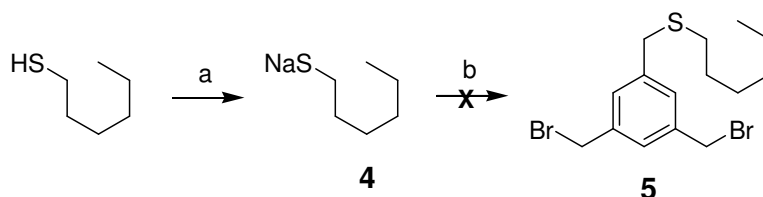
containing 2.5% concentrated sulfuric acid. 1,3,5-benzenetricarboxylate (**2**) was obtained quantitatively (quant.) as white needle-like crystalline solid after aqueous workup and extraction with *tert*-butyl methyl ether (TBME). **2** was then reduced to the corresponding triol **3** with LiAlH<sub>4</sub> by refluxing overnight in tetrahydrofuran (THF). After quenching the excess of reducing agent with few drops of water, the solvent was evaporated. The crude alcohol (**3**) was then substituted with bromines by refluxing overnight in 48% HBr in a water-toluene biphasic mixture. 1,3,5-tris(bromomethyl)benzene (**1**) was obtained as white needle like crystalline solid in 89% yield in three steps after purification with a short plug of silica gel.



**Scheme 3.1.2.** Synthesis of 1,3,5-tris(bromomethyl)benzene (**1**) (a) NBS, AIBN, dry CCl<sub>4</sub>, ↑↓, 44%; (b) MeOH, H<sub>2</sub>SO<sub>4</sub>, ↑↓ (c) LiAlH<sub>4</sub>, THF, ↑↓ (d) 48% HBr in water-toluene, ↑↓ 89% (3 steps).

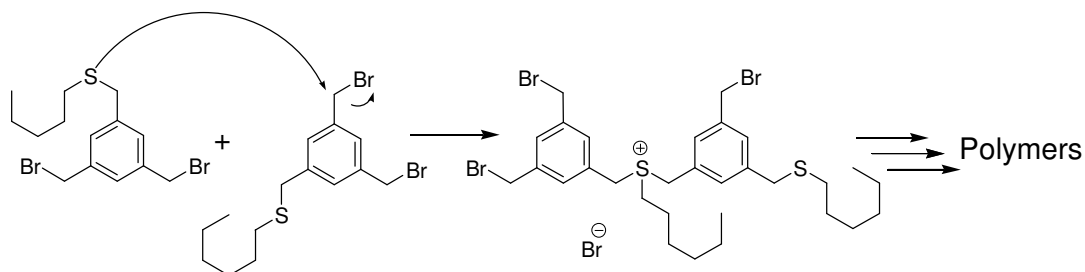
First attempts to synthesis the monohexylsulfanyl derivative were based on a nucleophilic substitution of sodium *n*-hexylthiolate (**4**) on **1**. Sodium *n*-hexylthiolate (**4**) was synthesized easily reacting dissolved sodium metal in ethanol (EtOH) with *n*-thiohexane for 2 hours at room temperature (RT). The formed white residue was washed extensively with TBME yielding 97% of **4** as white powder. Then, one equivalent of **4** was added to **1** in dry THF under Argon. Although, polar solvents like acetonitrile (MeCN) and *N,N*-dimethylformamide (DMF) were common solvents for substitution of benzylic bromines with thiols, THF was

preferred not only because of the low solubility of **1** in acetonitrile but also the toxicity and difficult removal of DMF as a solvent. Monitoring the course of reaction by thin-layer chromatography (TLC) displayed the formation of 3 new compounds within 10 minutes, probably representing the mono-, di- and trithiolated compounds respectively. It was also noticed that some amounts of the reaction mixture applied to TLC plate remained on the baseline. However, after an aqueous workup and purification by column chromatography isolation of neither the desired compound nor of the side products could be achieved.



**Scheme 3.1.3.** Strategy to synthesize (3,5-bis(bromomethyl)benzyl)(hexyl)sulfane, **5** (a) Na, EtOH, RT, 97%; (b) **1**, THF.

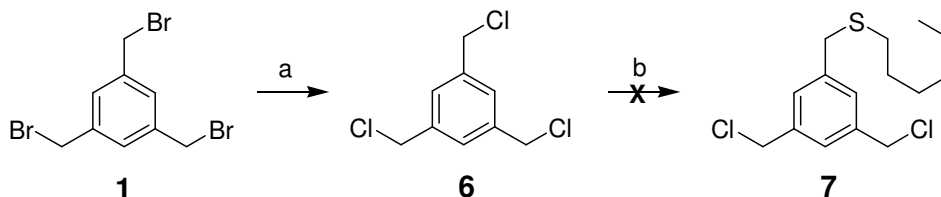
The failure of isolation of these compounds could be because of decomposition or polymerization of the mixture during the purification by column chromatography. Probably the nucleophilic character of the alkylbenzylthiol still allowed attacking benzylbromides of the neighboring molecule. Thus, as long as sterically not very demanding alkyl chains were used there seems to be an intrinsic problem with these bifunctional structures. Hence the benzylic bromines were probably reacting with the benzylic thioethers of the other molecules during purification leading the formation of sulfonium salts. Kugelrohr distillation, as alternative purification methods, also failed. Probably the increased temperature even increased the reaction between benzylic bromines and benzylic thioethers and led to polymerization *de novo*.



**Scheme 3.1.4.** Suggested mechanism for polymerization of bis(bromomethyl)benzylsulfane, **5**.

Basicity of the leaving group is one of the factors affecting  $S_N2$  reactions. In general, the weaker the basicity of a group, the greater its leaving ability. Weak bases do not share their electrons well since their electrons are farther away from the nucleus, making them easier for their bonds to be broken. Therefore,  $S_N2$  reaction rates of compounds increases going down in the same periodic group. The relative  $S_N2$  reaction rate of bromide (around 10000) is 50 times faster than chloride (around 200, where fluoride is 1). Therefore replacing benzylic bromides with chlorides could increase the stability of the desired compound and might prevent its polymerization during its isolation.

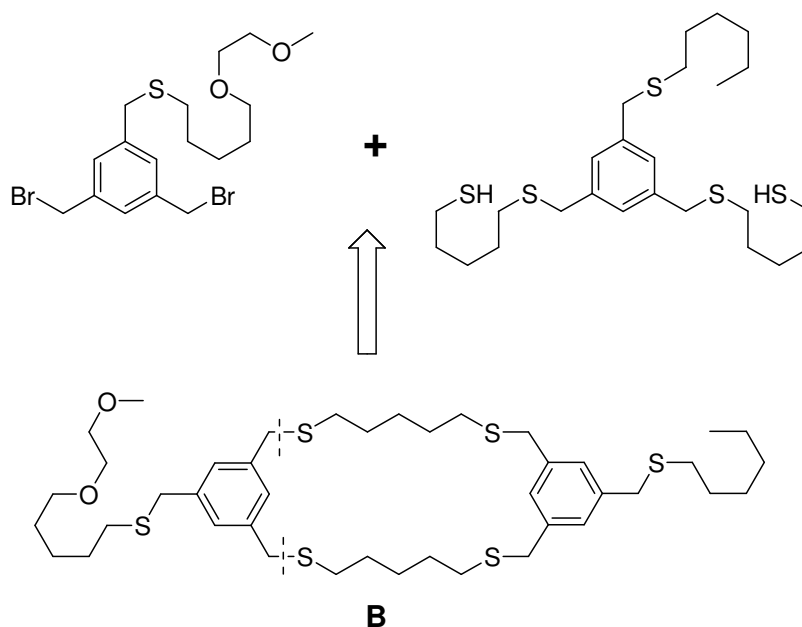
The exchange of bromine atoms to chlorine atoms is an equilibrium reaction but this could be driven to completion by using a large excess of chloride anions as nucleophiles. Thus, 5 equivalents of lithium chloride was added to **1** in dry DMF under Argon and the desired compound 1,3,5-tris(chloromethyl)benzene (**6**) was obtained quantitatively after aqueous workup and extraction with TBME. Using again the nucleophilic substitution of **4** on **6** in THF led to formation of three new compounds, probably representing the mono-, di- and trithiolated compounds respectively, determined by TLC. However, all attempts to isolate 3,5-bis(chloromethyl)benzyl sulfane (**7**) failed *de novo*.



**Scheme 3.1.5.** Strategy to synthesize (3,5-bis(chloromethyl)benzyl)(hexyl)sulfane, **7** (a) LiCl, DMF, RT, 99%; (b) **4**, THF, RT.

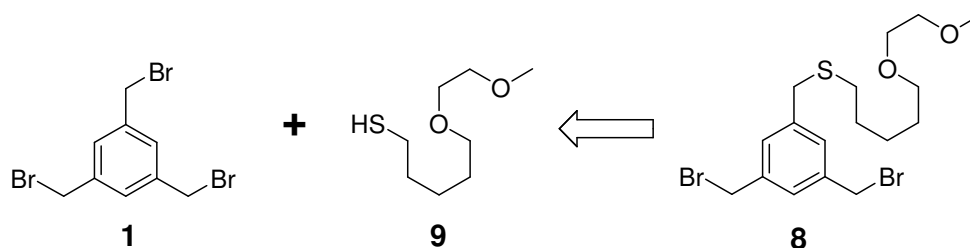
These unexpected problems to synthesize the monohexylsulfanyl building block led to reconsideration of the strategy for the synthesis of asymmetric ligand **B**. Although the synthesis of this asymmetrical ligand requires more steps, the polarity of its chain was expected to be useful for improved the separation features of the desired compound in column chromatography and to enhance its solubility in more polar organic solvents. On the other hand, dithiol building block can be synthesized first by substituting the two leaving groups with a dithiol that carries one of the thiols masked by a protection group and then substituting the remaining leaving group with thiohexane. This strategy was explained in detail below (Scheme 3.1.6).





**Scheme 3.1.6.** Retrosynthetic analysis of asymmetric ligand **B**.

For the the synthesis of the more polar thioalkyl chain required for building block (**8**) a reaction between **1** and the chain-like molecule (**9**) comprising a terminal thiol and a polar ethylene glycol subunit was considered.

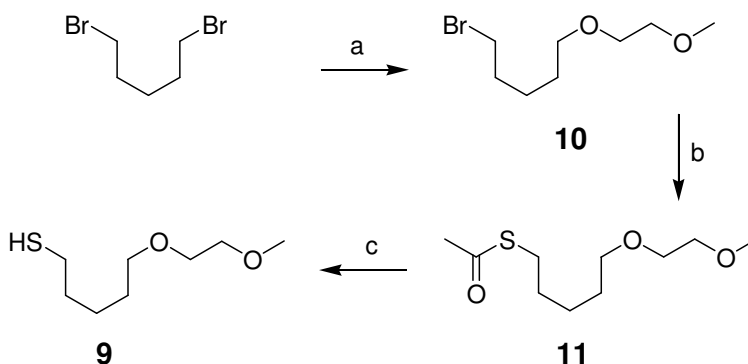


**Scheme 3.1.7.** Retrosynthetic analysis of polar group containing building block.

The synthesis of 5-(2'-methoxyethoxy)pentane-1-thiol (**9**) could be performed starting from commercially available 1,5-dibromopentane. Substitution of one bromine with 2-methoxyethanol and of the other bromine with a masked sulfur atom provided an ideal precursor of the target structure **9**. In order to profit from the increased polarity during the purification by column chromatography, the introduction of the polar 2-methoxyethanol group was considered first. Therefore, 1,5-dibromopentane was treated with equimolar amounts of

2-methoxyethanol and 1.2 equivalents of sodium hydride (NaH) in THF. The course of the reaction was monitored by TLC using a potassium permanganate solution as developing agent. The TLC showed that the formation of products was very slow. Completion was not even observed after overnight stirring at RT. For that reason, the mixture was heated to reflux. After overnight reflux, the consumption of 2-methoxyethanol and appearance of the two new well separated spots, probably representing the mono and di- substituted products, were observed on the TLC plate. After carefully quenching of excess NaH with water, the crude was separated by column chromatography following aqueous workup and extraction with TBME. 1-bromo-5-(2'-methoxyethoxy)pentane (**10**) was isolated in a low yield of %24 as colorless oil. However, the low yield was compensated by scaling up of the synthesis.

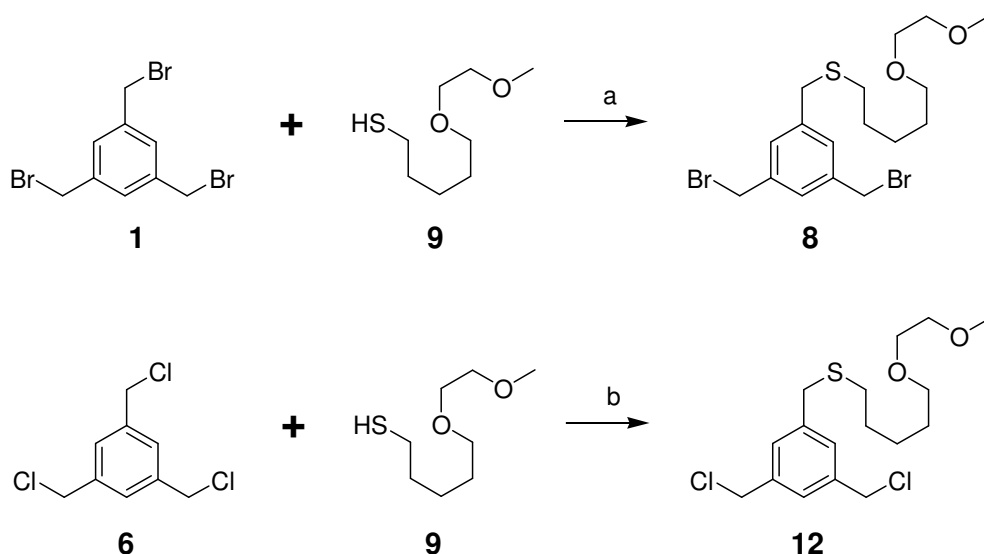
An elegant method for substitution of the remaining halogen of **10** with a sulfur atom was made using a thioacetate salt, followed by removal of the acetyl protection group in the next step. Thus, the introduction of the thioacetate group was performed by reacting equimolar amounts of **10** and potassium thioacetate (KSAc) in DMF at RT. The reaction was allowed to stir overnight. S-5-(2-methoxyethoxy)pentyl-thioacetate (**11**) was obtained quantitatively as white powder by column chromatography. The acetyl protection group was then removed in one hour (h) using one molar (M) NaOH in refluxing MeOH. After an aqueous workup extraction with TBME, **9** was obtained in 89% yield as colorless oil.



**Scheme 3.1.8.** Synthesis of the polar chain (a) 2-Methoxyethanol, NaH, THF,  $\uparrow\downarrow$ , 24%; (b) KSAc, DMF, RT, quant. (c) NaOH, MeOH,  $\uparrow\downarrow$ , 89%.

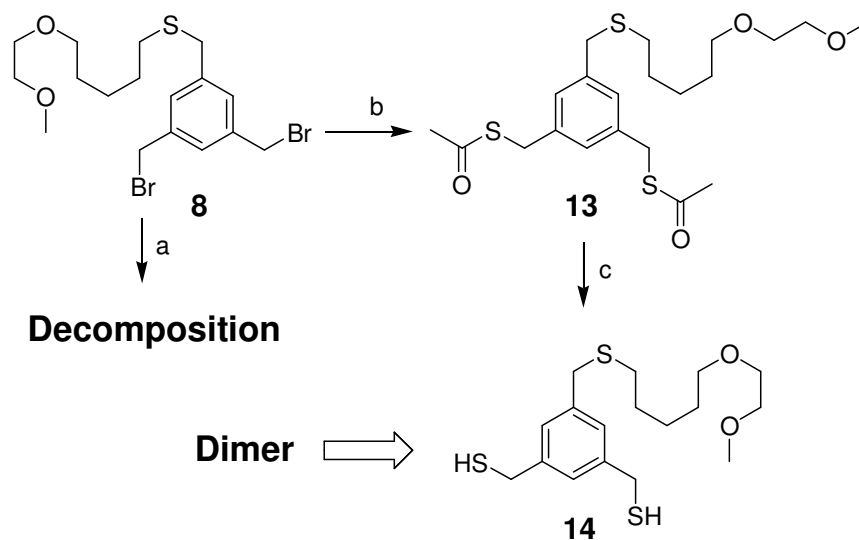
The synthesis of the dibromo building block **8** was achieved by the nucleophilic attack of **9** and **1** in THF at RT. One equivalent of NaH dispersed in 60% mineral oil was used as a base to deprotonate the thiol **9**. The consumption of **9** and formation of new products was observed by TLC in 30 minutes. The excess sodium hydride was quenched with a few drops of water and the crude was obtained after extraction with TBME. Then, the desired product

was isolated in 46% yield as colorless oil after purification by column chromatography. Di- and tris- substituted derivatives of **8** were also obtained as side products in lower yields. On the other hand, the obtained compound **8** was found to decompose even under inert atmosphere and cold storage. Most likely this decomposition reaction, which is due to the high reactivity of benzylic bromines towards thioethers, again took place (Scheme 3.1.4). To improve the stability of the dihalide building block, 1,3,5-tris(chloromethyl)benzene comprising considerably weaker leaving groups than its trisbromo derivative was used. Under similar conditions that were used to synthesize **8**, the desired dichloro building block (3,5-bis(chloromethyl)benzyl)(5-(2-methoxyethoxy)pentyl)sulfane (**12**) was obtained as colorless oil with a little higher yield, 47%, than before. More importantly, compound **12** displayed considerably improved stability as decomposition under inert atmosphere and cold storage was not detected.



**Scheme 3.1.9.** Synthesis of first building block; NaH, THF, RT, 46% for a and 47% for b.

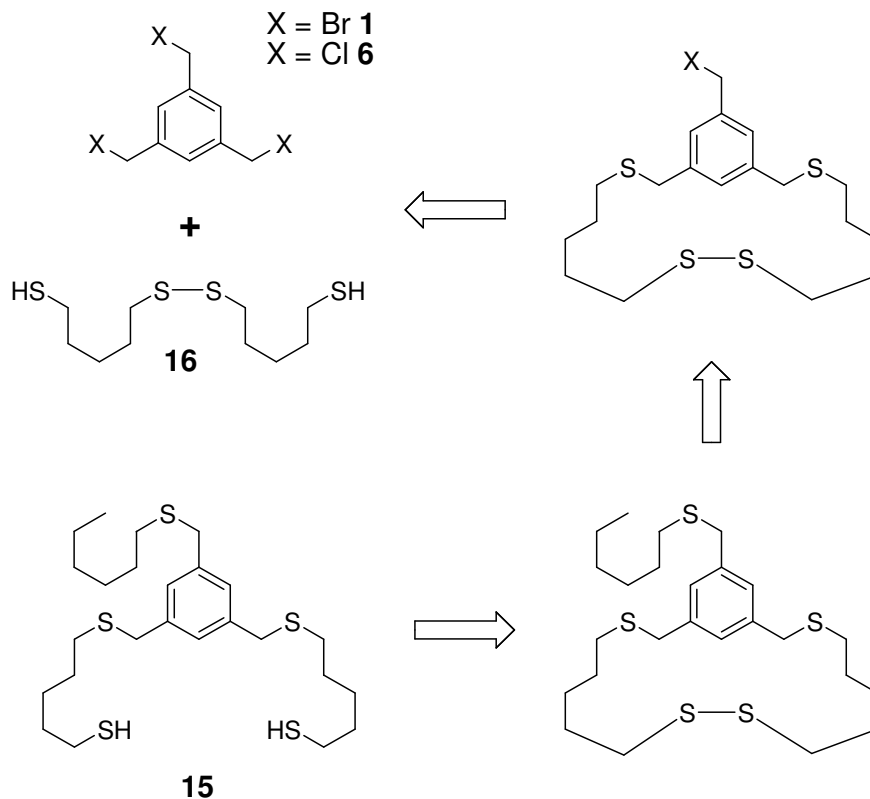
Another strategy to prevent the decomposition of **8** was to substitute bromines with sulfur atoms and to extend the synthesis towards the synthesis of dithiol building blocks. This way, it might be possible to couple the dithiol building block with another dihalide building block for the synthesis of target ligand **B**. Under similar conditions that were used for the synthesis of **9**, the dibromide **8** was reacted with two equivalents of potassium thioacetate. The dithiol building block **14** was obtained as colorless oil in two steps with 90% isolated yield after column chromatography.



**Scheme 3.1.10.** Alternative synthesis of first building block (a) under inert atmosphere and cold storage (b) KSAc, DMF, RT, 99%; (c) NaOH, MeOH,  $\uparrow\downarrow$ , 90%.

The second building block should contain thioalkyl chain for improved solubility and dithiol functionality in order to perform a ring closing reaction with the dibromo building block **8**. Due to the difference in the nature of thiol containing chains, they have to be substituted into the tris(halomethyl)benzene core separately, either inserting the thioalkyl chain first, then dithiol functionality or introducing the thioalkyl chain following the substitution of the thiol functionalities. Nevertheless, inserting the thioalkyl chain at the first step may result in the decomposition of the product as observed previously during the synthesis of **5**. For this reason, the introduction of the thiol functionalities was considered first. However, inserting the dithiol functionality has one major drawback; free thiols may as well lead to polymerization. Therefore, free thiols should be protected before reacting with tris(halomethyl)benzene core. Unfortunately, there are not many choices as a protection groups for thiols under basic conditions. Moreover, protection groups need to be cleaved for performing a reaction with first building block **8** in order to achieve ring closing synthesis. Furthermore, it was found that available protection groups may not be efficient to prevent decomposition of the product. Therefore, a reversible thiol-disulfide formation was considered. The thiol functionalities could be synthesized as dithioalkyldisulfide, substituted into the benzylic core. The remaining leaving group could be substituted with a thioalkyl chain. In the final step, the disulfide bond could be broken to form the free thiols. This strategy had a clear superiority than the use of a protection group as it eliminates inefficient

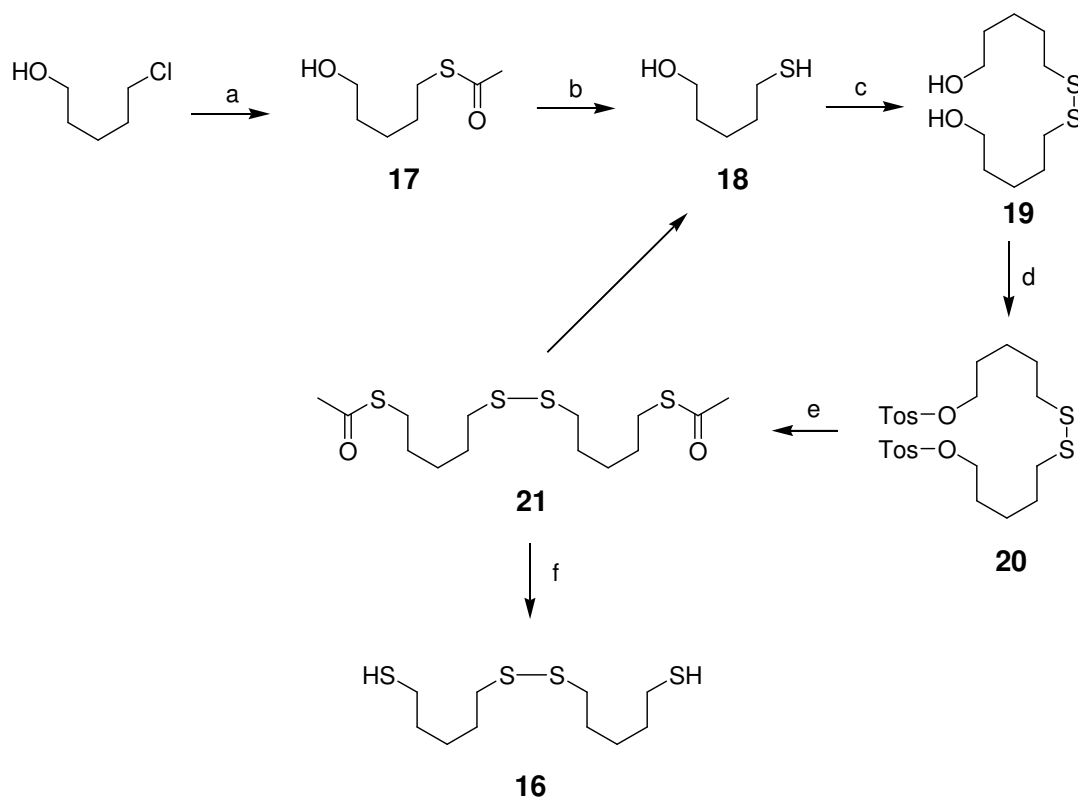
and time consuming protection-deprotection steps while reducing the danger of decomposition of the desired product **15**.



**Scheme 3.1.11.** Retrosynthetic analysis of second building block.

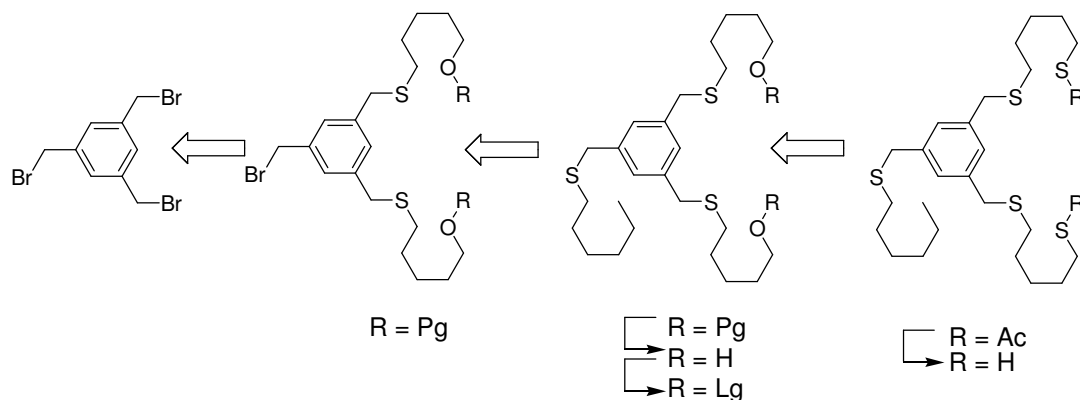
The dithiol chain, 5,5'-disulfanediyldipentane-1-thiol (**16**) was synthesized from commercially available 5-chloropentane-1-ol. First, 5-chloropentane-1-ol was reacted with equimolar amounts of potassium thioacetate in DMF for the introduction of the thioacetate group. Following a similar procedure for the synthesis of **11**, S-5-hydroxypentyl thioacetate (**17**) was obtained quantitatively as white powder. The acetyl protection group was removed under basic conditions similar to the procedure for the synthesis of **9**. The pure 5-mercaptopentane-1-ol (**18**) was obtained in 79% yield as colorless oil. Then **18** was oxidized to the disulfide 5,5'-disulfanediyldipentane-1-ol (**19**) by dropwise addition of 0.5 M methanolic iodine solution. The completion of reaction was confirmed by the persistent brown color of the solution. The excess iodine was quenched by washing with 10%  $\text{Na}_2\text{S}_2\text{O}_3$  solution. **19** was isolated in 89% yield as colorless oil after column chromatography.

It is known that alcohols do not easily undergo substitution reactions when they are reacted with nucleophiles. Thus, alcohols must first be transformed into a better leaving group in order to undergo substitution with nucleophiles. Tosylates or mesylates salts are commonly used reagents for converting alcohols into better leaving groups. Hence, the alcohol groups of **19** were substituted with better leaving groups, in our case tosyls, in order to insert dithiol functionality. The synthesis of 5,5'-disulfanediybis(pentane-5,1-diyl) bis(4-methylbenzenesulfonate) (**20**) was performed by reacting one equivalent of **19** with five equivalents of *p*-toluenesulfonyl chloride (*p*-TSCl) in pyridine containing dichloromethane (DCM). Triethylamine (TEA) can also be used as a base for sulfonation instead of pyridine due to ease of removal. However, pyridine is a much better base for sulfonation as it forms a complex with tosyl chloride by rendering the attack of the alcohol on the sulfur easier, acting as a nucleophilic catalyst. After overnight stirring at RT, the ditosylate **20** was obtained in 97% yield as white powder by column chromatography. The substitution of tosyl groups with sulfur atoms was performed using potassium thioacetate following similar conditions to the synthesis of **9**. S,S'-5,5'-disulfanediybis(pentane-5,1-diyl) dithioacetate (**21**) was obtained quantitatively as white powder. Although, previous substitution of leaving groups with potassium thioacetate and subsequent removal of acetyl protection groups to free thiol was performed successfully with excellent yields, the yield of deprotection of dithioacetate **21** was very low, only 6%. The analysis of deprotection reaction products showed the formation of **18** as the main product. Apparently, the acetyl deprotection conditions were too harsh and mainly led to cleavage of disulfide bond. The cleavage of disulfide bond may be caused by treatment of **21** at high temperature in presence of strong base. Therefore, various acids and bases were used for the removal of acetyl protection group without heat treatment. However, these acids and bases were either too strong leading 0 to 5% yield of desired compound and favoring the formation of **18** by cleaving the disulfide bond again or not efficient by removing the acetyl protecting group.



**Scheme 3.1.12.** Strategy towards synthesis of second building block, (a) KSAc, DMF, RT, quant.; (b) NaOH, MeOH,  $\uparrow\downarrow$ , 79%; (c) 0.5 M methanolic iodine, MeOH, RT, 89%; (d) *p*-TsCl, pyridine, DCM, RT, 97%; (e) KSAc, DMF, RT, quant.; (f) NaOH, MeOH,  $\uparrow\downarrow$ , 6%.

The low yield of deprotection of diethanethioate **21** and the unexpected problems confronted during the synthesis of monothiosubstituted dibromomethylbenzene **5** compelled us to revise the synthetic strategy in a more efficient and elaborate way. Dithiol containing 1,3,5-tris(mercaptomethyl)benzene building block could be synthesized by disubstitution of 1,3,5-tris(bromomethyl)benzene with polar thioalkyl chains. The resulting dithioalkyl substituted monobromomethylbenzene compound could be further treated with hexanethiol for the formation of 1,3,5-tris(mercaptomethyl)benzene building block. After the removal of protection groups, alcohol groups could be converted to suitable leaving groups. Finally, dithiol containing tris(mercaptomethyl)benzene building block could be synthesized by treating the precursor with potassium thioacetate and removal of acetyl protection groups respectively.



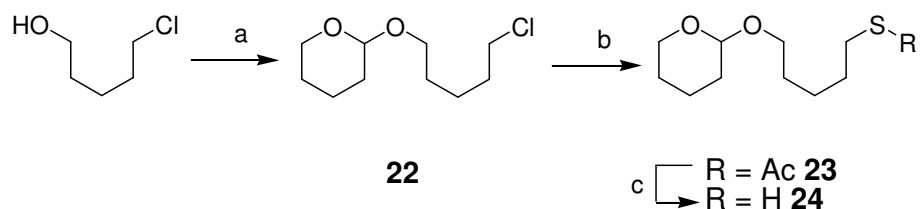
**Scheme 3.1.13.** Retrosynthetic analysis of 1,3,5- tris(mercaptopomethyl)benzene building block.

Dithioalkyl substituted monobromomethylbenzene compound building block could be synthesized by reacting one equivalent of **1** with two equivalents of **18**. However, **18** was not commercially available and it had to be synthesized. Although, the synthesis of **18** was performed starting from commercially available 5-chloropentan-1-ol, the alcoholic end had to be protected before substitution with **1** in order to reduce unwanted side products such as benzoethers. However, the protection of alcoholic end of **18** may also result in the protection of thiolic end since most of the protection groups and reaction conditions for protecting the alcohol and thiol groups are similar.

The alcohol protecting group should be resistant under basic conditions since the nucleophilic substitution conditions and removal of acetyl groups of thioacetate were performed in basic medium. In order to profit from the polarity of alcohol for easier purification, the protection group should not reduce the polarity of the compound. These limitations render the usage of alkyl, benzyl or silyl ethers, and common acid labile alcohol protecting reagents obsolete, since they will reduce the polarity of the molecule. Esters or benzyl esters can not be selected as an efficient protection group either, since they can not only lead to cleavage of the thiobenzyl bond during the deprotection but also be deprotected during the removal of the acetyl protection groups of sulfur. Although methoxymethyl (MOM) ethers are stable under basic conditions and provide polarity for purification, their precursor (MOM-Cl) is harmful and known as human carcinogen. Based on these limitations, methoxyethoxymethyl chloride (MEM-Cl) or 3,4-dihydro-2H-pyran (DHP) can be used. DHP was selected and applied as an alcohol protection group as it requires milder deprotection conditions than the MEM-Cl.



5-chloropentan-1-ol was thus reacted in a nucleophilic substitution reaction with 1.2 equivalents of DHP in DCM using pyridinium *p*-toluenesulfonate (PPTS) as catalyst. After stirring overnight at RT, the 2-(5-chloropentyloxy)-tetrahydro-2H-pyran (**22**) was obtained quantitatively as colorless oil by column chromatography. After the protection of alcohol group with THP, **22** was treated with one equivalent of potassium thioacetate in DMF leading to introduction of the thioacetate group. The reaction was allowed to stir overnight at RT and S-5-(tetrahydro-2H-pyran-2-yloxy)pentyl ethanethioate (**23**) was obtained quantitatively by column chromatography as white powder. The removal of acetyl group was performed under similar basic conditions for deprotection of **11**. 5-(tetrahydro-2H-pyran-2-yloxy)pentane-1-thiol (**24**) was isolated in 88% yield as colorless oil by column chromatography.

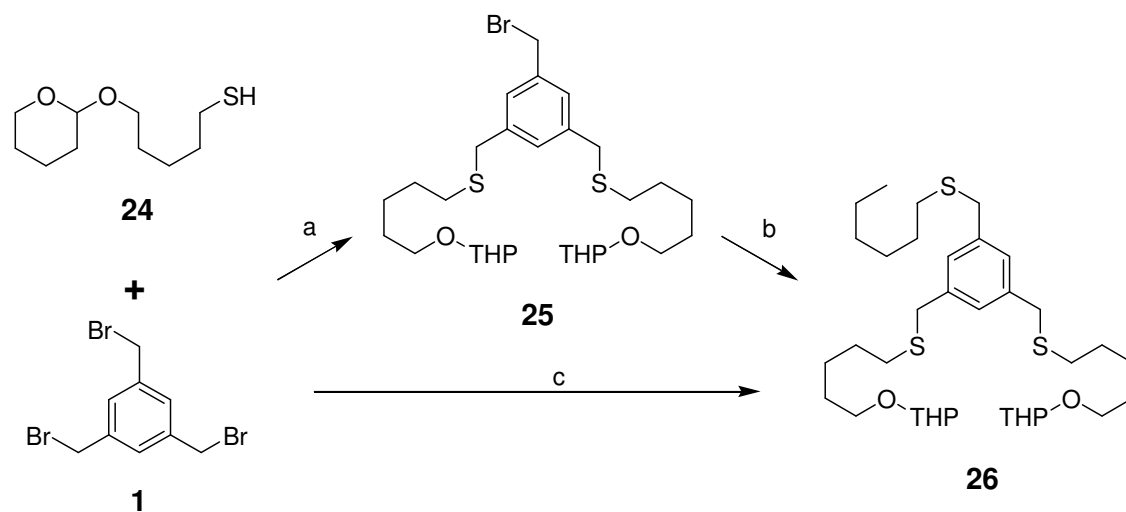


**Scheme 3.1.14.** Synthesis of polar thio building block. (a) PPTS, DCM, RT, 95%; (b) KSAc, DMF, RT, quant.; (c) NaOH, MeOH,  $\uparrow\downarrow$ , 88%.

The synthesis of dithiol containing 1,3,5-tris(mercaptomethyl)benzene building block was performed in two steps. First, **1** was treated with two equivalents of dithiol **24** in THF at RT using sodium hydride as a base. The TLC revealed that the reaction was completed in half an hour, indicating the effectiveness of the reaction conditions. After quenching the excess sodium hydride with water and aqueous work up which was followed by the extraction with TBME, the crude was purified by column chromatography and bis-THP-protected-alcohol (bromomethyl)benzene (**25**) was isolated in 42% yield as colorless oil. Mono and tri-substituted side products were also isolated in lower yields. For the introduction of thioalkyl chain, commercially available hexanethiol was chosen and treated with equimolar amounts of **25** in THF. 2,2'-(5,5'-(5-(hexylthiomethyl)-1,3-phenylene)bis-(methylene)bis-(sulfanediy))bis-(pentane-5,1-diyl)bis-(oxy)bis-(tetrahydro-2H-pyran) (**26**) was isolated in 61% yield as colorless oil after purification by column chromatography. The total yield is 26% after two steps reaction.

The yield of **26** was lower than expected for a one-to-one substitution reaction. This was also interesting since the reaction conditions proved to be efficient previously. Therefore, the

low yield could be a result of the decomposition of **25**. Hence, the stability of **25** was examined and it was found that **25** decomposed under inert atmosphere and cold storage in a few days, most likely in accordance with the suggested mechanism in scheme 3.1.4.

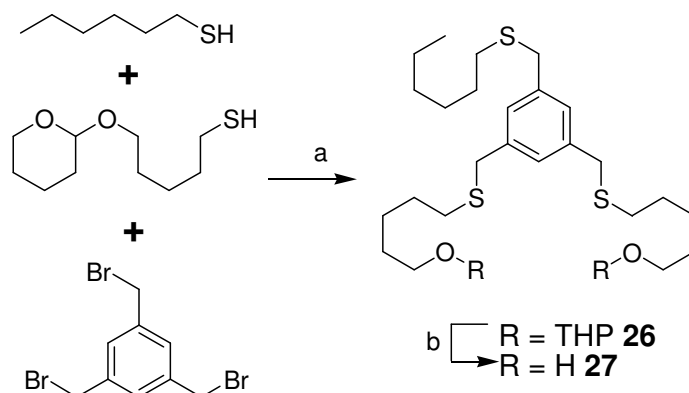


**Scheme 3.1.15.** Synthesis of tris(mercaptomethyl)benzene building block. (a) NaH, THF, RT, 42%; (b) hexanethiol, NaH, THF, RT, 61%, the total yield is 26% after two step reaction; (c) hexanethiol, NaH, THF, RT, 28% using one pot reaction method.

The total yield of **26** was found to be low, only 26%, after a two step reaction. While, one pot reaction can lead to more side products, the statistical yield of the desired compound is 33%, a little higher than the total yield of the two steps. Moreover, a one pot reaction method has the advantage of reducing the total synthesis steps and saving time. Thus, the synthesis of **26** was performed in one pot using two equivalents of dithiol **24**, one equivalent of hexanethiol and 3.3 equivalents of sodium hydride in THF. Aqueous work up and extraction with TBME followed by column chromatography gave the desired product **26** in 28% yield, close to the statistical yield and a little higher than the two-step approach.

Then, the deprotection of THP ethers was achieved quantitatively under milder condition using PPTS in refluxing EtOH. The course of the deprotection reaction was monitored by TLC. Due to the slow proton exchange mechanism between the solvent and THP protected compound of the deprotection reaction, the mono deprotection of THP was first observed. After overnight reflux, the fully deprotected 5,5'-(5-(hexylthiomethyl)-1,3-phenylene) bis-(methylene)bis-(sulfanediy) dipentan-1-ol (**27**) was obtained quantitatively by purification with a short plug of silica gel. The stepwise deprotection mechanism and possibility to isolate

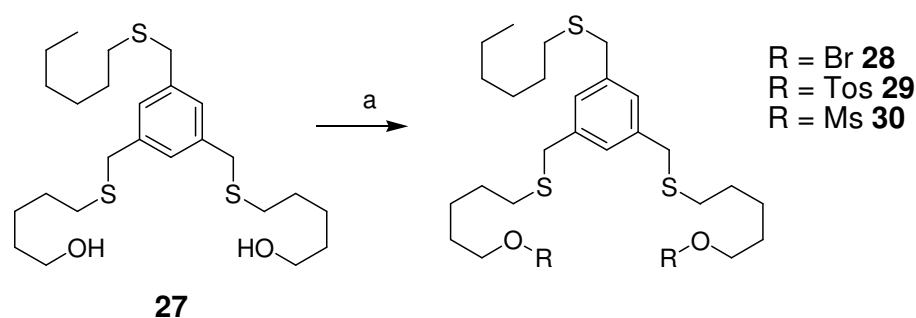
mono alcohol-mono THP (**27**) compound can be further expanded to the synthesis of tetrameric ligands in future.



**Scheme 3.1.16.** One pot synthesis and deprotection of THP of 1,3,5-tris(mercaptomethyl)benzene building block. (a) NaH, THF, RT, 28%; (b) PPTS, EtOH,  $\uparrow\downarrow$ , 99%.

After the fully deprotection of THP ethers, alcohol groups of diol **27** were exchanged with a better leaving group in order to perform a ring closing reaction by coupling with the first building block **8**. Phosphorus tribromide ( $\text{PBr}_3$ ) can be used to convert alcohols into the alkyl bromides. The high reactivity of bromine towards sulfur atoms could be very useful in a ring closing reaction. Moreover, the highly non-polar final product would be easier to separate from highly polar starting compound by column chromatography. Thus, two equivalents of  $\text{PBr}_3$  were added dropwise into the solution of **27** in THF at  $0^\circ\text{C}$ . The mixture was allowed to reach RT and left to stir under Ar. After an overnight reaction, two new spots were determined by TLC, probably representing the mono- and dibrominated compounds respectively. However, the newly formed compounds were found very unstable during the purification attempts. It was also noticed that large amount of mixture remained on the baseline of the TLC plate even in presence of highly polar eluents. Further, the crude turned into a darkish color after the removal of solvent before transferring to the silica gel column or K $\ddot{u}$ gelrohr for purification. The purification of the crude failed because of the high instability of the newly formed products. It is plausible that the substitution reaction easily took place but the high reactivity of bromines towards benzylic thiols led to decomposition of product during purification as suggested in scheme 3.1.4. For performing substitution reactions, conversion of diol **27** into more suitable leaving groups, such as tosylate and mesylates, were considered. The exchange of diol into sulfonates was studied since they can be introduced easily under mild conditions. Hence, one equivalent of diol **27** was dissolved in

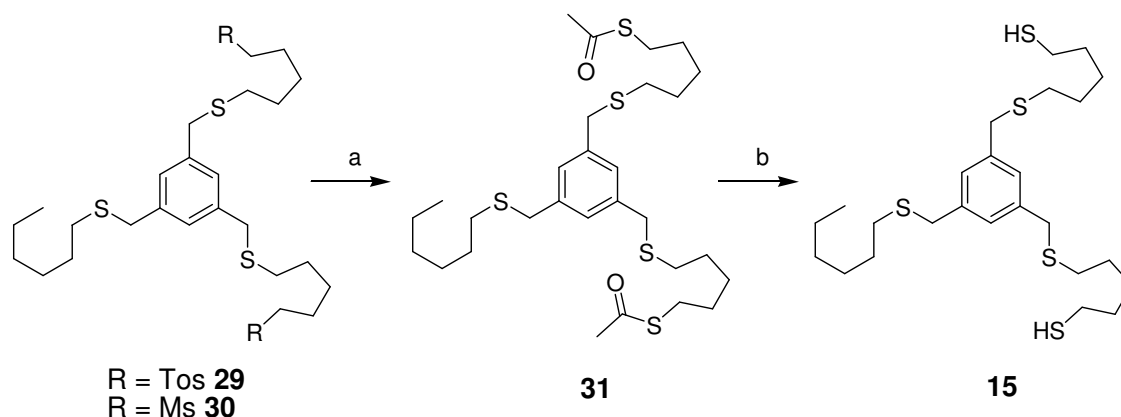
dry DCM. Then two equivalents of pyridine, a common base, and three equivalents of *p*-TsCl or methanesulfonyl chloride (MsCl), in case for mesylation, were added to the previous solution at 0°C. The reaction was run overnight at RT and the completion of the reaction was confirmed by TLC. After aqueous workup and extraction with TBME followed by purification by column chromatography, the tosylate **29** and the mesylate **30** were isolated in moderate yields of 59% and 41% respectively as colorless oil. However, the decomposition of sulfonates was observed even under Argon and below 0°C. Interestingly, both tosylate **29** and mesylate **30** displayed higher stability in DCM or TBME solutions even at room temperature unlike oily (dry) states.



**Scheme 3.1.17.** Synthesis of 1,3,5-tris(mercaptomethyl)benzene building block. (a) PBr<sub>3</sub>, THF, 0°-RT for R = Br; Pyridine, *p*-TsCl, DCM, RT, 59% for R = Tos, and 41% for mesylchloride for R = Ms.

To prevent the decomposition of these precious building blocks, further substitution of leaving groups into sulfur atoms using potassium thioacetate and deprotection to the free thiol was considered. Sulfonates **29** and **30** were reacted with two equivalents of potassium thioacetate in DMF. Acetyl protected thiol product **31** was isolated by column chromatography in a good yield as colorless oil. However, the yield of the thioacetate substitution was lower than similar previous substitutions. It is plausible that monosubstituted complex might react intra or intermolecularly with the sulfonate end which led to formation of a cyclic compound or disulfonate dimer respectively. Then the dimer might be reacted with another monosubstituted thioacetate complex for the formation of oligomers and even polymers as suggested in scheme 3.1.4.

In the final synthetic step, the acetyl protection groups were removed using a new method under milder conditions. The reaction of dithioacetate **31** with 0.25 equivalents of sodium methoxide (NaOMe) in dry MeOH provided the desired dithiol building block **32** quantitatively as colorless oil.

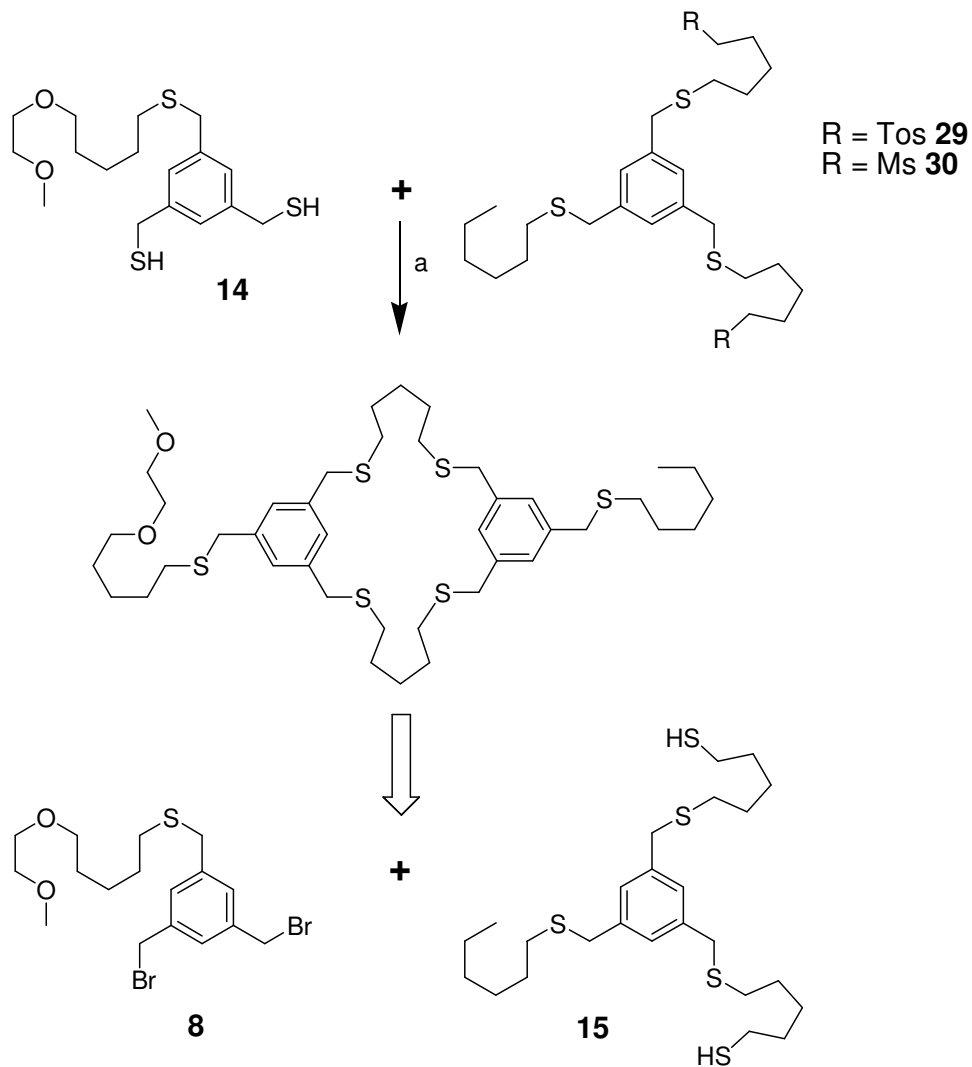


**Scheme 3.1.18.** Synthesis of of dithiol building block. (a) KSAc, DMF, RT, 69%; (b) NaOMe, MeOH, RT, quant., R are either tosyl or mesyl groups.

The synthesis of dithiol **15** from **29** or **30** provided the opportunity to choose different building blocks for the synthesis of dimer **B**. The ring closing reaction for the synthesis of dimer **B** might be performed either by the reaction between dibromo **8** and dithiol **15**, or by the reaction between dithiol **14** and disulfonate **29** or **30**. The synthesis of dithiols **14** and **15** both required two more steps of reactions starting from **8** and **29** or **30** respectively. Both of the building blocks **8** and **14** required the synthesis of alcohol protected thiol precursors **9**. On the other hand, the synthesis of second building blocks, disulfonates or **15** required the synthesis of alcohol protected thiol precursors **18**. Both of the precursors **9** and **18** could be synthesized in three steps from the commercially available starting materials. However, **14** could be synthesized in three steps starting from **1** whereas the synthesis of **15** needed double amount of reactions than **14**, a total of six steps starting from **1**. More importantly, the last two steps for synthesizing **15** reduced the amount of valuable building block. Therefore, it would be convenient to use dithiol **14** and ditosylate **29** or **30**, for the synthesis of ligand **B** for these reasons.

In a final synthetic step, 0.2 mmol dithiol **14** and 0.2 mmol ditosylate **29** were dissolved separately in 10 mL of THF. These solutions were simultaneously added with a rate of one drop per minute into 50 mL of THF solution containing 2.2 equivalents of sodium hydrate at room temperature. The dithiol **14** were activated with sodium hydrate in the reaction medium as the thiol salts blocked the needle and prevented dropwise addition of **14** to the reaction mixture. After the completion of addition of reactants to the reaction medium, the mixture allowed to stir overnight at room temperature. By using high dilution conditions (from  $4.10^{-5}$

M to  $333.10^{-5}$  M of reactants), the target compound, dimer **B**, was obtained as white solid in a yield of 16% by chromatographic purification. The yield of dimer **B** was a little higher, 19% when dimesylate **30** were used instead of ditosylate **29** due to the higher activity of tosylates towards leaving and thus increasing the polymerization possibility during the ring closing reaction. However, the total yield of last two steps was 9.44% for ditosylate **29**, while the yield was 7.79% for the mesylate **30** pathway.



**Scheme 3.1.19.** Synthesis of dimer **B**. (a) NaH, THF, RT, 19% using mesylated building blocks, and 16% using tosylated building blocks. R is either tosyl or mesyl group.

## Ligand Exchange Experiments

After the full characterization of dimer **B**, ligand exchange experiments were conducted using Schmid's clusters,  $\text{Au}_{55}(\text{PPh}_3)_{12}\text{Cl}_6$ . Schmid's clusters are soluble in common organic solvents and their solutions are dark red colored. Previous ligand exchange studies of Schmid's clusters by Pankau *et al.* [92] were performed in two-phase experimental setup using aqueous soluble ligands and organic soluble Schmid's clusters. The progress of the ligand exchange was monitored by color change of the phases. However, both Schmid's clusters and our multidentate thioether ligand **B** are soluble in organic solvents which render the observation of color change like in two-phase system obsolete. Therefore, the ligand exchange between the phosphine ligands and ligand **B** had to be confirmed using other analytical methods. It is well known that characteristic phosphorus peak of Schmid's clusters at  $\delta = 34.5$  ppm disappears in successful ligand exchange studies [91]. The removal of phosphine ligands can be easily monitored by  $^{31}\text{P}$ -NMR measurements. In addition to the disappearance of phosphorus peak by  $^{31}\text{P}$ -NMR measurements, one can expect much sharper  $^1\text{H}$ -NMR signals for the triphenylphosphine ligands attached to gold atoms after successful ligand exchange since the triphenylphosphine signals in Schmid's clusters are broadened because of the nearby gold atoms. Moreover, it was anticipated the broadening of thioether peaks of the dimer **B** around 2.2 and 2.4 ppm where the main interaction of thioethers with the  $\text{Au}_{55}$  clusters will occur.

A fast ligand exchange between the phosphine and the dimer **B** can be expected due to the monophasic transfer medium and structural flexibility of dimer **B**. Therefore, one equivalent of solid  $\text{Au}_{55}$  clusters were added directly into the NMR tube containing two equivalents of dimer **B** dissolved in  $\text{CD}_2\text{Cl}_2$ . The color of the solution changed quickly from colorless to dark reddish-brown upon addition of  $\text{Au}_{55}$  clusters and the ligand exchange studies were performed using NMR techniques. Interestingly, neither  $^1\text{H}$ -NMR nor  $^{31}\text{P}$ -NMR spectra showed changes in the signals. Thus, a slow ligand exchange reaction was considered. To minimise the oxidation of reactants, the NMR tube was sealed under vacuum and investigated regularly over a period of five days as a long term NMR study. A solution of Schmid's clusters and a solution of ligand **B** were also monitored separately under similar conditions as control experiment.

After five days of monitoring, it was found that the peak broadening belonging to triphenylphosphine ligand of  $\text{Au}_{55}$  clusters at 7.6 ppm became more visible in  $^1\text{H}$ -NMR

spectrum, proving the instability of  $Au_{55}$  clusters in  $CD_2Cl_2$  as reported earlier <sup>[69]</sup>. On the other hand, the expected broadening of thioether peaks of the dimer **B** around 2.2 and 2.4 ppm as a sign of their interaction with gold clusters was not observed. The small changes and broadening of peaks at the  $^1H$ -NMR spectra could be probably caused by coagulation of  $Au_{55}$  clusters into bulk gold. Moreover, a non-dispersible shiny gold film was formed on the surface of NMR tube preventing to observe the inside of the NMR tube which prevented further observation by naked eye.

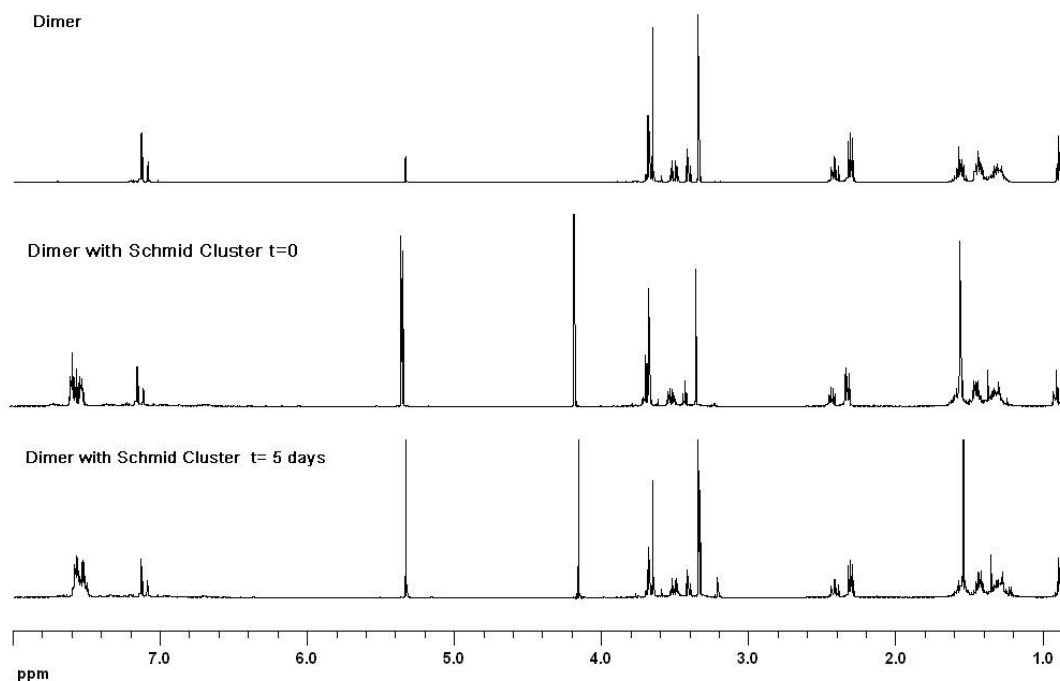


**Figure 3.1.2.**  $^1H$ -NMR Spectrum at 500MHz in  $CD_2Cl_2$  of dimer, dimer with gold nanoparticles at  $t=0$  and with gold nanoparticles at  $t=5$  days.



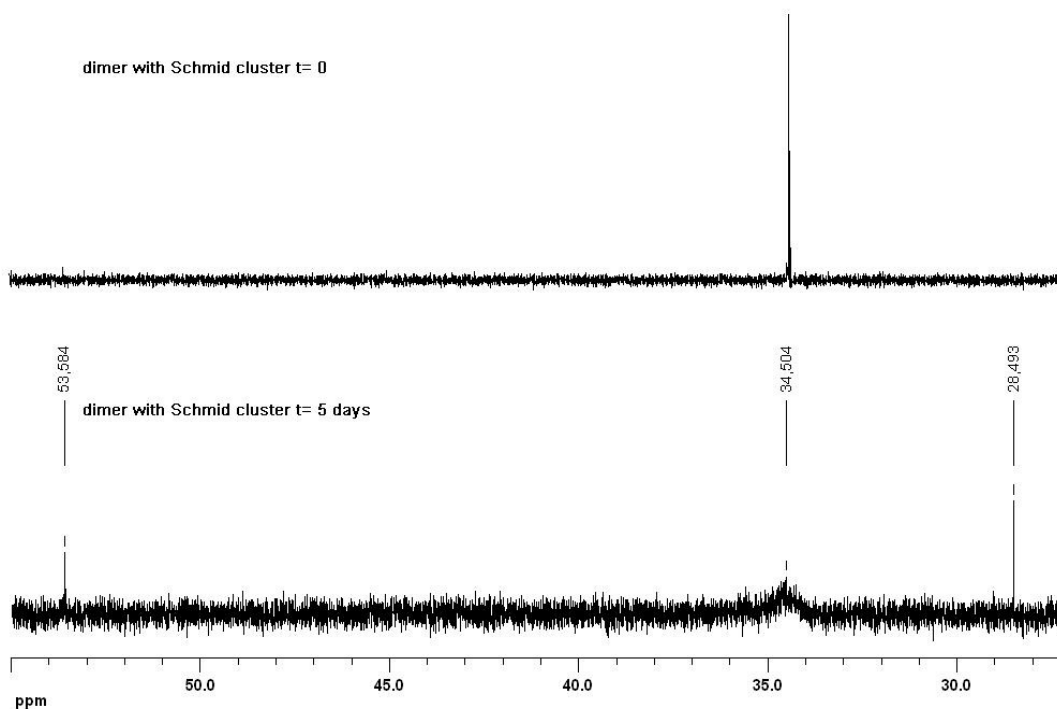


**Figure 3.1.3.**  $^{31}\text{P}$ -NMR Spectrum at 200MHz in  $\text{CD}_2\text{Cl}_2$  of dimer with gold nanoparticles at  $t=0$  and with gold nanoparticles at  $t=5$  days.

During the ligand exchange studies of  $\text{Au}_{55}$  clusters, Hutchison et. al. [88] observed a new peak formation in  $^{31}\text{P}$ -NMR spectra at 16.00 ppm arising from the formation of  $\text{AuPPh}_3\text{Cl}$  due to the decomposition of  $\text{Au}_{55}$  clusters. In contrast to Hutchison findings, two new peaks were noticed at 53.58 ppm and 28.49 ppm in  $^{31}\text{P}$ -NMR spectrum at 200 MHz in  $\text{CD}_2\text{Cl}_2$  after 5 days. These two peaks may be arising by the change in gold cluster shape and size. In addition to that, it was observed that the peak at 34.50 ppm belonging to the triphenylphosphine ligand of the  $\text{Au}_{55}$  clusters was shortened and became broadened with time stating the instability of Schmid's clusters in solution.

The findings in  $^1\text{H}$ -NMR and lack of phosphine peak at 16.00 ppm in  $^{31}\text{P}$ -NMR spectra supports the coagulation of  $\text{Au}_{55}$  clusters rather than the decomposition. It was already proven that the coagulation of  $\text{Au}_{55}$  clusters is thermodynamically favored [18]. Moreover, the coagulation of  $\text{Au}_{55}$  clusters was reported when the ligand exchange is slow [91].

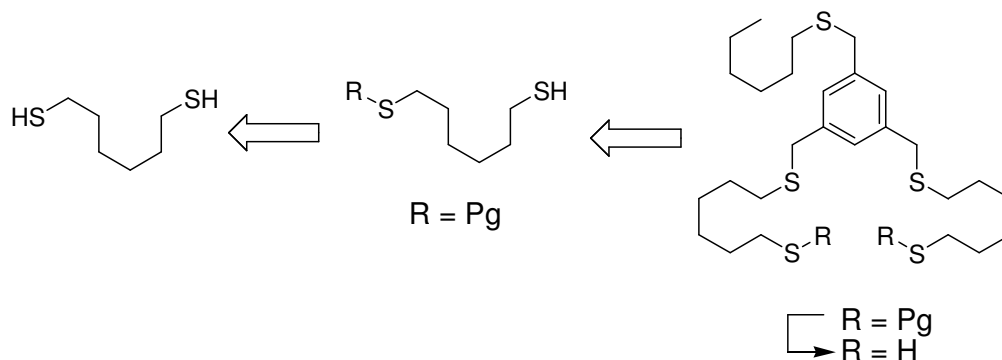
To overcome the coagulation of  $\text{Au}_{55}$  clusters due to the slower ligand exchange rate, the previously reported successful use of two phase ligand exchange method were considered.

Although, previously reported biphasic ligand exchanges were performed using organic soluble Schmid cluster and water soluble ligands, water soluble Au<sub>55</sub> clusters, Au<sub>55</sub>PPh<sub>3</sub>SO<sub>4</sub>, were used since the dimer **B** is soluble in organic phase. The dimer **B** was dissolved in DCM whereas Au<sub>55</sub> clusters were dissolved in deionised water. The mixture was then stirred for 7 days under Argon at room temperature. The organic layer stayed colorless, while the water layer remained reddish due to the presence of water soluble gold clusters indicating that the expected ligand exchanged did not occur. These findings were further supported by the <sup>1</sup>H-NMR and <sup>31</sup>P-NMR spectra of the organic part which did not show any broadening or appearance of new peaks arising from the interaction of dimer **B** with Au<sub>55</sub> clusters. In contrast to organic soluble counterparts only a little coagulation of water soluble Au<sub>55</sub> clusters was observed in the aqueous phase.

The two phase method for the ligand exchange reactions between the water soluble Schmid's clusters and organic soluble ligand **B** was clearly unsuccessful. On the other hand, it was observed that quick coagulation of Schmid's clusters into bigger clusters during monophasic ligand exchange studies with ligand **B**. It may be probable that the ligand **B** was exchanging with phosphine ligands only by covering half of the gold cluster and these half covered gold clusters coagulates before the completion of full ligand exchange. Another reason leading to the failure of successful ligand exchange may be the distance between the 1,3,5-tris(mercaptomethyl)benzene cores. In contrast to previous theoretical calculations, the distance between the 1,3,5-tris(mercaptomethyl)benzene cores may not be long enough to cover half of the gold cluster surface <sup>[172]</sup>. To test this hypothesis, the synthesis of a similar ligand with six carbon chain as a linker between the benzothioether cores was performed starting from commercially available 1,6-hexanedithiol.

The choice of 1,6-hexanedithiol as a starting material will reduce the required total synthesis steps comparing to 6-chloropentan-1-ol which could be used to synthesis 6-mercaptopentan-1-ol. Unlike 6-mercaptopentan-1-ol, 1,6-hexanedithiol is commercially available. Moreover, 1,6-hexanedithiol could be directly monoprotected and react with the 1,3,5-tris(bromomethyl)benzene core unlike protection of alcohol, substitution of chloride with potassium thioacetate and removal of acetyl group in case of choosing 6-chloropentan-1-ol as starting material. In addition to that, removal of protecting group of 1,3,5-tris(mercaptomethyl)benzene dithiol could be performed in one step to synthesize the final compound. The desired 1,3,5-tris(mercaptomethyl)benzene dithiol building block could be easily obtained in further two steps, one pot reaction following the removal of protection

groups, allowing the total synthesis in three steps starting from commercially available material.

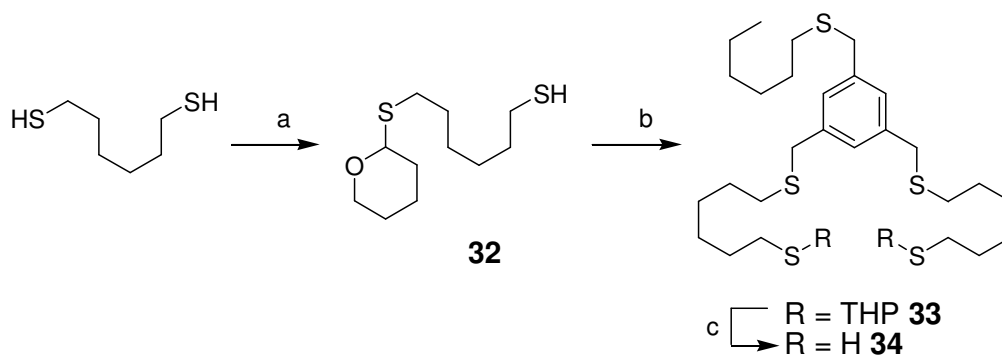


**Scheme 3.1.20.** Retrosynthetic analysis of 1,3,5-tris(mercaptomethyl)benzene dithiol building block.

THP was preferred again as a protection group for thiols as a result of the suitable protection group requirements mentioned above. In addition to that, THP provided not only the opportunity of selective deprotection towards the possibility to perform tetramer synthesis but also provided enough polarity for easier purification of desired compounds by column chromatography.

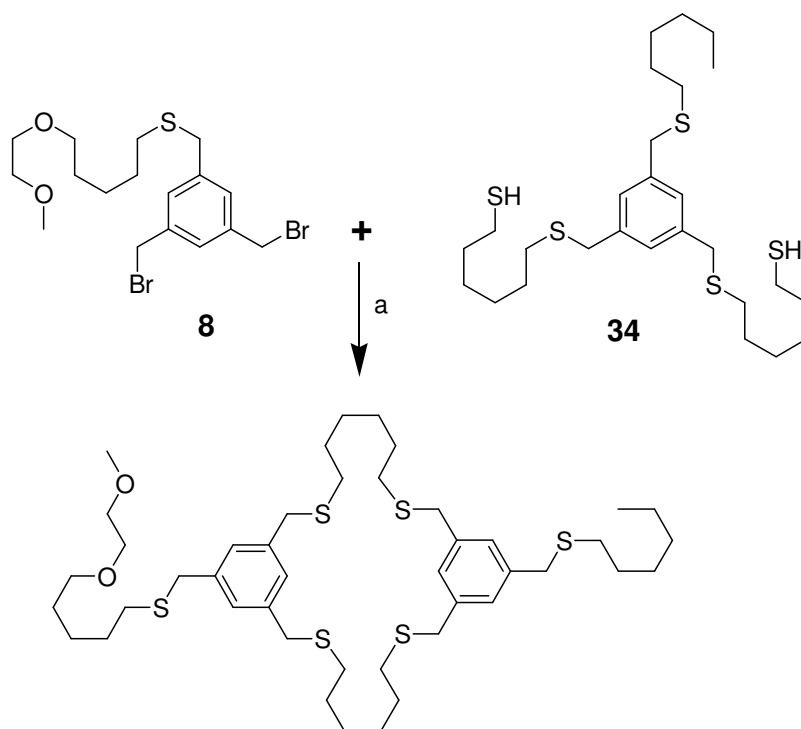
The monoprotection of 1,6-hexanedithiol with THP was achieved in 79% yield by using high dilution condition in DCM after overnight stirring at RT and usual work-up with water. The pure product, 6-(tetrahydro-2H-pyran-2-ylthio)-hexane-1-thiol (**32**) was isolated easily by column chromatography thanks to the polarity of the protection group. The synthesis of fully THP protected dithiol building block (**33**) was performed using one pot reaction under similar conditions of synthesis for compound **26** and obtained in 43% yield as slightly yellowish oil. In the next step, THP protection groups were cleaved using PPTS in refluxing EtOH. The 6,6'-(5-(hexylthiomethyl)-1,3-phenylene)bis(methylene)bis(sulfaneyl)dihexane-1-thiol (**34**) was obtained in 55% yield as colorless oil by column chromatography. While the deprotection of THP from alcohols could be fully performed quantitatively by increasing reaction time, the complete removal of THP protection groups for thiols could not be performed quantitatively. Although, the yield of **34** was better than synthesizing of 1,3,5-tris(mercaptomethyl)benzene dithiol building block starting from 6-chloropentan-1-ol, more efficient deprotection methods were investigated. The cleavage of THP groups in two steps using  $\text{AgNO}_3$  in MeOH/  $\text{H}_2\text{O}$ / MeCN mixture following reaction with  $\text{H}_2\text{S}$  in chloroform or HBr

in MeOH/ THF/ Benzene mixture were already known. However, these conditions could lead to unwanted cleavage of benzylic thioethers. Therefore, the conditions for selective cleavage of THP in the presence benzylic thioethers were considered. It was found that THP groups could be cleaved using trifluoroacetic acid (TFA) solution in DCM in the presence of triethylsilane ( $\text{Et}_3\text{SiH}$ ) which could be used as an efficient cation scavenger allowing the deprotection reactions at low concentrations of TFA <sup>[173]</sup>. The complete removal of THP protection groups were performed quantitatively using 4% TFA solution in DCM with 2.5 equivalents of triethylsilane, while benzylic thioethers remain intact and 1,3,5-tris(mercaptomethyl)benzene dithiol building block **34** was isolated quantitatively as colorless oil by purification with a short plug of silica gel.



**Scheme 3.1.21.** A new approach to the synthesis of a 1,3,5-tris(mercaptomethyl)benzene dithiol building block with six carbon chains as a linker between the aromatic cores. (a) DHP, PPTS, DCM, RT, 79%; (b) **1**, hexanethiol, NaH, THF, RT, 43%; (c)  $\text{Et}_3\text{SiH}$ , TFA, DCM, RT, 99%.

The synthesis of 1,3,5-tris(mercaptomethyl)benzene dithiol building block **34** was performed in three steps with a 57% yield starting from 1,3,5-tris(bromomethyl)benzene, in fewer steps and higher yields than the previously applied synthesis strategy. The ring closing reaction towards the synthesis of dimer **C** was performed between dibromo **8** and dithiol **34** using the previously mentioned conditions. After an overnight reaction, the dimer **C** was isolated in 22% yield as colorless oil by column chromatography.



**Scheme 3.1.22.** Synthesis of ligand C. (a) NaH, THF, RT, 22%.

Following the full characterization of ligand **C**, which has six carbon atoms containing alkyl chains for bridging the 1,3,5-tris(mercaptomethyl)benzene cores, the ligand exchange reactions with Schmid's clusters were studied with the help of NMR techniques. Unfortunately, increasing the carbon chain between the 1,3,5-tris(mercaptomethyl)benzene cores led to similar observations as in the ligand exchange of the dimer **B** which has five carbon atoms containing alkyl chain between the 1,3,5-tris(mercaptomethyl)benzene cores.

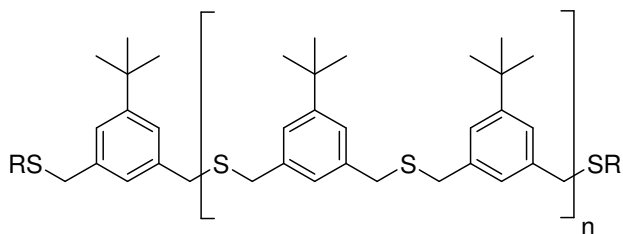
In summary, the synthesis of different length hexathioether ligands was performed. The ligand exchange reactions using Schmid's clusters were investigated under a varying of conditions. However, it was found out that the ligand exchange reactions were slower than the coagulation of  $Au_{55}$  clusters showing that the benzothioether ligands do not enwrap and efficiently stabilize the nanoparticles. These results indicate that the benzothioether wrapped  $Au_{55}$  clusters could not be achieved by ligand exchange reactions in contrast to previous findings<sup>[92]</sup>. The coagulation of  $Au_{55}$  clusters in the presence of benzothioether ligands and the designing of bulkier ligands should be investigated in the future.

### 3.2. Towards the synthesis of new gold nanoparticles stabilized by thioether based ligands

An important breakthrough for the synthesis of gold nanoparticles was achieved in 1994 by Brust and Schiffrin, who improved Faraday's two-phase method using alkane thiols to form highly stable monolayer protected gold nanoparticles<sup>[77]</sup>. Further investigations reported that the size of gold nanoparticles can be adjusted by varying the thiol-gold ratios, employed conditions and the nature of the ligand shell<sup>[81]</sup>. Several researchers expanded the Brust-Schiffrin method using other sulfur based ligands such as disulfides or thioethers for the synthesis of gold nanoparticles<sup>[93, 94, 174-178]</sup>.

Generally speaking, disulfides do not stabilize gold nanoparticles as well as thiols, and thioethers do not bind gold nanoparticles as strongly as thiols because of a weaker Au-S interaction<sup>[93]</sup>. Moreover, the first studies of thioether stabilized gold nanoparticles showed much larger core sizes and broader size distributions than thiol ligands, probably because of the weak bonding nature of the thioethers<sup>[176-177]</sup>. To compensate for the weak interaction between gold nanoparticles and thioethers, multiple thioethers containing ligands were required for producing stable and well-ordered monolayers<sup>[177-179]</sup>.

Recent studies from our lab showed that linear oligomeric multidentate thioether ligands can be used for the synthesis of gold nanoparticles via the two-phase method developed by Brust and Schiffrin for the synthesis of alkyl thiolate protected gold nanoparticles<sup>[160]</sup>.



**Scheme 3.2.1.** Linear oligomeric multidentate thioether ligand where n is 1 to 3 and R is a benzyl group.

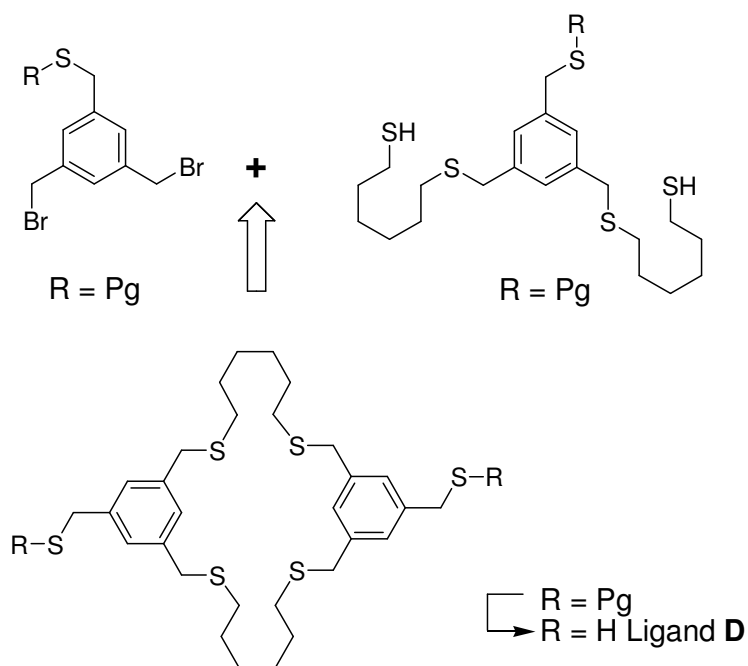
The synthesis of linear oligomeric multidentate thioether ligands shown in scheme 3.2.1, and their ability to stabilize gold nanoparticles was reported<sup>[160]</sup>. It was found that the stability of

the formed nanoparticles increased with the length of the stabilizing oligomer. Moreover, particles stabilized by the pentameric thioether ligand show a large size distribution while a much narrower size distribution was observed by using heptameric thioether ligands.<sup>[160]</sup>

In the light of these findings, the synthesis of gold nanoparticles via the two-phase method developed by Brust and Schiffrin using cyclic multidentate thioether ligands was considered due to their similar structural motifs with oligomeric multidentate thioether ligands<sup>[77]</sup>. Moreover, the central thioether cavity of cyclic multidentate thioether ligands may act as a template for the synthesis of predefined size gold nanoparticles. By varying the size of the central thioether ring of cyclic multidentate thioether ligands, the size of the desired gold particles could be dictated as has already been shown for ions by crown ethers. However, due to the unsuccessful results during the ligand exchange studies, the weak binding of thioethers to the gold particles should be modified. Therefore, a thiol-thioether hybrid multidentate ligand could lead to promising results for the direct synthesis of gold nanoparticles. While the central thioether ring could serve as a template for the synthesis of predefined size of gold nanoparticles, the thiol parts of the ligands could support additional binding to gold nanoparticles resulting in improved stability of gold clusters.

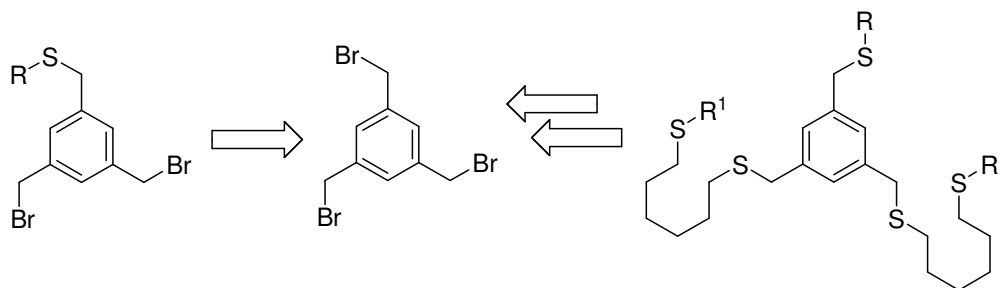
As mentioned above, Schmid's clusters have a perfect size for applications in future electronic devices. The theoretical calculations made for suitable ligands for Schmid's clusters states that the 1,3,5-tris(mercaptomethyl)benzene which are occupying [111] faces of gold clusters should be separated with a chain consisting of five or six carbon atoms<sup>[172]</sup>.

Under the light of these findings, a cyclic thiol-thioether hybrid multidentate ligand whose 1,3,5-tris(mercaptomethyl)benzene cores separated by five or six carbon atom could be a successful candidate for the synthesis of gold nanoparticles using Brust-Schiffrin method. A promising cyclic thiol-thioether hybrid multidentate ligand could be synthesized by a ring closing reaction between a monothioether substituted dibromomethylbenzene with one masked, two free thiols substituted 1,3,5-tris(mercaptomethyl)benzene building block. Once the ring closing reaction was performed, the cyclic thiol-thioether hybrid multidentate ligand can be obtained by removal of protection groups on the thiol end.



**Scheme 3.2.2.** Retrosynthetic analysis of cyclic thiol-thioether hybrid multidentate ligand **D**.

Retrosynthetic analysis depicted in scheme 3.2.2 led to build of a new type of ligand **D**. The easiest way to synthesis modified ligand **D** was to use one masked benzylic thiol and two leaving group with 1,3,5-tris(mercaptomethyl)benzene building block. Both building blocks would be easily accessible from 1,3,5-trimethylbenzene or 1,3,5-benzenetricarboxylic acid in few steps as performed before for the synthesis of previous building blocks. The 1,3,5-tris(mercaptomethyl)benzene building block could be synthesized from monothioether substituted dibromomethylbenzene in a few more straightforward steps.



**Scheme 3.2.3.** Retrosynthetic analysis building blocks. R and R<sup>1</sup> are different protection groups.

Nevertheless, the choice of suitable protecting group for the synthesis of monothioether substituted dibromomethylbenzene will be the most challenging step due to the the high



reactivity of sulfur in the presence of leaving groups which caused the low stability and led to decomposition of desired compound, possibly by polymerization as suggested before in scheme 3.1.4. Consequently, the suitable protecting group for the masked thiol had to be highly stable under conditions used for the nucleophilic substitution reaction, proper cleavage conditions without leading the cleavage of benzylic sulfides, easy to purify after deprotection and preferably higher selectivity towards mono functionalization.

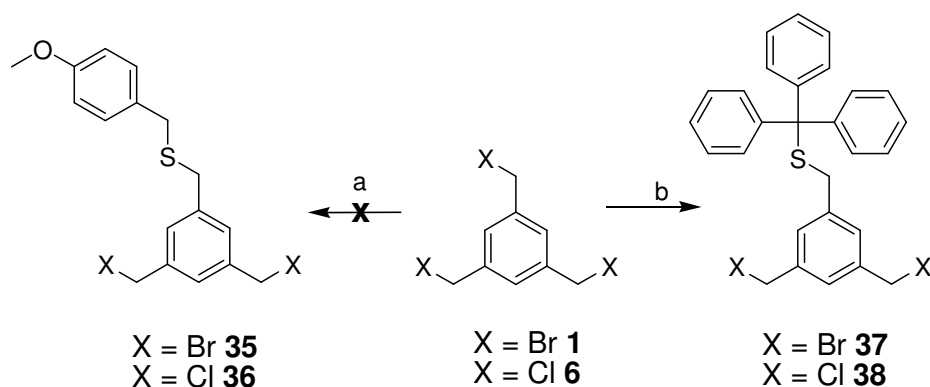
All these requirements made general thiol protection groups such as the S-acetyl group or other thioesters useless due to their easy cleavage under basic conditions, which are frequently used for nucleophilic substitution reactions. Alkyl thioethers were not considered as a suitable protection group not only because of the relatively harsh deprotection conditions<sup>[161]</sup> but also most of them lack bulkiness for preventing the reaction of benzylic thiols with the leaving groups.

All these limitations show that *p*-methoxy benzyl (PMB) or trityl could be used as suitable protection group. It has been described that sterically demanding protecting groups like trityl or PMB derivatives are suitable for monosubstitution reactions<sup>[180-181]</sup>. They are not only stable under basic reaction conditions, but also are reasonably bulky to prevent undesired intra or intermolecular reactions which lead to decomposition or polymeration of the desired product. However, PMB and trityl derived protecting groups are highly sensitive under acidic conditions and may be cleaved during column chromatography purification<sup>[161]</sup>. On the other hand, while PMB groups are much more resistant to cleavage under acidic conditions than trityl groups thanks to the electron donating abilities of *p*-methoxy moiety, their deprotection generally requires use of similar reagents as are used for the cleavage of benzyl thioethers<sup>[161]</sup>. Therefore, suitable deprotection conditions for selective cleavage of PMB in the presence of benzylic thioethers are required. After a literature search, it was found that mercury salts could also be used in the selective cleavage of PMB groups in the presence of benzyl sulfides despite their toxicity<sup>[161]</sup>.

As was explained above, PMB and trityl groups were considered as suitable protection group for the synthesis of monothioether substituted dibromomethylbenzene. Both of the protection groups PMB and trityl are commercially available as *p*-methoxybenzylmercaptane and triphenylmethyl mercaptane respectively. It is evident that the PMB groups are more polar than trityl groups due to the existence of the ether part; hence their purification could

be easier than trityl counterparts. For this reason, one equivalent of **1** was reacted with one equivalent of PMB in the presence of sodium hydride as base in THF at RT. Formation of well separated new spots, probably belonging to the mono and di- substituted products, on the TLC plate was observed after 30 minutes of reaction. After an aqueous workup and extraction with TBME, the crude mixture was subjected to silica gel column for purification. However, it was found that the desired product (3,5-bis(bromomethyl)benzyl)(4-methoxybenzyl)sulfane (**35**) and side products were decomposing during purification. It is most likely that the PMB group bulkiness is not enough to protect benzylic thiols from the attack of benzylic bromines and causing the decomposition of product by polymerization as happened before. Therefore, mono-PMB protection reaction was performed under similar conditions using less reactive leaving group containing 1,3,5-tris(chloromethyl)benzene. Although, the formation of new products was identified by TLC, the pure product (3,5-bis(chloromethyl)benzyl)(4-methoxybenzyl)sulfane (**36**) could not be obtained by column chromatography. The purification via K ugelrohr was also failed.

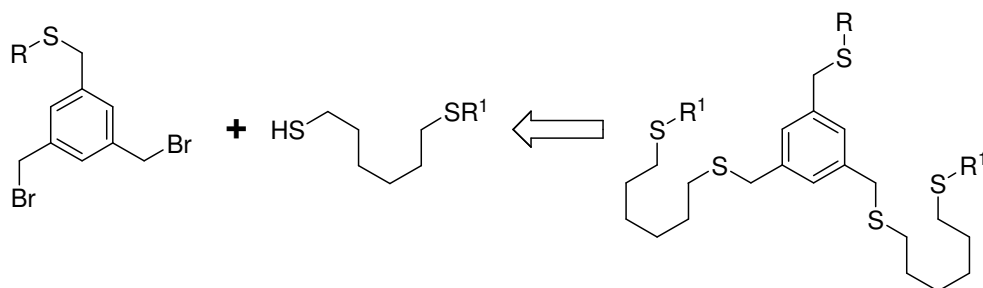
After the unsuccessful monoprotection attempts using PMB, trityl groups emerged as the only suitable candidate for the protection group. Therefore, the mono protection of 1,3,5-tris(mercaptomethyl)benzene using triphenylmethyl mercaptan was performed under similar conditions. The formation of new products was observed on TLC plate after 30 minutes of reaction as in the case of PMB. Similar workup procedure was applied and the desired product (3,5-bis(bromomethyl)benzyl)(trityl)sulfane (**37**) was isolated in 46% as white powder by column chromatography. The yield was similar, 49% when 1,3,5-tris(chloromethyl)benzene was used as starting material. The slow decomposition of **38** was observed while (3,5-bis(chloromethyl)benzyl)(trityl)sulfane (**38**) showed no sign of decomposition even storage at room temperature.



**Scheme 3.2.4.** Synthesis of bis(halomethyl)benzylsulfane. (a) 4-methoxybenzylmercaptane, NaH, THF, RT; (b) Triphenylmethyl mercaptan NaH, THF, RT, 46-48%.

Bis(halomethyl)benzylsulfane, **37** or **38**, can be also employed as precursors in the synthesis of one masked, two free thiols substituted 1,3,5-tris(mercaptomethyl)benzene building block. The one masked, two free thiols substituted 1,3,5-tris(mercaptomethyl)benzene building block could be easily synthesized by substituting the leaving groups of bis(halomethyl)benzylsulfane with monoprotected dithiol.

The one masked, two free thiols substituted 1,3,5-tris(mercaptomethyl)benzene building block could be synthesized by treating **38** with two equivalents of one free and one masked dithiol containing compound. Although less bulky protecting groups could be selected for masking one sulfur atom, the problem of selecting a proper protection group which can be cleaved in presence of trityl protection group arises. As stated earlier, nucleophilic substitution reactions usually require basic conditions which render useless to usage S-acetyl group or other thioesters groups as suitable protection groups. On the other hand, acidic deprotection conditions may also lead to deprotection of trityl protection groups. The suitable protection group for dithiol should be also cleaved leaving benzylic thioethers untouched. It was also desired that the protection group modifies the polarity of compound for easy purification by column chromatography.



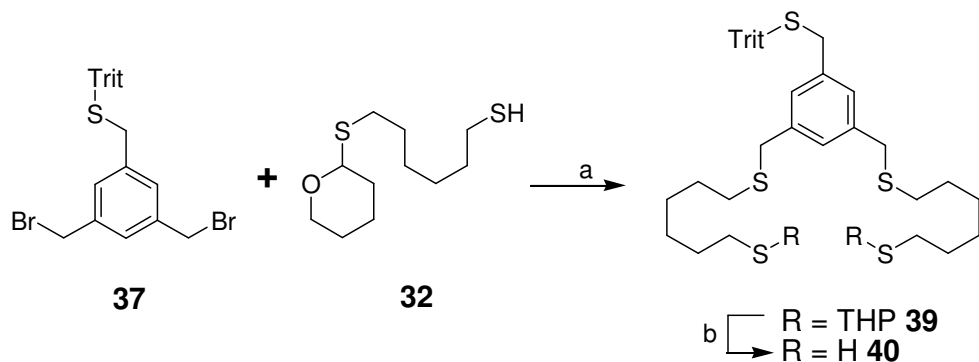
**Scheme 3.2.5.** Retrosynthetic analysis of 1,3,5-tris(mercaptomethyl)benzene building block where R and R<sup>1</sup> are different protection groups.

THP protection groups reasonably modify the polarity of compounds. They are also stable under basic conditions. But deprotection of THP groups from thiols requires harsh conditions or toxic mercury salts. A milder deprotection method using PPTS was performed for THP protection-deprotection of alcohol groups. This procedure was extended for the protection-deprotection of thiols with DHP as reported for the synthesis of **33** and **34**. Although, the deprotection efficiency was much lower than protection, monoprotected dithiol compound **32** was already synthesized and THP group may be cleaved mildly in presence of the trityl protection groups.

Bis(bromomethyl)benzylsulfane **37** was reacted with two equivalents of monoTHP protected dithiol **32** in THF using sodium hydrate as base. After aqueous workup and extraction with TBME, THP protected 1,3,5-tris(mercaptomethyl)benzene **39** was isolated easily in 96% yield as colorless oil thanks to the polarity of THP protection groups. In the next step, the removal of THP protection groups in the presence of trityl protection group was performed mildly using PPTS in refluxing EtOH. In addition to a starting material spot, two well separated spots were observed on TLC, probably representing mono and di- deprotected compounds after 24 hours of refluxing. A small sample taken from the reaction mixture and the yield of desired dithiol **40** was found around 30% (the yield was around 45% due the amount of consumed starting material). The reaction was refluxed another 24 hours, expecting the increase in desired compound yield. The analysis of a small sample taken from the reaction mixture showed similar yields, a little higher than 30%, for the amount of desired product **40**. The mild deprotection of THP group method is based on proton exchange between the solvent and compound. For this reason, the deprotection reaction was performed in more dilute solutions, in order to increase amount of the solvent atoms

which can exchange their protons with the compound **39** but the previously observed yield was obtained.

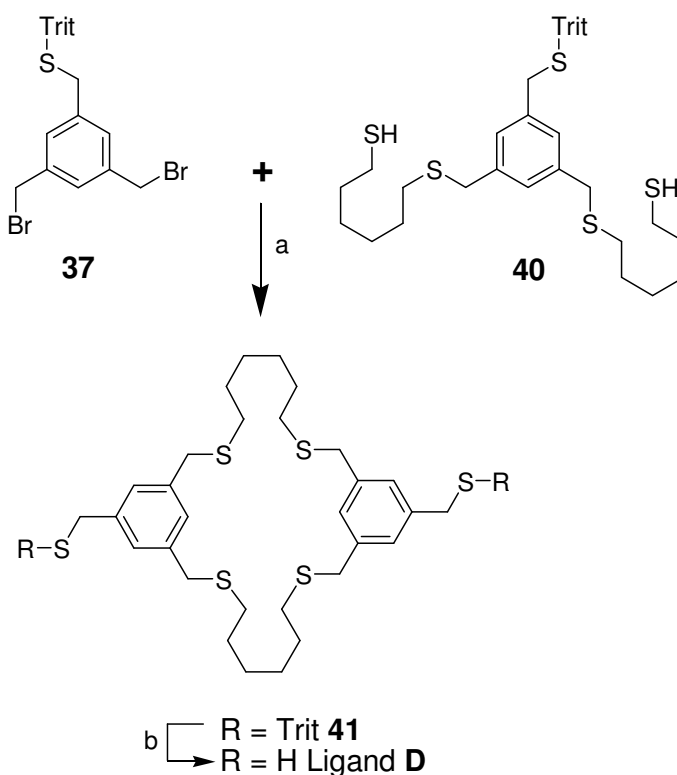
Oxygen being more electronegative than sulfur, has a higher proton tendency, thus EtOH may not prefer to exchange its proton with THP protected sulfur atoms. Therefore, the removal of THP groups using milder deprotection method was performed in alkylthiols to eliminate the electronegativity effect of solvent and to improve proton exchange between the solvent and compound **39**. The similar procedure for the deprotection of THP groups was repeated in n-propanethiol. The reaction were followed carefully, a small sample was taken every 12 hours and analyzed, but the improvement in the yield of desired compound **40** was not observed. It was likely that the proton exchange reaction reaches an equilibrium thus preventing the improvement of desired product yield. Although, this mild deprotection method for the cleavage of THP group was not very efficient, starting material and monodeprotected compounds could be isolated again, allowing their deprotection in subsequent runs to obtain more and more 1,3,5-tris(mercaptomethyl)benzene dithiol building block **40**.



**Scheme 3.2.6.** Alternative synthesis of 1,3,5-tris(mercaptomethyl)benzene dithiol building block. (a) NaH, THF, RT, 96%; (b) PPTS, EtOH,  $\uparrow\downarrow$ , 31% (45% due to the amount of consumed **39**).

Having two building blocks bis(halomethyl)benzylsulfane (**37** for bromo and **38** for chloro) and 1,3,5-tris(mercaptomethyl)benzene dithiol **40** at hand, the ring formation reaction was performed by dropwise addition of both building blocks in highly diluted medium with the help of a syringe pump. Again sodium hydrate was dissolved in reaction medium for *in situ* activation of dithiol **40** since activating them in syringe led to blocking of needle because of the formation of sulfonium salts. This strategy proved to be very effective, as the formation of new compound was observed right after the addition of building blocks. However, new spots which could be representing bigger chains, rings or polymer formations were also observed

by TLC after the addition of one fourth of starting materials into the reaction medium. The mixture was stirred half an hour more after the completion of addition of compounds and usual workup done before the purification via column chromatography. Side products such as bigger chains, rings or polymers formed in the reaction stuck to the silica gel and desired compound **41** could be purified easily with 32% yield as white powder. At the last step of the synthesis, the ligand **D** was obtained in 96% yield as colorless oil after deprotection of the trityl protecting groups using 4% TFA solution in DCM at the presence of triethylsilane following the previously mentioned conditions.



**Scheme 3.2.7.** Synthesis of ligand **D**, (a) NaH, THF, RT, 32%; (b) 4% TFA in DCM, triethylsilane, 96%.

The effectivity of ligand **D** for the direct synthesis of gold nanoparticles was carried out in a two-phase water-dichloromethane system. To protect the one-to-one ratio between the gold nanoparticles precursor and thiol-thioether moieties, the amount of added ligand **D** was normalized to the total number of thiol-thioethers. Therefore, a one-to-six ratio of ligand **D** to gold was used during the direct synthesis of nanoparticles. The synthesis was started by adding phase transfer agent, tetra-*n*-octylammonium bromide (TOAB), dissolved in toluene into the aqueous solution of the gold(III) precursor tetrachloroauric acid. The quick

discoloration of the aqueous phase and appearance of the orange color in the organic phase as a sign of transfer of gold salts into the organic phase was observed after vigorously stirring of the biphasic system. Then, a solution of the ligand **D** dissolved in toluene was added to the mixture. The formation of gold nanoparticles was performed by adding freshly prepared aqueous solution of the sodium borohydride to the strongly stirred two-phase system. After the addition of the reducing agent, the toluene phase turned dark brown, indicating the presence of gold nanoparticles in the organic part. Although, these were promising results proving for the formation of gold nanoparticles with ligand **D**, formation of a black precipitate was observed. Unfortunately, the black precipitate was insoluble and could not be re-dispersed in organic solvents hence purification and detailed analysis of formed complex could not be performed.

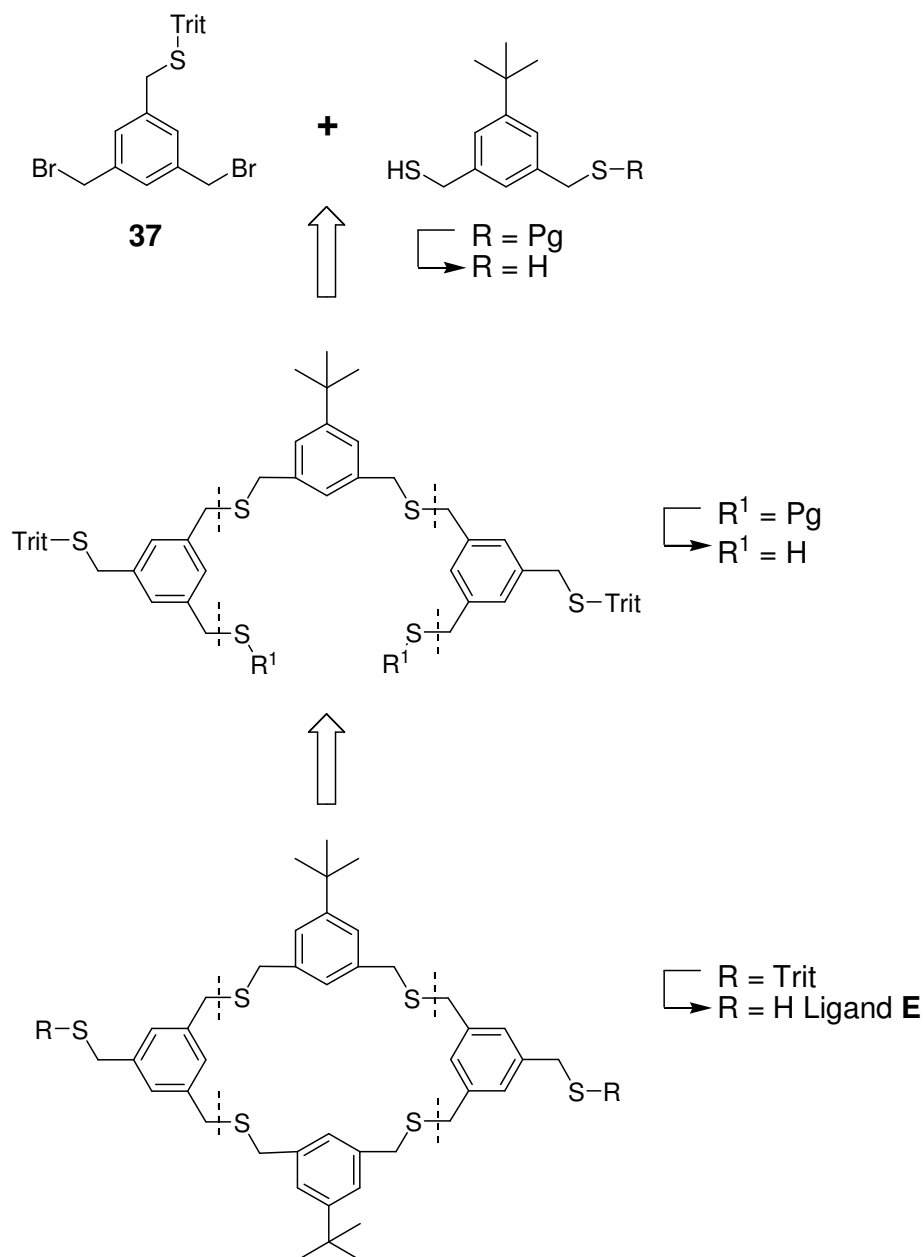
During the direct synthesis of gold nanoparticles with ligand **D**, several evidences of the formation of gold nanoparticles were observed. However, ligand-gold-phase transfer reagent mixture formed an insoluble black precipitate preventing further analysis. It is very probable that ligand **D** was missing bulkiness since they may not be efficient to keep gold nanoparticles separated and the formation of ligand-gold-phase transfer reagent complex might be happening.

As mentioned in the introduction, the suitable ligands should be bulkier or contain electrostatic atoms to prevent the coagulation of gold nanoparticles. Therefore, one can assume that ligand **D** should contain bulkier groups or charged atoms should be added in order to stabilize gold nanoparticles efficiently. The charged atoms could be inserted into ligand **D** by synthesizing new building blocks containing quaternary ammonium chains, or protonable components like alcohol, carboxylic acids etc. On the other hand, ligand **D** bulkiness could be easily improved by adding bulkier groups like *tert*-butyl or benzyl groups into the suitable places. The addition of bulkier groups close to thiols should be avoided in order to not decrease their ability to bind gold atoms. Hence, the most suitable position for addition of bulkier groups will be between the thioethers. Moreover, this could be achieved easily by replacing mono-THP protected dithiol (**32**) with a bulkier compound like mono-THP protected mercaptomethylbenzene (**45**).

The selection of suitable protection groups and the synthesis of bis(bromomethyl)benzylsulfane (**37**) were already explained in details above. Thus, the synthesis of new bulkier building block for bridging two 1,3,5-tris(mercaptomethyl)benzene

cores will be discussed here. While replacement of flexible alkyl bridges with benzylic building blocks may increase the bulkiness of the ligand, it can also lead to the problem of insolubility due to the increased stiffness of the final compound. Therefore, it will be a crucial decision to add good solubilizing groups to the bulky linkers. It is also known that *tert*-butyl groups could be used to improve solubility of the compounds due to their orthogonality which prevents stacking of molecules. Having bulkier than the linear alkyl chains and ability to improve solubility, it will be a wiser choice to add *tert*-butyl groups to the interlinking benzene groups while increasing the solubility and the bulkiness of the final compound. Therefore, *tert*-butylbenzene based compounds will be the most promising candidate for interlinking the 1,3,5-tris(mercaptomethyl)benzene cores instead of alkyl chains. A reaction between one equivalent of dibromomethylbenzylsulfane **37** and two equivalents of one masked and one free thiol containing *tert*-butylbenzylic compound might lead to precursors of ligand **E**. Then the trityl protected cyclic compound could be synthesized after removal of the protection group masking dithiols and followed by reaction with one equivalent of dibromomethylbenzylsulfane **37**. Finally, the ligand **E** could be obtained after the cleavage of trityl protection groups of the cyclic compound.





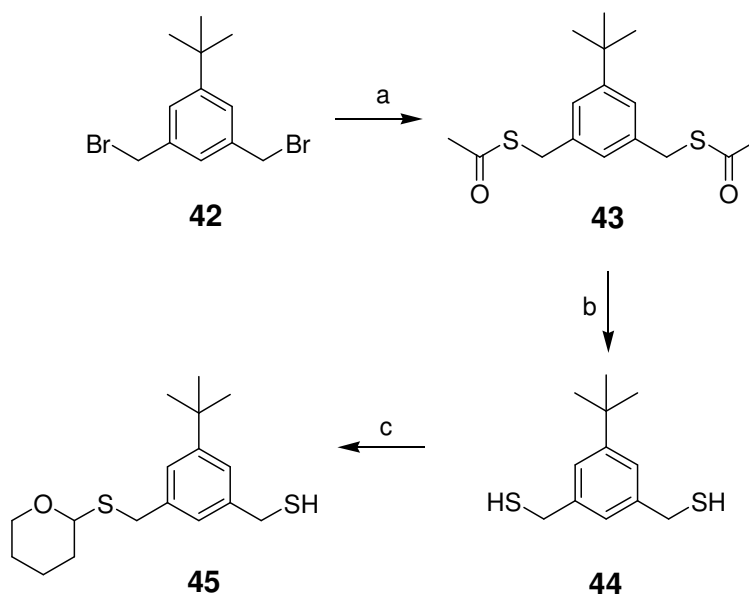
**Scheme 3.2.8.** Retrosynthetic analysis of ligand **E**.

The bulkier *tert*-butylbenzene based linkers could be synthesized in a benzylic bromination reaction with NBS starting from commercially available 5-*tert*-butyl-1,3-xylene. First, 1,3-bis(bromomethyl)-5-*tert*-butylbenzene (**42**) was synthesized in a good yield via benzylic bromination reaction started using AIBN as initiator and illumination with a 500 W halogen lamp from commercially available 5-*tert*-butyl-1,3-xylene in methyl formate solution instead of using human carcinogenic and environmentally hazardous carbon tetrachloride <sup>[118, 119]</sup>.

Then (5-*tert*-butyl-1,3-phenylene)dimethanethiol (**44**) was synthesized in two steps following the previously mentioned synthetic conditions.

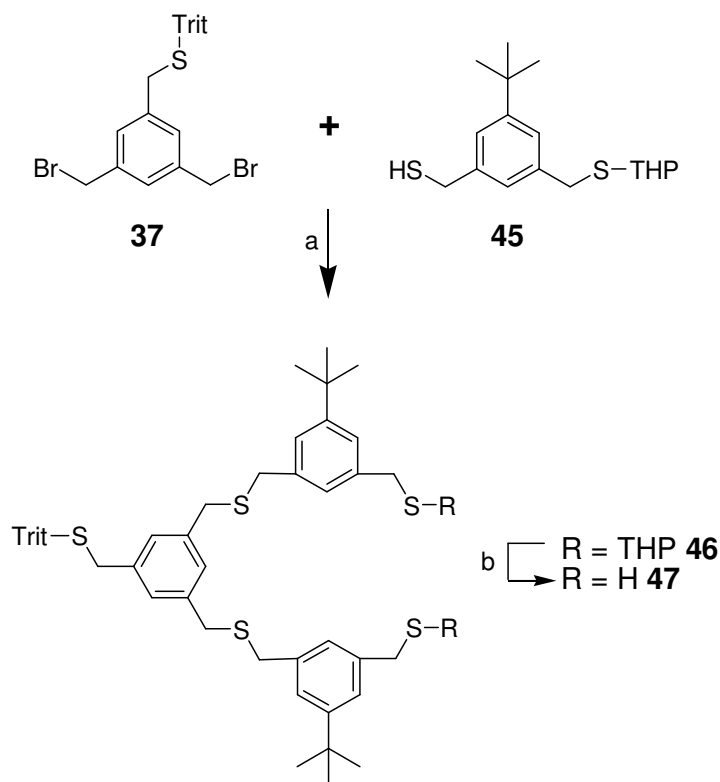
First, *tert*-butyl-phenylmethanedithioacetate **43** was synthesized in 93% yield by reacting one equivalent of **42** with 2.2 equivalents of potassium thioacetate. Then acetyl groups deprotected to the free thiols under basic conditions yielding 59% of *tert*-butyl-phenylmethanedithiol (**44**) as slightly yellow oily compound. The crude product was purified after basic workup and extraction with TBME. Interestingly, the yield of **44** was much lower than expected for the deprotection step. This could arise from the disulfide bond formation between the free thiols during the basic deprotection conditions or workup. **44** could also be synthesized alternatively in one pot reaction using thioacetic acid and potassium carbonate in two steps<sup>[182]</sup>. Although, this alternative synthesis way was much faster than previous one, it was not preferred because of strong pungent odour of thioacetic acid and lower yield, 45%, compared to the synthesis with potassium thioacetate.

As already mentioned in retrosynthetic analysis of ligand **E**, bis(bromomethyl)benzylsulfane **37** should be reacted with one masked and one free thiol containing *tert*-butylbenzylic building block towards the synthesise of ligand **E**. Due to their mild deprotection method in presence of highly acid labile trityl and acid labile benzothioether, THP was chosen again as a suitable protection group for masking one thiol of the (5-*tert*-butyl-1,3-phenylene)dimethanethiol (**44**). Therefore, DHP and **44** were reacted one-to-one ratio as described before and the desired compound, (3-*tert*-butyl-5-((tetrahydro-2H-pyran-2-ylthio)methyl)phenyl)methanethiol (**45**) was isolated by column chromatography in 62% yield, (77% yield due to the amount of consumed *t*-butyl-phenylmethanedithiol, **44**), as colorless oil.



**Scheme 3.2.9.** Synthesis of one masked, one free thiol containing *tert*-butylphenylic compound. (a) KSAc, DMF, RT, 91%; (b) NaOMe, MeOH, RT, 59%; (c) PPTS, DCM, RT, 62%, 77% due to the amount of consumed starting material.

The precursor of ligand **E** was synthesized from one equivalent of bis(bromomethyl)benzylsulfane **37** and two equivalents of mono THP protected-*tert*-butylphenylmethanethiol **45** in THF using 3.3 equivalents of sodium hydride as a base. After 30 minutes of stirring of the reaction mixture at RT, the excess of sodium hydride was carefully quenched with water. The general aqueous workup and extraction with TBME were applied. The crude was purified by column chromatography to give the pure semi cycle **46** in an excellent yield of 93% as white solid foam. In the next step, the THP groups were deprotected under mild conditions applied using PPTS as for the deprotection of previous compound **39**. Although, the yield of complete deprotection of THP groups while keeping trityl groups intact was a little better than in case of **39**, the yield of desired product was 39% (56% due to the consumed amount of starting material).



**Scheme 3.2.10.** A new approach to the synthesis of ligand with bulkier linker between the aromatic cores. (a) NaH, THF, RT, 93%; (b) PPTS, EtOH,  $\uparrow\downarrow$ , 39%; (56% due to the amount of consumed **46**).

The next reaction towards the synthesis of ligand **E** was the ring formation between **47** and **37** by dropwise addition of both building blocks in highly diluted medium with the help of syringe pump as was carried out in the synthesis of ligand **D**. Despite *in situ* activation of thiols and high dilution conditions, the formation of desired product was not observed by TLC. It was assumed that the formation of side products such as longer chains, bigger rings or polymers was happening as the sample spot from the reaction mixture remained on the baseline of the TLC plate even if highly polar solvents were used as eluent.

Based on this information, it seems very likely that the bulkier trityl protection groups were blocking the reaction between the free benzylic thiols of **47** and benzylic bromides of **37** by preventing cyclisation of the whole molecule and lead to formation of side products. The free benzylic thiols of bulkier interlinking group should be less flexible than less bulky alkyl thiols counterparts.

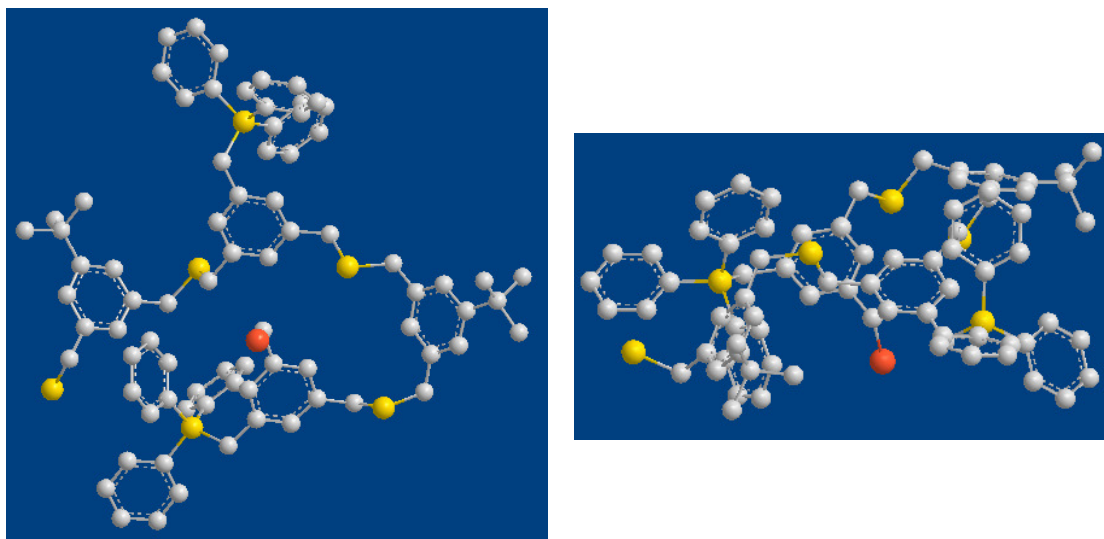
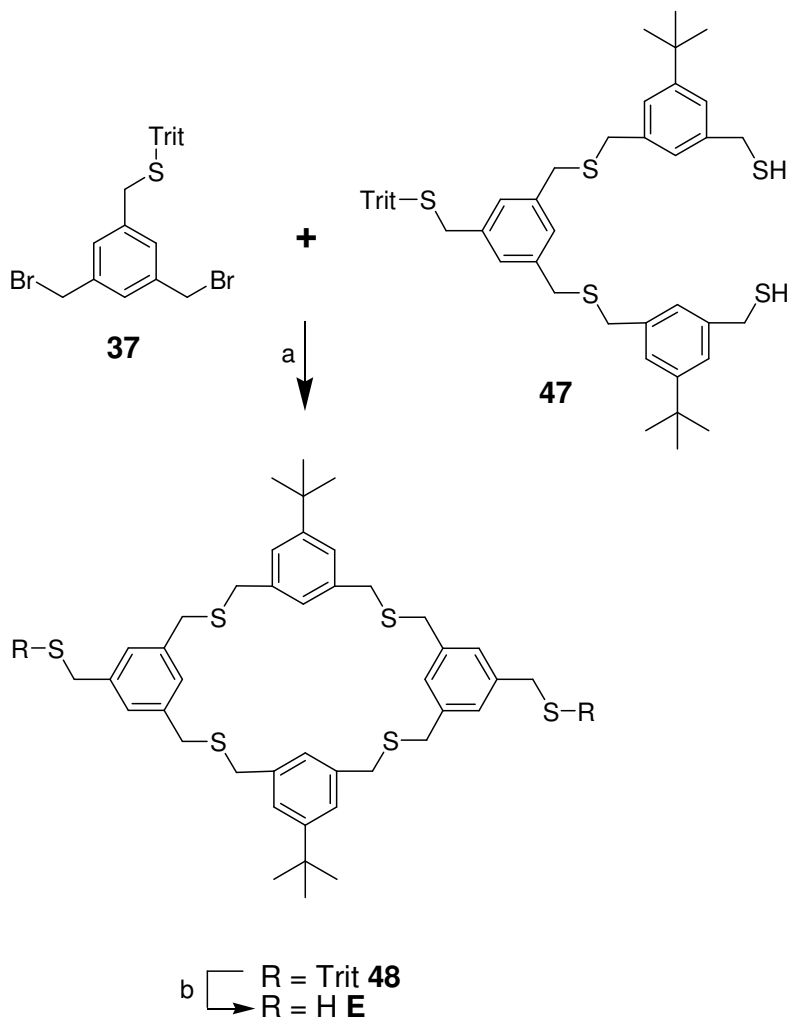


**Figure 3.2.1.** Balls and stick models of minimized energy calculations of uncyclised ligand with Chem 3D ver 11.0. Sulfur atoms are yellow, bromine atoms are red and carbon atoms are grey colored. Hydrogen atoms were omitted for clarity of the picture.

However, since the free rotation of single bonds around the carbon-carbon is assumed, the cyclisation reaction between **37** and **47** could be achieved under suitable conditions. It was rationalized that the desired ligand **E** could be obtained if the cyclization reaction performed using the more diluted conditions and cooler temperature in order to reduce the collision rate of molecules and thus to prevent unwanted intermolecular reactions. Therefore, the cyclisation reaction between **37** and **47** were repeated again in much more diluted conditions and varying temperatures from 0 °C to RT. 0.1 mmol dithiol **47** and 0.1 mmol dibromo **37** were dissolved separately in 20 mL of THF. These solutions were simultaneously added with a rate of one drop per minute to 100 mL of THF solution containing 2.2 equivalents of sodium hydrate at 0 °C. The appearance a new spot, indicating the formation of **48**, and the complete consummation of starting materials was confirmed by TLC analysis. After the completion of addition of reactants to the reaction medium, the mixture allowed to reach room temperature and stirred overnight under argon. The isolation of the new spot and fully characterization by spectroscopic methods verify the synthesis of **48** in 34% yields as white powder.

In a final synthetic step, the trityl protecting group was then removed from **48** using TFA (4% v/v) containing DCM in the presence of triethylsilane as cation scavenger similar to the deprotection of the cyclic benzothioether **41**. The apolar by-products of the deprotection

procedure were removed easily by column chromatography to give the pure ligand **E** in a yield of 53% as white powder.



**Scheme 3.2.11.** The synthesis of ligand **E** (a) NaH, THF, RT, 34%; (b) Et<sub>3</sub>SiH, TFA, DCM, RT, 53%.

Ligand **E** was employed for the direct preparation of gold nanoparticles using Brust-Schiffrin method. One-to-one ratio of thiol-thioether to gold equivalents was maintained to ensure compatibility with previous studies. Hence, a one-to-six ratio of ligand **E** to gold was used during the direct synthesis of nanoparticles. The synthesis was started by adding 131.2 mg (240  $\mu$ mol, 12 eq.) TOAB dissolved in 2.5 mL DCM into 203.9 mg (120  $\mu$ mol, 6 eq.) tetrachloroauric acid dissolved in 2.5 mL deionised water and the two-phase mixture stirred until the aqueous phase became colorless at room temperature. 15 mg (20  $\mu$ mol, 1 eq.) of ligand **E** dissolved in 2.5 mL DCM was added to the reaction mixture followed by a freshly

prepared solution of 36.3 mg (960  $\mu\text{mol}$ , 48 eq.) sodium borohydride in 2.5 mL water. After 10 minutes stirring, the resulting strongly colored dichloromethane phase was separated and the aqueous phase was washed twice with 10 mL of DCM. The combined organic fractions were dried over sodium sulfate, filtered and concentrated to a volume of ca. 1 mL. Ethanol (approx. 15 mL) was added to precipitate the particles, which were then centrifuged. The supernatant was discarded and the formed gold nanoparticles were collected for further analysis.

The pre-purification UV-Vis analysis of the particles stabilized with ligand **E** (blue line on figure 3.2.2) showed the presence of a very weak surface plasmon resonance band around 520 nm, stating that most of the gold nanoparticles size was less than 2nm.

It has already been reported that the phase transfer agent TOAB can itself act as stabilizer for gold nanoparticles<sup>[163]</sup>. Therefore, the newly formed gold nanoparticles should be purified in order to prove the stabilizing efficiency of the ligand **E**.

First of all, the nanoparticles were re-dissolved in toluene to get rid off the black precipitate which was probably coagulated gold nanoparticles depicted in UV-Vis as a small shoulder around 520 nm. It was observed that the UV-Vis spectrum of the particles stabilized with ligand **E** after redissolution in an organic solvent (red line on figure 3.2.2) was pointing towards the gold nanoparticles with a diameter less than 2 nm due to the disappearance of previously noted surface plasmon resonance band around 520 nm<sup>[162]</sup>. The phase transfer reagent (TOAB) had to be removed from the mixtures in order to receive clear information about the stabilizing efficiency of ligand **E**. Therefore, the nanoparticles were dissolved in few milliliters (mL) of DCM and concentrated to approximately 1 mL by using Rotavap and 24 mL of EtOH was added for precipitation of gold nanoparticles in order to remove the remaining phase transfer reagents. Usually precipitation procedures were repeated three times to ensure complete removal of excess phase transfer reagent but ligand **E** stabilized gold nanoparticles were reasonably soluble even in highly polar solvents such as ethanol. Although, the high solubility of gold nanoparticles stabilized by ligand **E** is suitable for removal of non-bounded ligands, it also led to loss of considerable amounts of nanoparticles. For this reason, further precipitations were omitted to prevent loss of thioether coated gold nanoparticles. The nanoparticles stabilized with ligand **E** were obtained as black-brown waxy solids after precipitation. The UV-Vis measurement was repeated for the nanoparticles purified by precipitation (green line on figure 3.2.2) and a spectra resembling

to the UV-Vis measurement after re-dissolution of gold nanoparticles (red line on figure 3.2.2) was detected.

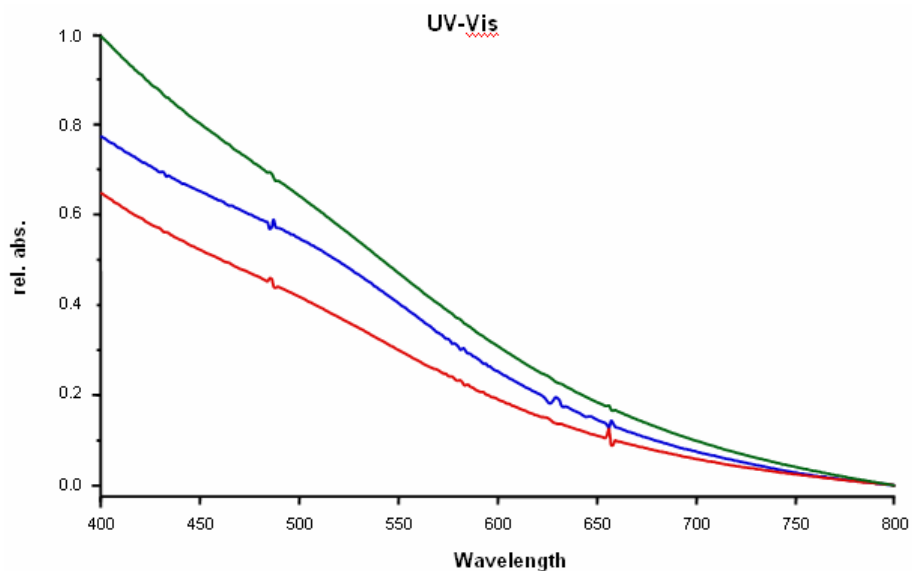


**Figure 3.2.2.** UV-Vis measurements of gold nanoparticles stabilized with bulky ligand **E**. UV-Vis measurements from the reaction mixture is showed by blue, redispersed nanoparticles by red and purified nanoparticles by green curves.

Although, UV-Vis measurement is very quick and useful to determine gold nanoparticles size, is not sufficient to prove the efficiency of ligands for stabilizing gold nanoparticles alone. Therefore, benzothioether stabilized gold nanoparticles were further investigated by  $^1\text{H-NMR}$  in  $\text{CD}_2\text{Cl}_2$ . The broadening of thiol and thioether signals arising from close Au-S interaction was observed on the  $^1\text{H-NMR}$  spectrum. However, the presence of phase transfer agent, TOAB, was also detected on the  $^1\text{H-NMR}$  spectrum confirming that the one purification by precipitation was not enough for complete removal of excess TOAB from the medium. Although, more purification by precipitation could be performed; the complete removal attempts of TOAB may lead to the decomposition of gold nanoparticles. It may be possible that some amount of the TOAB is required for the stabilization of gold nanoparticles stabilized by thioether dendrimers as reported by Luisa De Cola *et al.*,<sup>[164]</sup>.

The calculation of ligand-TOAB ratio was done based on comparison of integration of *t*-butyl groups of ligand **E** and alkyl chains of TOAB signals where a more accurate results can be obtained since the broadening of peaks was minimal due to their low interaction with gold



nanoparticles. The careful integration of these peaks and the interpretation of the  $^1\text{H-NMR}$  spectrum revealed a 1-to-0.9 ligand-to-TOAB ratio.

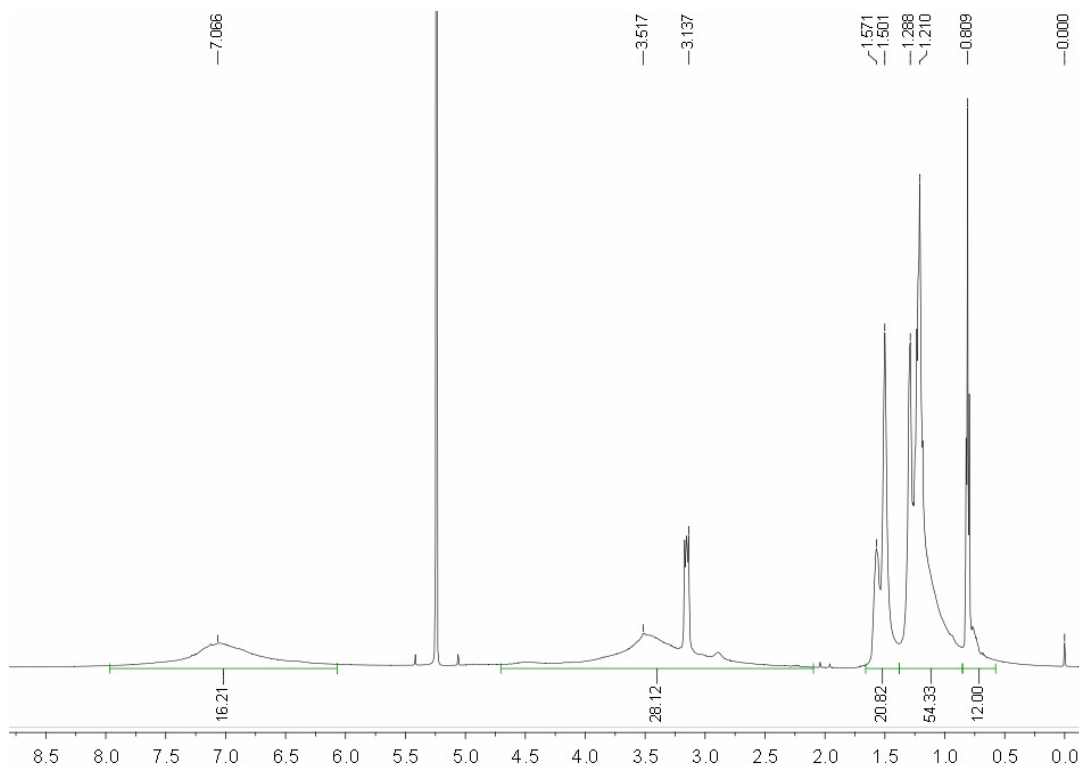


**Figure 3.2.3.**  $^1\text{H-NMR}$  Spectrum at 500MHz in  $\text{CD}_2\text{Cl}_2$  of ligand **E** with gold nanoparticles.

Beside spectroscopic analysis such as UV-Vis and  $^1\text{H-NMR}$  investigations, elemental analysis is a very useful technique for defining the TOAB-to-ligand ratio. From the nitrogen percentage of the elemental analysis, the amount of TOAB in the nanoparticles could be calculated as this is the only nitrogen source. However, the amount of nitrogen in the nanoparticles could not be detected by elemental analysis. This inconsistency could be arising due to the very low amount of nitrogen percentage of the whole complex. The pure TOAB contains 2.56% and the nitrogen amount of the whole complex could be very small for failing detection of it. Therefore, ligand-to-TOAB ratio was calculated using carbon-to-hydrogen ratio of the gold nanoparticles complexes. The results obtained from the elemental analysis showed 7.52-to-1 carbon-to-hydrogen ratio, 18.49% carbon and 2.46% hydrogen. This value is very consistent with our 1-to-0.9 ligand-to-TOAB ratio assumptions. The carbon-to-hydrogen ratio of pure ligand **E** is 9.62-to-1 whereas it is 5.62 for TOAB. 1-to-0.9 ligand-to-TOAB ratio leads 7.5-to-1 carbon-to-hydrogen ratio as obtained from the elemental

analysis. From these values, a mass proportion of 27% or 26.8% ligand-to-TOAB mixture was calculated based on the carbon or the hydrogen percentage respectively. These mass proportions also stated that the gold atoms were generating the remaining 73% of the total weight of the nanoparticles. Therefore, 1 g of the nanoparticles should be composed of 730 mg of gold atoms and 270 mg of organic components (ligand **E** and TOAB). The molecular weight of ligand **E** and TOAB are 749.25 g/mol and 546.80 g/mol respectively. The contribution of ligand **E** to the organic part of the nanoparticles will be 749.25 g/mol, while the contribution of TOAB will be 492.12 g/mol according to the 1-to-0.9 ligand **E** to TOAB ratio, concluding that the organic part of the nanoparticles should be 1241.37 g/mol. If 1 g nanoparticles contain 270 mg of organic components, then the 1 mol of nanoparticles should be 4597.67 g and the amount of gold atoms should be 3356.3 g. The atomic weight of gold is 196.97 g/mol. Therefore, 1 mol of ligand **E** and 0.9 mol of TOAB should stabilize 17 moles of gold atoms.

Transmission Electron Microscopy (TEM) measurements were performed after purification of nanoparticles stabilized by ligand **E**. The gold cores appeared well separated from each other by their protective layer and only occasional agglomerations were observed around the larger particles. This could be arisen from interlinking of two or more benzothioether stabilized gold nanoparticles due to the free thiol on the ligand. Free thiol at the end of the bulky ligand may also lead to formation of pseudo one dimensional arrangement of similar size nanoparticles. From the TEM pictures, one can clearly notice several linear nanoparticles chain formation where the chain length varies from 2 to 8 nanoparticles. However, the size and distance between the nanoparticles forming pseudo one dimensional arrangement showed a wide variation from 1.2 nm to 1.6 nm and 1.0 nm to 1.9 nm respectively.

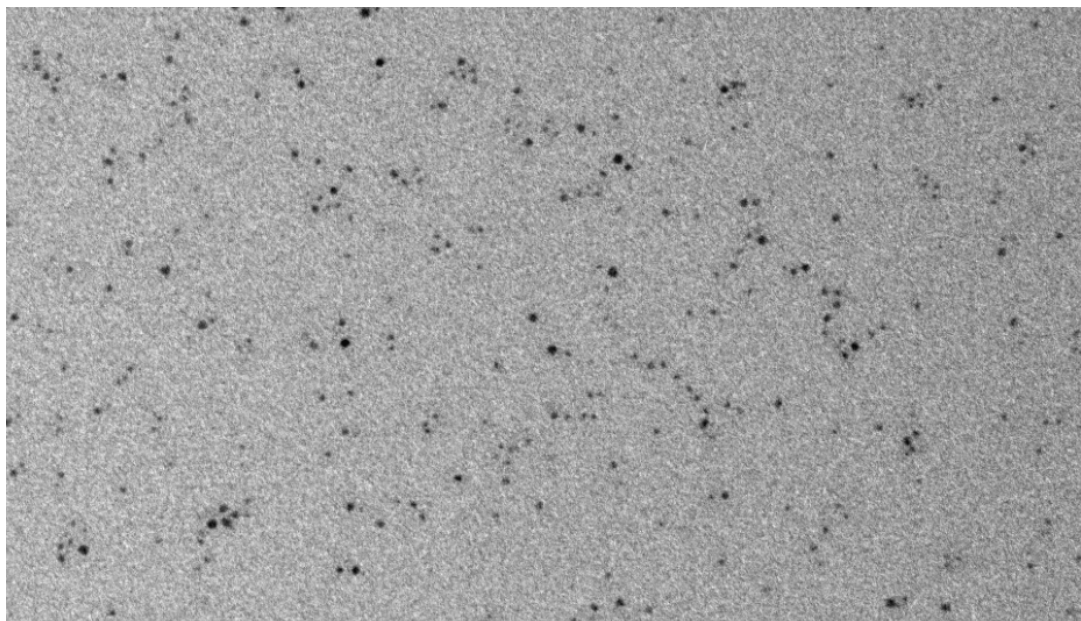


**Figure 3.2.4.** TEM picture of nanoparticles stabilized with ligand **E**. While the gold cores appear well separated and some pseudo 1D arrangement available, a few of stacks of gold nanoparticles can be observed around the larger particles.

The TEM pictures quality was enhanced using commercial image processing programs to reduce the measurement errors before the determination of particle sizes. The size distribution of particles was done carefully for a sample area of 100 nm x 600 nm and diameters of more than 400 nanoparticles were measured. The histogram in figure 3.2.5 showed narrow size distribution of nanoparticles ranging from 0.6 to 2.3 nm in which nearly 70% of the nanoparticles size lay between 0.9 nm to 1.2 nm. The particles larger than 2 nm or interlinked particles were probably insoluble and were purified from the mixture during the re-dissolution process. UV-Vis measurements were also supporting this observation as explained above.

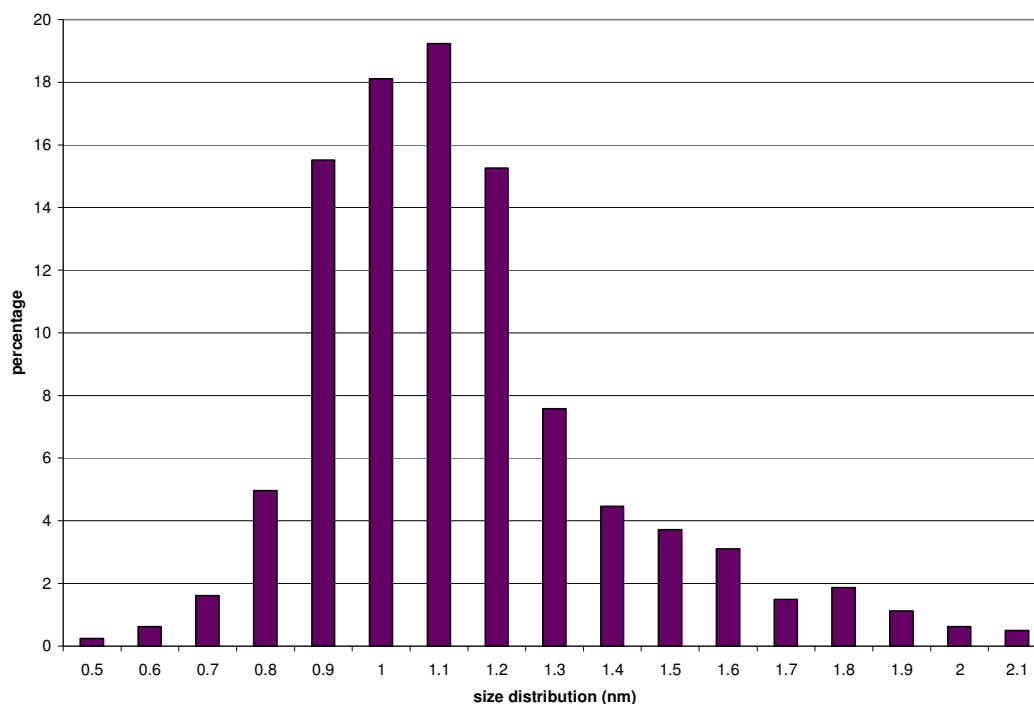


**Figure 3.2.5.** Histogram of nanoparticles stabilized with ligand **E**.

The elemental analysis results stated that 17 gold atoms were stabilized per ligand with TOAB whose ratio is 1-to-0.9. However, TEM measurements showed that the average size of gold nanoparticles stabilized with ligand was 1.1 nm. It was reported that the Au<sub>38</sub> cores synthesized with Brust-Schiffrin method have a core diameter of 1.1 nm<sup>[165]</sup>. In the light of these findings, it is more suitable that two of ligands **E** were templating the formation of one nanoparticle composed of 34 gold atoms.

Au<sub>13</sub> clusters sizes are determined as 0.8 nm<sup>[166]</sup>. The gold nanoparticles smaller than 1.1 nm may be formed in the thioether cavity of the bulky ligand and the free thiol branches of the ligands may wrap around the gold nanoparticles which is further supported from the calculations of the elemental analysis.

Simple energy minimization for molecular structure calculations (MM2) showed that the ligand **E** could have a bowl shape. The thioether atoms could have arranged a square like structure whose length is around 5.8-5.9 Å whereas thiol to thioether distance was measured 5.9-6.0 Å. On the other hand, the distance between the free thiols is 10.9-11.0 Å.

These measurements indicate that a cluster whose size is around 1 nm may fit into the ligand cavity. Finally, *tert*-butyl groups of bulky benzyl linkers pointing outwards of the bowl may serve to prevent coagulation of gold nanoparticles.

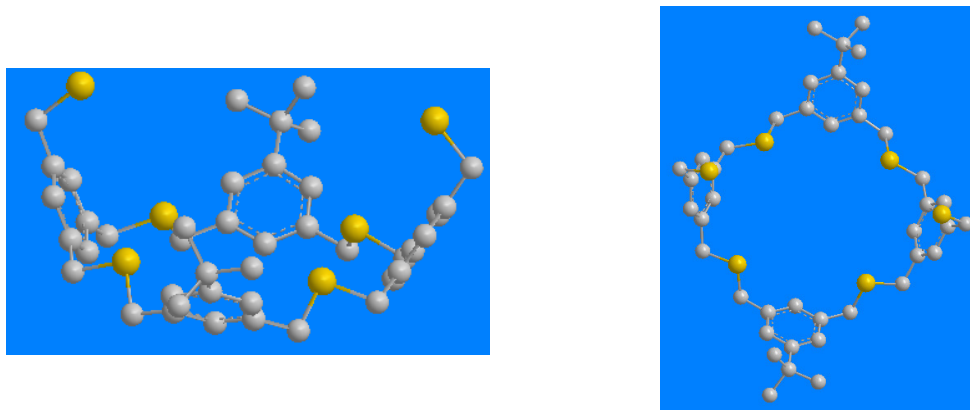


**Figure 3.2.6.** Balls and stick models of minimized energy calculations of ligand **E** with Chem 3D ver 11.0 from side (left) and top (right) view. Sulfur atoms are shown in yellow and carbons in grey colored. Hydrogen atoms were omitted for clarity of the picture.

For the nanoparticles larger than 1.1 nm, there are two possible explanations. First, it was clear from NMR data that TOAB was still present after purification by precipitation, and could therefore help to cover the surface of the nanoparticles which were not covered by the ligands. Alternatively, three or more ligand structures may also template the formation of larger gold nanoparticles.

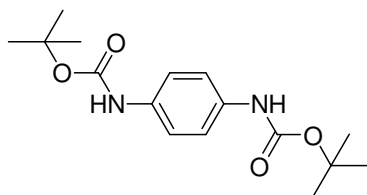
### 3.3 2D assemblies of preorganised molecules

#### 3.3.1 Towards protection group controlled surface chemistry

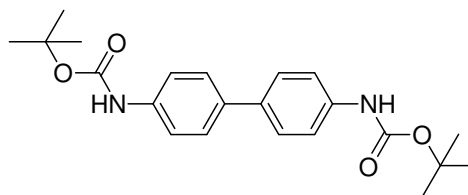
Di-*tert*-butyl dicarbonate (Boc-anhydride; Boc<sub>2</sub>O) is an extensively used reagent for the clean and rapid introduction Boc-protecting group for the amine functionality <sup>[167]</sup>. A *tert*-butyl carbamate (Boc) group is a common protecting group in organic synthesis frequently used in peptide and nucleoside syntheses as well as in heterocyclic chemistry. It is rather stable to hydrolysis under basic conditions and is inert to many other nucleophilic reagents. Deprotection is generally achieved under acidic conditions whereas it can be also obtained under basic conditions only in special cases, where the amine is highly activated, such as a pyrrole <sup>[168]</sup>. Furthermore, thermal deprotection methods have also been reported <sup>[169, 170]</sup>.

Besides common usage as a protection group, Boc groups can also play an important role in the self assembly of molecules by forming intermolecular hydrogen bonds due to the H-bond donor and H-bond acceptor capability. Being thermally cleavable and having self-assembly possibilities due to the H-bonding, Boc protected molecules are not only ideal candidates to arrange ordered structures but also to release active species at well defined positions as building blocks of a network consisting of interlinked deprotected molecules.

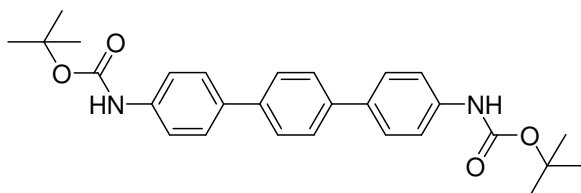
For the investigation of the potential of Boc groups which can act as intermolecular organizers for the formation of well-ordered molecular patterns, several fully Boc protected bi-functional arylamine precursors were synthesized from commercially available diamino precursors using Boc anhydride. The synthesis of fully protected bi-functional arylamine precursors were performed by reacting one equivalent of diamino precursor with three equivalents of  $\text{Boc}_2\text{O}$  in THF using three equivalents of triethylamine as a base. The mixtures were allowed to stir for 16h at RT under Argon. The crude was obtained after workup with water and extracted with DCM. The desired products were isolated by column chromatography in reasonable yields as white powder.



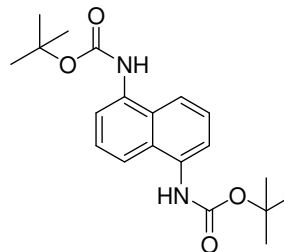
di-tert-butyl 1,4-phenylenedicarbamate, **49**



tert-butyl biphenyl-4,4'-diylidicarbamate, **50**



tert-butyl triphenyl-4,4'-diylidicarbamate, **51**



di-tert-butyl naphthalene-1,5-diylidicarbamate, **52**

**Figure 3.3.1.** Candidates for the formation of well-ordered molecular patterns.

The synthesized molecules potentials for self-assembly and intermolecular network formation were investigated by STM after deposition onto Cu(111) and Ag(111) surfaces.

The investigation of fully protected monophenylamine (**49**) and naphthalene diylldicarbamate (**52**) by STM showed no regular self-assembly pattern on neither Cu(111) nor Ag(111) surfaces. The fully protected triphenylamine (**51**) deposited on the Cu(111) surfaces by sublimation at RT showed self assembled structures. However, due to the changes in STM setup, it was unable to repeat the findings.

On the other hand, *tert*-butyl biphenyl-4,4'-diylldicarbamate, **50**, was successfully deposited to the both Cu(111) and Ag(111) surfaces. Upon deposition of **50** onto the Ag(111) surfaces, the structure of network identified as herringbone rearrangement. In high resolution STM images the bright lobes were assigned to *tert*-butyl groups of **50** while molecular backbone was noticed enabling the identification of the arrangement of individual molecules within the network<sup>[183-184]</sup>.

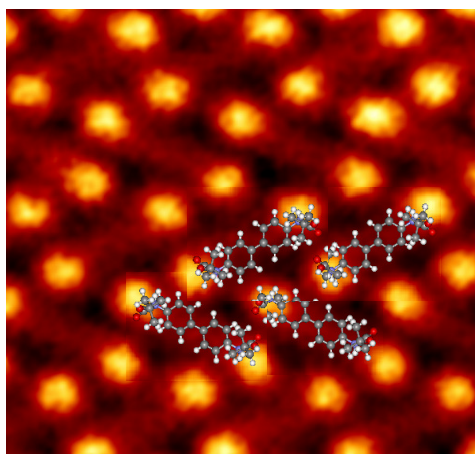


**Figure 3.3.2.** STM image ( $5.2 \times 4.8 \text{ nm}^2$ , 2 V, 20 pA, RT) of **50** on Ag(111).

Alternatively, STM images showed that the Boc protected 4,4'-diaminobiphenyl (**50**) forms two different but similar self-assembled structures for coverage  $\leq 1 \text{ ML}$  onto Cu (111) surfaces.

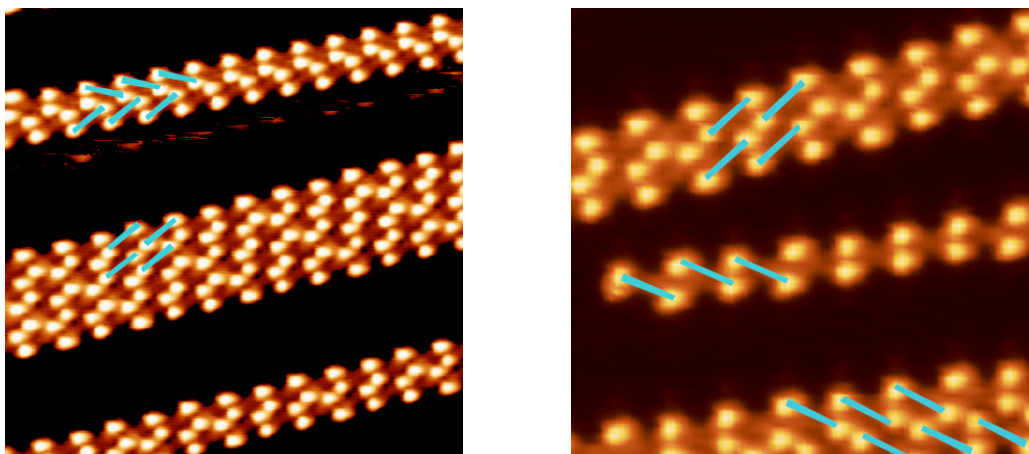


**Figure 3.3.3.** (a) Coexistence of both the parallel and the herringbone arrangements upon submonolayer coverage of **50** on Cu(111) ( $16 \times 16 \text{ nm}^2$ ;  $U_{\text{gap}} = 1.6 \text{ V}$ ,  $I_{\text{tunnel}} = 10 \text{ pA}$ ,  $77 \text{ K}$ ). (b) Closer view of submonolayer coverage of **50** on Cu(111) ( $10.8 \times 10.5 \text{ nm}^2$ ;  $U_{\text{gap}} = 1.21 \text{ V}$ ,  $I_{\text{tunnel}} = 10 \text{ pA}$ ,  $77 \text{ K}$ ).

Atomically resolved STM images showed that the aromatic backbones were oriented along the  $[11\bar{2}]$  direction. This led to determine the evolution of the self assembly of **50** starts with the formation of individual molecular rows which can be considered as the building block for both the parallel and the herringbone arrangements are aligned along the  $[01\bar{1}]$  direction. The position of the individual molecules forming parallel and herringbone arrangements is marked by the blue lines on STM images. The molecules are always located in the same position with regard to the underlying Cu(111) substrate thanks to the arrangement. The molecules within these rows interact with each other via H-bonds between the carbonyl oxygen atom of one molecule and a phenyl hydrogen atom of another molecule where the distance of the  $\text{O}\cdots\text{H}$  bond can be estimated to  $2.3\text{\AA}$ .

As can be seen from STM images of samples with higher molecular coverage, a densely packed arrangement can be reached either by keeping the same orientation of the 1D molecular rows during their assembly or by mirroring every second row at the  $[01\bar{1}]$  direction of the Cu substrate.



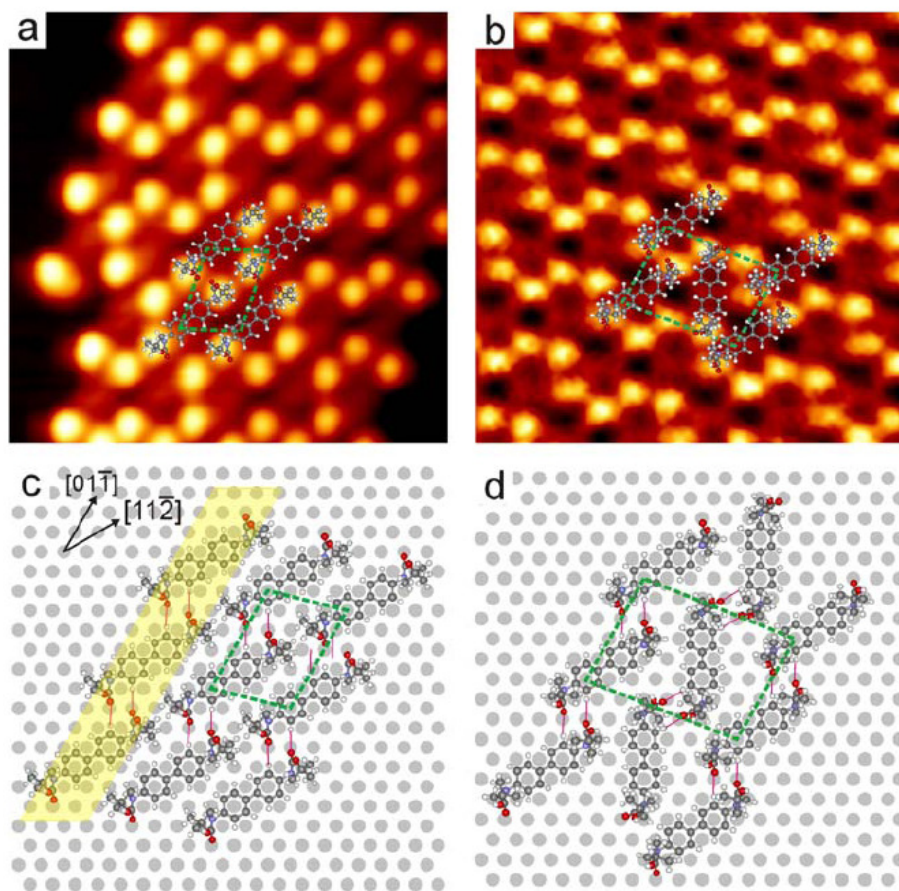


**Figure 3.3.4.** a) Parallel ( $7 \times 7 \text{ nm}^2$ , 10 pA, 1.6 V, 77 K) and b) herringbone ( $7 \times 7 \text{ nm}^2$ , 20 pA, 1.6 V, room temperature) arrangement of **50** on Cu(111). c), d) Suggested models for the two observed assembly structures. The unit cell is marked by green dots. The molecular row highlighted in yellow is the parent stripe motive which is stabilized by H-bonding (red lines) and which leads to both observed arrangements.

To induce intermolecular reactions within the self-assembled monolayers of **50**, temperature was applied as a trigger. It was expected to be able to profit from the rich chemistry of reactive intermediates potentially occurring during the deprotection of the Boc group to interlink the pre-organized molecular building blocks. For this purpose, the samples were heated and subsequently investigated after cooling to room temperature.

Observation of samples of **50** deposited on Ag(111) surfaces showed that after heating the samples at temperatures around  $200^\circ\text{C}$ , chainlike structures indicating the occurrence of a chemical reaction. From the disappearance of bright spots, it is suggested that the BOC groups are released and such, the remaining biphenyl units are interlinked.

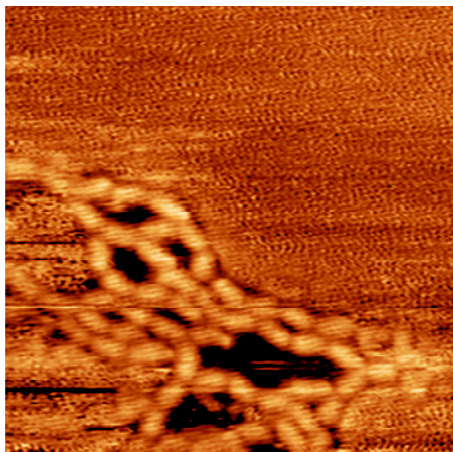


**Figure 3.3.5.** STM images of **50** on Ag(111) after heating samples to  $\sim 200^\circ\text{C}$ . ( $15 \times 15 \text{ nm}^2$ ,  $-1.18 \text{ V}$ ,  $6 \text{ pA}$ , RT).

Noteworthy, a considerable different and periodic molecular pattern was observed after heating the samples of **50** deposited on Cu(111) surfaces to  $196^\circ\text{C}$ . The number of bright spots arising from the bulky *tert*-butyl groups of the Boc protection groups was reduced considerably as expected for the deprotection of the Boc groups by heating.

A new pattern became visible in the upper part of figure 3.3.6 while the lower part shows the herringbone pattern of the doubly Boc protected biphenyl **50** as already observed before the heat treatment. The pattern seems to consist mainly of molecular rods still featuring terminal Boc groups but having about twice the length of the initial biphenyl rod **50**. Apparently, upon heating and subsequently investigated after cooling to RT each monomer loses one Boc group and two of these modified biphenyl units are interlinked towards a dimer. Therefore, a dimerization reaction must have taken place with the molecules immobilized on the surface since the desorption-reaction-readsorption mechanisms are very unlikely or even impossible under UHV conditions.

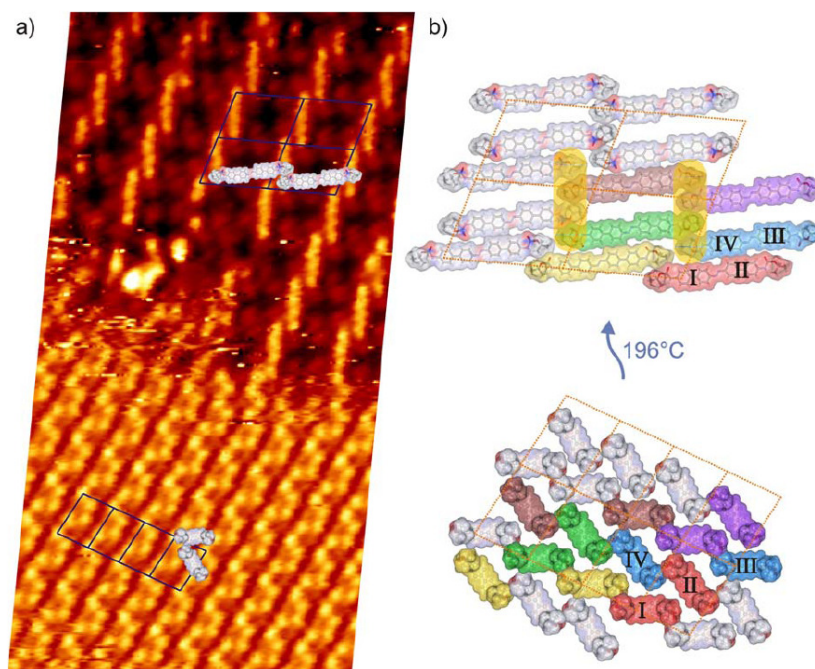


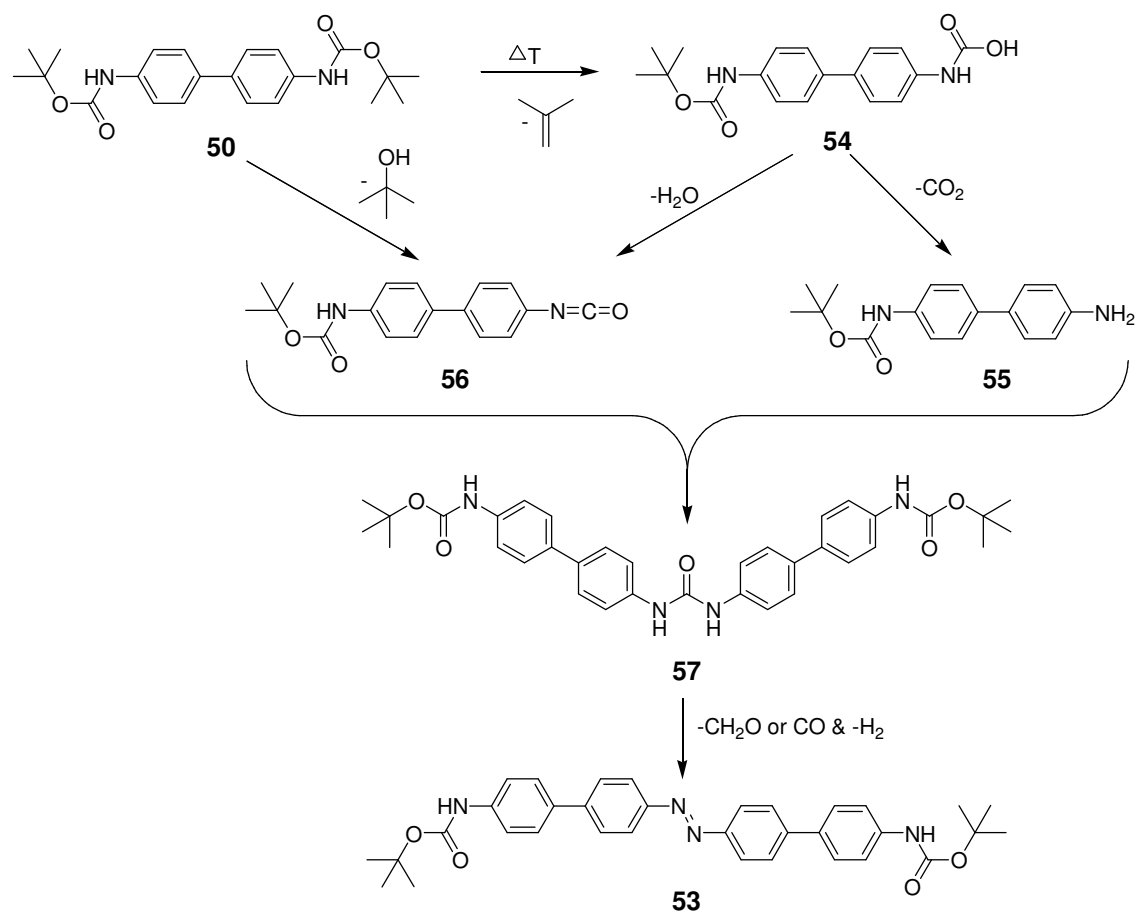
**Figure 3.3.6.** a) STM image ( $24 \times 12 \text{ nm}^2$ , 22 pA, 1.2 V) of **50** on Cu(111) annealed at  $196^\circ\text{C}$ . The drawn in molecules illustrate their arrangement in each of the two patterns. b) Hypothesized dimerization rearrangement of molecules explaining the transition from the herringbone arrangement of **50** to the double row arrangement of **54**.

Both biphenyl dimers must be interlinked quite rigidly since they aligned parallel to each other and parallel to the  $[11\bar{2}]$  direction. It is very probable that the interaction of lone pairs of oxygen of Boc groups and lone pairs of amine groups with the underlying Cu substrate plays an important role for the arrangement. More importantly, perfectly organized rows of dimers were formed as a result of selective deprotection of only one of both Boc groups of **50**. Although deprotection of a single protection group might be a consequence of electronic effects, a selection rule conveyed between the individual molecules was needed to allow the perfect transformation from the ordered monomer pattern into the double row dimer structure. For this, the deprotection of individual Boc groups induced by the spatial rearrangement of the neighboring molecules might be the underlying mechanism. Since a distance of approximately  $2.5 \text{ \AA}$  was measured, the azo structure  $\text{R-N=N-R}$  or the hydrazine structure  $\text{R-NH-NH-R}$  were taken into consideration in order to align both biphenyl subunits.

Considering the stiffness of parallel arrangement of the dimers, azo structure  $\text{R-N=N-R}$  was preferred. In fact, the weak signal corresponding for the linking azo unit  $\text{R-N=N-R}$  in the STM images were in line with the previous reported findings <sup>[188, 189]</sup>.

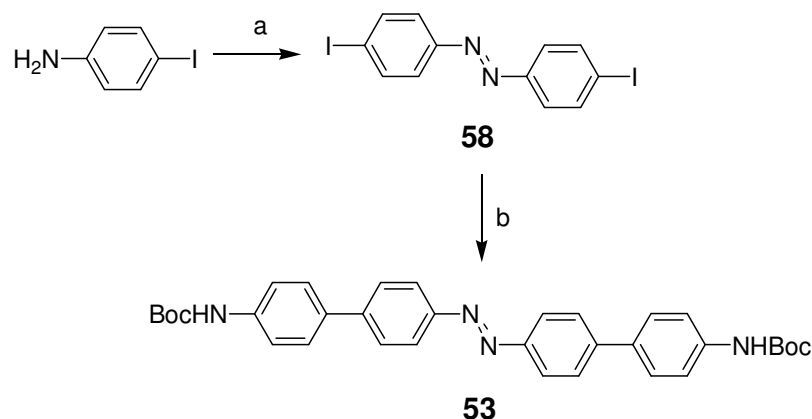
Formation of the dimers and their assembly into the double row pattern which took place via a coupling reaction between pairs of neighboring molecules were demonstrated in a quantitative manner in figure 3.3.6. One of the two subunits forming the dimer stayed in its position (molecules **I** and **III** in the lower part of Figure 3.3.6b), whilst the second rotated approximately 60° on the surface (molecules **II** and **IV**) to react with the first one, thus forming the pairs of dimers. It is plausible that the dimer pairs were stabilized by H-bonds between carbonyl oxygens and hydrogen atoms of the biphenyl core of the molecule <sup>[185]</sup>. Intercalating terminal *tert*-butyl groups separated these dimer pairs from each other.

A possible mechanism for monodeprotection of the **50** and formation of dimer can be explained by loss of isoprene moiety leading the formation of hydroxycarbamate upon heating. Then hydroxycarbamate may be decomposed to amine by decarboxylation or to isocyanate by condensation. Assisted by the coordination of the nitrogen lone-pair of **50** to the metal surface, the isocyanate **56** may even be formed directly by elimination of *tert*-butanol. Subsequently, the free amine **55** may react with the isocyanate **56** to form urea derivative **57** either by removal of formaldehyde or carbon monoxide (CO) and hydrogen. While urea derivatives in solution are rather stable and comparable reactions have not been reported yet, the coordination of CO on the metal surface might assist this reaction step on the metal surface. Furthermore, these hypothesized reaction steps would provide a potential explanation for the observed monodeprotection of **50**. The decreasing electron withdrawing character of the terminal substituents of **54**, **55** and **56** and also reduced electron-withdrawing ability of the central linker of **53** and **57** compared with **50** strengthens the stability of the second BOC protection group, hence providing a chemical argument for the observed monoprotection during the transformation from **50** to **53**.



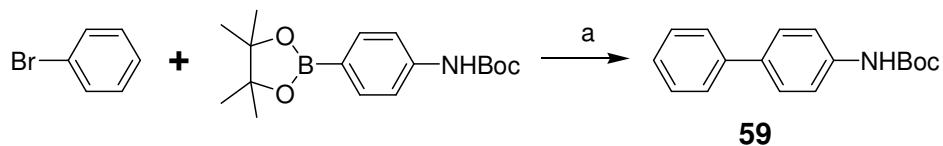
**Scheme 3.3.1.** Hypothesized chemical reaction sequence from the thermal transformation of the monomer **50** to the dimer **53** on the metal surface.

To investigate the chemical processes leading the coupling, azo derivative **53** was synthesized starting from commercially available *p*-iodoamine. 1,2-bis(4-iodophenyl)diazene was synthesized following a reported procedure<sup>[186]</sup>. The oxidation of *p*-iodoamine in refluxing DCM containing one-to-one ratio of  $KMnO_4$ - $FeSO_4$  led to synthesis azo benzene precursor in 18% yield as orange powder. Subsequent Suzuki coupling of 1,2-bis(4-iodophenyl)diazene, azo benzene precursor, with two equivalent of 4-(Boc amino)benzene boronic acid pinacol ester in refluxing toluene-EtOH mixture containing 2M  $Na_2CO_3$  as base yielded the desired orange colored compound **53** in 67% yield by column chromatography.



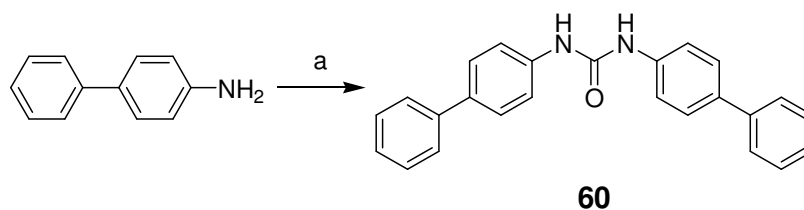
**Scheme 3.3.2.** Synthesis of biphenyl **53** (a)  $\text{KMnO}_4$ - $\text{FeSO}_4$ , DCM,  $\uparrow\downarrow$  18%; (b) 4-(Boc amino)benzene boronic acid pinacol ester,  $\text{Pd}(\text{PPh})_3$ , Toluene-EtOH,  $\text{Na}_2\text{CO}_3$ ,  $\uparrow\downarrow$ , 67%.

However, the deposition of **53** to the metal surface was failed because of its rather low decomposition temperature under UHV conditions. To test the hypothesis, model compounds were synthesized. A mono Boc functionalized biphenyl compound (**59**) was considered over compound **50** to reduce the number of potential reaction products. The model compound **59** was synthesized by Suzuki coupling reaction which conditions described above, between equimolar amounts of tert-Butyl-N-[4-(4,4,5,5-tetramethyl-1,2,3-dioxaborolan-2-yl)phenyl]carbamate (Boc protected amino boron ester) and *p*-bromobenzene. Following the usual workup, the desired compound **59** was obtained with 85% yield by column chromatography as an orange powder.



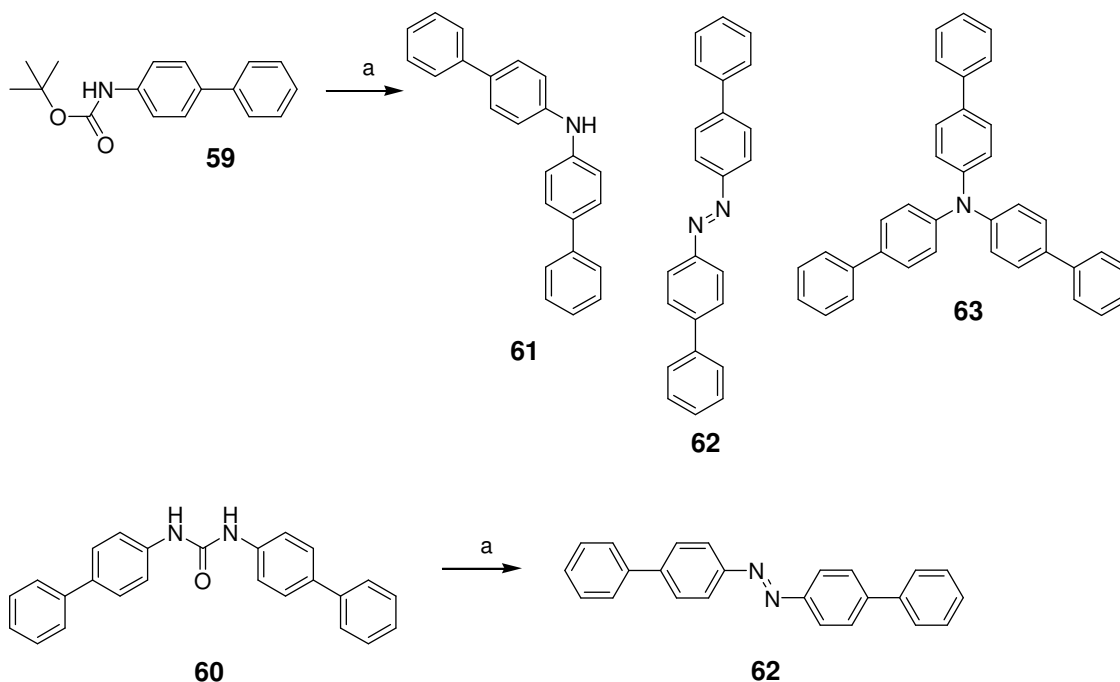
**Scheme 3.3.3.** Synthesis of biphenyl **59** (a)  $\text{Pd}(\text{PPh})_3$ , Toluene-EtOH,  $\text{Na}_2\text{CO}_3$ ,  $\uparrow\downarrow$ , 85%.

On the other hand, the model compound **61** was synthesized by condensation of 4-aminobiphenyl with bis-(trichloromethyl)carbonate (BTC) also known as triphosgene, in DCM at RT. 6 equivalents of 4-aminobiphenyl and 8 equivalents of 4-(dimethylamino)-pyridin (DMAP) was dissolved in DCM. One equivalent of BTC was added dropwise and the reaction mixture was stirred at RT. The formation of white solid was observed after 15 minutes of reaction. The solid was collected and washed extensively with DCM yielding 85% of **60** as white powder.



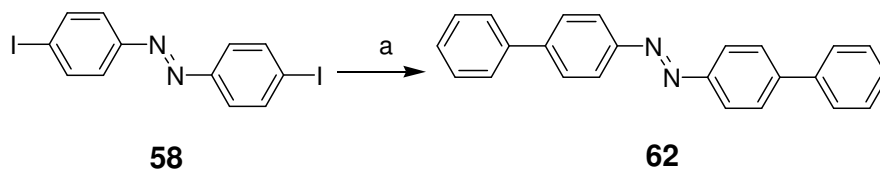
**Scheme 3.3.4.** Synthesis of **60** (a)  $\text{CO}(\text{OCCl}_3)_2$ , DMAP, DCM, RT 85%.

After the successful synthesis of both of the model compounds **59** and **60**, they were separately adsorbed on Ag nanoparticles and were heated under reduced pressure (0.1 mbar) to 200 °C for 6h to investigate the chemical processes leading to coupling under UHV conditions. Ag-particles have been preferred instead of Cu-particles as the surface purity of the later turned out to be troublesome due to oxidation processes. Three main reaction products were isolated by preparative thin layer chromatography (TLC) of the  $\text{CH}_2\text{Cl}_2$  extract of the particles. The MALDI-TOF spectra of the products showed signals corresponding to the structures **61-63**, thus supporting the formation of new N-N and N-C bonds under the reaction conditions.



**Scheme 3.3.5.** Simulation of surface reactions: Reaction products obtained by thermal decomposition of **59** on Ag nanoparticles. Thermal degradation of the urea derivative **60** to the azo derivative **62** on Ag nanoparticles. a) Ag(0), 0.1 mbar, 200 °C.

To support the hypothesized reaction sequence displayed in scheme 3.3.5 the so far unprecedented step from the urea derivative **57** to the azo derivative **53** was of particular interest. Indeed, a model reaction of urea **60** on Ag-particles under reaction conditions described above led to the formation of azo derivative **62** being identified by reversed phase HPLC as a reaction product in DMF extract. For the comparison of molecules, azo derivative **62** was synthesized following previously mentioned Suzuki coupling reaction conditions using two equivalents of phenylboronic acid pinacol ester and one equivalent previously synthesized 1,2-bis(4-iodophenyl)diazene. After overnight reaction, the solvent was removed, the crude dissolved in DCM and washed with water. The orange colored pure product was obtained by column chromatography with 85% yield.



**Scheme 3.3.6.** Synthesis of biphenyl **62** (a) phenylboronic acid pinacol ester, Pd(PPh)<sub>3</sub>, Toluene-EtOH, Na<sub>2</sub>CO<sub>3</sub>, ↑↓, 85%;

The analysis of the compounds and extracts is investigated by reverse phase HPLC. All three compounds have a common maximum absorption at 284 and 362nm. However, urea derivative **60** has a poor absorption at 362 nm. Hopefully, a much stronger signal can be recorded at 284nm. The analysis of the extracts displayed three main compounds: unreacted starting material **60**, an unknown reaction product and the expected azo derivative **62** supporting the idea of conversion of urea compound (**60**) to diazo compound **62** under UHV conditions. The unknown reaction product may be oligomeric derivatives of diazo compound **62** which are observed as cross or longer linear structures after heating samples to  $\geq 198^\circ\text{C}$ .



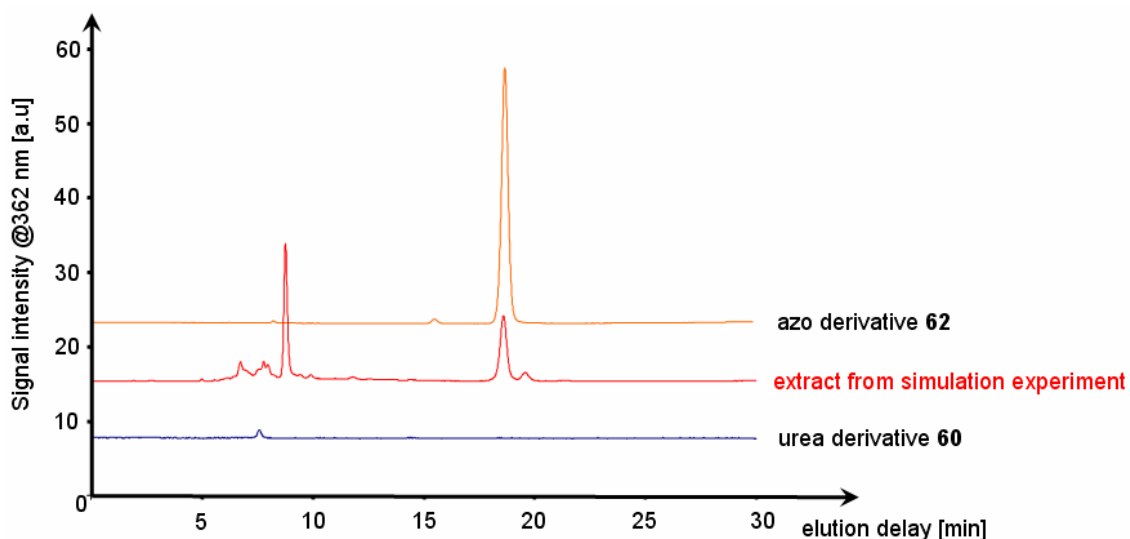


**Figure 3.3.7.** Reversed phase HPLC ( $\text{CH}_3\text{CN}$ , flow 0.4ml/min,  $\lambda_{\text{det}} = 362 \text{ nm}$ ,  $t = 25^\circ\text{C}$ ) of the azo derivative **62** (top), the DMF extract of the Ag nanoparticles (middle in red) and of the urea derivative **60** (bottom).

The formed dimer **53** has also two terminal Boc protected amines like **50** and they are in close proximity in the double-row arrangement. Therefore, the dimer **53** can be further react to give longer structures by applying higher temperatures. As expected, the formation of more complex interlinked structures surrounded by a mobile phase was observed by heating of **53**  $\geq 198^\circ\text{C}$  and subsequently investigated after cooling to RT<sup>[184, 187]</sup>.

Although, the structure of **53** and the structures of the resulting covalently linked molecules observed after heating  $\geq 198^\circ\text{C}$  and subsequently investigation after cooling to RT showed very interesting images, unfortunately, the very low yield and polymeric nature of the products prevented to their analysis by traditional surface techniques.

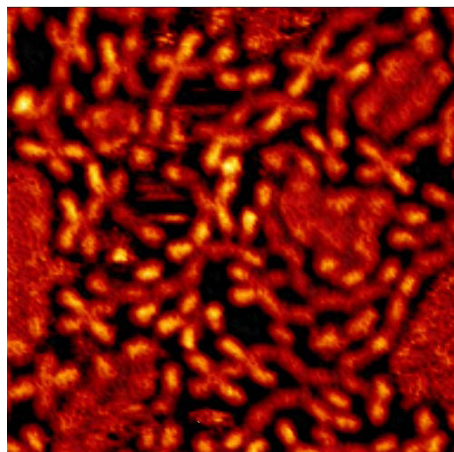


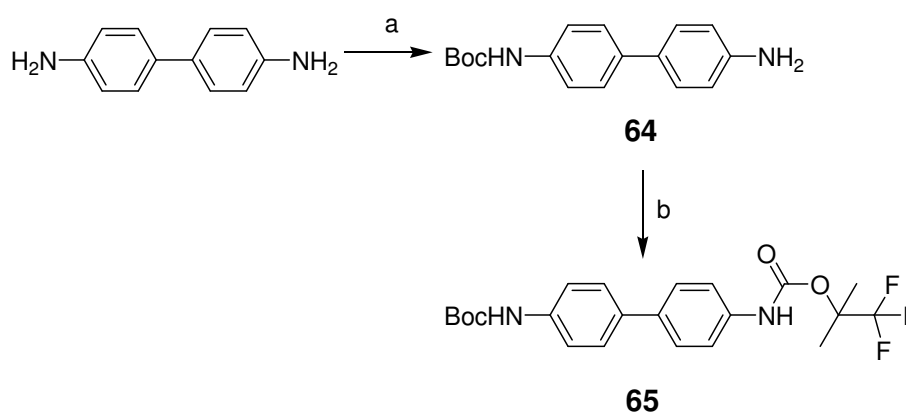
**Figure 3.3.8.** STM image ( $15 \times 15 \text{ nm}^2$ , 1.2 V, 20 pA) of 50 on Cu(111) annealed at temperatures  $> 198^\circ\text{C}$ . Chains and cross type structures consisting of interlinked biphenyl subunits were formed.

### 3.3.2 Towards the selective cleavage of protection group for controlling length of the interconnected structures

After these preliminary promising results, the selective cleavage of Boc protection groups which may lead to control of the length of the interconnected structures were investigated. If the cleavage of Boc groups can be performed in distinct temperatures, the length of the interconnected structures can be controlled. For this reason, one of the Boc groups should be cleaved at lower or much higher temperature than the other one. Increasing the cleavage temperature for Boc group is not only difficult to achieve while keeping the structure similar to original but also may lead problems during the evaporation of molecules for deposition on to the surfaces. On the other hand, reducing the cleavage temperature of one Boc groups can be achieved easily by replacing some of the hydrogen atoms with fluorine atoms. Fluorine containing compounds are well known for their reduction of melting or evaporating temperatures of molecules comparing to their non-fluorinated counterparts. For example, fluorides have been used in the past to reduce the melting temperatures of metals and ores, and to help them flow. Another advantage of fluorine atoms is not only its similar size to hydrogen atoms but also their ability to form H-bonding.

In the light of these information above, the desired molecule can be easily accessible by mono Boc protecting commercially available 4,4'-diaminobiphenyl (a.k.a. Benzidine) and following the nucleophilic substitution of remaining free amino site with fluorinated Boc derivative.

First, the synthesis of mono Boc protected benzidine derivative (**64**) was achieved using equimolar of benzidine and Boc anhydride in presence of one equivalent of triethylamine as a base in THF. The mixture was stirred overnight at RT under Argon. After usual workup with water and extraction with DCM, mono Boc protected benzidine derivative was obtained with 47% yield by column chromatography as white powder. For the synthesis of **65**, the remaining free amino site of **64** is reacted with 1,1,1-trifluoro-2-methylpropan-2-ol in presence of BTC following the procedure described above thus yielding 89% of **65** as white powder.



**Scheme 3.3.7.** Synthesis of **65** (a)  $\text{Boc}_2\text{O}$ ,  $\text{Et}_3\text{N}$ , THF, RT, 47%; (b) 1,1,1-trifluoro-2-methylpropan-2-ol,  $\text{CO}(\text{OCCl}_3)_2$ , DMAP, DCM, RT 89%.

Being the most electronegative element, replacing some hydrogen atoms of Boc group with fluorine atoms will affect the electron density of the whole molecule making slightly polar. The fluorinated Boc group of a molecule will be much more electronegative comparing to the non fluorinated Boc group. Therefore, one can expect that the fluorinated Boc groups will display more brightness than non fluorinated counterparts. Moreover, a head-to-tail coupling of monomers on the surface can be expected as a result of different polarity of Boc groups.

**65** was deposited at room temperature on both Cu(111) and Ag(111) surfaces for determination of self assembly pattern on the surfaces.

Upon deposition of **65** onto Ag(111) surface, the structure of network was identified as herringbone arrangement. However, the herringbone arrangement is not fully periodic displaying double and triple rows. The  $\text{O}\cdots\text{H}$  distance of neighboring molecules was

measured  $\sim 2.7$  Å. The evolution of the pattern starts with the formation of molecular blocks shown by green arrows as described the molecular model below. The formation of intermolecular H-bonding between the fluorinated Boc group of the molecule with the non-fluorinating end of the neighboring molecule which is parallel was observed. On the other hand, the formation of H-bonding between the fluorinated Boc groups of perpendicularly oriented neighboring molecules was observed too.

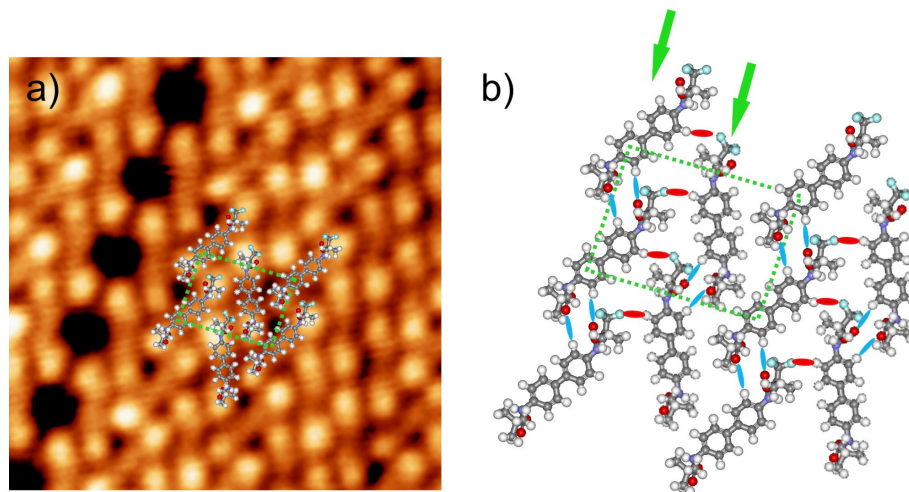


**Figure 3.3.9.** a) STM image ( $8 \times 8$  nm<sup>2</sup>, 1.7 V, 20 pA, RT) of the **65** adsorbed on Ag(111). b) The tentative molecular model shows molecular building blocks in green, hydrogen bonds blue for O...H red for F...H.

It should be noted that the formation of parallel arrangements in double or triple rows were also observed in addition to herringbone arrangement of **65** on Ag(111) surfaces.

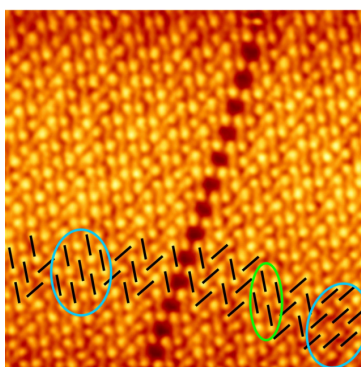


**Figure 3.3.10.** High resolution STM image of **65** on Ag (111) surface. Double row herringbone arrangement marked with green circles while triple row arrangements with blue circles ( $20 \times 20$  nm<sup>2</sup>, 1.7 V, 20 pA, RT).

On the other hand, molecules of **65** deposited on Cu(111) surfaces showed a parallel arrangement similar to the results obtained for double Boc protected biphenyl **50**. The STM images indicates that the intermolecular H-bonding were formed between the fluorinated Boc group of a molecule with the hydrogen of phenyl ring attached to the non-fluorinating Boc group of neighboring molecule resulting head-to-tail coupling of monomers.

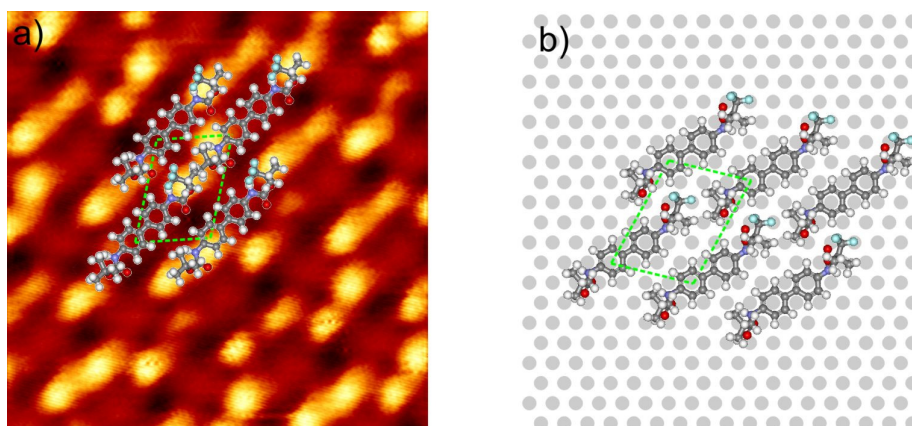


**Figure 3.3.11.** a) STM image ( $6 \times 5.9 \text{ nm}^2$ ,  $-1.8 \text{ V}$ ,  $20 \text{ pA}$ , RT) of biphenyl **65** adsorbed on Cu(111) and b) the tentative molecular model.

After the deposition of **65** onto Ag(111) and Cu(111) surfaces, the samples were heated and subsequently investigated upon cooled to room temperature to determine the temperature of formation of interlinked molecules.

It was found that the herringbone pattern formed during deposition onto the Ag(111) surfaces evolved into completely new arrangements after heating samples to around  $150^\circ\text{C}$ , much lower than its non fluorine containing counterpart, **50**, as expected. The formation of dimeric structures was observed. It is suggested that the fluorinated Boc group cleaves first due to the reasons explained previously and the formed unstable compounds react with the neighboring molecule resulting the formation of a dimer. The length of dimers is measured  $\sim 2.1 \text{ nm}$  which is also in good agreement with twice of the biphenyl unit length.

While dimeric structures are observed in majority after heating samples up to  $160^\circ\text{C}$ , some biphenyl units are observed to be linked up into even longer structures (between  $160\text{--}170^\circ\text{C}$ ). It is probable that dimers and trimers were forming spontaneously on the substrate surface. Longer structures, probably trimers, of **65** which were assembled in small islands were observed. The formation of trimeric structures assembled in a parallel pattern due to

the H-bonding interactions similar to dimeric arrangements was observed by heating samples at 168°C and subsequently investigation after cooled to room temperature. Mainly paralleled arrangement of trimeric structures was observed on STM images. Boc groups separated with a darker backbone were measured  $\sim 3.2$  nm consisting with the length of three interconnected biphenyl units.

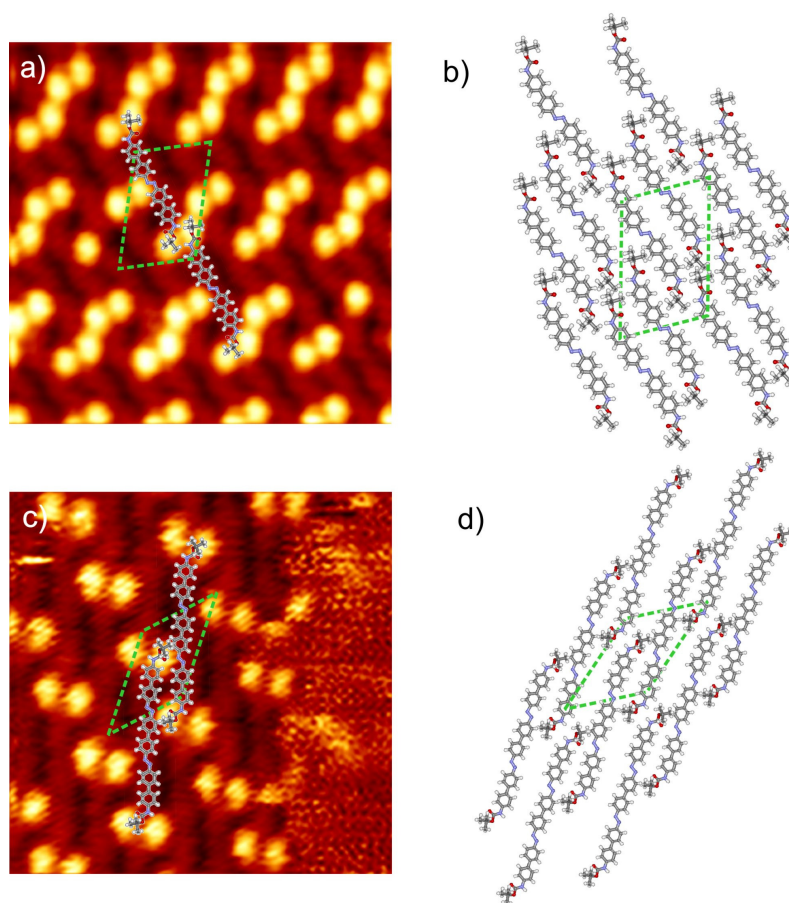


**Figure 3.3.12.** a) STM image of the dimeric arrangement of biphenyl **65** on Ag (111) after annealing the sample at 160°C ( $8 \times 8$  nm<sup>2</sup>, -1.8 V, 20 pA, RT), and b) corresponding molecular model. c) STM image of the trimeric structures formed after annealing the sample at 168°C ( $8 \times 8$  nm<sup>2</sup>, -1.9 V, 20 pA, RT), and d) schematic representation of the arrangement.

For temperatures larger than 168°C a considerable free space on the surface, some larger structures probably representing oligomers of **65** and small islands consisting of only trimeric structures were observed.

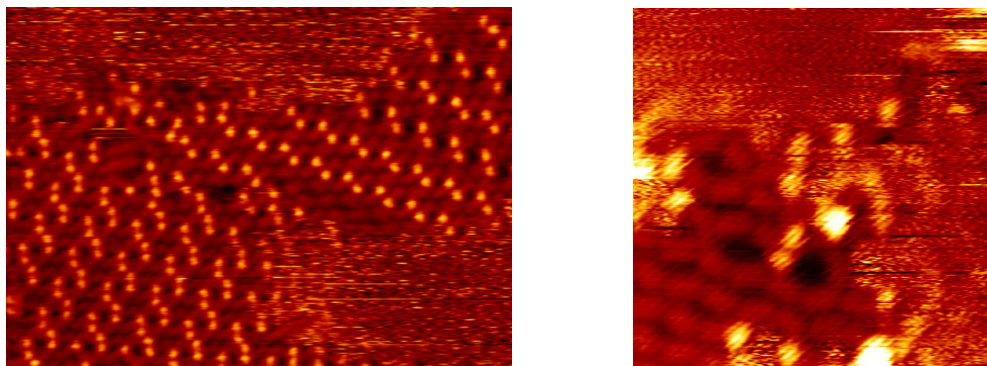


**Figure 3.3.13.** (a) STM image of **65** the surface after annealing the sample at 160°C showing the coexistence of dimeric and trimeric structures ( $24.9 \times 17.8 \text{ nm}^2$ , -1.9 V, 20 pA, RT). (b) Longer chains obtained after annealing **65** at 168°C. ( $10 \times 10 \text{ nm}^2$ , -1.9 V, 20 pA, RT)

The formation of longer molecules step by step may be possible if the fluorinated Boc group of a molecule cleaves first leaving a free amine behind which may then react the Boc protected side of the neighboring molecule. Therefore, **65** can form a dimer could be similar to its monomer, containing a Boc and a fluorinated Boc groups on opposite ends of the molecule, while being heavier than **50**. The increase of molecular length will not only reduce the dipole difference but also increased molecular weight will improve the stability of Boc groups by making their cleavage much more difficult than the monomer. Nevertheless, selective cleavage of fluorinated Boc group of the dimer can be still possible and may lead to trimer formation. Therefore, one can expect that the number of fluorine atoms will reduce due to the increase on number of cleaved fluorinated Boc groups. For this reason, **65** on Ag(111) surfaces were investigated by XPS at different temperatures. It was found that the number of fluorine atoms decreased drastically as a result of the desorption of the fluorinated Boc groups due to a dramatic decrease of the fluorine peak after treatment of the samples at elevated temperatures.

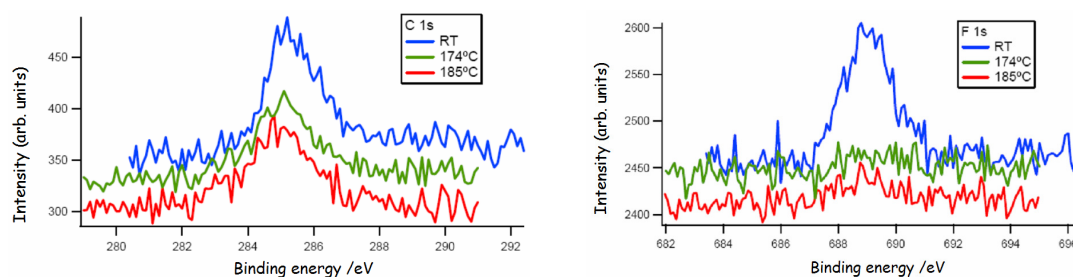


**Figure 3.3.14.** XPS measurements of **65** on Ag(111) at different annealing temperatures

The only parallel arrangement of samples observed on Cu(111) at RT were stable up to 150°C. Above this temperature, a new periodic pattern consisting of molecular rods which were measured twice the length of **65**, appeared which was stable in a wide temperature range of 150-180°C. It is the same dimeric arrangement obtained from biphenyl **50** after heat treatment at elevated temperatures. These dimers were probably arranged similar to the ones obtained before the heat treatment and showed the consistency with previous findings using biphenyl **50**. The dimers were held together thanks to the H-bonding between the carbonyl oxygen and hydrogen atoms of the biphenyl core of neighboring molecules.

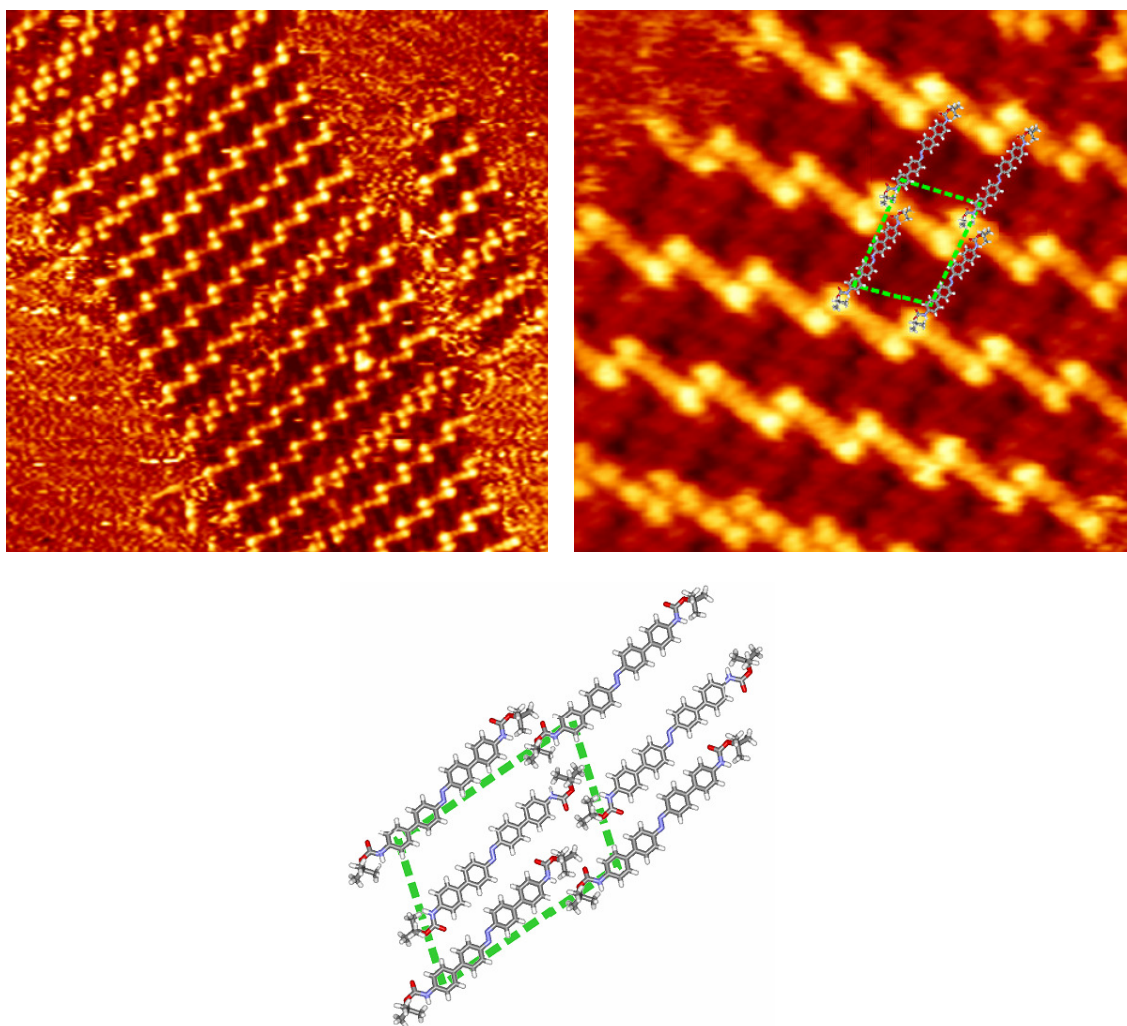


**Figure 3.3.15.** The STM images of **65** on Cu(111) surfaces (a) treated with heat at 157°C (30 x 30 nm<sup>2</sup>, 22 pA, 1.2 V) (b) treated with heat at 167°C. (11 x 11 nm<sup>2</sup>, 22 pA, 1.2 V). Below, the tentative model which represents the arrangement of the molecules.



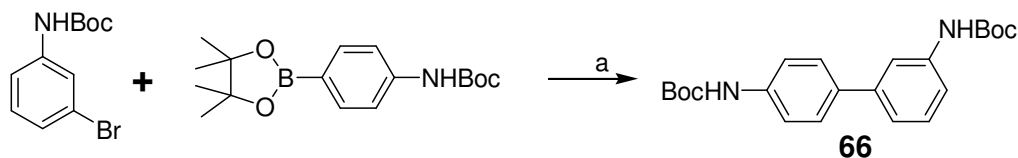
In short, the molecules of **65** deposited on Cu(111) was started to react with each other at 157°C. The formation of similar dimeric interlinked structures for **65** was observed at 167°C, much lower than its non fluorinated counterpart, **50**, as expected due to the reduction in melting temperature thanks to the fluorine atoms. Further heating of the samples led to decomposition of the structures. Although, the formation of interlinked structures of **65** happened at lower temperatures than **50** proved that the cleavage of fluorinated Boc group and formation of dimers happening first, the longer interconnected structures can not be observed.

On the other hand, the formation of interlinked dimeric structures of **65** on Ag(111) surface was observed at 160°C, 7°C lower than the ones on Cu(111) surfaces. The similar double row pattern for dimers of compound **50** on Cu(111) surface was detected. Surprisingly, the formation of linear trimers were observed upon heating the samples to 168°C which is very close to the temperature where dimer formation of **65** on Cu(111) surfaces. However, formation of trimer was unique to the **65** on Ag(111) surfaces. A linear trimer formation was neither observed for compound **50** on Cu(111) surface nor compound **65** on Cu(111) surface.

### 3.3.3 Self-Assembly pattern of asymmetric thermally inter-linkable structure

Until now, the self assembly of the symmetric or pseudo symmetric Boc protected biaminophenyl molecules on the Cu(111) and Ag(111) surfaces were investigated. The interlinking mechanisms of molecules were discussed in details. Moreover, the selective cleavage of Boc groups was succeeded by substituting some hydrogens of one Boc groups by fluorine atoms. Another possibility to perform selective cleavage of Boc groups could be achieved by changing positions of Boc groups. It is expected that the para positioned Boc group may cleave before the meta positioned Boc group due to the electronic reasons, thus by synthesizing asymmetric Boc protected biaminophenyl molecules. Moreover, 2D networks of asymmetric Boc protected biaminophenyl molecules could show different arrangement than symmetric or pseudo symmetric Boc protected biaminophenyl molecules due to the difference on their structures. Therefore, asymmetric Boc protected biaminophenyl molecules were synthesized to get a complete understanding about the self assembly and interlinking mechanism on Cu(111) and Ag(111) surfaces.

The asymmetric Boc protected biaminophenyl, di-*tert*-butyl biphenyl-3,4'-diyldicarbamate (**66**) was synthesized easily from commercially available *N*-(*tert*-Butoxycarbonyl)-3-bromoaniline and 4-(*N*-Boc-amino)phenylboronic acid pinacol ester by Suzuki reaction with 92% yield following similar procedures described before.



**Scheme 3.3.8.** Synthesis of asymmetric derivative of **50** (a) Pd(PPh)<sub>3</sub>, Toluene-EtOH, Na<sub>2</sub>CO<sub>3</sub>, ↑↓, 78%

Then asymmetric Boc protected biaminophenyl (**66**) was deposited on both Cu(111) and Ag(111) surfaces at room temperature and the samples were investigated by STM.

For low coverage of molecules of **66** on Ag(111) surface chain like structures and hexamers (flower like structures) were observed. The molecular chains were distributed randomly on the surface and exhibited no influence of the underlying silver substrate. The different conformations of the molecular chains formed by individual molecules of **66** were observed by STM.

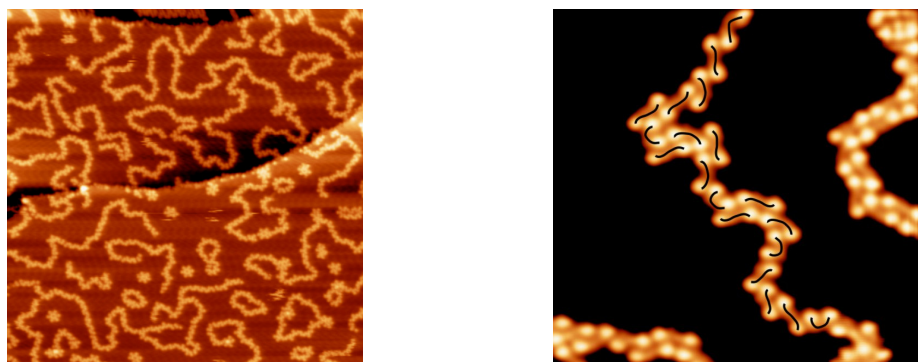


**Figure 3.3.16.** (a) Overview image of the molecular chains and flowers of **66** on Ag(111) formed at low coverage (100 x 100 nm<sup>2</sup>, 1.8 V, 20 pA, 77 K). (b) Randomly oriented single molecular rows with different molecular conformations. (15 x 14 nm<sup>2</sup>, -1.57 V, 20 pA, 77 K).

The flower like structures can clearly be identified that consisting of 6 molecules of **66**, thus revealing a six-fold symmetry. This hexamer has a side of length around 10Å. In order that a hexagon to be formed structure by intermolecular H-bonding interactions in a circular

arrangement; the two carbonyl oxygen atoms of the monomers should point to the opposite directions. As a result, the structures stabilized by 12 H-bonds between carbonyl oxygen and the phenyl hydrogen atoms of each neighboring molecule where the O...H distance is measured to be  $\sim 3$  Å.

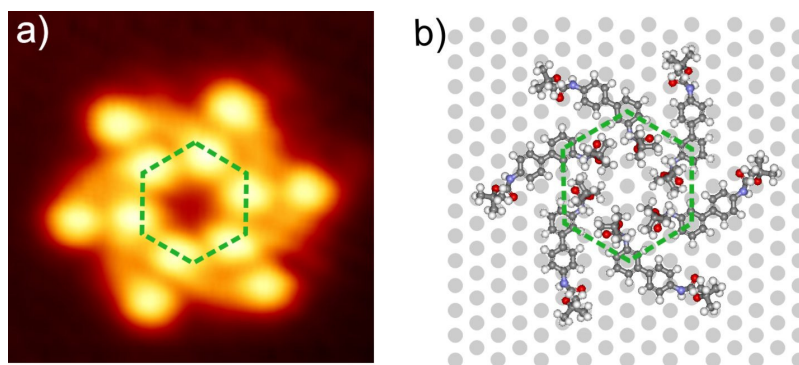


**Figure 3.3.17.** a) Closeup view of a hexamer consisting of six individual molecules of **66** ( $4.7 \times 4.7$  nm<sup>2</sup>, -1.57 V, 20 pA, 77 K). b) The tentative molecular model.

When increasing coverage of **66**, chains formed by double rows lying parallel to each other were observed. The uniformly arranged molecules showed same conformations in contrast to the arrangements at low coverage. Such a double row can be considered as a building block for the formation of the densely-packed arrangement at higher coverage due to the H-bonding interactions between the oxygen of carbonyl groups and hydrogens of phenyl rings.

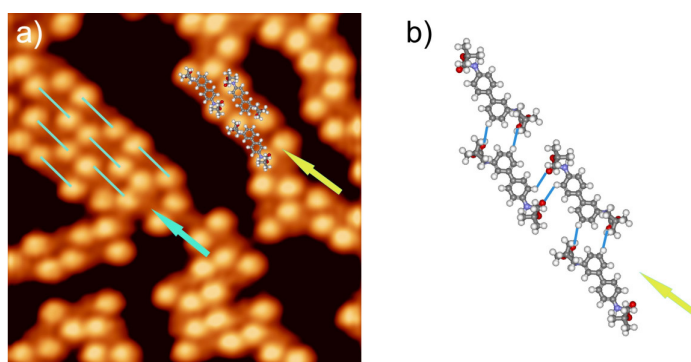


**Figure 3.3.18.** a) STM image of the molecular pattern at 0.5 ML ( $10 \times 10$  nm<sup>2</sup>, 1.57 V, 20 pA, 77 K). Evolution of the densely packed arrangement starts with the formation of double rows. A few molecules are inserted in the double row shown with a yellow arrow. The arrangement shown with a blue arrow is formed by the packing of two double rows and is a close-packed parallel arrangement which evolves into bigger islands at high coverage. b) Molecular model of the double row.

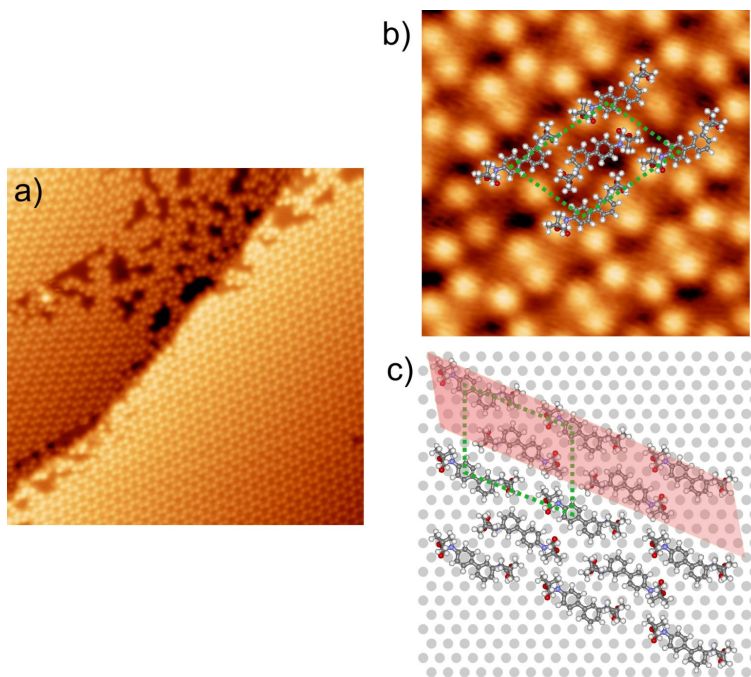


**Figure 3.3.19.** a) Overview of the close-packed parallel arrangement of biphenyl **66** on Ag(111) surface ( $40 \times 40 \text{ nm}^2$ , 1.2 V, 20 pA, 77 K). b) Molecules superimposed to the STM images ( $5.7 \times 5.7 \text{ nm}^2$ , 1.3 V, 20 pA, 77 K). c) Schematic representation of the arrangement double molecular row is highlighted by a red stripe.

To induce intermolecular reactions within the self-assembled monolayers of biphenyl **66**, temperature is exploited as a trigger for deprotection of Boc groups, as in the previous cases (biphenyl **50** and **65**).

The formation of new structures was observed when the samples was heated to  $155^\circ\text{C}$  and subsequently investigated after cooling to RT. It is clearly visible that the number of bright dots which correspond to the Boc groups was reduced along these rows indicating an interlinking of monomers into longer structures. The structure along the row at the border lying next to a monomer (indicated by a blue arrow) had twice the length of the monomer, hence corresponded to a dimer. On the other hand, the row inside the network was exclusively formed by the dimers that were rotated by  $180^\circ$  with respect to the neighboring dimer (indicated by a red arrow).

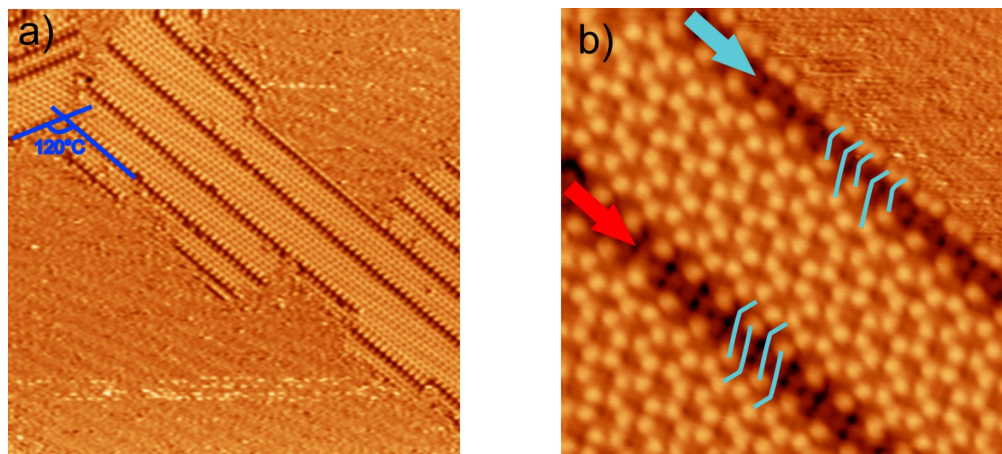


**Figure 3.3.20.** a) STM image of the structures which follow the principle directions of the underlying Ag(111) substrate ( $80 \times 80 \text{ nm}^2$ ,  $-1.94 \text{ V}$ ,  $20 \text{ pA}$ , RT). b) Mixture of monomers and dimers (indicated by red and blue arrows) of **66** ( $15 \times 15 \text{ nm}^2$ ,  $-1.94 \text{ V}$ ,  $20 \text{ pA}$ , RT).

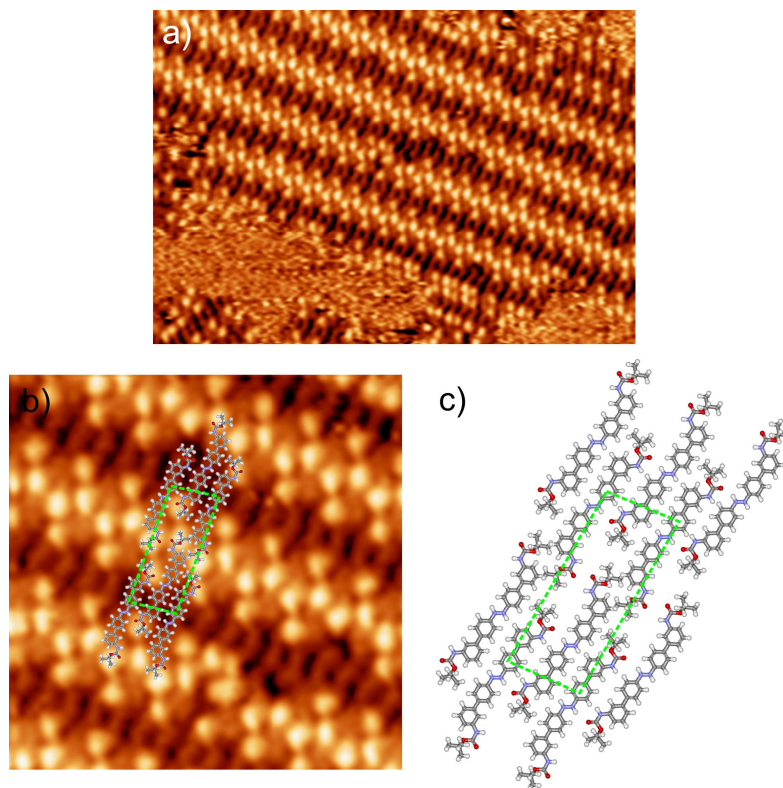


**Figure 3.3.21.** a and b) Dimers of **66** with different zoom view ( $29.8 \times 20.8 \text{ nm}^2$ ,  $-1.9 \text{ V}$ ,  $20 \text{ pA}$ , RT) ( $10 \times 10 \text{ nm}^2$ ,  $-1.9 \text{ V}$ ,  $20 \text{ pA}$ , RT). c) The tentative molecular model.

The dimers reacted further and revealed longer structures upon increasing the temperature to  $168^\circ\text{C}$ . It is probable that a monomer which loses a Boc group at para position forms an

unstable complex and reacts with two meta positioned Boc group containing dimer to form a trimer which has two meta positioned Boc group.

Similar dimeric and trimeric structures were previously obtained after annealing the self-assembled monolayers of biphenyl **50** and **65**. However, the dimeric pattern obtained after deprotection of biphenyl **66** displayed a distinct appearance in the STM images owing to the asymmetric shape of the molecule. Therefore, by selecting proper reaction temperature, it is possible to form well ordered 2D network structures mainly consisting of monomers, dimers or trimers.

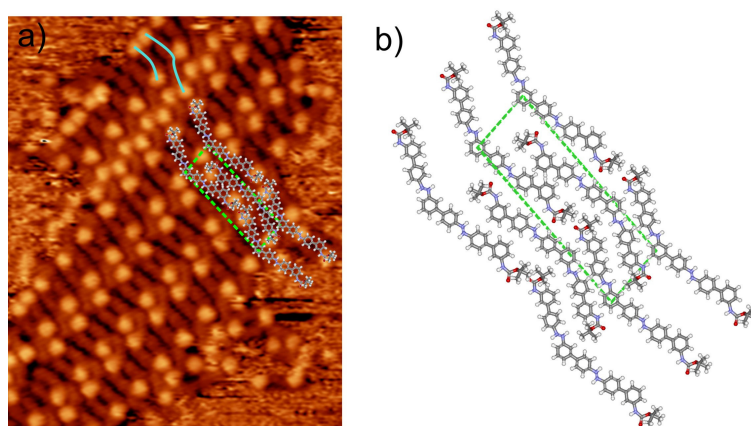


**Figure 3.3.22.** a) STM image of the trimeric structure at 168 °C. Monomers and dimers are marked in blue lines ( $13.6 \times 16.8 \text{ nm}^2$ , -1.9 V, 20 pA, RT) b) Tentative molecular model of the trimeric arrangement.

At low coverage, the molecules of **66** on Cu(111) organize mainly into double rows (building block) in which they are arranged in a parallel fashion with the same molecular conformation in contrast to their curved and disoriented chains on Ag(111) surfaces. Apart from this observation, the flower like structures are found to exist more frequently on Cu(111) surface.

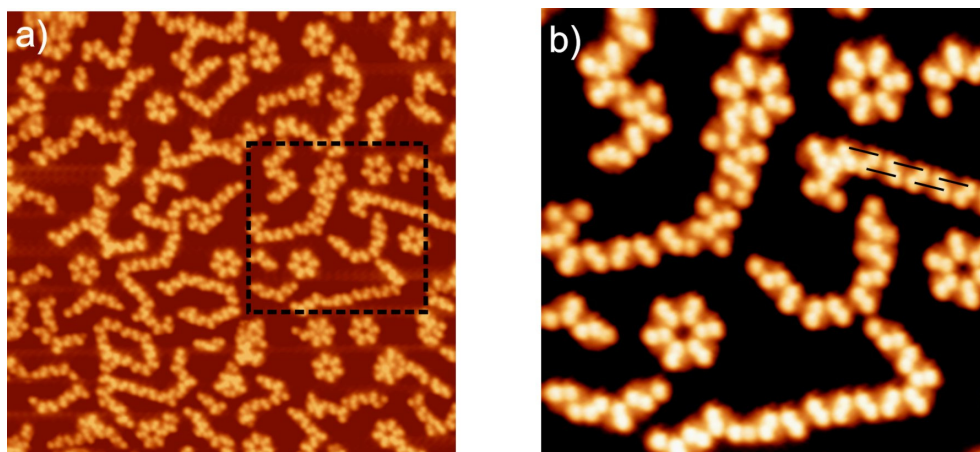


**Figure 3.3.23.** a) Chains and hexamers at low coverage on Cu(111) surfaces ( $50 \times 50 \text{ nm}^2$ , 1.1 V, 20 pA, 77 K). b) Closer view of molecules of **66** forming double rows marked in black lines in (a) ( $20 \times 20 \text{ nm}^2$ , 1.5 V, 20 pA, 77 K).

Further investigation of flower like structures on Cu(111) surfaces revealed that the molecules introduce a chiral signature to the hexameric structures. While the left hexamer are rotated counterclockwise, the molecules in the right hexamer are rotated in the opposite direction.

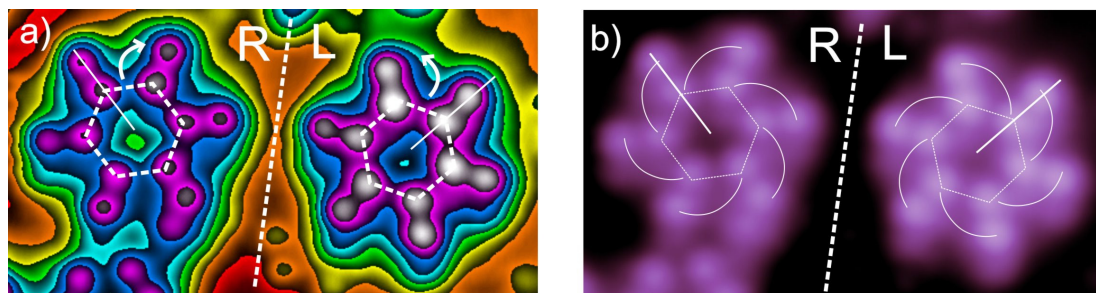


**Figure 3.3.24.** a) Enhanced STM image of left and right hexamers b) STM image in (a) with a normal contrast. ( $8.5 \times 4.7 \text{ nm}^2$ , 1.58 V, 20 pA, 77 K).

The growth mechanism of supramolecular structures of biphenyl **66** exhibited difference when formed on Cu(111) and Ag(111) surfaces. The randomly distributed chains displayed a better ordering and the hexamers mainly formed on Cu(111) at low coverage. The number and lengths of chains as well as the number of hexamers increased with increasing coverage density of molecules. Small islands of self-assembled molecules of **66** formed close to monolayer of molecules was deposited onto Cu(111) surfaces. On Ag(111) surfaces, the molecules started to form the parallel arrangement even at low molecular densities. When the coverage densities were increased, the 2D network arrangement of

molecules filled completely Ag(111) surfaces. On the other hand, molecules prefer to form only the chains formed by double rows and the hexameric structures on Cu(111) until all the free spaces between these structures are filled. This result indicated a random distribution of the chains and the double rows over the surface and no periodic order at high coverage.

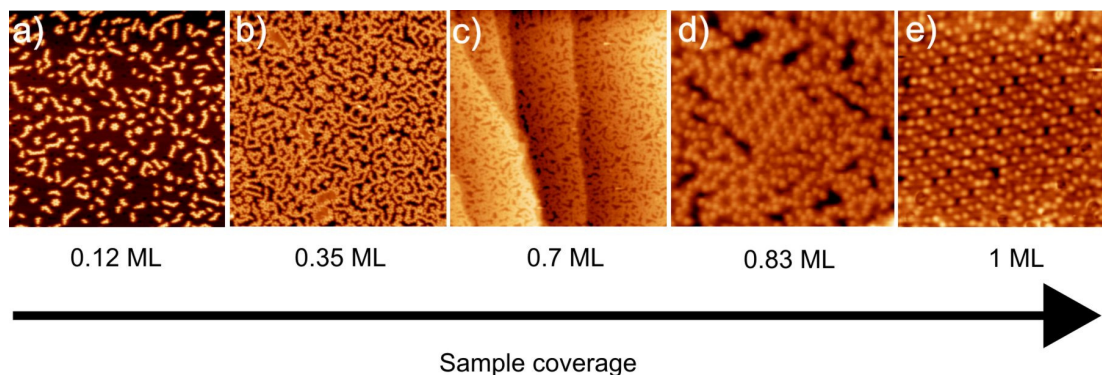


**Figure 3.3.25.** a) to e) Coverage dependent growth of self-assembled structures of **66** obtained by repeatedly adding molecules on Cu(111) surface. a) b) and c) ( $100 \times 100 \text{ nm}^2$ , 1.65 V, 20 pA, 77 K). (100 x 100 nm<sup>2</sup>, 1.65 V, 20 pA, 77 K). d) ( $19 \times 18 \text{ nm}^2$ , 1.6 V, 20 pA, 77 K (e);  $15 \times 15 \text{ nm}^2$ , -1.26 V, 20 pA, 77 K).

A closer look to these arrangements reveals that the molecules interact with each other dominantly in a parallel manner by H-bonds whereas a herringbone arrangement can be observed at some regions.

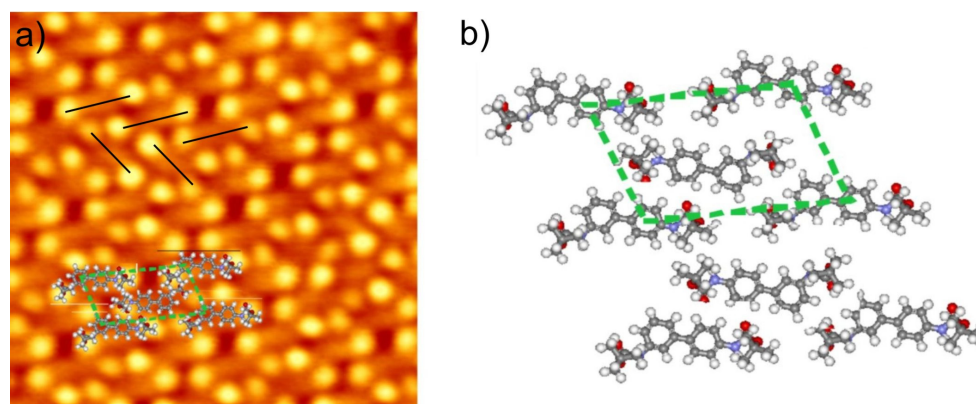


**Figure 3.3.26.** a) STM image of the parallel arrangement in which the unit cell and a few molecules are inserted to illustrate their arrangement ( $10 \times 10 \text{ nm}^2$ , -1.26 V, 20 pA, 77 K). Besides this structure, rarely a herringbone arrangement of the molecules can be observed, which is illustrated with black lines inside the network. b) Tentative molecular model of the close-packed parallel arrangement.

The molecules of asymmetric Boc protected biaminophenyl (**66**) deposited on Cu(111) disorganized upon heating to  $120^\circ\text{C}$  which is  $76^\circ\text{C}$  colder than the temperature on which



formation of interlinked structures for symmetric Boc protected biaminophenyl (**50**) was observed. The temperature difference between **66** and symmetric Boc protected biaminophenyl (**50**) can be explained by the structural differences, i.e. para vs meta. However, it was very interesting that any interlinked structures can be observed upon heating of **66**.

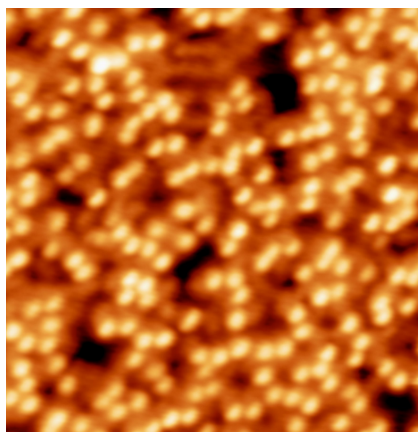


**Figure 3.3.27.** STM image of the sample after annealed at 160°C (12.7 x 12.8 nm<sup>2</sup>, 1.5 V, 20 pA, 77 K). Some interlinking is observed but there is no ordering of the structures.

On the other hand, the formation of interlinked dimeric structures of **66** on Ag(111) surface was observed at 165°C, 31°C lower than the temperature for interlinking symmetric Boc protected biaminophenyl (**50**) was observed, and 5°C higher than the temperature for interlinking of **65** on Ag(111) surfaces. Upon heating to 165°C, trimeric interlinked structures was observed for the **66** on Ag(111) surface similar to the interlinked structures of **65**. **66** and **65** showed similar interlinking pattern at very close temperatures. Therefore, the resulting interlinking structures and their interlinking temperature can be tuned by modifying the Boc protection group's substitution position or charge distribution.

## 4. SUMMARY AND CONCLUSIONS

Metal nanoparticles have received much attention as potentially effective materials showing novel electronic, optical, optoelectronic, magnetic, and thermal properties derived from the “quantum size effect”. Organized assemblies of metal nanoparticles are also expected to show novel and fascinating properties. For this reason, chemical control over the particle size in order to fabricate monodisperse metal nanoparticles is required.

In this work, we presented novel cyclic benzothioether ligands for ligand exchange studies of phosphine stabilized Au<sub>55</sub> nanoparticles. The ligand exchange reactions for better stabilized Au<sub>55</sub> clusters were examined. Moreover, direct synthesis of highly monodisperse gold nanoparticles was performed using novel cyclic benzothiol-thioether hybrid ligands. Model ligand **E** was studied closely for understanding the size, stability and dispersity of directly synthesized gold nanoparticles.

Our studies for the synthesis of monodisperse gold nanoparticles can be investigated in two parts. In the first part, ligands that are more stable than phosphines were designed according to the theoretical calculations. Then, we focused our attention to ligand exchange of well-defined, monodisperse Au<sub>55</sub>(PPh<sub>3</sub>)<sub>12</sub>Cl<sub>6</sub> clusters with cyclic benzothioether ligands. Mono and biphasic ligand exchange attempts to replace phosphine ligands with more stable benzothioether ligands could not be achieved. In fact, coagulation of Au<sub>55</sub> nanoparticles into bigger particles or even into bulk gold was observed. Hence, we concluded that cyclic benzothioether ligands were not suitable for stabilization of Au<sub>55</sub> clusters by ligand exchange reactions not only for their weak binding properties but also their lack of bulkiness to prevent coagulation, which essentially restricts the general applicability of this method.

In the second part of our search for better monodispersed gold nanoparticles, we focused on direct synthesis of gold nanoparticles with reduction of gold(III) precursors in the presence of our modified cyclic benzothioether ligands using two phase Brust-Schiffrin method. After the formation of gold nanoparticles with our bulkier benzothioether ligands, the properties of newly formed gold nanoparticles were investigated. Significantly, a very narrow size distribution with mainly 1.1 nm gold nanoparticles was obtained as demonstrated by TEM analysis. Calculations utilizing the characterization data showed that two of our bulky ligands stabilized one gold nanoparticle composed of 34 gold atoms. It was also observed that the

newly formed gold nanoparticles are additionally stabilized with the help of the ionic phase transfer reagent and showed very high stability in solution or solid phase.

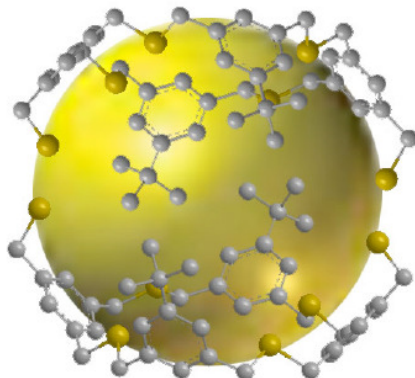


**Figure 4.1.** Suggested assembly of gold nanoparticles stabilized with two of ligands, **E**.

These studies proved cyclic benzothiol-thioether hybrid ligands as a good candidate for synthesis of highly stable and monodisperse gold nanoparticles using the bottom-up approach. Yet, in order to improve the yield of ligands for the large-scale production, more efficient synthesis methods and more suitable protection groups for sulfur atoms remain to be established. Moreover, the gold nanoparticles could not be fully purified and separated from each other due to the problems encountered during purification by precipitation. Therefore, benzothiol-thioether hybrid ligands stabilized gold nanoparticle formation should be studied to define not only the parameters for higher monodispersity and narrower size distribution but also the effect of the ligand/gold ratio and the synthesis conditions to achieve total control of the end products.

Organized molecular structures are of vital importance for the production of advanced functional surfaces in the field of nanotechnology. Recent studies revealed that design principles from supramolecular chemistry can be adapted to fabricate unique supramolecular aggregates at surfaces. A major challenge in bottom-up assembly of functional molecular nanosystems at surfaces is the formation of structures of large size using covalent or non-covalent bonds. 2D assembly of larger nanostructures from preorganised monomers was achieved using the concepts of supramolecular chemistry and protection group chemistry. Several Boc protected aromatic structures were synthesized and their ability to form ordered structures on surfaces were investigated. It was found that the Boc-protected diaminobiphenyl, **50**, self-assembled in two different arrangements on Cu(111) surface.

Annealing these arrangements at 196°C provided a well-ordered pattern consisting of dimers with terminal Boc groups. Further annealing of the samples at  $\geq 198^\circ\text{C}$  led to the formation of cross-type and chain-like structures. To understand the reactions leading the formation of more complex structures from the surface assembled preorganized molecules, bench side experiments were performed and the formation of new N-N and N-C covalent bonds between the monomers was identified which is facilitated by the release of the protecting groups under UHV conditions.

In the light of these promising results, fluorinated derivative of Boc-protected diaminobiphenyl (**65**) and asymmetric Boc-protected diaminobiphenyl (**66**) were synthesized for the study of more controlled covalent formation of preorganised molecules. Their coverage and self-assembly structures were investigated on Cu(111) and Ag(111) surfaces. Both of the molecules showed similar annealing temperatures for the covalent bond formation towards longer interconnected structures. While two different arrangements on Cu(111) and Ag(111) surfaces were observed for fluorinated derivative of Boc-protected diaminobiphenyl, asymmetric Boc-protected diaminobiphenyl showed only parallel arrangement structures only on Ag(111) structures.

These results reveal that using suitably designed protecting groups to arrange monomers on surfaces and inducing their cleavage by an external trigger allow the interlinking of the preorganized monomers. However, the principals underlying the formation of different structures on different surfaces remain to be investigated in details.

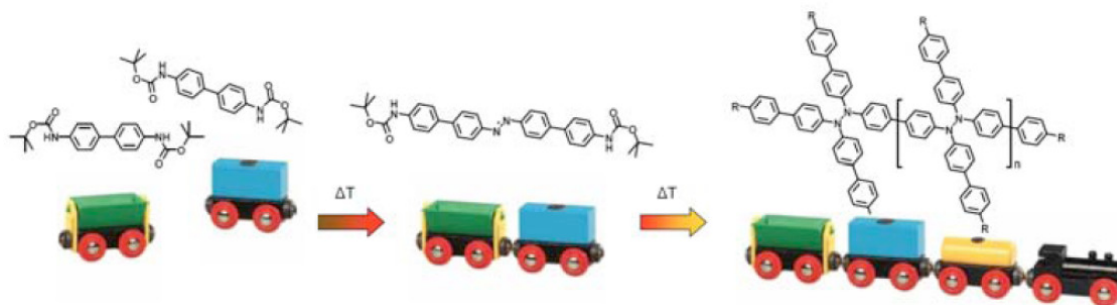


**Figure 4.2.** Preorganized pre-organized molecular building blocks interlinked on the surface

In conclusion, the assembly of the nanostructures with help of the protection groups may pave the way towards molecule-based covalently linked two dimensional functional structures which are so far only attainable at larger scale by lithography.

## 5. EXPERIMENTAL PART

### 5.1. General Remarks

All reactions were performed in dried standard glassware and inert atmosphere of Argon 6.0 obtained from *PanGas AG* (Dagmersellen, Switzerland). Evaporation and concentration of compounds *in vacuo* was done using a Büchi rotary evaporator. Drying of compounds and reagents were done using a RV5 high vacuum pump from Edwards.

Chemicals and reagents were used as received from *Fluka AG* (Buchs, Switzerland), *Acros AG* (Basel, Switzerland), and *Aldrich* (Buchs, Switzerland) in puriss. p. a. quality and used without further purification. Solvents for chromatography and extractions were distilled prior to use. Dry DCM was distilled from CaH<sub>2</sub>, THF from Na-benzophenone. HPLC-grade solvents were purchased from J. T. Baker and used for analytical HPLC. **Elemental analyses (EA)** were carried out by W. Kirsch on a *Perkin-Elmer Analytator 240*. The values are given in mass percent. **Melting points (MP)** were determined in °C using a *Stuart SMP3* apparatus and are uncorrected.

#### 5.1.1 Chromatographic methods

**Thin layer chromatography (TLC)** was performed on 0.25 mm precoated either 5x10 cm glass plates coated with silica gel 60 F<sub>254</sub> or 0.2 mm precoated basic alumina plates were used purchased from Merck AG (Darmstadt, Germany). Visualization of compounds was done at 254 nm (UV) and 366 nm (fluorescence). If necessary, the plates were stained by dipping into a KMnO<sub>4</sub> solution.

Description: TLC (SiO<sub>2</sub>, Alox) (solvent) R<sub>f</sub>

**Normal phase column chromatography** was done using silica gel 60 from Merck AG (Darmstadt, Germany) (0.043mm-0.060 mm, 230-400 mesh).

**High performance liquid chromatography (HPLC)** was done using HP1100 Series analytical HPLC on a Nucleosil 100-5 5.0µm SiO<sub>2</sub> column from Bischoff Chromatography NC-04 (250x4 mm). **Reverse phase column chromatography** was performed on Lichospher® 100 RP-18 silica gel from Merck (5µm particle size, 4x250 mm column) with HPLC-grade MeCN.

Description: HPLC (solvent system, length of program; detector wavelength), R<sub>t</sub>

### 5.1.2 Spectroscopic methods

**UV-Vis** spectra were recorded on an *Agilent* 8453 diode array detector spectrophotometer using optical 114-QS *Hellma* cuvettes (10 mm light path).

Description: UV-Vis (solvent), maxima wavelength ( $\lambda_{\max}$ ) in nm, (main bands, relative extinction coefficient in %)

**Electron impact (EI)** mass spectra and **fast atom bombardment (FAB)** mass spectra were recorded by *Dr. H. Nadig* on a *finnigan* MAT 95Q for EI-MS and on a *finnigan* MAT 8400 for FAB-MS in the mass spectrometry laboratory of the institute. As matrix for FAB-MS *m*-nitrobenzyl alcohol or glycine was used. **Electron spray ionization mass spectra (ESI-MS)** were recorded on a Bruker Esquire 3000plus. **Matrix-assisted laser desorption-ionization mass spectra in conjunction with time of flight (MALDI-TOF)** were recorded on a Perseptive Biosystems Vestec Mass Spectroscopy Products Voyager<sup>TM</sup> Elite Biospectrometry<sup>TM</sup> Research station. The samples for ESI-MS were prepared by dissolving the compounds in DCM and dilution with MeOH. For MALDI-TOF measurements 1-10 $\mu$ l of sample dissolved in DCM was placed on a 100-wells sample plate and measured without matrix. Peaks with intensity less than 10% were not considered.

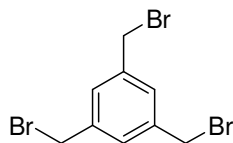
Description: MS type, mass peaks in  $m/z$

**Nuclear magnetic resonance (NMR)** were recorded on Bruker Avance250-MNR (250 MHz <sup>1</sup>H), Bruker DPX-NMR (400 MHz <sup>1</sup>H and 100 MHz for <sup>13</sup>C) or or a *Bruker* DRX-500 (500 MHz for <sup>1</sup>H and 125 MHz for <sup>13</sup>C) spectrometer at ambient temperature in the solvents indicated. Solvents were obtained from Cambridge Isotope Laboratories. CDCl<sub>3</sub> was filtered through basic alumina prior to use. All measurements were done at RT unless otherwise stated. The chemical shifts ( $\delta$ ) were given in ppm relative to TMS. The coupling constants *J*, were listed in Hz. The multiplicities of the signals were indicated *s* (singlet), *d* (doublet), *t* (triplet), *q* (quartet), *m* (multiplet) and *br* (broad). HMQC and HMBC measurement were done on Bruker DRX-NMR (600 MHz) Dr. D. Haussinger.

Description: <sup>1</sup>H-NMR (frequency, solvent):  $\delta$  in ppm, peak multiplicity, *J* in Hz

## 5.2. Synthetic Procedures for Gold Nanoparticles

Synthesis 1,3,5-tris(bromomethyl)benzene, **1**



Via Radical reaction

In a dry double neck 250 mL flask under Ar, mesitylene (5.0 g, 42 mmol, 1 eq.), *N*-bromosuccinimide (22.5 g, 127 mmol, 3 eq.) and  $\alpha,\alpha'$ -azoisobutylnitrile (25 mg, 0.15 mmol, as initiator) were heated to reflux in 125 mL dry  $\text{CCl}_4$  with stirring for 24 h. The mixture filtered to remove the succinimide and the filtrate washed with distilled  $\text{H}_2\text{O}$  (3 x 125 mL) and dried over anhyd.  $\text{Na}_2\text{SO}_4$ . The solvents were removed under reduced pressure. The resulting yellow oil was recrystallized in boiling light petroleum. The solvent was evaporated using Rotavap. The product was purified by recrystallization in ethylacetate to give product as white crystalline needles (6.59 g, 44%).

Via Reduction and bromination

In a dry double neck 500 mL flask under Ar, lithium aluminum hydride (2.23 g, 58.5 mmol, 3.6 eq.) was added to 150 mL of dry THF. Then, benzenetricarboxylate (**2**) (4 g, 15.8 mmol, 1 eq.) dissolved in 150 mL of dry THF was added dropwise at room temperature under vigorous stirring and an atmosphere of Ar. The mixture was refluxed O/N. The excess of reducing agent was destroyed by slow addition of water, and the solvent was evaporated. Then, 120 mL of a 48% HBr solution and 200 mL of toluene were added and heated to reflux for O/N. The organic layer was separated, and the aqueous portion was extracted with TBME (3 x 150 mL). The organic layers were combined, washed with 500 mL brine, dried over anhyd.  $\text{Na}_2\text{SO}_4$ . The solvent was evaporated using Rotavap. The crude material was purified through a short column of silica using *n*-hexane as eluent. The solvents were evaporated under high vacuum to afford the product as white crystalline needles (5.25 g, 93%).

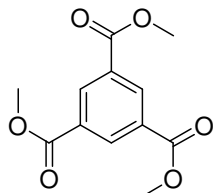
$\text{C}_9\text{H}_9\text{Br}_3$ ,      M.W. = 356.88 g/mol  
                          Exact Mass = 353.83 g/mol

TLC                 $\text{SiO}_2$ , Hexane (100%)  
                           $R_f$  = 0.3

Melting point 104–105°C

EI-MS	354.1[M <sup>+</sup> ],
<sup>1</sup> H-NMR	(400MHz, CDCl <sub>3</sub> ) δ= 7.33 (s, 3H); 4.44 (s, 6H)
<sup>13</sup> C-NMR	(100 MHz, CDCl <sub>3</sub> ) δ= 139.11; 129.62; 32.27;

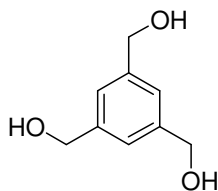
Synthesis trimethyl benzene-1,3,5-tricarboxylate, **2**



In a dry double neck 500 mL flask under Ar, benzenetricarboxylic acid (10 g, 47.5 mmol, 3.6 eq.) was added to 200 mL of MeOH solution which contains 2.5 mL concentrated sulfuric acid. The mixture was refluxed O/N. Upon cooling down, white needle like crystals formed. Saturated sodium carbonate solution was added until the solution became neutral. The solution was filtered; the crystals were washed excessively to remove sodium carbonate salts. The white needle like compound was dried open air to give product as white powder (11.38 g, 95%).

C <sub>12</sub> H <sub>12</sub> O <sub>6</sub> ,	M.W. = 252.22 g/mol Exact Mass = 252.06 g/mol
TLC	SiO <sub>2</sub> , Hexane-EtAc (5:1) R <sub>f</sub> = 0.3
Melting point	146–148 °C
EI-MS	252 [M <sup>+</sup> ],
<sup>1</sup> H-NMR	(250 MHz, CDCl <sub>3</sub> ) δ= 8.87 (s, 3H); 3.99 (s, 9H)

Synthesis benzene-1,3,5-triyltrimethanol, **3**

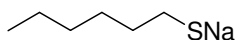




In a dry double neck 500 ml flask under Ar, lithium aluminum hydride (2.23 g, 58.5 mmol, 3.6 eq.) was added to 150 mL of dry THF. Then, benzenetricarboxylate (**2**) (4 g, 15.8 mmol, 1 eq.) dissolved in 150 mL of dry THF was added dropwise at room temperature under vigorous stirring and an atmosphere of Ar. The mixture was refluxed O/N. The excess of reducing agent was destroyed by slow addition of water, and the solvent was evaporated. The solution was filtered; the formed solids were washed excessively to remove aluminium salts. The colorless oily compound was obtained after evaporation of the solvent (2.39 g, 90%).

$C_9H_{12}O_3$ ,	M.W. = 168.19 g/mol
	Exact Mass = 168.08 g/mol
TLC	SiO <sub>2</sub> , CHCl <sub>3</sub> -MeOH (9:1)
	R <sub>f</sub> = 0.35
Melting point	76–78 °C
EI-MS	191.1 [M <sup>+</sup> ],
<sup>1</sup> H-NMR	(400 MHz, MeOD)
	δ = 7.24 (s, 3H); 4.60 (s, 6H)
<sup>13</sup> C-NMR	(100 MHz, MeOD)
	δ = 141.95; 124.49; 64.14

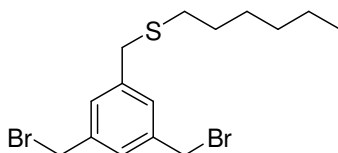
Synthesis sodium hexane-1-thiolate, **4**



In a dry 100 mL 2-necked flask equipped with a condenser and a magnetic stirrer, sodium metal (2.3 g, 0.1 mol, 1 eq.) was dissolved in 20 mL anhyd. EtOH over a period of 30 min. mercaptohexane (14.1 mL, 0.1 mol, 1 eq.) was then added slowly, and the resulting solution was stirred for another 2 h at RT. The solid residue obtained after evaporation of the solvent was washed with Et<sub>2</sub>O, isolated by filtration, and dried under vacuum leading the product as white solid (13.5 g, 97%).

$C_6H_{13}NaS$ ,	M.W. = 140.22 g/mol
	Exact Mass = 140.06g/mol
ESI-MS	140.1 [M <sup>+</sup> +Na],

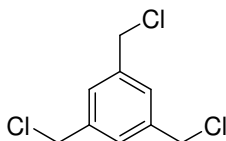
Synthesis (3,5-bis(bromomethyl)benzyl)(hexyl)sulfane, **5**



In a dry double neck 250 mL flask under Ar, 1,3,5-tris(bromomethyl)benzene (**1**) (3.57 g, 10 mmol, 1 eq.) was dissolved in 100 mL THF. Hexane-1-thiolate (**4**) (1.4 g, 10 mmol, 1 eq.) added slowly to the reaction mixture. Then the mixture was let to stir at RT for 30 minutes. The reaction mixture is poured into 75 mL water. Organic layer was collected. Water layer was extracted with TBME (3 x 75 mL). All the organic extracts were combined, washed with 150 mL brine, dried over anhyd. Na<sub>2</sub>SO<sub>4</sub>. The solvent was evaporated using Rotavap leaving yellowish oily crude. The purification attempts via column chromatography or distillation were failed.

TLC            SiO<sub>2</sub>, Hexane-EtAc (19:1)  
                   R<sub>f</sub> = 0.45

Synthesis 1,3,5-tris(chloromethyl)benzene, **6**



In a dry double neck 25 mL flask under Ar, 1,3,5-tris(bromomethyl)benzene (**1**) (3.57 g, 10 mmol, 1 eq.) and lithiumchloride (2.12 g, 50 mmol, 5 eq.) were dissolved in 15 mL dry DMF. The mixture is stirred 2 h at RT, under Ar. The reaction mixture is poured into 25 mL water. The mixture was extracted with TBME (3 x 25 mL). All the organic extracts were combined, washed twice with 25 mL brine, dried over anhyd. Na<sub>2</sub>SO<sub>4</sub>. The solvent was evaporated using Rotavap leading the product as white powder (2.23 g, 99%).

C<sub>9</sub>H<sub>9</sub>Cl<sub>3</sub>,        M.W. = 223.53 g/mol  
                   Exact Mass = 221.98 g/mol

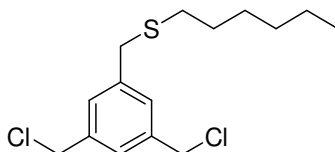
TLC            SiO<sub>2</sub>, Hexane (100%)  
                   R<sub>f</sub> = 0.3

<sup>1</sup>H-NMR        (400 MHz, CDCl<sub>3</sub>)  
                   δ = 7.38 (s, 3H.); 4.59 (s, 6H.);

<sup>13</sup>C-NMR        (100 MHz, CDCl<sub>3</sub>)

$\delta$ = 138.67, 128.64; 45.38

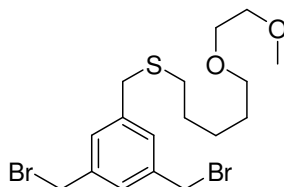
Synthesis (3,5-bis(bromomethyl)benzyl)(hexyl)sulfane, **7**



In a dry double neck 25 mL flask under Ar, 1,3,5-tris(chloromethyl)benzene (**6**) (0.22 g, 0.1 mmol, 1 eq.) was dissolved in 10 mL dry THF. Hexane-1-thiolate (**4**) (0.14 g, 1 mmol, 1 eq.) added slowly to the reaction mixture. Then the mixture was let to stir at RT for 30 minutes. The reaction mixture is poured into 10 mL water. Organic layer was collected. Water layer was extracted with TBME (3 x 10 mL). All the organic extracts were combined, washed with 25 mL brine, dried over anhyd.  $\text{Na}_2\text{SO}_4$ . The solvent was evaporated using Rotavap leaving yellowish oily crude. The purification attempts via column chromatography or distillation were failed.

TLC  $\text{SiO}_2$ , Hexane-EtAc (19:1)  
 $R_f = 0.45$

Synthesis (3,5-bis(bromomethyl)benzyl)(5-(2-methoxyethoxy)pentyl)sulfane, **8**

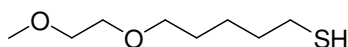


In a dry double neck 250 mL flask under Ar, 1,3,5-tris(bromomethyl)benzene (**1**) (3.57 g, 10 mmol, 1 eq.) and 5-(2-methoxyethoxy)pentane-1-thiol (**9**) (1.78 g, 10 mmol, 1 eq.) were dissolved in 100 mL dry THF. Sodium hydrate 60% dispersion in mineral oil (0.44 g, 11 mmol, 1.1 eq.) was added to the previous solution at 0°C. Then the mixture was let to stir at RT for 30 minutes. The reaction mixture is poured into 100 mL water. Organic layer was collected. Water layer was extracted with TBME (3 x 75 mL). All the organic extracts were combined, washed with 150 mL brine, dried over anhyd.  $\text{Na}_2\text{SO}_4$ . The solvent was evaporated using Rotavap. The crude was purified on a silica gel column (Hexane-EtAc 3:1) and the product was obtained as colorless oil (2.09 g, 46%).

$\text{C}_{17}\text{H}_{26}\text{Br}_2\text{O}_2\text{S}$  M.W. = 454.26 g/mol

	Exact Mass = 452 g/mol
TLC	SiO <sub>2</sub> , Hexane-EtAc (3:1) R <sub>f</sub> = 0.3
MALDI-MS	452.1 [M <sup>+</sup> ],
<sup>1</sup> H-NMR	(400MHz, CDCl <sub>3</sub> ) δ= 7.35 (s, 1H); 7.29 (s, 2H); 4.45 (s, 4H); 3.70 (s, 2H); 3.60-3.55 (m, 4H); 3.49 (t, J= 6.8 Hz, 2H); 3.4 (s, 3H); 2.43 (t, J= 7.6 Hz, 2H); 1.61-1.54 (m, 4H); 1.45-1.39 (m, 2H);
<sup>13</sup> C-NMR	(100 MHz, CDCl <sub>3</sub> ) δ= 140.51; 139.01; 129.90; 128.47; 72.39; 71.68; 70.45; 59.50; 46.37; 36.24; 31.84; 29.61; 29.59; 25.47;
E.A.	Calculated : C, 44.95%; H, 5.77%; Found : C, 45.11%; H, 5.69%;

Synthesis 5-(2-methoxyethoxy)pentane-1-thiol, **9**

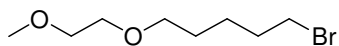


In a dry double neck 25 mL flask under Ar, 5-(2-methoxyethoxy)pentyl ethanethioate (**11**) (1.10 g, 5 mmol, 4 eq.), and sodiumthiomethoxide (0.07 g, 1.25 mmol, 1 eq.) were dissolved in 15 mL dry MeOH and the mixture was let to stir at RT for O/N. The reaction mixture was poured into 15 mL water, acidified with sat. NH<sub>4</sub>Cl and was extracted with DCM (3 x 25 mL). All the organic extracts were combined, washed with 50 mL brine, dried over anhyd. Na<sub>2</sub>SO<sub>4</sub>. The solvent was evaporated using Rotavap leading colorless oily product (0.89 g, 99%).

C <sub>8</sub> H <sub>18</sub> O <sub>2</sub> S	M.W. = 178.29 g/mol Exact Mass = 178.1 g/mol
TLC	SiO <sub>2</sub> , Hexane-EtAc (4:1) R <sub>f</sub> = 0.3
EI-MS	70eV 179.1 [M <sup>+</sup> ],
<sup>1</sup> H-NMR	(400MHz, CDCl <sub>3</sub> ) δ= 3.44-3.38 (m, 4H); 3.22 (t, J= 6.4 Hz, 2H); 3.24 (s, 3H); 2.38 (q, J <sub>1</sub> = 3.6 Hz, J <sub>2</sub> = 7.6 Hz, 2H); 1.53-1.43 (m, 4H); 1.58-1.48 (m, 4H); 1.36-1.32 (m, 2H); 1.21 (t, J= 7.6 Hz, 1H);

$^{13}\text{C-NMR}$	(100 MHz, $\text{CDCl}_3$ )
	$\delta = 72.26; 71.49; 70.20; 59.41; 34.07; 29.11; 25.20$
E.A.	Calculated : C, 53.89%; H, 10.18%;
	Found : C, 54.11%; H, 10.03%;

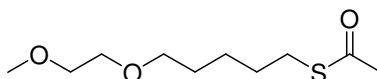
#### Synthesis 1-bromo-5-(2-methoxyethoxy)pentane, **10**



In a dry double neck 50 mL flask under Ar, sodium hydrate 60% dispersion in mineral oil (0.44 g, 11 mmol, 1.1 eq.) was dissolved in 10 mL dry THF and 2-methoxyethanol (0.73 mL, 10 mmol, 1 eq.) added dropwise to the previous solution at 0°C. All the sodium alkolate solution was added to the refluxing 1,5-dibromopentane (1.37 mL 10 mmol, 1 eq.) dissolved in 10 mL dry THF solution. The mixture was refluxed O/N under Ar. The solvent evaporated, the crude dissolved in 15 mL EtAc and filtered to get rid off salt. The filtrate was washed with water (2 x 25 mL) and with 25 mL brine, dried over anhyd.  $\text{Na}_2\text{SO}_4$ . The solvent was evaporated using Rotavap. The crude was purified on a silica gel column (Hexane-EtAc 6:1) and the product was obtained as colorless oil (0.54 g, 24%).

$\text{C}_8\text{H}_{17}\text{BrO}_2$ ,	M.W. = 225.12 g/mol
	Exact Mass = 224.04 g/mol
TLC	$\text{SiO}_2$ , Hexane-EtAc (6:1)
	$R_f = 0.3$
EI-MS	70eV
	225.1 [ $\text{M}^+$ ],
$^1\text{H-NMR}$	(400MHz, $\text{CDCl}_3$ )
	$\delta = 3.51\text{-}3.46$ (m, 4H); 3.40 (t, $J = 6.4$ Hz, 2H); 3.34 (t, $J = 6.8$ Hz, 4H); 3.32 (s, 1H); 1.85-1.78 (m, 7.6 2H); 1.60-1.52 (m, 2H); 1.47-1.39 (m, 2H);
$^{13}\text{C-NMR}$	(100 MHz, $\text{CDCl}_3$ )
	$\delta = 72.32; 71.49; 70.42; 59.41; 34.07; 32.96; 29.11; 25.20;$

#### Synthesis S-5-(2-methoxyethoxy)pentyl ethanethioate, **11**

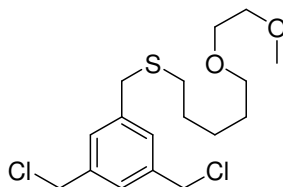


In a dry double neck 25 mL flask under Ar, 1-bromo-5-(2-methoxyethoxy)pentane (**10**) (2.25 g, 10 mmol, 1 eq.) and potassiumthioacetate, (2.51 g, 0.22 mol, 2.2 eq.) were dissolved in

10 ml anhyd. DMF. The mixture was let to stir at RT for O/N. The reaction mixture is poured into 10 mL water. The mixture was extracted with TBME (3 x 15 mL). All the organic extracts were combined, washed twice with 25 mL brine, dried over anhyd. Na<sub>2</sub>SO<sub>4</sub>. The solvent was evaporated using Rotavap leading colorless oily product (2.20 g, 99%).

C <sub>10</sub> H <sub>20</sub> O <sub>3</sub> S	M.W. = 220.33 g/mol Exact Mass = 220.11 g/mol
TLC	SiO <sub>2</sub> , Hexane-EtAc (4:1) R <sub>f</sub> = 0.2
EI-MS	70eV 220.1 [M <sup>+</sup> ],
<sup>1</sup> H-NMR	(400MHz, CDCl <sub>3</sub> ) δ= 3.51-3.46 ( <i>m</i> , 4H); 3.39 ( <i>t</i> , <i>J</i> = 6.4 Hz, 2H); 3.31 ( <i>s</i> , 3H); 2.79 ( <i>t</i> , <i>J</i> = 7.2 Hz, 2H); 2.25 ( <i>s</i> , 3H); 1.58-1.48 ( <i>m</i> , 4H); 1.39-1.30 ( <i>m</i> , 2H);
<sup>13</sup> C-NMR	(100 MHz, CDCl <sub>3</sub> ) δ= 194.45; 72.32; 71.52; 70.38; 59.41; 30.96; 29.73; 29.45; 29.36; 25.72
E.A.	Calculated : C, 54.51%; H, 9.15%; Found : C, 54.36%; H, 9.09%;

Synthesis (3,5-bis(bromomethyl)benzyl)(5-(2-methoxyethoxy)pentyl)sulfane, **12**



In a dry double neck 100 mL flask under Ar, 1,3,5-tris(chloromethyl)benzene (**6**) (2.23g, 10 mmol, 1 eq.) and 5-(2-methoxyethoxy)pentane-1-thiol (**9**) (1.78 g, 10 mmol, 1 eq.) was dissolved in 25 mL dry THF. Sodium hydrate 60% dispersion in mineral oil (0.44 g, 11 mmol, 1.1 eq.) was added to the previous solution at 0°C. Then the mixture was let to stir at RT for 30 minutes. The reaction mixture is poured into 30 mL water. Organic layer was collected. Water layer was extracted with TBME (3 x 25 mL). All the organic extracts were combined, washed with 75 mL brine, dried over anhyd. Na<sub>2</sub>SO<sub>4</sub>. The solvent was evaporated using Rotavap. The crude was purified on a silica gel column (Hexane-EtAc 3:1) and the product was obtained as colorless oil (1.72 g, 47%).

$C_{17}H_{26}Cl_2O_2S$  M.W. = 365.36 g/mol

Exact Mass = 364.10 g/mol

TLC  $SiO_2$ , Hexane-EtAc (4:1)

$R_f$  = 0.25

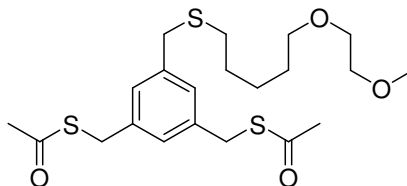
$^1H$ -NMR (400MHz,  $CDCl_3$ )

$\delta$  = 7.30 (s, 3H); 4.57 (s, 4H); 3.69 (s, 2H); 3.59-3.53 (m, 4H); 3.44 (t,  $J$  = 6.4 Hz, 2H); 3.38 (s, 3H); 2.41 (t,  $J$  = 7.8 Hz, 2H); 1.62-1.54 (m, 4H); 1.45-1.39 (m, 2H);

$^{13}C$ -NMR (100 MHz,  $CDCl_3$ )

$\delta$  = 140.40; 138.68; 129.39; 127.70; 72.39; 71.68; 70.45; 59.50; 46.07; 36.31; 31.87; 29.58; 29.44; 25.81;

Synthesis  $S,S'$ -(5-((5-(2-methoxyethoxy)pentylthio)methyl)-1,3-phenylene)bis (methylene) diethanethioate, **13**



In a dry double neck 25 mL flask under Ar, (3,5-bis(bromomethyl)benzyl)(5-(2-methoxyethoxy)pentyl)sulfane (**8**) (0.48 g, 1 mmol, 1 eq.), and potassiumthioacetate, (0.25 g, 22 mmol, 2.2 eq.) were dissolved in 2 mL anhyd. DMF. The mixture was let to stir at RT for O/N. The reaction mixture is poured into 10 mL water. The mixture was extracted with TBME (3 x 15 ml). All the organic extracts were combined, washed twice with 25 mL brine, dried over anhyd.  $Na_2SO_4$ . The solvent was evaporated using Rotavap leading colorless oily product (0.44 g, 99%).

$C_{21}H_{32}O_4S_3$  M.W. = 444.67 g/mol

Exact Mass = 444.15 g/mol

TLC  $SiO_2$ , Hexane-EtAc (4:1)

$R_f$  = 0.1

EI-MS 70eV

455.1 [ $M^+$ ]

$^1H$ -NMR (400MHz,  $CDCl_3$ )

$\delta$ = 7.10 (s, 2H); 7.07 (s, 1H); 4.07 (s, 4H); 3.61 (s, 2H); 3.57-3.48 (m, 4H); 3.45 (t,  $J$ = 6.8 Hz, 2H); 3.37 (s, 3H); 2.39 (t,  $J$ = 7.2 Hz, 2H); 2.34 (s, 6H); 1.65-1.55 (m, 4H); 1.45-1.35 (m, 2H);

$^{13}\text{C-NMR}$

(100 MHz,  $\text{CDCl}_3$ )

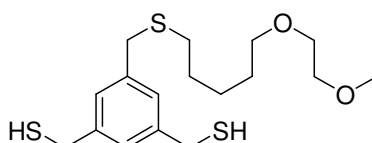
$\delta$ = 195.34; 139.95; 138.61; 128.63; 128.23; 72.38; 71.70; 70.44; 59.49; 36.38; 33.53; 31.87; 30.74; 29.60; 29.45; 25.82

E.A.

Calculated : C, 56.72%; H, 7.25%;

Found : C, 56.74%; H, 7.33%;

Synthesis (5-((5-(2-methoxyethoxy)pentylthio)methyl)-1,3-phenylene)dimethanethiol, **14**



In a dry double neck 25 mL flask under Ar, S,S'-((5-(2-methoxyethoxy)pentylthio)methyl)-1,3-phenylene)bis (methylene) diethanethioate (**13**) (0.44 g, 1 mmol, 4 eq.) and sodiumthiomethoxide (0.13 g, 0.25 mmol, 1 eq.) were dissolved in 5 mL dry MeOH and the mixture was let to stir at RT for O/N. The reaction mixture was poured into 10 mL water, acidified with sat.  $\text{NH}_4\text{Cl}$  and was extracted with DCM (3 x 15 mL). All the organic extracts were combined, washed with 50 mL brine, dried over anhyd.  $\text{Na}_2\text{SO}_4$ . The solvent was evaporated using Rotavap leading the colorless oily product (0.36 g, 99%).

$\text{C}_{17}\text{H}_{28}\text{O}_2\text{S}_3$  M.W. = 360.6 g/mol

Exact Mass = 360.13 g/mol

TLC

$\text{SiO}_2$ , Hexane-EtAc (4:1)

$R_f$  = 0.2

EI-MS

70eV

359.1 [ $\text{M}^+$ ]

$^1\text{H-NMR}$

(250 MHz,  $\text{CDCl}_3$ )

$\delta$ = 7.17 (s, 1H); 7.15 (s, 2H); 3.70 (t,  $J$ = 4 Hz, 4H); 3.66 (s, 2H); 3.55 (dxt, 4H); 3.44 (t,  $J$ = 6.8 Hz, 2H); 3.38 (s, 3H); 2.42 (t,  $J$ = 7.2 Hz, 2H); 1.77 (t,  $J$ = 7.6, 2H); 1.61-1.54 (m, 4H); 1.44-1.39 (m, 2H);

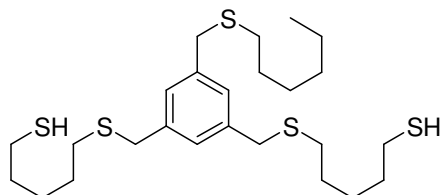
$^1\text{H-NMR}$

(400MHz,  $\text{CDCl}_3$ )



	$\delta$ = 7.17 (s, 1H); 7.15 (s, 2H); 3.70 (t, $J$ = 17.2 Hz, 6H); 3.60-3.55 (m, 4H); 3.44 (t, $J$ = 6.8 Hz, 2H); 3.38 (s, 3H); 2.45 (t, $J$ = 7.2 Hz, 2H); 1.77 (t, $J$ = 7.2 Hz, 2H); 1.61-1.54 (m, 4H); 1.45-1.39 (m, 2H);
$^{13}\text{C-NMR}$	(100 MHz, $\text{CDCl}_3$ ) $\delta$ = 142.20; 139.98; 127.66; 126.77; 72.39; 71.71; 70.45; 59.50; 36.48; 31.89; 29.62; 29.49; 29.11; 25.84;
E.A.	Calculated : C, 56.63%; H, 7.83%; Found : C, 55.93%; H, 7.67%;

Synthesis 5,5'-(5-(hexylthiomethyl)-1,3-phenylene)bis(methylene)bis(sulfaneydiyl) dipentane-1-thiol, **15**



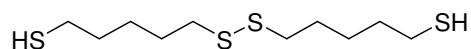
In a dry double neck 25 mL flask under Ar, S,S'-5,5'-(5-(hexylthiomethyl)-1,3-phenylene)bis(methylene)bis(sulfaneydiyl bis(pentane-5,1-diyl) diethanethioate (**31**) (58.9 mg, 0.1 mmol, 4 eq.), and sodiumthiomethoxide (13 mg, 0.025 mmol, 1 eq.) were dissolved in 2 mL dry MeOH and the mixture was let to stir at RT for O/N. The reaction mixture was poured into 10 mL water, acidified with sat.  $\text{NH}_4\text{Cl}$  and was extracted with DCM (3 x 15 mL). All the organic extracts were combined, washed with 50 mL brine, dried over anhyd.  $\text{Na}_2\text{SO}_4$ . The solvent was evaporated using Rotavap to give a colorless oily product (50.5 mg, 99%).

$\text{C}_{25}\text{H}_{44}\text{S}_5$	M.W. = 504.94 g/mol Exact Mass = 504.2 g/mol
TLC	$\text{SiO}_2$ , Hexane-EtAc (9:1) $R_f$ = 0.4
EI-MS	70eV 503.8 [ $\text{M}^+$ ],
$^1\text{H-NMR}$	(400 MHz, $\text{CDCl}_3$ ) $\delta$ = 7.12 (s, 3H); 3.66 (s, 6H); 2.64 (t, $J$ = 7.3 Hz, 6H); 2.47-2.40 (m, 4H); 1.72-1.23 (m, 22H); 0.87 (t, $J$ = 6.4 Hz, 3H);
$^{13}\text{C-NMR}$	(100 MHz, $\text{CDCl}_3$ )

$\delta$ = 139.57; 139.31; 133.53; 130.26; 128.39; 70.71; 36.49; 31.99; 31.83;  
31.53; 29.63; 28.98; 28.87; 25.02; 22.96; 22.06; 14.47

E.A.           Calculated     : C, 59.47%; H, 8.78%;  
                  Found            : C, 59.57%; H, 8.85%;

Synthesis 5,5'-disulfanediyldipentane-1-thiol, **16**



In a dry double neck 25 mL flask under Ar, S,S'-5,5'-disulfanediyldis(pentane-5,1-diyl) diethanethioate (**21**) (3.54 g, 10 mmol, 1 eq.) and sodium hydroxide (0.44 g, 11 mmol, 1 eq.) were dissolved in 10 mL dry MeOH. Then the mixture was refluxed O/N. The reaction mixture is poured into 50 ml water. The mixture was extracted with TBME (3 x 25 ml). All the organic extracts were combined, washed with 75 mL brine, dried over anhyd. Na<sub>2</sub>SO<sub>4</sub>. The solvent was evaporated using Rotavap leading yellowish oily crude. The crude material was purified through a short column of silica with using pure *n*-hexane as eluent. The solvents were evaporated under high vacuum to afford the product as white solid (0.16 g, 6%).

C<sub>10</sub>H<sub>22</sub>S<sub>4</sub>       M.W. = 270.54 g/mol

Exact Mass = 270.06 g/mol

TLC             SiO<sub>2</sub>, Hexane (100%)

R<sub>f</sub> = 0.45

EI-MS          70eV

270.1 [M<sup>+</sup>],

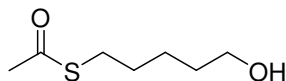
<sup>1</sup>H-NMR       (400MHz, CDCl<sub>3</sub>)

$\delta$ = 2.66 (*t*, *J*= 7.2 Hz, 4H); 2.52 (*q*, *J*<sub>1</sub>= 4.0 Hz, *J*<sub>2</sub>= 7.2 Hz, 4H); 1.71-1.58 (*m*, 8H); 1.51-1.43 (*m*, 4H); 1.33 (*t*, *J*= 7.6 Hz, 3H);

<sup>13</sup>C-NMR       (100 MHz, CDCl<sub>3</sub>)

$\delta$ = 39.19; 33.97; 28.98; 27.57; 24.88

Synthesis S-5-hydroxypentyl ethanethioate, **17**

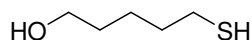


In a dry double neck 25 mL flask under Ar, 1-chloro-pentan-5-ol (2.25 g, 10 mmol, 1 eq.) and potassiumthioacetate (2.51 g, 0.22 mol, 2.2 eq.) were dissolved in 10 mL anhyd. DMF. The mixture was let to stir at RT for O/N. The reaction mixture is poured into 10 mL water. The

mixture was extracted with TBME (3 x 15 ml). All the organic extracts were combined, washed twice with 25 mL brine, dried over anhyd. Na<sub>2</sub>SO<sub>4</sub>. The solvent was evaporated using Rotavap to give product as colorless oil (1.62 g, 99%).

C <sub>7</sub> H <sub>14</sub> O <sub>2</sub> S	M.W. = 162.25 g/mol
	Exact Mass = 162.07 g/mol
TLC	SiO <sub>2</sub> , Hexane-EtAc (2:1)
	R <sub>f</sub> = 0.3
EI-MS	70eV
	162.1 [M <sup>+</sup> ],
<sup>1</sup> H-NMR	(400MHz, CDCl <sub>3</sub> )
	δ= 3.64 ( <i>t</i> , <i>J</i> = 6.4 Hz, 2H); 2.90 ( <i>t</i> , <i>J</i> = 6.4 Hz, 2H); 2.35 ( <i>s</i> , 3H); 1.69-1.48 ( <i>m</i> , 6H)
E.A.	Calculated : C, 51.82%; H, 8.70%;
	Found : C, 52.16%; H, 8.59%;

#### Synthesis 5-mercaptopentan-1-ol, **18**

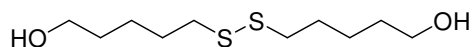


In a dry double neck 25 mL flask under Ar, S-5-hydroxypentyl ethanethioate (**17**) (1.62 g, 10 mmol, 1 eq.) and sodium hydroxide (0.44 g, 11 mmol, 1 eq.) were dissolved in 10 mL dry MeOH. Then the mixture was refluxed O/N. The reaction mixture is poured into 50 mL water. The mixture was extracted with TBME (3 x 25 mL). All the organic extracts were combined, washed with 75 mL brine, dried over anhyd. Na<sub>2</sub>SO<sub>4</sub>. The solvent was evaporated using Rotavap leading yellowish oily crude. The crude material was purified through a short column of silica with a 1-to-1 mixture of *n*-hexane-EtAc. The solvents were evaporated under high vacuum to afford the product as white solid (0.95 g, 79%).

C <sub>5</sub> H <sub>12</sub> OS	M.W. = 120.21 g/mol
	Exact Mass = 120.06 g/mol
TLC	SiO <sub>2</sub> , Hexane-EtAc (1:1)
	R <sub>f</sub> = 0.35
EI-MS	70eV
	120.1 [M <sup>+</sup> ],
<sup>1</sup> H-NMR	(250MHz, CDCl <sub>3</sub> )

$\delta$  = 3.65 (*t*,  $J$  = 6.0 Hz, 2H); 2.55 (*q*,  $J_1$  = 3.5 Hz,  $J_2$  = 7.25 Hz, 2H); 1.88 (*s*, 1H);  
1.68-1.52 (*m*, 6H); 1.36 (*t*,  $J$  = 7.6 Hz, 1H);

Synthesis 5,5'-disulfanediylpentan-1-ol, **19**



In a 100 mL beaker, 5-mercaptopentane-1-ol (**18**) (1.20 g, 10 mmol, 1 eq.) was dissolved in 10 mL methanol and and titrated with 0.5 M methanolic iodine until the reaction turned from colorless to a persistent yellow. The reaction was quenched with 10% sodium bisulfite to a colorless solution. The resulting mixture is poured into 25 mL water. Water layer was extracted with DCM (3 x 25 mL). All the organic extracts were combined, washed with 50 mL brine, dried over anhyd.  $\text{Na}_2\text{SO}_4$ . The solvent was evaporated using Rotavap. The crude material was purified through a short column of silica with a 1-to-1 mixture of *n*-hexane-EtAc. The solvents were evaporated under high vacuum to afford the product as colorless oil (1.06 g, 89%).

$\text{C}_{10}\text{H}_{22}\text{O}_2\text{S}_2$ , M.W. = 238.41 g/mol

Exact Mass = 238.11 g/mol

TLC  $\text{SiO}_2$ , Hexane-EtAc (1:1)

$R_f$  = 0.2

EI-MS 70eV

238.1 [ $\text{M}^+$ ],

$^1\text{H-NMR}$  (400 MHz,  $\text{CDCl}_3$ )

$\delta$  = 4.68 (*s, br*, 2H); 3.65 (*t*,  $J$  = 6.8 Hz, 4H); 2.69 (*t*,  $J$  = 6.8 Hz, 4H); 1.75-1.68 (*m*, 4H); 1.63-1.57 (*m*, 4H); 1.51-1.48 (*m*, 4H).

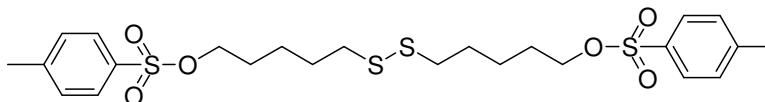
$^{13}\text{C-NMR}$  (100 MHz,  $\text{CDCl}_3$ )

$\delta$  = 63.12; 39.33; 32.67; 29.33; 25.04

E.A. Calculated : C, 50.38%; H, 9.30%;

Found : C, 50.76%; H, 9.19%;

Synthesis 5,5'-disulfanediylbis(pentane-5,1-diyl) bis(4-methylbenzenesulfonate), **20**



In a dry double neck 100 mL flask under Ar, 5,5'-disulfanediylpentan-1-ol (**19**) (2.38 g 10 mmol, 1 eq.) was dissolved in 10 mL dry DCM and pyridine (1.8 ml, 22 mmol, 2.2 eq.) was to

the reaction mixture. *p*-Toluenesulfonyl chloride (4.58 g, 24 mmol, 2.4 eq) dissolved in 12 mL dry DCM was added slowly to the previous mixture at 0°C. The reaction mixture was let to reach RT and stirred under Ar for O/N. The reaction mixture was quenched by adding 20 mL saturated NH<sub>4</sub>Cl solution. Organic layer was collected and extracted with sat. Na<sub>2</sub>SO<sub>4</sub> solution (2 x 25 mL) washed with 25 mL brine, dried over anhyd. Na<sub>2</sub>SO<sub>4</sub>. The solvent was evaporated using Rotavap. The crude was purified on a silica gel column (Hex-EtAc 9:1) and the product was obtained as colorless oil after evaporation of the solvents (5.30 g, 97%).

C<sub>24</sub>H<sub>34</sub>O<sub>6</sub>S<sub>2</sub>, M.W. = 546.78 g/mol

Exact Mass = 546.12 g/mol

TLC SiO<sub>2</sub>, Hexane-EtAc (9:1)

R<sub>f</sub> = 0.3

EI-MS 70eV

546.1 [M<sup>+</sup>],

<sup>1</sup>H-NMR (400 MHz, CDCl<sub>3</sub>)

δ = 7.77 (*d*, *J* = 4.8 Hz, 4H); 7.34 (*d*, *J* = 5.2 Hz, 4H); 4.01 (*t*, *J* = 5.2 Hz, 4H); 2.59 (*t*, *J* = 4.8 Hz, 4H); 2.44 (*s*, 6H); 1.71-1.55 (*m*, 9H); 1.46-1.38 (*m*, 4H)

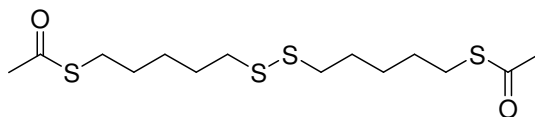
<sup>13</sup>C-NMR (100 MHz, CDCl<sub>3</sub>)

δ = 145.18; 133.48; 130.28; 128.29; 70.69; 38.88; 28.88; 28.86; 24.70; 22.06

E.A. Calculated : C, 52.72%; H, 6.27%;

Found : C, 52.76%; H, 6.19%;

Synthesis S,S'-5,5'-disulfanediybis(pentane-5,1-diyl) diethanethioate, **21**

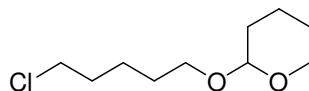


In a dry double neck 25 mL flask under Ar, 5,5'-disulfanediybis(pentane-5,1-diyl) bis(4-methylbenzenesulfonate) (**20**) (5.47 g 10 mmol, 1 eq.) and potassiumthioacetate, (2.51 g, 0.22 mol, 2.2 eq.) were dissolved in 10 mL anhyd. DMF. The mixture was let to stir at RT for O/N. The reaction mixture is poured into 10 mL water. The mixture was extracted with TBME (3 x 15 mL). All the organic extracts were combined, washed twice with 25 mL brine, dried over anhyd. Na<sub>2</sub>SO<sub>4</sub>. The solvent was evaporated using Rotavap leading colorless oily product (3.52 g, 99%).

C<sub>14</sub>H<sub>26</sub>O<sub>2</sub>S<sub>4</sub> M.W. = 354.62 g/mol

	Exact Mass = 354.08 g/mol
TLC	SiO <sub>2</sub> , Hexane-EtAc (9:1) R <sub>f</sub> = 0.4
EI-MS	70eV 354.5 [M <sup>+</sup> ],
<sup>1</sup> H-NMR	(400MHz, CDCl <sub>3</sub> ) δ= 2.89-2.82 ( <i>m</i> , 4H); 2.66 ( <i>t</i> , <i>J</i> = 7.2 Hz, 4H); 2.32 ( <i>s</i> , 6H); 1.75-1.42 ( <i>m</i> , 12H)
E.A.	Calculated : C, 47.42%; H, 7.39%; Found : C, 47.76%; H, 7.19%;

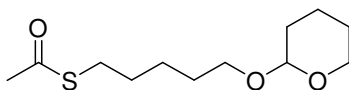
Synthesis 2-(5-chloropentyloxy)-tetrahydro-2H-pyran, **22**



In a dry double neck 100 mL flask under Ar, 5-chloro-pentan-1-ol, (1.16 ml, 10 mmol, 1 eq.), 3,4-Dihydro-2H-pyran (0.91 ml, 10 mmol, 1 eq.) and pyridinium p-toluenesulfonate (0.17 g, 1 mmol, 0.1 eq.) were dissolved in 30 mL anhyd. DCM. The mixture was let to stir at RT O/N. The reaction mixture is poured into 30 mL water. Organic layer was collected. Water layer was extracted with DCM (3 x 25 mL). All the organic extracts were combined, washed with 75 mL brine, dried over anhyd. Na<sub>2</sub>SO<sub>4</sub>. The solvent was evaporated using Rotavap. The crude was purified on a silica gel column (Hexane-EtAc 9:1) and the product was obtained as colorless oil (1.96 g, 95%).

C <sub>10</sub> H <sub>19</sub> ClO <sub>2</sub>	M.W. = 206.71 g/mol Exact Mass = 206.11 g/mol
TLC	SiO <sub>2</sub> , Hexane-EtAc (9:1) R <sub>f</sub> = 0.3
EI-MS	70eV 205.1 [M <sup>+</sup> ],
<sup>1</sup> H-NMR	(250 MHz, CDCl <sub>3</sub> ) δ= 4.57 ( <i>m</i> , 1H); 3.86-3.67 ( <i>m</i> , 2H); 3.52-3.30 ( <i>m</i> , 4H); 1.83-1.40 ( <i>m</i> , 12H)

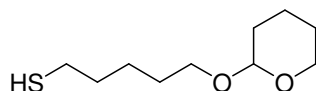
Synthesis S-5-(tetrahydro-2H-pyran-2-yloxy)pentyl ethanethioate, **23**



In a dry double neck 25 mL flask under Ar, 2-(5-chloropentyloxy)-tetrahydro-2H-pyran (**22**) (2.06 g, 10 mmol, 1 eq.), and potassiumthioacetate (2.51 g, 22 mmol, 2.2 eq.) were dissolved in 10 mL anhyd. DMF. The mixture was let to stir at RT for O/N. The reaction mixture is poured into 20 mL water. The mixture was extracted with TBME (3 x 25 mL). All the organic extracts were combined, washed twice with 50 mL brine, dried over anhyd. Na<sub>2</sub>SO<sub>4</sub>. The solvent was evaporated using Rotavap and the product was obtained as colorless oil (2.46 g, 99%).

C <sub>12</sub> H <sub>22</sub> O <sub>3</sub> S	M.W. = 246.37 g/mol
	Exact Mass = 246.13 g/mol
TLC	SiO <sub>2</sub> , Hexane-EtAc (6:1)
	R <sub>f</sub> = 0.35
EI-MS	70eV
	245.1 [M <sup>+</sup> ],
<sup>1</sup> H-NMR	(400 MHz, CDCl <sub>3</sub> )
	δ = 4.57 ( <i>t</i> , <i>J</i> = 7.2 Hz, 1H); 3.88-3.80 ( <i>m</i> , 1H); 3.78-3.72 ( <i>m</i> , 1H); 3.52-3.46 ( <i>m</i> , 1H); 3.42-3.36 ( <i>m</i> , 1H); 2.88 ( <i>t</i> , <i>J</i> = 7.2 Hz, 2H); 2.33 ( <i>s</i> , 3H); 1.76-1.40 ( <i>m</i> , 12H)
E.A.	Calculated : C, 58.50%; H, 9.00%;
	Found : C, 58.76%; H, 9.09%;

#### Synthesis 5-(tetrahydro-2H-pyran-2-yloxy)pentane-1-thiol, **24**

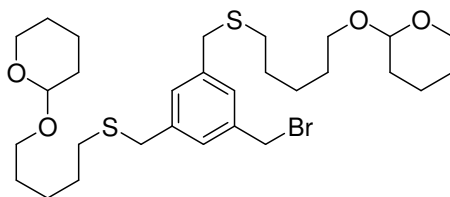


In a dry double neck 25 mL flask under Ar, S-5-(tetrahydro-2H-pyran-2-yloxy)pentyl ethanethioate (**23**) (1.23 g, 5mmol, 4 eq.) and sodiumthiomethoxide (0.07 g, 1.25 mmol, 1 eq.) were dissolved in 15 mL dry MeOH and the mixture was let to stir at RT for O/N. The reaction mixture was poured into 15 mL water, acidified with sat. NH<sub>4</sub>Cl and was extracted with DCM (3 x 25 mL). All the organic extracts were combined, washed with 50 mL brine, dried over anhyd. Na<sub>2</sub>SO<sub>4</sub>. The solvent was evaporated using Rotavap leaving and the product was obtained as colorless oil (2.02 g, 99%).

C <sub>10</sub> H <sub>20</sub> O <sub>2</sub> S	M.W. = 204.33 g/mol
	Exact Mass = 204.12 g/mol

TLC	SiO <sub>2</sub> , Hexane-EtAc (9:1) R <sub>f</sub> = 0.3
EI-MS	70eV 205.1 [M <sup>+</sup> ],
<sup>1</sup> H-NMR	(400 MHz, CDCl <sub>3</sub> ) δ= 4.55 ( <i>t</i> , <i>J</i> = 3.6 Hz, 1H); 3.87-3.81 ( <i>m</i> , 1H); 3.75-3.69 ( <i>m</i> , 1H); 3.50-3.45 ( <i>m</i> , 1H); 3.40-3.34 ( <i>m</i> , 1H); 2.51 ( <i>q</i> , <i>J</i> <sub>1</sub> = 3.6, <i>J</i> <sub>2</sub> = 9.6, 2H); 1.81-1.77 ( <i>m</i> , 1H); 1.72-1.41 ( <i>m</i> , 11H), 1.35 ( <i>t</i> , <i>J</i> = 3.6 Hz, 1H)
<sup>13</sup> C-NMR	(100 MHz, CDCl <sub>3</sub> ) δ= 99.28; 67.74; 62.76; 34.25; 31.16; 29.59; 25.87; 25.48; 24.94; 20.08
E.A.	Calculated : C, 58.78%; H, 9.87%; Found : C, 58.93%; H, 9.75%;

Synthesis 2,2'-(5,5'-(5-(bromomethyl)-1,3-phenylene)bis(methylene)bis(sulfanediyl) bis(pentane-5,1-diyl)) bis(oxy)bis(tetrahydro-2H-pyran), **25**



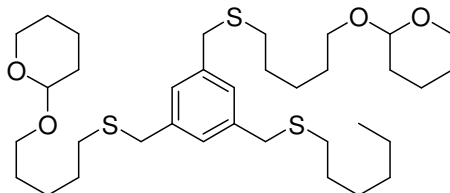
In a dry double neck 250 mL flask under Ar, 1,3,5-tris(bromomethyl)benzene (**1**) (1.78 g, 5 mmol, 1 eq.) and 5-(tetrahydro-2H-pyran-2-yloxy)pentane-1-thiol (**24**) (2.04 g, 10 mmol, 2 eq.) was dissolved in 100 mL dry THF. Sodium hydrate 60% dispersion in mineral oil (0.44 g, 11 mmol, 2.2 eq.) was added to the previous solution at 0°C. Then the mixture was let to stir at RT for 30 minutes. The reaction mixture is poured into 100 mL water. Organic layer was collected. Water layer was extracted with TBME (3 x 75 mL). All the organic extracts were combined, washed with 150 mL brine, dried over anhyd. Na<sub>2</sub>SO<sub>4</sub>. The solvent was evaporated using Rotavap. The crude was purified on a silica gel column (Hexane-EtAc 4:1) to give product as colorless oil (1.32 g, 43.6%).

C <sub>29</sub> H <sub>47</sub> BrO <sub>4</sub> S <sub>2</sub>	M.W. = 603.72 g/mol Exact Mass = 602.21 g/mol
TLC	SiO <sub>2</sub> , Hexane-EtAc (4:1) R <sub>f</sub> = 0.25
EI-MS	70eV



	603.1 [M <sup>+</sup> ],
<sup>1</sup> H-NMR	(400 MHz, CDCl <sub>3</sub> ) $\delta$ = 7.20 (s, 2H); 7.18 (s, 1H); 4.55 (t, <i>J</i> = 2.8 Hz, 2H); 4.43 (s, 2H); 3.85-3.81 (m, 2H); 3.71-3.66 (m, 2H); 3.64 (s, 2H); 3.50-3.43 (m, 2H); 3.36-3.30 (m, 2H)
<sup>13</sup> C-NMR	(100 MHz, CDCl <sub>3</sub> ) $\delta$ = 139.96; 138.57; 129.74; 128.46; 99.24; 67.74; 62.75; 36.32; 33.62; 31.77; 31.16; 29.72; 29.47; 25.96; 25.88; 20.11
E.A.	Calculated : C, 57.69%; H, 7.85%; Found : C, 58.03%; H, 7.75%;

Synthesis 2,2'-(5,5'-(5-(hexylthiomethyl)-1,3-phenylene)bis(methylene)bis(sulfanediyl) bis(pentane-5,1-diyl))bis(oxy)bis(tetrahydro-2H-pyran), **26**



In a dry double neck 25 mL flask under Ar, 2,2'-(5,5'-(5-(bromomethyl)-1,3-phenylene)bis(methylene)bis(sulfanediyl) bis(pentane-5,1-diyl)) bis(oxy)bis(tetrahydro-2H-pyran) (**25**) (1.2g, 2 mmol, 1 eq.) and sodium hexane-1-thiolate (**4**) (0.28 g, 2 mmol, 1 eq.) was dissolved in 10 mL dry THF. The mixture was let to stir at RT for 30 minutes. The reaction mixture is poured into 25 mL water. Organic layer was collected. Water layer was extracted with TBME (3 x 15 mL). All the organic extracts were combined, washed with 50 mL brine, dried over anhyd. Na<sub>2</sub>SO<sub>4</sub>. The solvent was evaporated using Rotavap. The crude was purified on a silica gel column (Hexane-EtAc 4:1) and the product product was obtained as colorless oil (0.78 g, 61.4%).

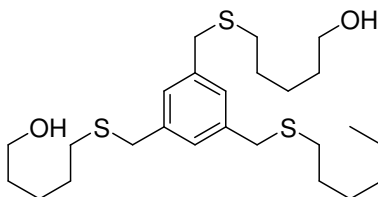
Via one pot reaction

In a dry double neck 100 mL flask under Ar, 1,3,5-tris(bromomethyl)benzene (**1**) (1.78 g, 5 mmol, 1 eq.), 5-(tetrahydro-2H-pyran-2-yloxy)pentane-1-thiol (**24**) (2.04 g, 10 mmol, 2 eq.) and hexane-1-thiol (1.4 ml, 5 mmol, 1 eq.) were dissolved in 50 mL dry THF. Sodium hydrate 60% dispersion in mineral oil (1.32 g, 33 mmol, 3.3 eq.) was added to the previous solution at 0°C. Then the mixture was let to stir at RT for 30 minutes. The reaction mixture is poured into 100 mL water. Organic layer was collected. Water layer was extracted with TBME (3 x 75 mL). All the organic extracts were combined, washed with 150 mL brine, dried

over anhyd. Na<sub>2</sub>SO<sub>4</sub>. The solvent was evaporated using Rotavap. The crude was purified on a silica gel column (Hexane-EtAc 4:1) and the product was obtained as colorless oil (1.15 g, 36%).

C <sub>35</sub> H <sub>60</sub> O <sub>4</sub> S <sub>3</sub>	M.W. = 641.04 g/mol
	Exact Mass = 640.37 g/mol
TLC	SiO <sub>2</sub> , Hexane-EtAc (4:1)
	R <sub>f</sub> = 0.35
EI-MS	70eV
	640.1 [M <sup>+</sup> ],
<sup>1</sup> H-NMR	(400 MHz, CDCl <sub>3</sub> )
	δ = 7.12 (s, 3H); 4.55 (t, J = 2.4 Hz, 2H); 3.88-3.84 (m, 2H); 3.74-3.69 (m, 2H); 3.66 (s, 6H); 3.51-3.46 (m, 2H); 3.38-3.33 (m, 2H); 2.40 (dxt, J <sub>1</sub> = 4.0 Hz, J <sub>2</sub> = 9.2 Hz, 6H); 1.95-1.09 (m, 32H); 0.87 (t, J = 6.4 Hz, 3H)
<sup>13</sup> C-NMR	(100 MHz, CDCl <sub>3</sub> )
	δ = 139.49; 128.34; 128.31; 99.30; 67.78; 62.78; 36.49; 31.87; 31.84; 31.77; 31.17; 29.77; 29.62; 29.52; 28.99; 25.99; 25.89; 22.96; 20.11; 14.46
E.A.	Calculated : C, 65.58%; H, 9.43%;
	Found : C, 65.92%; H, 9.67%;

Synthesis 5,5'-(5-(hexylthiomethyl)-1,3-phenylene)bis(methylene)bis(sulfanediyl) dipentan-1-ol, **27**

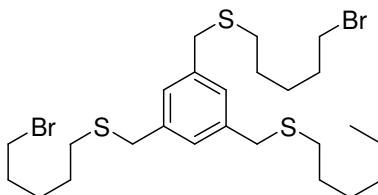


In a dry double neck 25 mL flask under Ar, 2,2'-(5,5'-(5-(hexylthiomethyl)-1,3-phenylene)bis(methylene)bis(sulfanediyl) bis(pentane-5,1-diyl))bis(oxy)bis(tetrahydro-2H-pyran) (**26**) (1.28 g, 2 mmol, 1 eq.) and pyridinium p-toluenesulfonate (0.34 g, 0.2 mmol, 0.1 eq.) were dissolved in 10 ml anhyd. EtOH and the mixture were let to stir at 55 °C for O/N. The solvent was evaporated using Rotavap. The crude was purified on a silica gel column (Hexane-EtAc 1:1) and the product was obtained as colorless oil (0.73 g, 77%).

C <sub>25</sub> H <sub>44</sub> O <sub>2</sub> S <sub>3</sub>	M.W. = 472.81 g/mol
---	---------------------

	Exact Mass = 472.25 g/mol
TLC	SiO <sub>2</sub> , Hexane-EtAc (1:1) R <sub>f</sub> = 0.35
ESI-MS	495.1 [M <sup>+</sup> + Na]
<sup>1</sup> H-NMR	(400 MHz, CDCl <sub>3</sub> ) δ = 7.12 (s, 3H); 3.66 (s, 6H); 3.61 (t, J = 6 Hz, 4H); 2.41 (t, J = 7.2 Hz, 6H); 1.61-1.51 (m, 8H); 1.48-1.391 (m, 6H); 1.34-1.24 (m, 8H); 0.87 (t, J = 6.8 Hz, 3H);
<sup>13</sup> C-NMR	(100 MHz, CDCl <sub>3</sub> ) δ = 139.41; 128.38; 128.33; 63.10; 36.51; 32.66; 31.98; 31.84; 31.73; 29.39; 28.99; 25.42; 22.96; 14.46
E.A.	Calculated : C, 63.51%; H, 9.38%; Found : C, 63.73%; H, 9.27%;

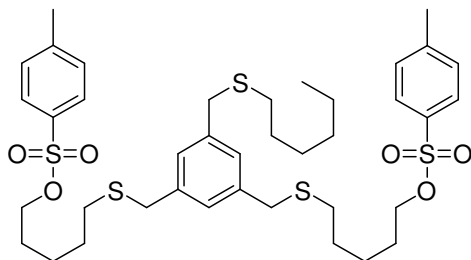
Synthesis (5-(hexylthiomethyl)-1,3-phenylene)bis(methylene)bis((5-bromopentyl) sulfane),  
**28**



In a dry double neck 25 mL flask under Ar, 5,5'-(5-(hexylthiomethyl)-1,3-phenylene)bis(methylene)bis(sulfanediyl) dipentan-1-ol (**27**) (47.28 mg, 0.1 mmol, 1 eq.) was dissolved in 1 mL dry THF. Phosphorus tribromide (23.5 μL, 0.25 mmol, 2.5 eq.) was added dropwise to the previous solution at 0°C. The mixture was let to stir at RT for O/N. The reaction mixture is poured into 20 mL icy water. Organic layer was collected. Water layer was extracted with TBME (3 x 15 mL). All the organic extracts were combined, washed with 25 mL brine, dried over anhyd. Na<sub>2</sub>SO<sub>4</sub>. The solvent was evaporated using Rotavap leaving yellowish oily crude. The purification attempts via column chromatography or distillation were failed.

C <sub>25</sub> H <sub>42</sub> Br <sub>2</sub> S <sub>3</sub>	M.W. = 596.60 g/mol
	Exact Mass = 596.08 g/mol
TLC	SiO <sub>2</sub> , Hexane-EtAc (9:1) R <sub>f</sub> = 0.35

Synthesis 5,5'-(5-(hexylthiomethyl)-1,3-phenylene)bis(methylene)bis(sulfanediyl)bis(pentane-5,1-diyl) bis(4-methylbenzenesulfonate), **29**



In a dry double neck 25 mL flask under Ar, 5,5'-(5-(hexylthiomethyl)-1,3-phenylene)bis(methylene)bis(sulfanediyl) dipentane-1-ol (**27**) (0.47 g, 1 mmol, 1 eq.) and pyridine, (0.16 mL, 2 mmol, 2 eq.) were dissolved in 2 mL dry DCM. *p*-Toluenesulfonyl chloride (0.42 g, 2.2 mmol, 2.2 eq.) dissolved in 1 mL dry DCM was added dropwise to the previous solution at 0°C and the mixture was let to stir at RT for O/N. The reaction mixture was diluted with 10 mL DCM and was quenched by slow addition of 15 mL sat NH<sub>4</sub>Cl solution water. Organic layer was collected. Water layer was extracted with DCM (3 x 15 mL). All the organic extracts were combined, washed with 50 mL sat. Na<sub>2</sub>CO<sub>3</sub> and 50 mL brine, dried over anhyd. Na<sub>2</sub>SO<sub>4</sub>. The solvent was evaporated using Rotavap. The crude was purified on a silica gel column (Hexane-EtAc 3:2) and the product was obtained as colorless oil (0.46 g, 59%).

C<sub>39</sub>H<sub>56</sub>O<sub>6</sub>S<sub>5</sub> M.W. = 781.18 g/mol

Exact Mass = 780.27 g/mol

TLC SiO<sub>2</sub>, Hexane-EtAc (3:1)

R<sub>f</sub> = 0.3

EI-MS 70eV

779.3 [M<sup>+</sup>]

<sup>1</sup>H-NMR (400 MHz, CDCl<sub>3</sub>)

δ = 7.75 (d, 2H); 7.35 (d, 2H); 7.10 (s, 2H); 7.09 (s, 1H); 3.99 (t, *J* = 6.8 Hz, 4H); 3.66 (s, 2H); 3.63 (s, 4H); 2.44 (s, 6H); 2.39 (t, *J* = 7.2 Hz, 3H); 2.35 (t, *J* = 6.8 Hz, 4H); 1.66-1.46 (m, 10H); 1.41-1.25 (m, 10H); 0.87 (t, *J* = 6.4 Hz, 3H);

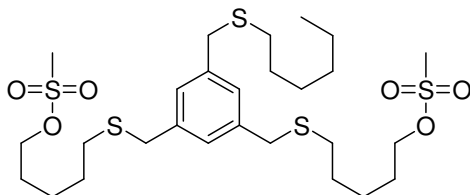
<sup>13</sup>C-NMR (100 MHz, CDCl<sub>3</sub>)

δ = 139.57; 139.31; 133.53; 130.26; 128.39; 128.28; 70.71; 36.49; 31.99; 31.83; 31.53; 29.63; 28.98; 28.87; 25.02; 22.96; 22.06; 14.47

E.A. Calculated : C, 59.96%; H, 7.23%;

Found : C, 59.71%; H, 7.12%;

Synthesis 5,5'-(5-(hexylthiomethyl)-1,3-phenylene)bis(methylene)bis(sulfanediyl)bis(pentane-5,1-diyl) dimethanesulfonate, **30**



In a dry double neck 25 mL flask under Ar, 5,5'-(5-(hexylthiomethyl)-1,3-phenylene)bis(methylene)bis(sulfanediyl) dipentan-1-ol (**27**) (0.47 g, 1 mmol, 1 eq.) and pyridine, (0.16 mL, 2 mmol, 2 eq.) were dissolved in 2 mL dry DCM. Methanesulfonyl chloride (0.17 mL, 2.2 mmol, 2.2 eq.) was added dropwise to the previous solution at 0°C and the mixture was let to stir at RT for O/N. The reaction mixture was diluted with 10 mL DCM and was quenched by slow addition of 15 mL sat NH<sub>4</sub>Cl solution water. Organic layer was collected. Water layer was extracted with DCM (3 x 15 mL). All the organic extracts were combined, washed with 50 mL sat Na<sub>2</sub>CO<sub>3</sub> and 50 mL brine, dried over anhyd. Na<sub>2</sub>SO<sub>4</sub>. The solvent was evaporated using Rotavap. The crude was purified on a silica gel column (Hexane-EtAc 1:1) and the product was obtained as colorless oil (0.26 g, 41%).

C<sub>27</sub>H<sub>48</sub>O<sub>6</sub>S<sub>5</sub> M.W. = 628.99 g/mol

Exact Mass = 628.21 g/mol

TLC SiO<sub>2</sub>, Hexane-EtAc (1:1)

R<sub>f</sub> = 0.3

EI-MS 70eV

627.4 [M<sup>+</sup>],

<sup>1</sup>H-NMR (400 MHz, CDCl<sub>3</sub>)

δ = 7.11 (s, 3H); 4.21 (t, J = 6.4 Hz, 4H); 3.68 (s, 6H); 2.99 (s, 6H); 2.41 (t, J = 7.2 Hz, 6H); 1.81-1.72 (m, 6H); 1.64-1.54 (m, 10H); 1.36-1.21 (m, 6H); 0.86 (t, J = 6.4 Hz, 3H);

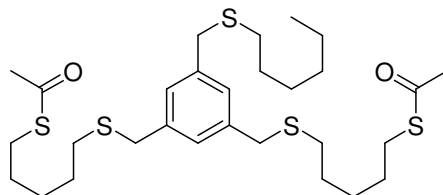
<sup>13</sup>C-NMR (100 MHz, CDCl<sub>3</sub>)

δ = 139.60; 139.32; 128.42; 128.29; 70.21; 37.80; 36.50; 32.02; 31.83; 31.55; 29.64; 29.15; 28.99; 28.98; 25.06; 22.96; 14.47

E.A. Calculated : C, 51.56%; H, 7.69%;

Found : C, 51.11%; H, 7.62%;

Synthesis S,S'-5,5'-(5-(hexylthiomethyl)-1,3-phenylene)bis(methylene)bis(sulfanediyl) bis(pentane-5,1-diyl) diethanethioate, **31**



In a dry double neck 25 ml flask under Ar, 5,5'-(5-(hexylthiomethyl)-1,3-phenylene)bis(methylene)bis(sulfanediyl)bis(pentane-5,1-diyl) bis(4-methylbenzenesulfonate) (**29**) (0.78 g, 1 mmol, 1 eq.), and potassiumthioacetate, (0.25 g, 22 mmol, 2.2 eq.) were dissolved in 2 mL anhyd. DMF. The mixture was let to stir at RT for O/N. The reaction mixture is poured into 20 mL water. The mixture was extracted with DCM (3 x 25 mL). All the organic extracts were combined, washed twice with 50 mL brine, dried over anhyd. Na<sub>2</sub>SO<sub>4</sub>. The solvent was evaporated using Rotavap leading colorless oil as product (0.25g, 42%).

C<sub>29</sub>H<sub>48</sub>O<sub>2</sub>S<sub>5</sub> M.W. = 589.02 g/mol

Exact Mass = 588.23 g/mol

TLC SiO<sub>2</sub>, Hexane-EtAc (3:1)

R<sub>f</sub> = 0.25

EI-MS 70eV

587.3 [M<sup>+</sup>],

<sup>1</sup>H-NMR (400 MHz, CDCl<sub>3</sub>)

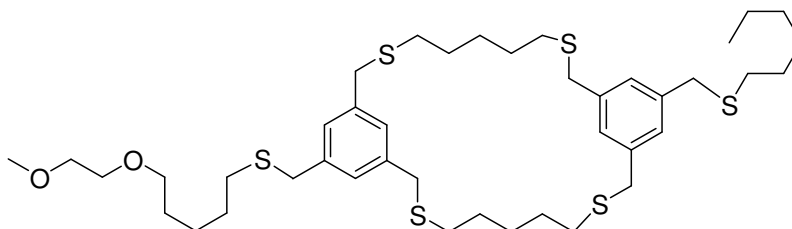
δ = 7.12 (s, 3H); 3.66 (s, 6H); 3.61 (s, 4H); 2.84 (t, *J* = 7.2 Hz, 4H); 2.39 (t, *J* = 7.2 Hz, 6H); 2.32 (s, 6H); 1.59-1.49 (m, 10H); 1.44-1.19 (m, 10H); 0.87 (t, *J* = 6.8 Hz, 3H);

<sup>13</sup>C-NMR (100 MHz, CDCl<sub>3</sub>)

δ = 196.30; 139.53; 139.38; 128.38; 128.31; 36.49; 31.92; 31.85; 31.62; 31.06; 29.63; 29.56; 29.33; 29.11; 29.00; 28.37; 22.97; 14.47

E.A. Calculated : C, 59.13%; H, 8.21%;

Found : C, 59.23%; H, 8.20%;

Synthesis of ligand **B** for enwrapping Au<sub>55</sub> nanoparticles

In a dry double neck 100 mL flask, sodium hydrate 60% dispersion in mineral oil (0.18 mg, 0.44 mmol, 2.2 eq.) dissolved in 50 mL anhyd. DMF. (5-((5-(2-methoxyethoxy)pentylthio)methyl)-1,3-phenylene)dimethanethiol (**14**) (72.12 mg, 0.2 mmol, 1 eq.), and 5,5'-(5-(hexylthiomethyl)-1,3-phenylene)bis-(methylene)bis-(sulfanediy)bis-(pentane-5,1-diyl)bis-(4-methylbenzenesulfonate), **29**, (or 126 mg 5,5'-(5-(hexylthiomethyl)-1,3-phenylene)bis-(methylene)bis-(sulfanediy)bis-(pentane-5,1-diyl) dimethanesulfonate, (**30**) (156.22 mg, 0.2 mmol, 1 eq.) dissolved in 10 mL anhyd. DMF separately were added to the previous solution dropwise at RT. The mixture was let to stir at RT for O/N. The reaction mixture was poured into 10 mL water. The mixture was extracted with TBME (3 x 50 mL). All the organic extracts were combined, washed twice with 100 mL brine, dried over anhyd. Na<sub>2</sub>SO<sub>4</sub>. The solvent was evaporated using Rotavap. The crude was purified on a silica gel column (Hexane-EtAc 4:1) and the desired product(s) were obtained as colorless oil (for **29**, 25.52 mg, 16% yields and for **30**, 30.29 mg, and 18%).

C<sub>42</sub>H<sub>68</sub>O<sub>2</sub>S<sub>6</sub> M.W. = 797.38 g/mol

Exact Mass = 796.35 g/mol

TLC SiO<sub>2</sub>, Hexane-EtAc (4:1)

R<sub>f</sub> = 0.25

MALDI 819.19 [M<sup>+</sup>+Na],

<sup>1</sup>H-NMR (400 MHz, CDCl<sub>3</sub>)

δ = 7.11 (s, 4H); 7.09 (s, 2H); 3.63 (s, 12H); 3.58-3.50 (m, 4H); 3.44 (t, J = 7.2 Hz, 2H); 3.63 (s, 3H); 2.39 (dxt, J<sub>1</sub> = 1.2 Hz, J<sub>2</sub> = 7.2 Hz, 4H); 2.29 (t, J = 6.4 Hz, 8H); 1.60-1.22 (m, 26H); 0.87 (t, J = 6.4 Hz, 3H);

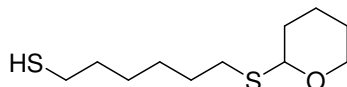
<sup>13</sup>C-NMR (100 MHz, CDCl<sub>3</sub>)

δ = 139.82; 139.75; 139.37; 139.36; 128.36; 72.38; 71.71; 70.45; 59.50; 36.48; 31.94; 31.84; 31.26; 29.63; 29.49; 29.18; 28.99; 28.60; 25.84; 22.96; 14.47

E.A. Calculated : C, 63.26; H, 8.60;

Found : C, 63.10; H, 8.46;  
 GPC THF, 210 nm, 16.68 min, (90.07% pure)

Synthesis 6-(tetrahydro-2H-pyran-2-ylthio)hexane-1-thiol, **32**



In a dry double neck 25 mL flask under Ar, hexane-1,6-dithiol, (1.5 g, 10 mmol, 1 eq.), 3,4-Dihydro-2H-pyran, (1.1 ml, 12 mmol, 1 eq.) and pyridinium p-toluenesulfonate (0.25 g, 1 mmol, 0.1 eq.) were dissolved in 15 mL anhyd. DCM. The mixture was let to stir at RT O/N. The reaction mixture is poured into 30 mL water. Organic layer was collected. Water layer was extracted with DCM (3 x 15 mL). All the organic extracts were combined, washed with 50 mL brine, dried over anhyd. Na<sub>2</sub>SO<sub>4</sub>. The solvent was evaporated using Rotavap. The crude was purified on a silica gel column (Hex-EtAc 9:1) and the product was obtained as colorless oil (0.98 g, 41.9%, 79.2% yield due to the amount of consumed starting material).

C<sub>11</sub>H<sub>22</sub>OS<sub>2</sub> M.W. = 234.42 g/mol  
 Exact Mass = 234.11 g/mol

TLC SiO<sub>2</sub>, Hexane-EtAc (9:1)  
 R<sub>f</sub> = 0.3

EI-MS 70 eV  
 234.1 [M<sup>+</sup> + Na]

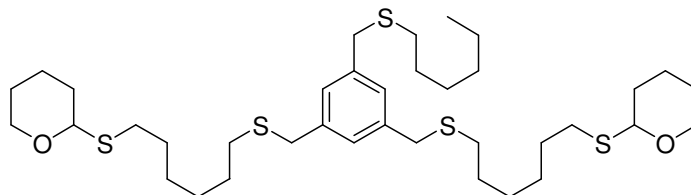
<sup>1</sup>H-NMR (400 MHz, CDCl<sub>3</sub>)  
 δ= 4.87-4.82 (*m*, 1H); 4.11-4.05 (*m*, 1H); 3.52-3.47 (*m*, 1H); 2.72-2.44 (*m*, 4H); 1.98-1.44 (*m*, 14H); 1.34 (*t*, *J*= 6.8, 2H);

<sup>13</sup>C-NMR (100 MHz, CDCl<sub>3</sub>)  
 δ= 82.69; 65.03; 34.00; 31.85; 30.61; 29.80; 28.05; 26.02; 24.90; 22.20

E.A. Calculated : C, 56.36%; H, 9.46%;  
 Found : C, 56.58%; H, 9.22%;



Synthesis 2,2'-(6,6'-(5-(hexylthiomethyl)-1,3-phenylene)bis(methylene) bis(sulfanediyl) bis(hexane-6,1-diyl))bis(sulfanediyl)bis(tetrahydro-2H-pyran), **33**



In a dry double neck 25 mL flask under Ar, 1,3,5-tris(bromomethyl)benzene (**1**) (1.78 g, 5 mmol, 1 eq.), 6-(tetrahydro-2H-pyran-2-ylthio)hexane-1-thiol (**32**) (2.34 g, 10 mmol, 1 eq.) and hexane-1-thiol (1.4 mL, 5 mmol, 1 eq.) were dissolved in 15 mL anhyd. THF. Sodium hydrate 60% dispersion in mineral oil (1.32 g, 33 mmol, 3.3 eq.) was added to the previous solution at 0°C. Then the mixture was let to stir at RT for 30 minutes. The reaction mixture is poured into 50 mL water. Organic layer was collected. Water layer was extracted with TBME (3 x 25 mL). All the organic extracts were combined, washed with 75 mL brine, dried over anhyd. Na<sub>2</sub>SO<sub>4</sub>. The solvent was evaporated using Rotavap. The crude was purified on a silica gel column (Hex-EtAc 9:1) and the product was obtained as colorless oil (1.51 g, 43%).

C<sub>37</sub>H<sub>64</sub>O<sub>2</sub>S<sub>5</sub> M.W. = 701.23 g/mol

Exact Mass = 700.35 g/mol

TLC SiO<sub>2</sub>, Hexane-EtAc (9:1)

R<sub>f</sub> = 0.2

EI-MS 70eV

700.1 [M<sup>+</sup>],

<sup>1</sup>H-NMR (400 MHz, CDCl<sub>3</sub>)

δ = 7.12 (s, 3); 4.86-4.82 (m, 2H); 4.12-4.06 (m, 2H); 3.67 (s, 6H); 3.52-3.48 (m, 2H); 2.72-2.48 (m, 4H); 2.40 (t, J = 7.2, 6H); 1.95-1.28 (m, 38H); 0.88 (t, J = 6.4 Hz, 3H);

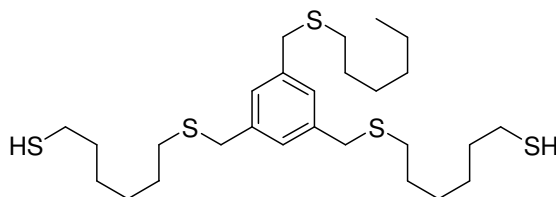
<sup>13</sup>C-NMR (100 MHz, CDCl<sub>3</sub>)

δ = 139.51; 139.40; 128.36; 128.31; 82.71; 65.01; 36.49; 31.90; 31.86; 31.86; 31.71; 30.60; 29.96; 29.63; 29.25; 29.00; 28.58; 26.03; 22.96; 22.21; 14.63

E.A. Calculated : C, 63.37%; H, 9.20%;

Found : C, 63.08%; H, 9.03%;

Synthesis 5,5'-(5-(hexylthiomethyl)-1,3-phenylene)bis(methylene)bis(sulfaneyl) dipentane-1-thiol, **34**



In a dry double neck 25 mL flask under Ar, 2,2'-(6,6'-(5-(hexylthiomethyl)-1,3-phenylene)bis(methylene)bis(sulfaneyl)bis-(hexane-6,1-diyl))bis(sulfaneyl)bis-(tetrahydro-2H-pyran) (**33**) (0.70 g, 1 mmol, 1 eq.) and pyridinium p-toluenesulfonate (0.5 g, 0.2 mmol, 0.2 eq.) were dissolved in 10 mL anhyd. EtOH and the mixture were let to stir at 55°C for O/N. The solvent was evaporated using Rotavap. The crude was purified on a silica gel column (Hex-EtAc 9:1) and the product was obtained as colorless oil (0.05 g, 9% and 25.4% due to the amount of consumed starting material).

$C_{27}H_{48}S_5$  M.W. = 533.00 g/mol

Exact Mass = 532.24 g/mol

TLC  $SiO_2$ , Hexane-EtAc (9:1)

$R_f$  = 0.35

EI-MS 70eV

531.7 [ $M^+$ ],

$^1H$ -NMR (400 MHz,  $CDCl_3$ )

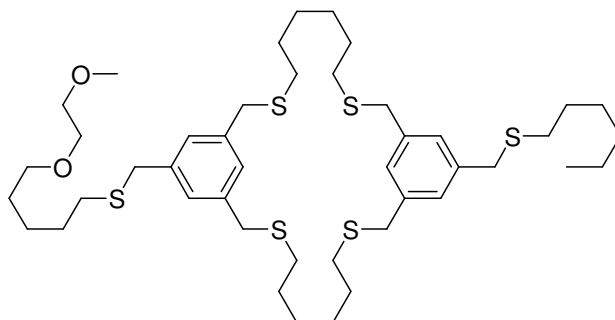
$\delta$  = 7.13 (s, 3H); 3.67 (s, 6H); 2.50 (q,  $J_1$  = 3.6 Hz,  $J_2$  = 12.4 Hz, 4H); 2.41 (t,  $J$  = 7.2 Hz, 6H); 1.61-1.21 (m, 26H); 0.88 (t,  $J$  = 7.5 Hz, 3H);

$^{13}C$ -NMR (100 MHz,  $CDCl_3$ )

$\delta$  = 139.54; 139.39; 128.39; 128.31; 36.52; 33.95; 31.96; 31.85; 31.68; 29.64; 29.07; 27.94; 24.88; 22.97; 14.47

E.A. Calculated : C, 60.84%; H, 9.08%;

Found : C, 60.92%; H, 9.01%;

Synthesis of ligand **C** for enwrapping Au<sub>55</sub> nanoparticles

In a dry double neck 100 mL flask, sodium hydrate 60% dispersion in mineral oil (0.18 mg, 0.44 mmol, 2.2 eq.) dissolved in 50 mL anhyd. DMF. 5,5'-(5-(hexylthiomethyl)-1,3-phenylene)bis(methylene)bis(sulfaneydiyl) dipentane-1-thiol (**34**) (106.6 mg, 0.2 mmol, 1 eq.), and (3,5-bis(bromomethyl)benzyl)(5-(2-methoxyethoxy)pentyl)sulfane (**8**) (90.85 mg, 0.2 mmol, 1 eq.) dissolved separately in 10 mL anhyd. DMF and were added dropwise to the previous solution at RT. The mixture was let to stir at RT for O/N. The reaction mixture is poured into 10 mL water. The mixture was extracted with TBME (3 x 50 mL). All the organic extracts were combined, washed twice with 100 mL brine, dried over anhyd. Na<sub>2</sub>SO<sub>4</sub>. The solvent was evaporated using Rotavap. The crude was purified on a silica gel column (Hexane-EtAc 4:1) and the product was obtained as colorless oil (for **34** 25.52 mg, 16%, and for **30**, 30.29 mg, 18%).

C<sub>44</sub>H<sub>72</sub>O<sub>2</sub>S<sub>6</sub> M.W. = 825.43 g/mol

Exact Mass = 824.39 g/mol

TLC SiO<sub>2</sub>, Hexane-EtAc (4:1)

R<sub>f</sub> = 0.25

MALDI 824.19 [M<sup>+</sup>+Na],

<sup>1</sup>H-NMR (400 MHz, CDCl<sub>3</sub>)

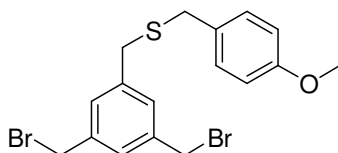
δ = 7.11 (s, 4H); 7.09 (s, 2H); 3.66 (s, 12H); 3.55 (m, 4H); 3.44 (t, J = 6.8 Hz, 2H); 3.38 (s, 3H); 2.40 (m, 2H); 2.29 (t, J = 7.2 Hz, 12H); 1.62-1.18 (m, 28H); 0.87 (t, J = 6.4 Hz, 3H);

<sup>13</sup>C-NMR (100 MHz, CDCl<sub>3</sub>)

δ = 139.82; 139.75; 139.36; 128.36; 72.38; 71.71; 70.45; 59.50; 36.48; 31.94; 31.84; 31.36; 29.63; 29.49; 29.18; 28.99; 28.59; 25.84; 22.96; 14.47

E.A. Calculated : C, 64.02; H, 8.79;

Found : C, 63.90; H, 8.56;

Synthesis (3,5-bis(bromomethyl)benzyl)(4-methoxybenzyl)sulfane, **35**

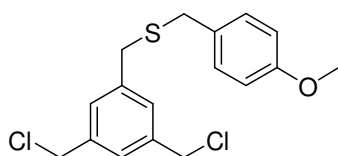
In a dry double neck 250 mL flask under Ar, 1,3,5-tris(bromomethyl)benzene (**1**) (3.57 g, 10 mmol, 1 eq.) was dissolved in 100 ml THF. Methoxybenzylmercaptane (2.3 ml, 11 mmol, 1.1 eq.) and sodium hydrate 60% dispersion in mineral oil (660 mg, 11 mmol, 1.1 eq.) added slowly to the reaction mixture. Then the mixture was let to stir at RT for 30 minutes. The reaction mixture is poured into 75 mL water. Organic layer was collected. Water layer was extracted with TBME (3 x 75 mL). All the organic extracts were combined, washed with 150 mL brine, dried over anhyd. Na<sub>2</sub>SO<sub>4</sub>. The solvent was evaporated using Rotavap leaving yellowish oily crude. The purification attempts via column chromatography or distillation were failed.

C<sub>17</sub>H<sub>18</sub>Br<sub>2</sub>OS M.W. = 430.20 g/mol

Exact Mass = 427.94 g/mol

TLC SiO<sub>2</sub>, Hexane-EtAc (5:1)

R<sub>f</sub> = 0.6

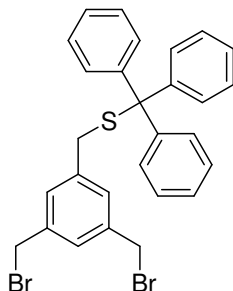
Synthesis (3,5-bis(chloromethyl)benzyl)(4-methoxybenzyl)sulfane, **36**

In a dry double neck 250 mL flask under Ar, 1,3,5-tris(chloromethyl)benzene (**6**) (2.24g, 10 mmol, 1 eq.) was dissolved in 100 mL THF. Methoxybenzylmercaptane, (2.3 ml, 11 mmol, 1.1 eq.) and sodium hydrate 60% dispersion in mineral oil (660 mg, 11 mmol, 1.1 eq.) added slowly to the reaction mixture. Then the mixture was let to stir at RT for 30 minutes. The reaction mixture is poured into 75 mL water. Organic layer was collected. Water layer was extracted with TBME (3 x 75 mL). All the organic extracts were combined, washed with 150 mL brine, dried over anhyd. Na<sub>2</sub>SO<sub>4</sub>. The solvent was evaporated using Rotavap leaving yellowish oily crude. The purification attempts via column chromatography or distillation were failed.

C<sub>17</sub>H<sub>18</sub>Cl<sub>2</sub>OS M.W. = 341.30 g/mol

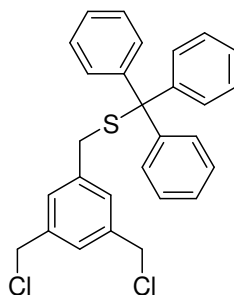
Exact Mass = 340.05 g/mol  
 TLC SiO<sub>2</sub>, Hexane-EtAc (5:1)  
 R<sub>f</sub> = 0.6

Synthesis of (3,5-bis(bromomethyl)benzyl)(triphenyl)sulfane, **37**



In a dry double neck 100 mL flask under Ar, 1,3,5-tris(bromomethyl)benzene (**1**) (3.57 g, 10 mmol, 1 eq.), triphenylmethanethiol (2.76 g, 10 mmol, 1 eq.) and sodium hydrate 60% dispersion in mineral oil (0.66 g, 11 mmol, 1.1 eq.) were dissolved in 60 mL THF. Then the mixture was let to stir at RT for 30 minutes. The reaction mixture is poured into 75 mL water. Organic layer was collected. Water layer was extracted with TBME (3 x 50 mL). All the organic extracts were combined, washed with 150 mL brine, dried over anhyd. Na<sub>2</sub>SO<sub>4</sub>. The solvent was evaporated using Rotavap. The crude was purified on a silica gel column (Hexane-DCM 4:1) and the product was obtained as white powder (2.54 g, 46%).

C<sub>28</sub>H<sub>24</sub>Br<sub>2</sub>S M.W. = 552.36 g/mol  
 Exact Mass = 550.00 g/mol  
 TLC SiO<sub>2</sub>, Hexane-DCM (4:1)  
 R<sub>f</sub> = 0.25  
 EI-MS 70eV  
 549.1 [M<sup>+</sup>],  
<sup>1</sup>H NMR (400 MHz, CDCl<sub>3</sub>)  
 δ = 7.48-7.42 (*m*, 6H), 7.35-7.20 (*m*, 10H), 7.01 (*s*, 2H), 4.39 (*s*, 4H), 3.32 (*s*, 2H)  
<sup>13</sup>C NMR (100 MHz, CDCl<sub>3</sub>)  
 δ = 144.51; 138.73; 138.42; 129.77; 129.64; 128.29; 128.02; 126.85; 67.30; 36.41; 32.66  
 E.A. Calculated : C, 60.88%; H, 4.38%;  
 Found : C, 61.08%; H, 4.21%;

Synthesis of (3,5-bis(chloromethyl)benzyl)(trityl)sulfane, **38**

In a dry double neck 100 mL flask under Ar, 1,3,5-tris(chloromethyl)benzene (**6**) (2.22 g, 10 mmol, 1 eq.), triphenylmethanethiol (2.76 g, 10 mmol, 1 eq.) and sodium hydrate 60% dispersion in mineral oil (0.66 g, 11 mmol, 1.1 eq.) were dissolved in 60 mL THF. Then the mixture was let to stir at RT for 30 minutes. The reaction mixture is poured into 75 mL water. Organic layer was collected. Water layer was extracted with TBME (3 x 50 mL). All the organic extracts were combined, washed with 150 mL brine, dried over anhyd. Na<sub>2</sub>SO<sub>4</sub>. The solvent was evaporated using Rotavap. The crude was purified on a silica gel column (Hexane-DCM 4:1) and the product was obtained as white powder (2.22 g, 48%).

C<sub>28</sub>H<sub>24</sub>Cl<sub>2</sub>S M.W. = 463.46 g/mol

Exact Mass = 462.10 g/mol

TLC SiO<sub>2</sub>, Hexane-DCM (4:1)

R<sub>f</sub> = 0.25

EI-MS 70eV

461.14 [M<sup>+</sup>],

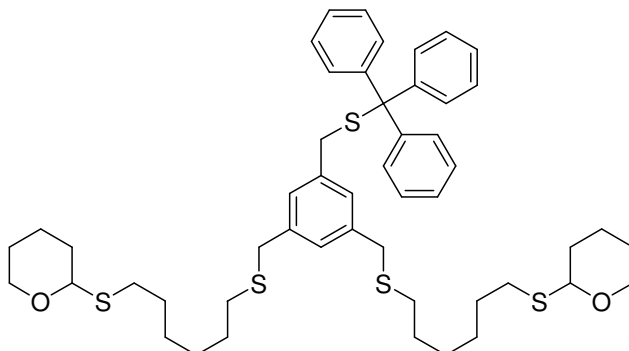
<sup>1</sup>H-NMR (250 MHz, CDCl<sub>3</sub>)

δ = 7.49 - 7.44 (*m*, 6H); 7.35 - 7.20 (*m*, 10H); 7.03 (*s*, 2H); 4.47 (*s*, 4H); 3.34 (*s*, 2H);

E.A. Calculated : C, 72.56%; H, 5.22%;

Found : C, 72.80%; H, 5.12%;

Synthesis of 2,2'-(6,6'-(5-(tritylthiomethyl)-1,3-phenylene)bis(methylene)bis(sulfanediyl)bis(hexane-6,1-diy))bis(sulfanediyl)bis(tetrahydro-2H-pyran), **39**



In a dry double neck 25 mL flask under Ar, (3,5-bis(bromomethyl)benzyl)(trityl)sulfane (**38**) (0.55 g, 1 mmol, 1 eq.), 6-(tetrahydro-2H-pyran-2-ylthio)hexane-1-thiol (**32**) (0.51 g, 2.2 mmol, 2.2 eq.) and sodium hydrate 60% dispersion in mineral oil (0.12 g, 3 mmol, 3 eq.) was dissolved in 15 mL dry THF. Then the mixture was let to stir at RT for 30 minutes. The reaction mixture is poured into 25 mL water. Organic layer was collected. Water layer was extracted with TBME (3 x 15 mL). All the organic extracts were combined, washed with 50 mL brine, dried over anhyd. Na<sub>2</sub>SO<sub>4</sub>. The solvent was evaporated using Rotavap. The crude was purified on a silica gel column (Hexane-EtAc 5:1) and the product was obtained as colorless oil (0.83 g, 96%).

C<sub>50</sub>H<sub>66</sub>O<sub>2</sub>S<sub>5</sub> M.W. = 859.37 g/mol

Exact Mass = 858.37 g/mol

TLC SiO<sub>2</sub>, Hexane-EtAc (5:1)

R<sub>f</sub> = 0.2

MALDI 881.59 [M<sup>+</sup>+Na],

<sup>1</sup>H-NMR (400 MHz, CDCl<sub>3</sub>)

δ = 7.49 -7.43 (*m*, 6H); 7.38-7.22 (*m*, 9H); 7.10 (*s*, 1H); 6.96 (*s*, 2H); 4.87-4.83 (*m*, 2H); 4.13-4.07 (*m*, 2H); 3.64 (*s*, 4H); 3.53-3.48 (*m*, 2H); 2.71-2.49 (*m*, 4H); 2.40 (*t*, *J* = 7.2, 4H); 1.95-1.24 (*m*, 30H);

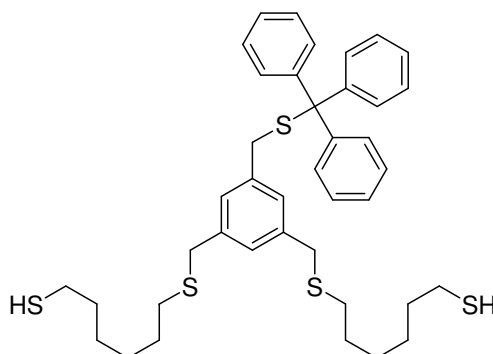
<sup>13</sup>C-NMR (100 MHz, CDCl<sub>3</sub>)

δ = 145.07; 139.39; 137.91; 130.03; 128.57; 128.43; 128.37; 127.12; 82.70; 67.86; 65.03; 37.18; 36.43; 31.87; 31.80; 30.69; 30.22; 29.51; 28.97; 28.88; 26.04; 22.23

E.A. Calculated : C, 69.88%; H, 7.74%;

Found : C, 69.70%; H, 7.61%;

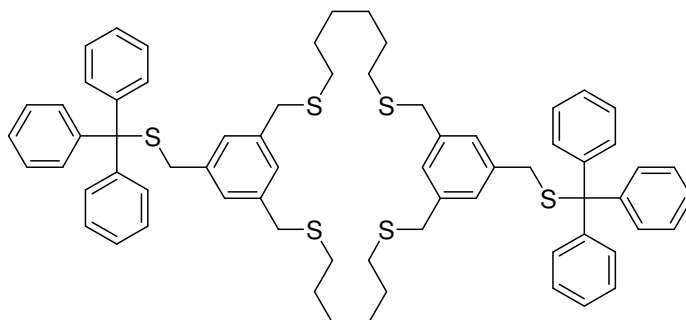
Synthesis of 6,6'-(5-(tritylthiomethyl)-1,3-phenylene)bis(methylene)bis(sulfanediyl) dihexane-1-thiol, **40**



In a dry double neck 25 mL flask under Ar, 2,2'-(6,6'-(5-(tritylthiomethyl)-1,3-phenylene)bis(methylene)bis(sulfanediyl))bis(hexane-6,1-diyl))bis(sulfanediyl)bis(tetrahydro-2H-pyran) (**39**) (0.43 g, 0.5 mmol, 1 eq.) and pyridinium p-toluenesulfonate (0.5 g, 0.2 mmol, 0.2 eq.) were dissolved in 10 mL anhyd. EtOH and the mixture were let to stir at 55°C for O/N. The solvent was evaporated using Rotavap. The crude was purified on a silica gel column (Hexane-EtAc 4:1) and the product was obtained as colorless oil (0.11 g, 31.1%, and 45.4% due to the amount of consumed starting material).

$C_{40}H_{50}S_5$	M.W. = 691.15 g/mol Exact Mass = 690.25 g/mol
TLC	SiO <sub>2</sub> , Hexane-EtAc (4:1) $R_f = 0.4$
MALDI	713.43 [ $M^+ + Na$ ],
<sup>1</sup> H-NMR	(400 MHz, CDCl <sub>3</sub> ) $\delta = 7.45$ ( <i>d</i> , $J = 7.6$ Hz, 6H); 7.32-7.22 ( <i>m</i> , 9H); 7.08( <i>s</i> , 1H); 6.93 ( <i>s</i> , 2H); 3.62 ( <i>s</i> , 4H); 3.29 ( <i>s</i> , 2H); 2.48 ( <i>q</i> , $J_1 = 3.4$ Hz, $J_2 = 7.8$ Hz 4H); 2.37 ( <i>t</i> , $J = 7.2$ Hz, 4H); 1.59-1.18 ( <i>m</i> , 18H);
<sup>13</sup> C-NMR	(100 MHz, CDCl <sub>3</sub> ) $\delta = 145.08$ ; 139.41; 137.93; 130.04; 128.58; 128.36; 127.13; 37.21; 36.48; 34.22; 31.78; 31.26; 29.49; 28.66; 28.31; 25.91; 24.93;
E.A.	Calculated : C, 69.51%; H, 7.29%; Found : C, 69.25%; H, 7.31%;

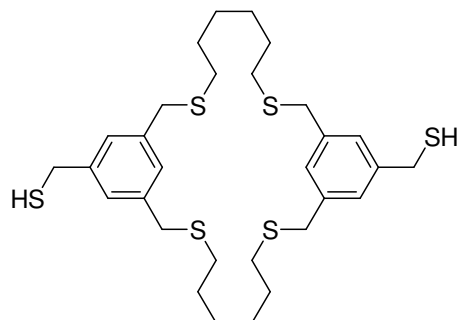


Synthesis of protected ligand **D** for enwrapping Au<sub>55</sub> nanoparticles, **41**

In a dry double neck 100 mL flask, sodium hydrate 60% dispersion in mineral oil (0.09 mg, 0.44 mmol, 2.2 eq.) was dissolved in 50 ml dry THF under Ar. Then 6,6'-(5-(tritylthiomethyl)-1,3-phenylene)bis(methylene)bis(sulfaneyl) dihexane-1-thiol (**40**) (69.15 mg, 0.1 mmol, 1 eq.) and (3,5-bis(bromomethyl)benzyl)(trityl)sulfane (**37**) (55.24 mg, 0.1 mmol, 1 eq.) dissolved separately in 5 mL dry THF were added dropwise to the previous solution at RT. The mixture was let to stir at RT for O/N. The reaction mixture is poured into 10 mL water. The mixture was extracted with TBME (3 x 50 mL). All the organic extracts were combined, washed twice with 100 mL brine, dried over anhyd. Na<sub>2</sub>SO<sub>4</sub>. The solvent was evaporated using Rotavap. The crude was purified on a silica gel column (Hexane-EtAc 5:1) and the product was obtained as colorless oil (34.61 mg, 32%).

C <sub>68</sub> H <sub>72</sub> S <sub>6</sub>	M.W. = 1081.69 g/mol Exact Mass = 1080.40 g/mol
TLC	SiO <sub>2</sub> , Hexane-EtAc (5:1) R <sub>f</sub> = 0.25
MALDI	1103.09 [M <sup>+</sup> +Na],
<sup>1</sup> H-NMR	(400 MHz, CDCl <sub>3</sub> ) δ= 7.52 -7.44 ( <i>m</i> , 12H); 7.36-7.24 ( <i>m</i> , 18H); 7.03 ( <i>s</i> , 2H); 6.92 ( <i>s</i> , 4H); 3.58 ( <i>s</i> , 8H); 3.27 ( <i>s</i> , 4H); 2.26 ( <i>t</i> , <i>J</i> = 7.2 Hz, 8H); 1.62-1.21 ( <i>m</i> , 16H);
<sup>13</sup> C-NMR	(100 MHz, CDCl <sub>3</sub> ) δ= 145.07; 139.35; 138.16; 130.04; 128.60; 128.40; 127.16; 67.88; 37.22; 36.26; 31.23; 29.54; 28.82;
E.A.	Calculated : C, 75.51; H, 6.71; Found : C, 75.85; H, 6.60;

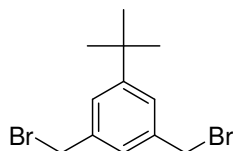
Synthesis of ligand **D** for enwrapping Au<sub>55</sub> nanoparticles



In a dry double neck 25 mL flask under Ar, protected ligand **D** (**41**) (27.04 mg, 0.025 mmol, 1 eq) was dissolved in 5 mL anhyd. DCM. Then triethylsilane (0.014 ml, 0.075 mmol, 3 eq.) and trifluoroacetic acid (0.2 ml, 4% v/v in DCM) was added to the previous solution. The mixture was let to stir at RT for 15 min. The reaction mixture is poured into 5 mL sat. NaHCO<sub>3</sub> solution. The mixture was extracted with DCM (3 x 5 mL). All the organic extracts were combined, washed twice with 25 mL brine, dried over anhyd. Na<sub>2</sub>SO<sub>4</sub>. The solvent was evaporated using Rotavap. The crude was purified on a silica gel column (Hexane-EtAc 9:1) and the product was obtained as colorless oil (11.64 mg, 78%).

C <sub>30</sub> H <sub>44</sub> S <sub>6</sub>	M.W. = 597.06 g/mol
	Exact Mass = 596.18 g/mol
TLC	SiO <sub>2</sub> , Hexane-EtAc (9:1)
	R <sub>f</sub> = 0.25
MALDI	619.92 [M <sup>+</sup> +Na],
<sup>1</sup> H-NMR	(400 MHz, CDCl <sub>3</sub> )
	δ= 7.14 (s, 4H); 7.10 (s, 2H); 3.71 (d, J= 3.6 Hz, 4H); 3.65 (s, 8H); 2.33 (t, J= 7.2 Hz, 8H); 1.76 (t, J= 6.8 Hz, 2H); 1.48-1.40 (m, 8H); 1.30-1.22 (m, 8H);
<sup>13</sup> C-NMR	(100 MHz, CDCl <sub>3</sub> )
	δ= 142.24; 139.65; 128.57; 127.54; 36.33; 31.32; 29.52; 29.15; 28.77
E.A.	Calculated : C, 60.35; H, 7.43;
	Found : C, 60.69; H, 7.31;

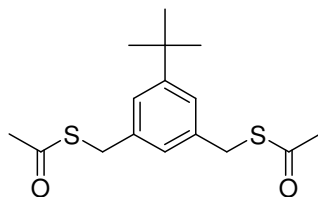
Synthesis of 1,3-Bis(bromomethyl)-5-*tert*-butylbenzene, **42**



In a dry double neck 250 mL flask under Ar, N-Bromosuccinimide (30.17 g, 170 mmol, 2.1 eq) and 5-*tert*-butyl-*m*-xylene (15.0 mL, 12.98 g, 80 mmol, 1 eq) were dissolved in methyl formate (150 mL). 2,2'-Azobis(2-methylpropionitrile) (75 mg) was then added and the reaction mixture was illuminated by a 500 W halogen lamp for 3 hours. The solvent was evaporated by using a rotary evaporator and the residue was redissolved in DCM. All the organic extracts were combined, washed twice with 75 mL brine, dried over anhyd. Na<sub>2</sub>SO<sub>4</sub>. The solvent was evaporated using Rotavap. The residue was recrystallized from dichloromethane-hexane twice to give the product as white crystals (18.02 g, 70%).

C <sub>12</sub> H <sub>16</sub> Br <sub>2</sub>	M.W. = 320.06 g/mol Exact Mass = 317.96 g/mol
TLC	SiO <sub>2</sub> , Hexane-EtAc (9:1) R <sub>f</sub> = 0.35
MALDI	316.92 [M <sup>+</sup> +Na],
<sup>1</sup> H-NMR	(400 MHz, CDCl <sub>3</sub> ) δ = 7.34 ( <i>br</i> , 2H); 7.27 ( <i>br</i> , 1H); 4.49 ( <i>s</i> , 4H); 1.34 ( <i>s</i> , 9H);
<sup>13</sup> C-NMR	(100 MHz, CDCl <sub>3</sub> ) δ = 153.06; 138.42; 127.32; 126.78; 35.20; 33.97; 31.61;
E.A.	Calculated : C, 45.03; H, 5.04; Found : C, 45.33; H, 5.21;

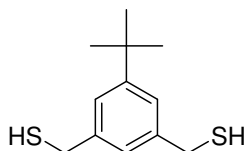
Synthesis of S,S'-(5-*tert*-butyl-1,3-phenylene)bis(methylene) diethanethioate, **43**



In a dry double neck 100 mL flask under Ar, 1,3-Bis(bromomethyl)-5-*tert*-butylbenzene (3.20 g, 10 mmol, 1 eq.) and potassium thioacetate (2.51 g, 22 mmol, 2.2 eq.) were dissolved in 10 mL anhyd. DMF. Then the mixture was let to stir at RT for O/N. The mixture was let to stir at RT for. The reaction mixture is poured into 20 mL water. The mixture was extracted with TBME (3 x 25 mL). All the organic extracts were combined, washed twice with 75 mL brine, dried over anhyd. Na<sub>2</sub>SO<sub>4</sub>. The solvent was evaporated using Rotavap and the product was obtained as white powder (2.82 g, 91%).

$C_{16}H_{22}O_2S_2$	M.W. = 310.47 g/mol Exact Mass = 310.11 g/mol
TLC	SiO <sub>2</sub> , Hexane-EtAc (9:1) R <sub>f</sub> = 0.2
MP	140-142 °C
MALDI	310.0 [M <sup>+</sup> +Na],
<sup>1</sup> H-NMR	(400 MHz, CDCl <sub>3</sub> ) δ= 7.18 (s, 2H); 7.01 (s, 1H); 4.09 (s, 4H); 2.35 (s, 6H); 1.29 (s, 9H);
<sup>13</sup> C-NMR	(100 MHz, CDCl <sub>3</sub> ) δ= 195.54; 152.51; 137.87; 126.75; 126.82; 125.39; 35.07; 33.97; 31.67; 30.75
E.A.	Calculated : C 61.90%, H 7.14% Found : C 62.22%, H 7.06%

Synthesis of (5-*tert*-Butyl-1,3-phenylene)dimethanethiol, **44**

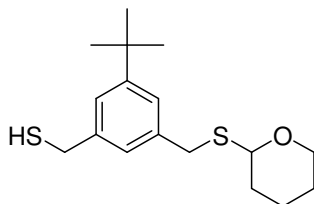


In a dry double neck 25 ml flask under Ar, 1,3-bis(bromomethyl)-5-*tert*-butylbenzene (**42**) (3.20 g, 10 mmol, 1 eq) and thiourea (1.77 g, 23.3 mmol, 2.5 eq) was dissolved in 40 ml dry DMSO under an atmosphere of argon. Then the mixture was let to stir at RT for O/N. The mixture was poured into a 50 mL 1M ice cold aqueous sodium hydroxide solution, which was then acidified with 1M hydrochloric acid. The mixture was extracted with DCM (3 x 50 mL). All the organic extracts were combined, washed twice with 75 mL brine, dried over anhyd. Na<sub>2</sub>SO<sub>4</sub>. The solvent was evaporated using Rotavap and the product was obtained by kugelrohr distillation (2 x 10<sup>-1</sup> mbar, 195 °C) as white powder (1.34 g, 64%).

$C_{12}H_{18}S_2$	M.W. = 226.40 g/mol Exact Mass = 226.08 g/mol
TLC	SiO <sub>2</sub> , Hexane-EtAc (9:1) R <sub>f</sub> = 0.4
EI-MS	70eV 225.1 [M <sup>+</sup> ],

$^1\text{H-NMR}$	(400 MHz, $\text{CDCl}_3$ ) $\delta$ = 7.22 (s, 2H); 7.14 (s, 1H); 3.74 (d, $J$ = 7.2 Hz, 4H); 1.78 (t, $J$ = 7.2 Hz, 2H); 1.33 (s, 9H).
$^{13}\text{C-NMR}$	(100 MHz, $\text{CDCl}_3$ ) $\delta$ = 152.56; 141.55; 125.30; 124.31; 35.17; 31.75; 29.52
E.A.	Calculated : C, 63.66; H, 8.01; Found : C, 63.39; H, 7.89;

Synthesis of (3-*tert*-butyl-5-((tetrahydro-2H-pyran-2-ylthio)methyl)phenyl)methanethiol, **45**



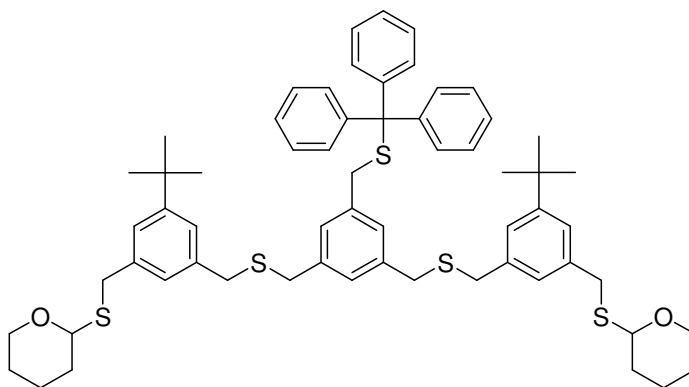
In a dry double neck 25 mL flask under Ar, (5-*tert*-Butyl-1,3-phenylene)dimethanethiol (**44**) (2.26 g, 10 mmol, 1 eq.), 3,4-Dihydro-2H-pyran (1.1 ml, 12 mmol, 1 eq.) and pyridinium *p*-toluenesulfonate (0.25 g, 1 mmol, 0.1 eq.) were dissolved in 15 mL anhyd. DCM. The mixture was let to stir at RT O/N. The reaction mixture is poured into 30 mL water. Organic layer was collected. Water layer was extracted with DCM (3 x 15 mL). All the organic extracts were combined, washed with 50 mL brine, dried over anhyd.  $\text{Na}_2\text{SO}_4$ . The solvent was evaporated using Rotavap. The crude was purified on a silica gel column (Hexane-EtAc 9:1) and the product was obtained as colorless oil (0.99 g, 31.9%, 45.2% due to the amount of consumed starting material).

$\text{C}_{17}\text{H}_{26}\text{OS}_2$	M.W. = 310.52 g/mol Exact Mass = 310.14 g/mol
TLC	$\text{SiO}_2$ , Hexane-EtAc (9:1) $R_f$ = 0.3
EI-MS	70eV 310.1 [ $\text{M}^+$ ],
$^1\text{H-NMR}$	(400 MHz, $\text{CDCl}_3$ ) $\delta$ = 7.21 (s, 2H); 7.11 (s, 1H); 4.75-4.69 (m, 1H); 4.15-4.08 (m, 1H); 3.87 (s, 1H); 3.76-3.70 (m, 3H); 3.58-3.49 (m, 1H); 1.98-1.84 (m, 3H); 1.61-1.44 (m, 4H); 1.32 (t, $J$ = 6.4, 9H);
$^{13}\text{C-NMR}$	(100 MHz, $\text{CDCl}_3$ )

$\delta$ = 152.21; 141.28; 138.92; 126.20; 125.33; 124.07; 81.26; 65.07; 35.10;  
34.60; 31.76; 31.29; 29.55; 26.04; 22.19

E.A.            Calculated     : C, 65.76%; H, 8.44%;  
                  Found             : C, 65.96%; H, 8.65%;

Synthesis of 2,2'-5,5'-(5-(tritylthiomethyl)-1,3-phenylene)bis(methylene)bis(sulfaneyl) bis(methylene)bis(3-tert-butyl-5,1-phenylene)bis(methylene)bis(sulfaneyl) bis(tetrahydro-2H-pyran), **46**



In a dry double neck 25 mL flask under Ar, (3,5-bis(bromomethyl)benzyl)(trityl)sulfane (**45**) (0.55 g, 1 mmol, 1 eq.), (3-tert-butyl-5-((tetrahydro-2H-pyran-2-ylthio)methyl)phenyl)methanethiol (0.68 g, 2.2 mmol, 2.2 eq.) and sodium hydrate 60% dispersion in mineral oil (0.12 g, 3 mmol, 3 eq.) was dissolved in 15 mL dry THF. The mixture was let to stir at RT for 30 minutes. The reaction mixture is poured into 25 mL water. Organic layer was collected. Water layer was extracted with TBME (3 x 15 mL). All the organic extracts were combined, washed with 50 mL brine, dried over anhyd. Na<sub>2</sub>SO<sub>4</sub>. The solvent was evaporated using Rotavap. The crude was purified on a silica gel column (Hexane-EtAc 9:1) and the product was obtained as colorless oil (0.94 g, 93%)

C<sub>62</sub>H<sub>74</sub>O<sub>2</sub>S<sub>5</sub>    M.W. = 1011.57 g/mol

Exact Mass = 1010.43 g/mol

TLC             SiO<sub>2</sub>, Hexane-EtAc (9:1)

R<sub>f</sub> = 0.2

MALDI         1033.92 [M<sup>+</sup>+Na],

<sup>1</sup>H-NMR        (400 MHz, CDCl<sub>3</sub>)

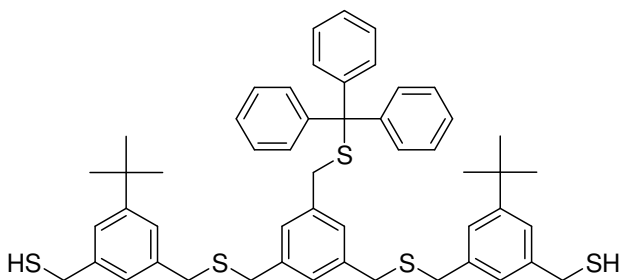
$\delta$ = 7.47 (*d*, *J*=6.4 Hz, 6H); 7.30 (*t*, *J*=6.8 Hz, 6H); 7.22 (*t*, *J*=6.8 Hz, 5H); 7.14 (*s*, 2H); 7.09 (*s*, 1H); 7.07 (*s*, 2H); 6.94 (*s*, 2H); 4.72-4.65 (*m*, 2H); 4.14-4.08

(*m*, 2H); 3.76 (*dxd*,  $J_1=20.6$  Hz,  $J_2=13.2$  Hz, 4H); 3.54 (*d*,  $J=4.8$  Hz, 8H); 3.48-3.42 (*m*, 2H); 3.29 (*s*, 2 H); 1.98-1.84 (*m*, 4H); 1.61-1.44 (*m*, 6H); 1.32 (*t*,  $J=6.4$ , 18H)

$^{13}\text{C-NMR}$  (100 MHz,  $\text{CDCl}_3$ )  
 $\delta =$  151.91; 145.60; 139.09; 138.71; 138.18; 138.01; 130.04; 128.82; 128.77; 128.38; 127.20; 127.13; 125.25; 125.05; 81.25; 67.89; 65.04; 37.21; 36.37; 35.93; 35.04; 34.66; 31.80; 31.32; 26.04; 22.21

E.A. Calculated : C, 73.61%; H, 7.37%;  
 Found : C, 73.95%; H, 7.32%;

Synthesis of 5,5'-(5-(tritylthiomethyl)-1,3-phenylene)bis(methylene)bis(sulfanediyl)bis(methylene) bis(3-tert-butyl-5,1-phenylene)dimethanethiol, **47**



In a dry double neck 25 ml flask under Ar, 2,2'-5,5'-(5-(tritylthiomethyl)-1,3-phenylene)bis(methylene)bis-(sulfanediyl)bis-(methylene)bis-(3-tert-butyl-5,1-phenylene)bis(methylene)bis-(sulfanediyl)bis-(tetrahydro-2H-pyran) (**46**) (0.51 g, 0.5 mmol, 1 eq.) and pyridinium *p*-toluenesulfonate (0.5 g, 0.2 mmol, 0.2 eq.) were dissolved in 10 mL anhyd. EtOH and the mixture were let to stir at 55°C for O/N. The solvent was evaporated using Rotavap. The crude was purified on a silica gel column (Hexane-EtAc 9:1) and the product was obtained as colorless oil (0.10 g, 23.7% and 39.6% due to the amount of consumed starting material).

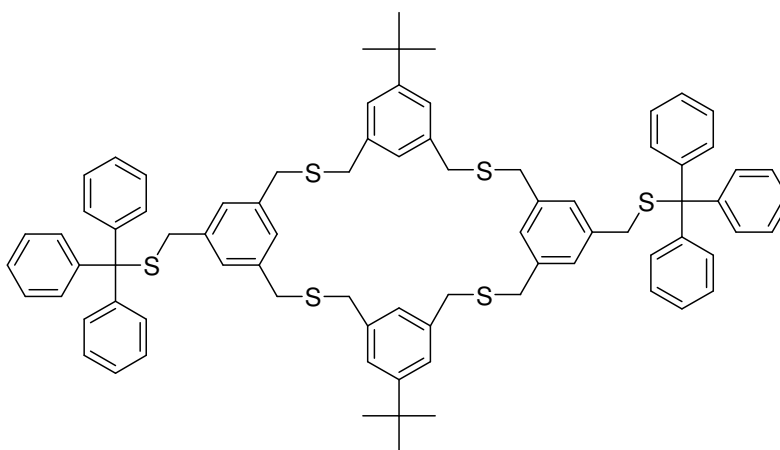
$\text{C}_{52}\text{H}_{58}\text{S}_5$  M.W. = 843.34g/mol  
 Exact Mass = 842.31 g/mol  
 TLC  $\text{SiO}_2$ , Hexane-EtAc (9:1)  
 $R_f = 0.25$   
 MALDI 865.36 [ $\text{M}^+ + \text{Na}$ ],  
 $^1\text{H-NMR}$  (400 MHz,  $\text{CDCl}_3$ )

$\delta$ = 7.46 (*t*, *J*= 4.8 Hz, 8H); 7.34-7.04 (*m*, 14H); 6.94 (*s*, 2H); 3.67 (*d*, *J*= 4.8 Hz, 4H); 3.53 (*d*, *J*= 4.4 Hz, 8H); 3.30 (*s*, 2H); 1.74 (*t*, *J*= 4.8 Hz, 2H); 1.29 (*s*, 18H);

$^{13}\text{C-NMR}$  (100 MHz,  $\text{CDCl}_3$ )  
 $\delta$ = 152.29; 145.18; 141.34; 138.43; 138.00; 130.09; 128.39; 128.33; 126.31; 125.24; 125.20; 67.90; 37.22; 36.22; 35.11; 31.26; 29.53

E.A. Calculated : C, 74.06%; H, 6.93%;  
 Found : C, 74.32%; H, 6.91%;

Synthesis of protected ligand **E** for direct synthesis of nanoparticles, **48**



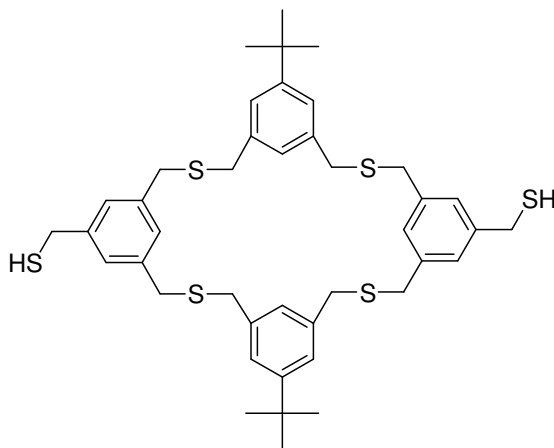
In a dry double neck 250 mL flask, sodium hydrate 60% dispersion in mineral oil (0.09 mg, 0.44 mmol, 2.2 eq.) dissolved in 100 ml dry THF under Ar. Then 5,5'-(5-(tritylthiomethyl)-1,3-phenylene)bis-(methylene)bis-(sulfanediyl)bis-(methylene)bis-(3-tert-butyl-5,1-phenylene)dimethanethiol, (**47**) (84.33 mg, 0.1 mmol, 1 eq.) and (3,5-bis(bromomethyl)benzyl)(trityl)sulfane (**37**) (55.24 mg, 0.1 mmol, 1 eq.) were dissolved separately in 5 ml dry THF and were added dropwise to the previous solution at 0°C. After the completion of addition of reactants, the mixture was let to reach RT and let to stir for O/N. The reaction mixture is poured into 10 mL water. The mixture was extracted with TBME (3 x 50 mL). All the organic extracts were combined, washed twice with 100 mL brine, dried over anhyd.  $\text{Na}_2\text{SO}_4$ . The solvent was evaporated using Rotavap. The crude was purified on a silica gel column (Hexane-EtAc 9:1) and the product was obtained as white solid (41.95 mg, 32%).

$\text{C}_{80}\text{H}_{80}\text{S}_6$  M.W. = 1233.88 g/mol



	Exact Mass = 1232.46 g/mol
TLC	SiO <sub>2</sub> , Hexane-EtAc (9:1) R <sub>f</sub> = 0.45
MALDI	1255.68 [M <sup>+</sup> +Na],
<sup>1</sup> H-NMR	(400 MHz, CDCl <sub>3</sub> ) δ= 7.45 ( <i>d</i> , <i>J</i> = 4.0 Hz, 12H); 7.33-7.18 ( <i>m</i> , 24H); 6.96 ( <i>s</i> , 4H); 6.92 ( <i>s</i> , 1H); 6.84 ( <i>s</i> , 1H); 3.52 ( <i>d</i> , <i>J</i> = 7.2 Hz, 16H); 3.28 ( <i>s</i> , 4H); 1.27 ( <i>s</i> , 18H);
<sup>13</sup> C-NMR	(100 MHz, CDCl <sub>3</sub> ) δ= 152.28; 145.07; 138.03; 130.05; 129.09; 128.40; 128.35; 127.15; 125.07; 109.96; 67.87; 36.02; 35.10; 31.82; 30.13 152.29; 145.18; 141.34; 138.00;; 128.39; 128.33; 126.31; 125.24; 125.20;
E.A.	Calculated : C, 77.87; H, 6.54; Found : C, 77.99; H, 6.45;

#### Synthesis of ligand **E** for direct synthesis of nanoparticles, **49**



In a dry double neck 25 mL flask under Ar, protected ligand **E** (61.69 mg, 0.05 mmol, 1 eq) was dissolved in 5 mL anhyd. DCM. Then triethylsilane (0.028 ml, 0.15 mmol, 3 eq.) and trifluoroacetic acid (0.2 ml 4% v/v in DCM) was added to the previous solution. The mixture was let to stir at RT for 15 min. The reaction mixture is poured into 5 mL sat. NaHCO<sub>3</sub> solution. The mixture was extracted with DCM (3 x 5 mL). All the organic extracts were combined, washed twice with 25 mL brine, dried over anhyd. Na<sub>2</sub>SO<sub>4</sub>. The solvent was evaporated using Rotavap. The crude was purified on a silica gel column (Hexane-EtAc 9:1) and the product was obtained as colorless oil (19.85 mg, 53%).

C<sub>42</sub>H<sub>52</sub>S<sub>6</sub> M.W. = 749.25 g/mol

	Exact Mass = 748.24 g/mol
TLC	SiO <sub>2</sub> , Hexane-EtAc (9:1) R <sub>f</sub> = 0.3
<sup>1</sup> H-NMR	(400 MHz, CDCl <sub>3</sub> ) δ= 7.22 (s, 4H); 7.14 (s, 4H); 6.97 (s, 2H); 6.87 (s, 2H); 3.68 (d, J= 7.6 Hz, 4H); 3.58 (d, J= 7.2 Hz, 16H); 1.76 (t, J= 7.6 Hz, 2H); 1.31 (s, 18H);
E.A.	Calculated : C, 67.33; H, 7.00; Found : C, 67.71; H, 6.90;

### Gold Nanoparticle Formation, Purification and Size Distribution Measurement

Gold nanoparticle syntheses were carried out on a 20 - 30 μmol scale with respect to the Au equivalents. Tetrachloroauric acid (*n* equivalents, where *n* is the number of sulphur atoms in the used ligand) was dissolved in 2.5 mL deionized water. A solution of tetraoctylammonium bromide (*2n* equivalents) in 2.5 mL DCM was added and the two-phase mixture stirred until the aqueous phase became colourless. The ligand (1 equivalent) was dissolved in 2.5 mL DCM and then added to the reaction mixture, followed by a freshly prepared solution of sodium borohydride in 2.5 mL of water. After 10 min of stirring, the resulting strongly coloured DCM phase was separated and the aqueous phase was extracted with DCM (2 x 5 mL). The combined organic fractions were dried over magnesium sulphate, filtered and concentrated to a volume of *ca.* 1 mL. Approximately 15 mL ethanol was added to precipitate the particles, which were then centrifuged. The supernatant was discarded. After redispersion in DCM, the nanoparticles were either left in that solvent or evaporated to dryness using a rotary evaporator.

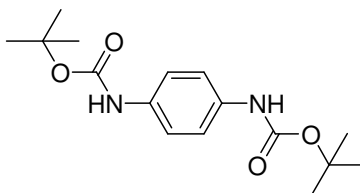
Sample preparation consists of depositing the nanoparticles onto a suitable TEM substrate (typically a SiO/Cu or SiO<sub>2</sub> TEM grid). For optimal analysis, a dilute nanoparticle sample is aerosoled onto the grid in order to ensure well-spaced, uniform distributions of particles on the surface. The sample is placed into the microscope and micrographs at a suitable magnification (-200,000 x) are obtained. In order to ensure that there is no bias in the size analysis, several images representing diverse regions of the TEM grid and several hundreds to thousands of nanoparticles are taken. This helps to avoid artificial size separation or skewing as a result of drying effects or aggregation. Analysis of the obtained micrographs can be the most difficult aspect of the size analysis.

Following developing of the positive film, the images are digitized and undergo image manipulations in Adobe Photoshop or CorelDraw software to enhance the contrast of the nanoparticles. First, the positive film is inverted, yielding black spots (nanoparticles) on a gray background then, levels adjustment increases contrast, by lightening the background and darkening the nanoparticles. Finally, unsharp mask is used to further enhance contrast between the nanoparticles and the background, but may also increase background noise, which is eliminated using a Gaussian blur. Throughout the many steps, every effort is taken to avoid distorting the nanoparticle size distribution.

The digitally enhanced image is then opened in the software Image J and threshold adjusted to highlight the nanoparticles over the background and then automated size analysis is carried out. Because nanoparticle aggregates and background noise can influence particle size measurements, nanoparticles with a circularity less than 0.75 (1 being a perfect circle) are removed as possible aggregates. This series of steps is carried out for each of the obtained images, and the average core diameter and size-distribution is calculated in MS Excel.

### 5.3. Synthetic Procedures for 2D assemblies of preorganized structures

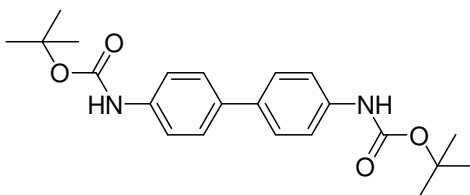
Synthesis of di-*tert*-butyl 1,4-phenylenedicarbamate, **49**



In a dry double neck 100 mL flask under Ar, *p*-phenylenediamine (0.54 g, 5 mmol, 1 eq.) was dissolved in 25 mL THF. Triethylamine (1.5 mL, 11 mmol, 2.2 eq.) was added to the solution. Di-*tert*-butyl dicarbonate (2.71 g, 12.5 mmol, 2.5 eq.) was dissolved in 25 mL in dry THF and added slowly to the reaction mixture. Then the mixture was let to stir at RT for overnight. The reaction was quenched by addition of 25 mL water. The organic layer was separated. The water layer was extracted with DCM (3 x 15 mL). All the organic extracts were combined, washed with 25 mL sat.  $\text{NH}_4\text{Cl}$ , dried over anhyd.  $\text{Na}_2\text{SO}_4$ . The solvent was evaporated using Rotavap. The product was purified by recrystallization in ethylacetate and the product was obtained as white solid (0.68 g, 44%).

$C_{16}H_{24}N_2O_4$ ,	M.W. = 308.37 g/mol
	Exact Mass = 308.17 g/mol
TLC	SiO <sub>2</sub> , EtAc (100%)
	R <sub>f</sub> = 0.8
ESI-MS	331.1 [M <sup>+</sup> + Na],
EI-MS	70eV
	308.1 [M <sup>+</sup> ],
<sup>1</sup> H-NMR	(400 MHz, DMSO, d <sub>6</sub> )
	δ = 9.16 (s, 2H); 7.31 (s, 4H); 1.47 (s, 18H)
<sup>13</sup> C-NMR	(100 MHz, DMSO, d <sub>6</sub> )
	δ = 153.61; 134.31; 127.12; 119.26; 79.90; 28.99
E.A.	Calculated : C, 62.32%; H, 7.84%, N, 9.08%
	Found : C, 62.29%; H, 7.60%, N, 9.15%

Synthesis of *tert*-butyl biphenyl-4,4'-diyl dicarbamate, **50**

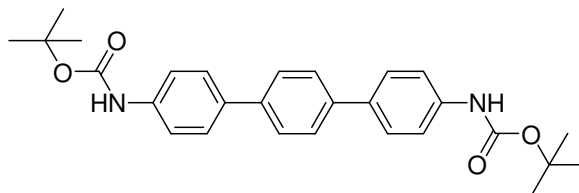


In a dry double necked 25 mL flask under Ar, di-*tert*-butyl dicarbonate (1.18g, 5 mmol, 2.5 eq.) was dissolved in 5 mL dry THF and triethylamine (0.55 ml, 4 mmol, 2 eq.) was added to the solution. Benzidine (0.37 g, 2 mmol, 1 eq.) was dissolved in 5 mL dry THF and was added dropwise to the reaction mixture. Then the mixture was let to stir at RT for O/N in the dark. The reaction was quenched by addition of 15 mL water. The organic layer was separated. The water layer was extracted with DCM (3 x 15 mL). All the organic extracts were combined, washed with 25 mL sat. NH<sub>4</sub>Cl, dried over anhyd. Na<sub>2</sub>SO<sub>4</sub>. The solvent was evaporated using Rotavap. The crude was purified on a silica gel column (Hexane-EtAc 1:1) and the product was obtained as white solid (0.45 g, 58%).

$C_{22}H_{28}N_2O_4$ ,	M.W. = 384.47 g/mol
	Exact Mass = 384.20 g/mol
TLC	SiO <sub>2</sub> , Hexane-EtAc (1:1)
	R <sub>f</sub> = 0.7
EI-MS	70eV

	384.1 [M <sup>+</sup> ],
<sup>1</sup> H-NMR	(400 MHz, DMSO, d <sub>6</sub> ) δ= 9.38 (s, 2H); 7.49 (s, 8H); 1.46 (s, 18H)
<sup>13</sup> C-NMR	(100 MHz, DMSO, d <sub>6</sub> ) δ= 153.61; 139.35; 134.31; 127.12; 119.26; 79.90; 28.99;
E.A.	Calculated : C, 68.73%; H, 7.34%, N, 7.29% Found : C, 68.48%; H, 7.19%, N, 7.22%

#### Synthesis of tert-butyl terphenyl-4,4'-diylidicarbamate, **51**

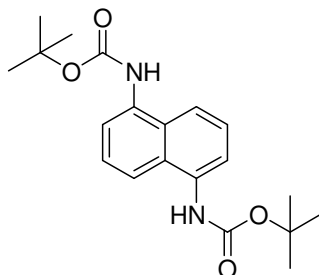


In a dry double necked 25 mL flask under Ar, di-*tert*-butyl dicarbonate (1.18g, 5 mmol, 2.5 eq.) was dissolved in 5 mL dry THF and triethylamine (0.55 ml, 4 mmol, 2 eq.) is added to the solution. Terphenyl (0.52 g, 2 mmol, 1 eq.) dissolved in 5 mL dry THF was added dropwise to the reaction mixture. Then the mixture was let to stir at RT for overnight in the dark. The reaction was quenched by addition of 15 mL water. The organic layer was separated. The water layer was extracted with DCM (3 x 15 mL). All the organic extracts were combined, washed with 25 mL sat. NH<sub>4</sub>Cl, dried over anhyd. Na<sub>2</sub>SO<sub>4</sub>. The solvent was evaporated using Rotavap. The product was recrystallized in THF to give as white solid (0.29 g, 32%).

C <sub>28</sub> H <sub>32</sub> N <sub>2</sub> O <sub>4</sub> ,	M.W. = 460.56 g/mol Exact Mass = 460.24 g/mol
TLC	SiO <sub>2</sub> , Hexane-EtAc (1:1) R <sub>f</sub> = 0.5
EI-MS	70eV 460.1 [M <sup>+</sup> ],
<sup>1</sup> H-NMR	(400 MHz, DMSO, d <sub>6</sub> ) δ= 9.46 (s, 2H); 7.69 (s, 4H); 7.49 (dxd, J <sub>1</sub> = 4.8 Hz, J <sub>2</sub> = 13.2 Hz, 8H); 1.49 (s, 18H)
<sup>13</sup> C-NMR	(100 MHz, DMSO, d <sub>6</sub> ) δ= 152.50; 139.41; 136.92; 128.12; 127.24; 119.75; 79.52; 28.32

E.A.	Calculated	: C, 73.02%; H, 7.00%, N, 6.08%;
	Found	: C, 73.32%; H, 6.87%, N, 5.99%;

Synthesis of di-*tert*-butyl naphthalene-1,5-diylidicarbamate, **52**



In a dry double necked 25 mL flask under Ar, di-*tert*-butyl dicarbonate (1.18g, 5 mmol, 2.5 eq.) was dissolved in 5 mL dry THF and triethylamine (0.55 ml, 4 mmol, 2 eq.) is added to the solution. Naphthalene-1,5-diamine, (0.32 g, 2 mmol, 1 eq.) dissolved in 5 mL dry THF was added dropwise to the reaction mixture. Then the mixture was let to stir at RT for overnight in the dark. The reaction was quenched by addition of 15 mL water. The organic layer was separated. The water layer was extracted with DCM (3 x 15 mL). All the organic extracts were combined, washed with 25 mL sat. NH<sub>4</sub>Cl, dried over anhyd. Na<sub>2</sub>SO<sub>4</sub>. The solvent was evaporated using Rotavap. The product was recrystallized in EtAc to give as white solid (0.24 g, 34%).

C<sub>16</sub>H<sub>24</sub>N<sub>2</sub>O<sub>4</sub>, M.W. = 358.43 g/mol

Exact Mass = 358.19 g/mol

TLC SiO<sub>2</sub>, EtAc (100%)

R<sub>f</sub> = 0.8

ESI-MS 381.1 [M+Na]<sup>+</sup>,

EI-MS 70eV

358.3 [M<sup>+</sup>],

<sup>1</sup>H-NMR (400 MHz, DMSO, d<sub>6</sub>)

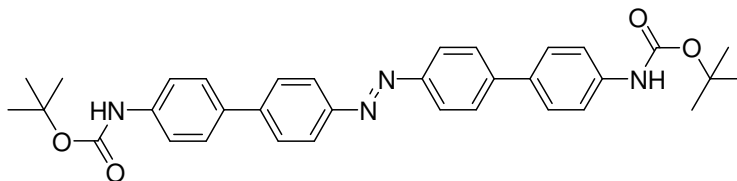
δ = 9.16 (s, 2H); 7.56 (dxd, J<sub>1</sub> = 4.8 Hz, J<sub>2</sub> = 11.2 Hz, 4H); 7.37 (t, J = 4.8 Hz, 2H); 6.96 (dxd, J<sub>1</sub> = 4.4 Hz, J<sub>2</sub> = 12.4 Hz, 2H); 1.47 (s, 18H)

<sup>13</sup>C-NMR (100 MHz, DMSO, d<sub>6</sub>)

δ = 152.50; 141.01; 126.33; 125.32; 111.76; 105.08; 79.50; 28.49;

E.A.	Calculated	: C, 67.02%; H, 7.31%, N, 7.82%
------	------------	---------------------------------

	Found	: C, 66.69%; H, 7.20%, N, 7.55%
--	-------	---------------------------------

Synthesis of (E)-di-tert-butyl 4',4''-(diazene-1,2-diyl)bis(biphenyl-4',4-diyl)dicarbamate, **53**

In a 25 mL double necked flask under Ar, (E)-1,2-bis(4-iodophenyl)diazene (**59**) (86.95 mg, 0.2 mmol, 1 eq), and 4-(Boc-amino)benzeneboronic acid pinacol ester (143.8 mg, 0.44 mmol, 2.2 eq) were dissolved in degassed 14 mL toluene/ethanol (6:1) containing 1 mL 2M Na<sub>2</sub>CO<sub>3</sub>. Then, Pd(PPh<sub>3</sub>)<sub>4</sub> (26 mg, 0.02 mmol, 10% mol eq.) was added and the mixture was refluxed under Ar O/N. The solvent was evaporated. The crude mixture was dissolved in 50 mL DCM and washed with water (2 x 50 mL). The organic layer was collected, washed with 50 mL brine and dried over anhydrous Na<sub>2</sub>SO<sub>4</sub>. The solvent was evaporated using Rotavap. The crude was purified on a silica gel column (DCM 100%) and the product was obtained as an orange solid (75.7 mg, 67%).

C<sub>34</sub>H<sub>36</sub>N<sub>4</sub>O<sub>4</sub>, M.W. = 564.67 g/mol

Exact Mass = 564.27 g/mol

TLC SiO<sub>2</sub>, (DCM 100%).

R<sub>f</sub> = 0.25

EI-MS 70eV

564.3 [M<sup>+</sup>],

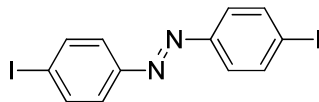
<sup>1</sup>H-NMR (400 MHz, DMSO-*d*<sub>6</sub>)

δ = 9.54 (s, 2H); 7.98 (d, *J* = 8Hz, 4H); 7.88 (d, *J* = 8Hz, 4H); 7.72 (d, *J* = 8Hz, 4H); 7.60 (d, *J* = 8Hz, 4H); 1.50 (s, 18H)

<sup>13</sup>C-NMR not soluble

E.A. Calculated : C, 72.32%; H, 6.43%; N, 9.92%

Found : C, 71.97%; H, 6.21%; N, 9.53%

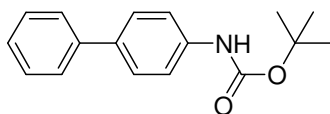
Synthesis of (E)-1,2-bis(4-bromophenyl)diazene, **58**

In a dry double neck 100 mL flask under Ar, 4-iodo-aniline (2.19 g, 10 mmol, 1 eq.) was dissolved in 25 mL dry DCM. Equal amount of oxidant (3 g KMnO<sub>4</sub> and 3 g FeSO<sub>4</sub>·7H<sub>2</sub>O) was prepared by grinding in a mortar and added to the solution. The mixture was refluxed

under Ar for O/N. The solution was filtered, dried over Na<sub>2</sub>SO<sub>4</sub> and was evaporated using Rotavap. The crude was purified on a silica gel column (Hexane-DCM 3:1) and the product was obtained as yellow powder (0.78 g, 18%).

C <sub>12</sub> H <sub>8</sub> I <sub>2</sub> N <sub>2</sub>	M.W. = 434.01 g/mol Exact Mass = 433.88 g/mol
TLC	SiO <sub>2</sub> , Hexane-DCM (3:1) R <sub>f</sub> = 0.3
EI-MS	70eV 433.8 [M <sup>+</sup> ]
MP	242-244 °C
<sup>1</sup> H-NMR	(400 MHz, CDCl <sub>3</sub> ) δ = 7.86 (d, J=8.0 Hz, 4H); 7.64 (d, J=8.0 Hz, 4H)
<sup>13</sup> C-NMR	(100 MHz, CDCl <sub>3</sub> ) δ = 152.13; 138.84; 124.94; 98.55

Synthesis of tert-butyl biphenyl-4-ylcarbamate, **59**



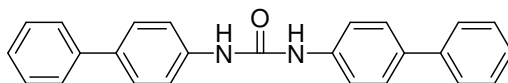
In a dry 25 mL double necked flask under Ar, bromobenzene (0.22 mL, 2 mmol, 1 eq.) and 4-(Boc-amino)benzeneboronic acid pinacol ester (0.64g, 2 mmol, 1 eq.) were dissolved in degassed 14 mL toluene/ethanol (6:1) containing 1mL 2M Na<sub>2</sub>CO<sub>3</sub>. Then, Pd(PPh<sub>3</sub>)<sub>4</sub> (0.12g, 0.2 mmol, 1 eq.) was added and the mixture was refluxed under Ar O/N. The reaction was stopped, the solvent evaporated. The crude was dissolved in 25 mL DCM and washed with 25mL water then with 25 mL brine. The water layer was extracted with DCM (3 x15 mL). All the organic extracts were combined, dried over anhyd. Na<sub>2</sub>SO<sub>4</sub>. The solvent was evaporated using Rotavap. The crude was purified on a silica gel column (Hexane-EtAc 4:1) and the product was obtained as white solid (0.46 g, 85%).

C <sub>17</sub> H <sub>19</sub> NO <sub>2</sub> ,	M.W. = 269.34 g/mol Exact Mass = 269.14 g/mol
TLC	SiO <sub>2</sub> , (Hexane-EtAc 4:1). R <sub>f</sub> = 0.4
EI-MS	70eV



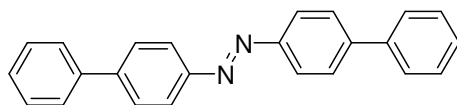
	269.2 [M <sup>+</sup> ],
<sup>1</sup> H-NMR	(400 MHz, CDCl <sub>3</sub> ) $\delta$ = 7.57-7.52 ( <i>m</i> , 4H); 7.44-7.40 ( <i>m</i> , 4H); 7.33 ( <i>t</i> , 0.34 H, <i>J</i> = 12.0 Hz); 7.31 ( <i>t</i> , 0.51 H, <i>J</i> = 20.0 Hz); 7.29 ( <i>t</i> , 0.17 H, <i>J</i> = 20.0 Hz); 6.52 ( <i>s</i> , 1H); 1.52 ( <i>s</i> , 9H)
<sup>13</sup> C-NMR	(100 MHz, CDCl <sub>3</sub> ) $\delta$ = 153.13; 141.04; 138.06; 136.35; 129,14; 128.03; 127.18; 119.21; 81.05; 28.76
E.A.	Calculated : C, 75.81%; H, 7.11%, N, 5.20% Found : C, 75.56%; H, 7.17%, N, 5.14%

#### Synthesis of 1,3-Bis(4-iodophenyl)urea, **60**



In a dry 25 mL double necked flask under Ar, 4-biphenylamine (113.30 mg, 0.67 mmol, 6 eq.) and DMAP (109.13 mg, 0.92 mmol, 8 eq.) were dissolved in 2 mL dry DCM. Then, BTC (32.64 mg, 0.11 mmol, 1 eq.) dissolved in 2 mL dry DCM added dropwise to the previous solution at RT. The solution was stirred 15 min additional after addition of all BTC. White turbid solution mixture was filtered. The filter cake was washed extensively with DCM and let to dry at open air to obtain the product as white solid (103.07 mg, 85%).

C <sub>25</sub> H <sub>20</sub> N <sub>2</sub> O,	M.W. = 364.44 g/mol Exact Mass = 364.16 g/mol
MALDI	364.82 [M <sup>+</sup> ],
<sup>1</sup> H-NMR	(400 MHz, DMSO- <i>d</i> <sub>6</sub> ) $\delta$ = 8.85 ( <i>s</i> , 2H); 7.67-7.58 ( <i>m</i> , 12H); 7.45 ( <i>t, br, J</i> = 8.0 Hz, 4H); 7.32 ( <i>t, br, J</i> = 7.6 Hz, 2H)
<sup>13</sup> C-NMR	not soluble enough
E.A.	Calculated : C, 82.39%; H, 5.53%, N, 7.69% Found : C, 82.77%; H, 5.32%, N, 7.59%
UV-Vis	(MeCN) $\lambda$ = 284 and 306
RP-HPLC	(100% MeCN, flow 0.4ml/min, $\lambda_{det}$ = 284 and 306 nm, T= 25 °C) R <sub>t</sub> = 7.6 min, purity 99%

Synthesis of 1,2-di(biphenyl-4-yl)diazene, **62**

In a 25 mL double necked flask under Ar, (E)-1,2-bis(4-iodophenyl)diazene (**58**) (108.5 mg, 0.25 mmol, 1 eq), and phenylboronic acid pinacol ester (116.2mg, 0.6 mmol, 2.2 eq) were dissolved in degassed 14 mL toluene/ethanol (6:1) containing 1mL 2M Na<sub>2</sub>CO<sub>3</sub>. Then, Pd(PPh<sub>3</sub>)<sub>4</sub> (28.9 mg, 0.025 mmol, 10%mol eq.) was added and the mixture was refluxed under Ar O/N. The solvent is evaporated. The crude mixture is dissolved in 50 mL DCM and washed with water (2 x 50 mL). The organic layer was collected, washed with 50 mL brine and dried over anhydrous Na<sub>2</sub>SO<sub>4</sub>. The solvent was evaporated using Rotavap. The crude was purified on a silica gel column (DCM 100%) and the product was obtained as an orange solid (284.25 mg, 85%).

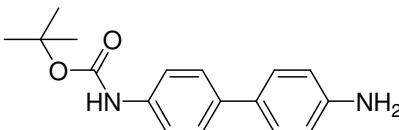
C <sub>24</sub> H <sub>18</sub> N <sub>2</sub> ,	M.W. = 334.41 g/mol
	Exact Mass = 334.15 g/mol
TLC	SiO <sub>2</sub> , (DCM 100%).
	R <sub>f</sub> = 0.35
EI-MS	70eV
	334.2 [M <sup>+</sup> ]
MP	253-255 °C
<sup>1</sup> H-NMR	(400 MHz, THF- <i>d</i> <sub>4</sub> )
	δ= 8.03 ( <i>d</i> , <i>J</i> = 6.8 Hz, 4H); 7.84 ( <i>d</i> , <i>J</i> = 7.2 Hz, 4H); 7.73 ( <i>d</i> , <i>J</i> = 5.6 Hz, 4H); 7.46 ( <i>t</i> , <i>J</i> = 11.2 Hz, 4H); 7.36 ( <i>t</i> , <i>J</i> = 11.6 Hz, 2H)
<sup>13</sup> C-NMR	not soluble enough
E.A.	Calculated : C, 86.20; H, 5.43; N, 8.38
	Found : C, 85.79; H, 5.66; N, 8.25
UV-VIS	(MeCN) λ= 362
RP- HPLC	(100% MeCN, flow 0.4ml/min, λ <sub>det</sub> = 362nm, T= 25 °C)
	R <sub>t</sub> = 18.7min, purity 99%

**Simulation of the surface reactions**

The reaction conditions were mimicked by adsorbing **59** (5 mg, 0.0186 mmol) dissolved in dichloromethane on Ag nanoparticles with a diameter of about (2±1) μm (1.01 g) by evaporation of the solvent at the rotavap. Subsequently, the surface functionalized particles

were treated at 200°C and 0.1 mbar for 6h in a glass reaction vessel. To analyze the emerging organic compounds, the particles were extracted extensively with DCM. After concentration of the eluent and preparative TLC three new compounds have been isolated together with considerable amounts of unreacted starting material **59**. Analysis by MALDI-ToF displayed their molecular weights of 321.12, 334.11 and 471.22 suggesting the structures **61-63** displayed in Scheme 3.3.5 as reaction products. In a similar procedure the urea derivative **60** (5 mg, 0.0137 mmol) was dissolved in DMF and immobilized on Ag nanoparticles with a diameter of about (2±1) µm (1.01g) by evaporation of the solvent at reduced pressure. After similar treatment of the particles as described above, the cooled down particles were extracted with DMF. The solvent of the extract was removed under reduced pressure and the remaining material was redissolved in acetonitrile for subsequent analysis by reversed phase HPLC. The analysis of the extract displayed three main compounds: unreacted starting material **60**, an unknown reaction product and the expected azo derivative **62**.

#### Synthesis of tert-butyl 4'-aminobiphenyl-4-ylcarbamate, **64**



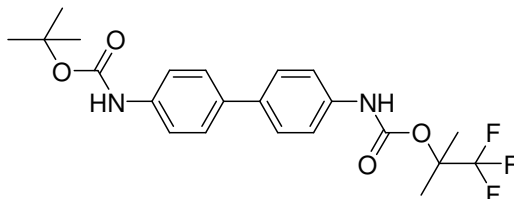
In a dry double necked 25 mL flask under Ar, di-*tert*-butyl dicarbonate (1.09 g, 5 mmol, 1 eq.), triethylamine (1.4 mL, 10 mmol, 2 eq.) and benzidine (0.92 g, 5 mmol, 1 eq.) were dissolved in 15 mL dry THF. The mixture was let to stir at RT for O/N in the dark. The reaction was quenched by addition of 15 mL water. The organic layer was separated. The water layer was extracted with DCM (3 x 15 mL). All the organic extracts were combined, dried over anhyd. Na<sub>2</sub>SO<sub>4</sub>. The solvent was evaporated using Rotavap. The crude was purified on a silica gel column (Hexane-EtAc 1:1) and the product was obtained as white solid (0.67 g, 47%).

C <sub>17</sub> H <sub>20</sub> N <sub>2</sub> O <sub>2</sub> ,	M.W. = 284.35 g/mol
	Exact Mass = 284.15 g/mol
TLC	SiO <sub>2</sub> , Hexane-EtAc (1:1)
	R <sub>f</sub> = 0.3
ESI-MS	285.2 [M <sup>+</sup> ],
<sup>1</sup> H-NMR	(250 MHz, DMSO- <i>d</i> <sub>6</sub> )

$\delta$  = 9.31 (s, 1H); 7.43 (d,  $J$  = 3.2 Hz, 4H); 7.31 (d,  $J$  = 6.8 Hz, 2H); 6.62 (d,  $J$  = 6.8 Hz, 2H); 5.15 (s, 2H); 1.49 (s, 9H)

E.A.            Calculated     : C, 71.81%; H, 7.09%, N, 9.85%  
                  Found            : C, 71.90%; H, 7.14%, N, 9.65%

Synthesis of tert-butyl (1,1,1-trifluoro-2-methylpropan-2-yl) [1,1'-biphenyl]-4,4'-diylldicarbamate, **65**



In a dry 25 mL double necked flask under Ar, BTC (89.02 mg, 0.3 mmol, 1 eq.) was dissolved in 3 mL dry DCM. 1,1,1-trifluoro-2-methylpropan-2-ol (98.5  $\mu$ L, 0.9 mmol, 3 eq.) and DMAP (219.9 mg, 1.8 mmol, 6 eq.) were dissolved in 3 mL dry DCM and were added slowly to the previous solution at 0°C. The mixture allowed to reach RT and stirred under Ar. tert-butyl 4'-aminobiphenyl-4-ylcarbamate (**64**) (255.93 mg, 0.9 mmol, 3 eq.) and DMAP (219.9 mg, 1.8 mmol, 6 eq.) were dissolved in 3 mL dry DCM and added dropwise to the previous solution at RT. The solution was stirred 15 min additional after the completion of addition. White turbid solution mixture was filtered. The reaction was diluted with 10 mL DCM and quenched by addition of 15 mL water. The organic layer was separated and washed with 15 mL 0.5 M HCl, 15 mL water, 15 mL 5% Na<sub>2</sub>S<sub>2</sub>O<sub>3</sub>, 15 mL 2.5% NaHCO<sub>3</sub> and 15 mL brine. Organic extracts were dried over anhyd. Na<sub>2</sub>SO<sub>4</sub>. The solvent was evaporated using Rotavap. The crude was purified on a silica gel column (Hexane-EtAc 1:1) and the product was obtained as white solid (390.21 mg, 89%).

C<sub>22</sub>H<sub>25</sub>F<sub>3</sub>N<sub>2</sub>O<sub>4</sub> M.W. = 438.44 g/mol

Exact Mass = 438.18 g/mol

TLC            SiO<sub>2</sub>, Hexane-EtAc (1:1)

R<sub>f</sub> = 0.5

EI-MS        437.82 [M<sup>+</sup>],

<sup>1</sup>H-NMR      (400 MHz, DMSO-*d*<sub>6</sub>)

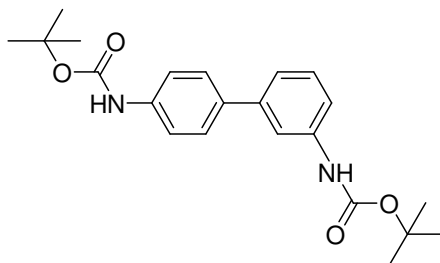
$\delta$  = 9.84 (s, 1H); 9.39 (s, 1H); 7.54-7.50 (*m*, 8H); 1.70 (s, 6H); 1.47 (s, 9H)

<sup>13</sup>C-NMR      (100 MHz, DMSO-*d*<sub>6</sub>)

$\delta$  = 153.60; 151.74; 139.50; 138.39; 135.14; 134.11; 127.22; 119.69; 119.26;  
79.93; 28.99; 20.30

E.A.            Calculated     : C, 60.27%; H, 5.75%, N, 6.39%  
                  Found             : C, 60.62%; H, 5.69%, N, 6.33%

#### Synthesis of di-tert-butyl biphenyl-3,4'-diyldicarbamate, **66**



In a 25 mL double necked flask under Ar, N-(*tert*-Butoxycarbonyl)-3-bromoaniline (272.14 mg, 1 mmol, 1 eq), and 4-(N-Boc-amino)phenylboronic acid pinacol ester (319.21 mg, 1 mmol, 1 eq) were dissolved in degassed 14 mL toluene/ethanol (6:1) containing 1 mL 2M Na<sub>2</sub>CO<sub>3</sub>. Then, Pd(PPh<sub>3</sub>)<sub>4</sub> (57.78 mg, 0.05 mmol, 5%mol eq.) was added and the mixture was refluxed under Ar O/N. The solvent is evaporated. The crude mixture is dissolved in 50 mL DCM and washed with water (2 x 50 mL). The organic layer was collected, washed with 50 mL brine and dried over anhydrous Na<sub>2</sub>SO<sub>4</sub>. The solvent was evaporated using Rotavap. The crude was purified on a silica gel column (Hexane-EtAc 4:1) and the product was obtained as an orange solid (299.9 mg, 78%).

C<sub>22</sub>H<sub>28</sub>N<sub>2</sub>O<sub>4</sub>,    M.W. = 384.47 g/mol

Exact Mass = 384.20 g/mol

TLC                SiO<sub>2</sub>, Hexane-EtAc 4:1

R<sub>f</sub> = 0.3

EI-MS             70eV

384.1 [M],

<sup>1</sup>H-NMR          (400 MHz, CDCl<sub>3</sub>)

$\delta$  = 7.58 (s, 1H); 7.53 (t, *J* = 2.8 Hz, 1H); 7.51 (t, *J* = 2.8 Hz, 1H); 7.41 (d, *J* = 4.0 Hz, 2H); 7.35-7.28 (m, 2H); 7.24 (t, *J* = 1.6 Hz, 0.5H); 7.22 (t, *J* = 1.6 Hz, 0.5H); 6.53 (s, 2H); 1.53 (s, 18H)

<sup>13</sup>C-NMR          (100 MHz, CDCl<sub>3</sub>)

$\delta$  = 153.16; 141.94; 139.16; 138.20; 135.95; 129.74; 128.08; 121.94; 119.11; 117.48; 117.27; 81.04; 28.77

## Experimental Part

---

E.A.            Calculated    : C, 68.73%; H, 7.34%, N, 7.29%  
                 Found         : C, 68.82%; H, 7.34%, N, 7.06%

## 6. REFERENCES

- [1] P. Mulvaney, *MRS Bull.* **2001**, *26*, 1009.
- [2] U. Kreibig, M. Vollmer, *Optical Properties of Metal Clusters*, Springer-Verlag, Berlin, **1995**.
- [3] L. M. Liz-Marzán, *Materials today*, **2004**, *7*, 26.
- [4] L. M. Liz-Marzán, *Langmuir*, **2006**, *22*, 32.
- [5] F. Antonii, *Panacea Aurea-Auro Potabile*, Bibliopolio Frobeniano, Hamburg, **1618**.
- [6] J. Kunckels, *Nuetliche Observationes oder Anmerkungen von Auro und Argento Potabili*, Schutzens, Hamburg, **1676**.
- [7] H. H. Helcher, *Aurum Potabile oder Gold Tinstur*, J. Herbord Klossen, Breslau and Leipzig, **1718**.
- [8] W. Ostwald, *Kolloid Z.*, **1909**, *4*, 5.
- [9] M. Faraday, *Phil. Trans. R. Soc. Lond.*, **1857**, *147*, 145.
- [10] B. L. Cushing, V. L. Kolesnichenko, C. J. O'Connor, *Chem. Rev.* **2004**, *104*, 3893.
- [11] G. Mie, *Ann. Phys.* **1908**, *25*, 377.
- [12] A. P. Alivisatos, *J. Phys. Chem.* **1996**, *100*, 13226.
- [13] M. Amman, K. Mullen, E. Ben-Jacob, *J. Appl. Phys.* **1989**, *65*, 339.
- [14] J. B. Barner, S. T. Ruggiero, *Phys. Rev. Lett.* **1987**, *59*, 809.
- [15] M. C. Daniel, D. Astruc, *Chem. Rev.* **2004**, *104*, 293
- [16] C. Schonenberger, H. van Houten, C. W. Beenakker, *J. Phys. B*, **1993**, *189*, 218.
- [17] H. Grabert, M. H. Devoret, *NATO ASI Series, Series B, Physics, Vol. 294*, Plenum Press, New York, **1992**.
- [18] G. Schmid, *Chem. Rev.* **1992**, *92*, 1709.
- [19] K. J. Klabunde, J. Stark, O. Koper, C. Mohs, D. G. Park, S. Decker, Y. Jiang, I. Lagadic, D. J. Zhang, *J. Phys. Chem.* **1996**, *100*, 12142.
- [20] N. L. Rosi, C. A. Mirkin, *Chem. Rev.* **2005**, *105*, 1547.
- [21] R. Shenhar, V. M. Rotello, *Acc. Chem. Res.* **2003**, *36*, 549.
- [22] E. Katz, I. Willner, *Angew. Chem. Int. Ed. Engl.* **2004**, *43*, 6042.
- [23] C. Burda, X. B. Chen, R. Narayanan, M. A. El-Sayed, *Chem. Rev.* **2005**, *105*, 1025.

## References

---

- [24] P. Buffat, J. P. Borel, *Phys. Rev. A*, **1976**, *13*, 2287.
- [25] S. W. Chen, R. S. Ingram, M. J. Hostetler, J. J. Pietron, R. W. Murray, T. G. Schaaff, J. T. Khoury, M. M. Alvarez, R. L. Whetten, *Science*, **1998**, *280*, 2098.
- [26] A. C. Templeton, M. P. Wuelfing, R. W. Murray, *Acc. Chem. Res.* **2000**, *33*, 27.
- [27] M. J. Hostetler, S. J. Green, J. J. Stokes, R. W. Murray, *J. Am. Chem. Soc.* **1996**, *118*, 4212.
- [28] M. J. Hostetler, A. C. Templeton, R. W. Murray, *Langmuir*, **1999**, *15*, 3782.
- [29] A. A. Guzelian, U. Banin, A. V. Kadavanich, X. Peng, A. P. Alivisatos, *Appl. Phys. Lett.* **1996**, *69*, 1432.
- [30] P. Mulvaney, *Langmuir*, **1996**, *12*, 788.
- [31] C. F. Bohren, D. R. Huffman, *Absorption and Scattering of Light by Small Particles*, John Wiley & Sons, New York, **1984**.
- [32] A. J. Haes, R. P. Van Duyne, *J. Am. Chem. Soc.* **2002**, *124*, 10596.
- [33] D. C. Hone, A. H. Haines, D. A. Russell, *Langmuir*, **2003**, *19*, 7141.
- [34] R. Kubo, A. Kawabata, S. Kobayashi, *Annu. Rev. Mater. Sci.* **1984**, *14*, 49.
- [35] R. L. Johnston, *Phil. Trans. R. Soc. A*, **1998**, *356*, 211.
- [36] O. D. Haberlen, S. C. Chung, M. Stener, N. Rosch, *J. Chem. Phys.* **1997**, *106*, 5189.
- [37] C. N. R. Rao, G. U. Kulkarni, P. J. Thomas, P. P. Edwards, *Chem. Eur. J.* **2002**, *8*, 29.
- [38] P. Marquardt, L. Borngen, G. Nimtz, R. Sonnberger, H. Gleiter, J. Zhu, *Phys. Lett. A*, **1986**, *114*, 39.
- [39] G. Schmid, *Adv. Eng. Mater.* **2001**, *3*, 737.
- [40] M. A. El-Sayed, *Acc. Chem. Res.* **2001**, *34*, 257.
- [41] T. G. Schaaff, M. N. Shafiqullin, J. T. Khoury, I. Vezmar, R. L. Whetten, W. G. Cullen, P. N. First, C. GutierrezWing, J. Ascensio, M. J. JoseYacaman, *J. Phys. Chem. B*, **1997**, *101*, 7885.
- [42] D. L. Feldheim, C. D. Keating, *Chem. Soc. Rev.* **1998**, *27*, 1.
- [43] R. S. Ingram, M. J. Hostetler, R. W. Murray, T. G. Schaaff, J. T. Khoury, R. L. Whetten, T. P. Bigioni, D. K. Guthrie, P. N. First, *J. Am. Chem. Soc.* **1997**, *119*, 9279.
- [44] L. J. de Jongh, *Appl. Organomet. Chem.* **1998**, *12*, 393.
- [45] G. Schon, U. Simon, *Colloid. Polym. Sci.* **1995**, *273*, 101.



- [46] C. Schonenberger, H. Vanhouten, H. C. Donkersloot, *Europhys. Lett.* **1992**, *20*, 249.
- [47] D. V. Averin, K. K. Likharev, *J. Low Temp. Phys.* **1986**, *62*, 345.
- [48] A. E. Hanna, M. Tinkham, *Phys. Rev. B*, **1991**, *44*, 5919.
- [49] P. J. Thomas, G. U. Kulkarni, C. N. R. Rao, *Chem. Phys. Lett.* **2000**, *321*, 163.
- [50] D. L. Feldheim, B. E. Eaton, *ACS Nano*, **2007**, *1*, 154.
- [51] G. Schmid, B. Corain, *Eur. J. Inorg. Chem.* **2003**, 3081.
- [52] G. Schmid, U. Simon, *Chem. Commun.* **2005**, 697.
- [53] R. C. Thiel, R. E. Benfield, R. Zanoni, H. H. A. Smit, M. W. Dirken, *Struct. Bond.* **1993**, *81*, 1.
- [54] R. Narayanan, M. A. El-Sayed, *J. Phys. Chem. B*, **2005**, *109*, 12663.
- [55] M. Haruta, T. Kobayashi, H. Sano, N. Yamada, *Chem. Lett.* **1987**, 405.
- [56] M. Valden, X. Lai, D. W. Goodman, *Science*, **1998**, *281*, 1647.
- [57] R. Meyer, C. Lemire, S. K. Shaikhutdinov, H. Freund, *Gold Bull.* **2004**, *37*, 72.
- [58] D. H. Everett, *Basic Principles of Colloid Science*, Royal Society of Chemistry, London, **1988**.
- [59] J. Turkevich, P. C. Stevenson, J. Hillier, *Discuss. Faraday Soc.* **1951**, *11*, 55
- [60] G. Frens, *Nature: Phys. Sci.* **1973**, *241*, 20.
- [61] F. Cariati, L. Naldini, *Inorg. Chim. Acta*, **1971**, *5*, 172.
- [62] L. Malatesta, L. Naldini, G. Simonette, F. Cariati, *Chem. Commun.* **1965**, 212.
- [63] M. McPartlin, R. Mason, L. Malatesta, *J. Chem. Soc. D.* **1969**, 334.
- [64] B. K. Teo, X. Shi, H. Zhang, *J. Am. Chem. Soc.* **1992**, *114*, 2743.
- [65] G. Schmid, R. Pfeil, R. Boese, F. Bandermann, S. Meyer, G. H. M. Calis, Y. W. A. van der Velden, *Chem. Ber.* **1981**, *114*, 3634.
- [66] P. Braunstein, H. Lehner, D. Matt, *Inorg. Synth.* **1990**, *27*, 218.
- [67] J. P. Fackler, C. J. Mcneal, R. E. P. Winpenny, L. H. Pignolet, *J. Am. Chem. Soc.* **1989**, *111*, 6434.
- [68] D. H. Rapoport, W. Vogel, H. Colfen, R. Schlogl, *J. Phys. Chem. B*, **1997**, *101*, 4175.
- [69] G. Schmid, *Struct. Bond.* **1985**, *62*, 51.

## References

---

- [70] H. G. Boyen, G. Kastle, F. Weigl, B. Koslowski, C. Dietrich, P. Ziemann, J. P. Spatz, S. Riethmuller, C. Hartmann, M. Moller, G. Schmid, M. G. Garnier, P. Oelhafen, *Science*, **2002**, *297*, 1533.
- [71] G. Schmid, R. Pfeil, R. Boese, F. Bandermann, S. Meyer, G. H. M. Calis, W. A. Vandervelden, *Chem. Ber. Recl.* **1981**, *114*, 3634.
- [72] J. O. Bovin, R. Wallenberg, D. J. Smith, *Nature*, **1985**, *317*, 47.
- [73] G. Schmid, *Inorg. Synth.* **1990**, *27*, 214.
- [74] J. Petroski, M. H. Chou, C. Creutz, *Inorg. Chem.* **2004**, *43*, 1597.
- [75] G. H. Woehrle, L. O. Brown, J. E. Hutchison, *J. Am. Chem. Soc.* **2005**, *127*, 2172.
- [76] G. H. Woehrle, M. G. Warner, J. E. Hutchison, *J. Phys. Chem. B*, **2002**, *106*, 9979.
- [77] M. Brust, M. Walker, D. Bethell, D. J. Schiffrin, R. Whyman, *J. Chem. Soc. Chem. Commun.* **1994**, 801.
- [78] V. J. Gandubert, R. B. Lennox, *Langmuir*, **2005**, *21*, 6532.
- [79] S. Rucareanu, V. J. Gandubert, R. B. Lennox, *Chem. Mater.* **2006**, *18*, 4674.
- [80] A. G. Kanaras, F. S. Kamounah, K. Schaumburg, C. J. Kiely, M. Brus, *Chem. Commun.* **2002**, 2294
- [81] M. J. Hostetler, J. E. Wingate, C. J. Zhong, J. E. Harris, R. W. Vachet, M. R. Clark, J. D. Londono, S. J. Green, J. J. Stokes, G. D. Wignall, G. L. Glish, M. D. Porter, N. D. Evans, R. W. Murray, *Langmuir*, **1998**, *14*, 17.
- [82] J. F. Hicks, A. C. Templeton, S. W. Chen, K. M. Sheran, R. Jasti, R. W. Murray, J. Debord, T. G. Schaaf, R. L. Whetten, *Anal. Chem.* **1999**, *71*, 3703.
- [83] J. F. Hicks, D. T. Miles, R. W. Murray, *J. Am. Chem. Soc.* **2002**, *124*, 13322.
- [84] A. C. Templeton, M. J. Hostetler, C. T. Kraft, R. W. Murray, *J. Am. Chem. Soc.* **1998**, *120*, 1906.
- [85] A. C. Templeton, M. J. Hostetler, E. K. Warmoth, S. W. Chen, C. M. Hartshorn, V. M. Krishnamurthy, M. D. E. Forbes, R. W. Murray, *J. Am. Chem. Soc.* **1998**, *120*, 4845.
- [86] D. Li, G. L. Jones, J. R. Dunlap, F. Hua, B. Zhao, *Langmuir*, **2006**, *22*, 3344.
- [87] F. Hua, M. T. Swihart, E. Ruckenstein, *Langmuir*, **2005**, *21*, 6054.
- [88] G. H. Woehrle, L. O. Brown, J. E. Hutchison, *J. Am. Chem. Soc.* **2005**, *127*, 2172.
- [89] G. Schmid, R. Pugin, J. O. Malm, J. O. Bovin, *Eur. J. Inorg. Chem.* **1998**, 813.
- [90] G. Schmid, R. Pugin, W. Meyer-Zaika, U. Simon, *Eur. J. Inorg. Chem.* **1999**, 2051.
- [91] L. O. Brown, J. E. Hutchison, *J. Am. Chem. Soc.* **1997**, *119*, 12384.

- [92] W. M. Pankau, S. Mönninghoff, G. von Kiedrowski, *Angew. Chem. Int. Ed.* **2006**, *45*, 1889.
- [93] Porter, Lon A., D. Ji, S. L. Westcott, M. Graupe, R. S. Czernuszewicz, N. J. Halas, T. R. Lee, *Langmuir*, **1998**, *14*, 7378.
- [94] A. Manna, P.-L. Chen, H. Akiyama, T.-X. Wei, K. Tamada, W. Knoll, *Chem. Mater.* **2003**, *15*, 20.
- [95] R. L. Donkers, Y. Song, R. W. Murray, *Langmuir*, **2004**, *20*, 4703.
- [96] A. K. Boal, F. Ilhan, J. E. DeRouchey, T. Thurn-Albrecht, T. P. Russell, V. M. Rotello, *Nature*, **2000**, *404*, 746.
- [97] A. K. Boal, V. M. Rotello, *J. Am. Chem. Soc.* **2002**, *124*, 5019.
- [98] A. Badia, L. Cuccia, L. Demers, F. Morin, R. B. Lennox, *J. Am. Chem. Soc.* **1997**, *119*, 2682.
- [99] A. C. Templeton, S. Chen, S. M. Gross, R. W. Murray, *Langmuir*, **1999**, *15*, 66.
- [100] G. M. Whitesides, J. C. Love, *Sci. Am.* **2001**, *285*, 38.
- [101] H. J. Levinson, W. H. Arnold, in *Handbook of Microlithography, Micromachining, and Microfabrication, Vol. 1 of SPIE Press monograph* (Ed.: P. Rai-Choudhury), SPIE Optical Engineering Press, Bellingham, **1997**.
- [102] F. Gerrina, in *Handbook of Microlithography, Micromachining, and Microfabrication, Vol. 1 of SPIE Press monograph* (Ed.: P. Rai-Choudhury), SPIE Optical Engineering Press, Bellingham, **1997**.
- [103] B. Michel, A. Bernard, A. Bietsch, E. Delamarque, M. Geissler, D. Juncker, H. Kind, J.-P. Renault, H. Rothuizen, H. Schmid, P. Schmidt-Winkel, R. Stutz, H. Wolf, *IBM J. Res. Develop.* **2001**, *45*, 697.
- [104] E. F. Wassermann, M. Thielen, S. Kirsch, A. Pollmann, H. Weinforth, A. Carl, *J. Appl. Phys.* **1998**, *83*, 1753.
- [105] A. N. Boto, P. Kok, D. S. Abrams, S. L. Braunstein, C. P. Williams, J. P. Dowling, *Phys. Rev. Lett.* **2000**, *85*, 2733.
- [106] D. Mijatovic, J. C. T. Eijkel, A. van den Berg, *Lab. Chip.* **2005**, *5*, 492.
- [107] S. Y. Chou, P. R. Krauss, P. J. Renstrom, *Science*, **1996**, *272*, 85.
- [108] S. Y. Chou, C. Keimel, J. Gu, *Nature*, **2002**, *417*, 835.
- [109] R. P. Feynman, *Eng. Sci.* **1960**, *23*, 22.
- [110] J. M. Lehn, *Angew. Chem. Inter. Ed.* **1988**, *27*, 89.
- [111] J. M. Lehn, *Pure Appl. Chem.* **1994**, *66*, 1961.

- [112] J.-M. Lehn, *Supramolecular chemistry—concepts and perspectives*, VCH, Weinheim, **1995**.
- [113] S. Stepanow, M. Lingenfelder, A. Dmitriev, H. Spillmann, E. Delvigne, N. Lin, X. Deng, C. Cai, J. V. Barth, K. Kern, *Nat. Mater.* **2004**, *3*, 229.
- [114] N. Lin, A. Dmitriev, J. Weckesser, J. V. Barth, K. Kern, *Angew. Chem. Inter. Ed.* **2002**, *41*, 4779.
- [115] J. A. Theobald, N. S. Oxtoby, M. A. Phillips, N. R. Champness, P. H. Beton, *Nature*, **2003**, *424*, 1029.
- [116] M. Stöhr, M. Wahl, C. H. Galka, Till Riehm, T. A. Jung, L. H. Gade, *Angew. Chem. Inter. Ed.* **2005**, *44*, 7394.
- [117] J. V. Barth, J. Weckesser, N. Lin, A. Dmitriev, K. Kern, *Appl. Phys. A*, **2003**, *76*, 645.
- [118] R. van Hameren, P. Schon, A. M. van Buul, J. Hoogboom, S. V. Lazarenko, J. W. Gerritsen, H. Engelkamp, P. C. M. Christianen, H. A. Heus, J. C. Maan, T. Rasing, S. Speller, A. E. Rowan, J. A. A. W. Elemans, R. J. M. Nolte, *Science*, **2006**, *314*, 1433.
- [119] J. P. Rabe, S. Buchholz, *Science*, **1991**, *253*, 424.
- [120] S. B. Michael de Wild, Hitoshi Suzuki, Hisao Yanagi, Derck Schlettwein, Stanislav Ivan, Alexis Baratoff, Hans-Joachim Guentherodt, Thomas A. Jung,, *ChemPhysChem*, **2002**, *3*, 881.
- [121] T. Yokoyama, S. Yokoyama, T. Kamikado, Y. Okuno, S. Mashiko, *Nature*, **2001**, *413*, 619.
- [122] E. Fischer, *Ber. Deutsch Chem. Ges.* **1894**, *28*, 2985.
- [123] P. Ehrlich, *Studies on immunity*, Wiley, New York, **1906**.
- [124] M. Albrecht, *Naturwissenschaften*, **2007**, *94*, 951.
- [125] F. Hibbert, J. Emsley, *Adv. Phys. Org. Chem.* **1990**, *26*, 255.
- [126] J. Pranata, S. G. Wierschke, W. L. Jorgensen, *J. Am. Chem. Soc.* **1991**, *113*, 2810.
- [127] G. M. Whitesides, J. P. Mathias, C. T. Seto, *Science*, **1991**, *254*, 1312.
- [128] G. Binnig, H. Rohrer, C. Gerber, E. Weibel, *Phys. Rev. Lett.* **1982**, *49*, 57.
- [129] K. Eichhorst-Gerner, A. Stabel, G. Moessner, D. Declercq, S. Valiyaveetil, V. Enkelmann, K. Müllen, J. P. Rabe, *Angew. Chem. Int. Ed.* **1996**, *35*, 1492.
- [130] S. De Feyter, A. Gesquiere, M. M. Abdel-Mottaleb, P. C. M. Grim, F. C. De Schryver, C. Meiners, M. Sieffert, S. Valiyaveetil, K. Mullen, *Acc. Chem. Res.* **2000**, *33*, 520.
- [131] S. De Feyter, P. C. M. Grim, J. van Esch, R. M. Kellogg, B. L. Feringa, F. C. De Schryver, *J. Phys. Chem. B*, **1998**, *102*, 8981.

- [132] J.V. Barth, J. Weckesser, C. Cai, P. Günter, L. Bürgi, O. Jeandupeux, K. Kern, *Angew. Chem. Int. Ed.* **2000**, *39*, 1230.
- [133] J. V. Barth, J. Weckesser, G. Trimarchi, M. Vladimirova, A. De Vita, C. Cai, H. Brune, P. Gunter, K. Kern, *J. Am. Chem. Soc.* **2002**, *124*, 7991.
- [134] M. Bohringer, K. Morgenstern, W.-D. Schneider, R. Berndt, *Angew. Chem. Int. Ed.* **1999**, *38*, 821.
- [135] M. Bohringer, K. Morgenstern, W.-D. Schneider, R. Berndt, F. Mauri, A. De Vita, R. Car, *Phys. Rev. Lett.* **1999**, *83*, 324.
- [136] M. Bohringer, W.-D. Schneider, R. Berndt, *Surf. Rev. Lett.* **2000**, *7*, 666.
- [137] S. B. Lei, C. Wang, S. X. Yin, H. N. Wang, F. Xi, H. W. Liu, B. Xu, L. J. Wan, C. L. Bai, *J. Phys. Chem. B*, **2001**, *105*, 10838.
- [138] A. Dmitriev, N. Lin, J. Weckesser, J. V. Barth, K. Kern, *J. Phys. Chem. B*, **2002**, *106*, 6907.
- [139] S. Griessl, M. Lackinger, M. Edelwirth, M. Hietschold, W. M. Heckl, *Single Mol.* **2002**, *3*, 25.
- [140] D. L. Keeling, N. S. Oxtoby, C. Wilson, M. J. Humphry, N. R. Champness, P. H. Beton, *Nano Lett.* **2003**, *3*, 9.
- [141] R. Otero, M. Schöck, L. M. Molina, E. Lægsgaard, I. Stensgaard, B. Hammer, F. Besenbacher, *Angew. Chem. Int. Ed.* **2005**, *44*, 2270.
- [142] J. A. Zerkowski, C. T. Seto, D. A. Wierda, G. M. Whitesides, *J. Am. Chem. Soc.* **1990**, *112*, 9025.
- [143] J.-M. Lehn, M. Mascal, A. DeCian, J. Fischer, *J. Chem. Soc. Chem. Commun.* **1990**, *6*, 479
- [144] L. M. A. Perdigao, N. R. Champness, P. H. Beton, *Chem. Commun.* **2006**, *5*, 538.
- [145] D. L. Keeling, M. J. Humphry, R. H. J. Fawcett, P. H. Beton, C. Hobbs, L. Kantorovich, *Phys. Rev. Lett.* **2005**, *94*, 146104.
- [146] C. Bobisch, T. Wagner, A. Bannani, R. Moller, *J. Chem. Phys.* **2003**, *119*, 9804.
- [147] A. Langner, S. T. Tait, N. Lin, C. Rajadurai, M. Ruben, K. Kern, *Proc. Natl. Acad. Sci. U.S.A.*, **2007**, *104*, 17927.
- [148] A. Nitzan, M. A. Ratner, *Science*, **2003**, *300*, 1384.
- [149] A. P. Cote, A. I. Benin, N. W. Ockwig, M. O'Keeffe, A. J. Matzger, O. M. Yaghi, *Science*, **2005**, *310*, 1166.
- [150] S.-W. Hla, L. Bartels, G. Meyer, K.-H. Rieder, *Phys. Rev. Lett.* **2000**, *85*, 2777.
- [151] S. W. Hla, G. Meyer, K.-H. Rieder, *Chem. Phys. Lett.* **2003**, *370*, 431.

- [152] Y. Okawa, M. Aono, *Nature*, **2001**, *409*, 683.
- [153] T. Takami, H. Ozaki, M. Kasuga, T. Tsuchiya, A. Ogawa, Y. Mazaki, D. Fukushi, M. Uda, M. Aono, *Angew. Chem. Int. Ed.* **1997**, *36*, 2755.
- [154] A. Miura, S. De Feyter, M. M. S. Abdel-Mottaleb, A. Gesquiere, P. C. M. Grim, G. Moessner, M. Sieffert, M. Klapper, K. Mullen, F. C. De Schryver, *Langmuir*, **2003**, *19*, 6474.
- [155] L. Grill, M. Dyer, L. Lafferentz, M. Persson, M. V. Peters, S. Hecht, *Nat. Nano*, **2007**, *2*, 687.
- [156] M. I. Veld, P. Iavicoli, S. Haq, D. B. Amabilino, R. Raval, *Chem. Commun.* **2008**, 1536
- [157] N. A. A. Zwaneveld, R. Pawlak, M. Abel, D. Catalin, D. Gigmes, D. Bertin, L. Porte, *J. Am. Chem. Soc.* **2008**, *130*, 6678.
- [158] L. R. MacGillivray, J. L. Atwood, *Angew. Chem. Int. Ed.* **1999**, *38*, 1018.
- [159] M. Brust, M. Walker, D. Bethell, D. J. Schiffrin, R. Whyman, *J. Chem. Soc., Chem. Commun.* **1994**, 801.
- [160] T. Peterle, A. Leifert, J. Timper, A. Sologubenko, U. Simon, M. Mayor, *Chem. Commun.* **2008**, 3438.
- [161] T. W. Greene, P. G. M. Wuts, *Protective Groups in Organic Synthesis*, Wiley & Sons, Hoboken, New Jersey, **2006**.
- [162] M. M. Alvarez, J. T. Khoury, T. G. Schaaff, M. N. Shafigullin, I. Vezmar, R. L. Whetten, *J. Phys. Chem. B*, **1997**, *101*, 3706.
- [163] K. G. Thomas, J. Zajicek, P. V. Kamat, *Langmuir*, **2002**, *18*, 3722.
- [164] A. D'Aléo, R. M. Williams, F. Osswald, P. Edamana, U. Hahn, J. van Heyst, F. D. Tichelaar, F. Vögtle, L. De Cola, *Adv. Funct. Mater.* **2004**, *14*, 1167.
- [165] J. Kim, D. Lee, *J. Am. Chem. Soc.* **2006**, *128*, 4518.
- [166] L. D. Menard, S.-P. Gao, H. Xu, R. D. Twesten, A. S. Harper, Y. Song, G. Wang, A. D. Douglas, J. C. Yang, A. I. Frenkel, R. G. Nuzzo, R. W. Murray, *J. Phys. Chem. B*, **2006**, *110*, 12874.
- [167] D. S. Tarbell, Y. Yamamoto, B. M. Pope, *Proc. Natl. Acad. Sci. U.S.A.* **1972**, *69*, 730.
- [168] I. Hasan, E. R. Marinelli, L.-C. C. Lin, F. W. Fowler, A. B. Levy, *J. Org. Chem.* **1981**, *46*, 157.
- [169] H. H. Wasserman, G. D. Berger, K. R. Cho, *Tetrahedron Lett.* **1982**, *23*, 465.
- [170] V. H. Rawal, M. P. Cava, *Tetrahedron Lett.* **1985**, *26*, 6141.

- [171] J. Kimling, M. Maier, B. Okenve, V. Kotaidis, H. Ballot, and A. Plech, *J. Phys. Chem. B* **2006**, 110, 15700.
- [172] W.M. Pankau, K. Verbist, G. von Kiedrowski, *Chem. Commun.* **2001**, 519.
- [173] X. Moreau, J.-M. Campagne, *J. Org. Chem.* **2003**, 68, 5346.
- [174] T. Yonezawa; K. Yasui; N. Kimizuka, *Langmuir*, **2001**, 17, 271.
- [175] K. Torigoe, K. Esumi, *J. Phys. Chem. B*, **1999**, 103, 2862.
- [176] E. J. Shelley, D. Ryan, S. R. Johnson, M. Couillard, D. Fitzmaurice, P. D. Nellist, Y. Chen, R. E. Palmer, J. A. Preece, *Langmuir*, **2002**, 18, 1791-1795.
- [177] X. M. Li, M. R. de Jong, K. Inoue, S. Shinkai, J. Huskens, D. N. Reinhoudt, *J. Mater. Chem.* **2001**, 11, 1919.
- [178] E. U. Thoden van Velzen, J. F. J. Engbersen, D. N. Reinhoudt, *J. Am. Chem. Soc.*, **1994**, 116, 3597.
- [179] M. M. Maye, S. C. Chun, L. Han, D. Rabinovitch, C.-J. Zhong, *J. Am. Chem. Soc.* **2002**, 124, 4958-4959.
- [180] S-W. Tam-Chang, J. C. Mason, *Tetrahedron*, **1999**, 55, 13333.
- [181] T. G. M. Dhar, L. A. Borden, S. Tyagarajan, K. E. Smith, T. A. Branchek, R. L. Weinschank, C. Gluchowski, *J. Med. Chem.* **1994**, 37, 2334.
- [182] C.-C. Han, R. Balakumar, *Tetrahedron Lett.* **2006**, 47, 8255.
- [183] F. Moresco, G. Meyer, K.-H. Rieder, J. Ping, H. Tang, C. Joachim, *Surf. Sci.* **2002**, 499, 94.
- [184] T. A. Jung, R. R. Schlittler, G. K. Gimzewski, *Nature*, **1997**, 386, 696.
- [185] S. Weigelt, C. Busse, L. Petersen, E. Rauls, B. Hammer, K. V. Gothelf, F. Besenbacher, T. R. Linderoth, *Nat. Mater.* **2006**, 5, 112.
- [186] N. A. Noureldin, J. W. Bellegarde, *Synthesis*, **1999**, 6, 939.
- [187] S. Berner, M. Brunner, L. Ramoino, H. Suzuki, H.-J. Güntherodt, T. A. Jung, *Chem. Phys. Lett.* **2001**, 175.
- [188] J. Henzl, M. Mehlhorn, H. Gawronski, K. H. Rieder, K. Morgenstern, *Angew. Chem. Int. Ed.* **2006**, 45, 603.
- [189] M. J. Comstock, N. Levy, A. Kirakosian, J. Cho, F. Lauterwasser, J. H. Harvey, D. A. Strubbe, J. M. J. Frechet, D. Trauner, S. G. Louie, M. F. Crommie, *Phys. Rev. Lett.* **2007**, 99, 038301.

## 7. CURRICULUM VITAE

### M. A. Umut SOYDANER

Date of Birth / Place: 17 June 1977 / Istanbul

Marital Status : Married, one child

Nationality : Turkish

e-mail: umut.soydaner@stud.unibas.ch

#### EDUCATION:

**Ph.D. Chemistry**, University of Basel, Basel, 2005- 2010

Thesis: Organising molecules at the solid/liquid interface

Research advisor: Prof. Dr. Marcel Mayor

**M. Sc. Chemistry**, University of Basel, Basel, 2004-2005

Thesis: Synthesis and Computational Study of *Meso*-perhalogenated Protoporphyrin-IX Complexes: Toward Hybrid CYP Enzymes

Research advisors: Prof. Wolf D. Woggon and Prof. Markus Meuwly

**MBA**, Galatasaray University, İstanbul, 2001- 2004

Thesis: Investigation of Successful Customer Relationship Management for Banks

Research advisor: Prof. Dr. M.Yaman Öztekin

**B. Sc. Chemistry**, Department of Chemistry, Middle East Technical University (METU), Ankara, 1996- 2001

#### RESEARCH EXPERIENCES:

**University of Basel**, Basel, Teaching assistant of General Chemistry for Pharmaceutical students, 2005-2009

**Sabancı University**, Istanbul, Research Assistant under the supervision of Prof. Dr. Alpay Taralp, 2002-2003,

**GlaxoWellcome**, Internship, Department of Production and Department of Quality& Assurance in Microbiology and Chemistry, February 1999 and August 1999

**Colgate-Palmolive**, Internship, Department of Quality& Assurance August 1998